

Dissertationsreihe am Institut für Hydromechanik
der Universität Karlsruhe (TH)
Heft 2006/3

Coupled 3D hydrodynamic models for
submarine outfalls: Environmental hydraulic
design and control of multiport diffusers

Tobias Bleninger



Tobias Bleninger

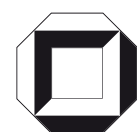
**Coupled 3D hydrodynamic models for submarine outfalls:
Environmental hydraulic design and control of multiport diffusers**

Dissertationsreihe am Institut für Hydromechanik
der Universität Karlsruhe (TH)

Heft 2006/3

Coupled 3D hydrodynamic models for submarine outfalls: Environmen- tal hydraulic design and control of multiport diffusers

von
Tobias Bleninger



universitätsverlag karlsruhe

Dissertation, genehmigt von der
Fakultät für Bauingenieur-, Geo- und Umweltwissenschaften
der Universität Fridericiana zu Karlsruhe (TH), 2006
Referenten: Prof. Gerhard H. Jirka, Ph.D., Prof. Dr.-Ing. E.h. Hermann H. Hahn, Ph.D.,
Prof. Peter A. Davies, University of Dundee, UK

Impressum

Universitätsverlag Karlsruhe
c/o Universitätsbibliothek
Straße am Forum 2
D-76131 Karlsruhe
www.uvka.de



Dieses Werk ist unter folgender Creative Commons-Lizenz
lizenziert: <http://creativecommons.org/licenses/by-nc-nd/2.0/de/>

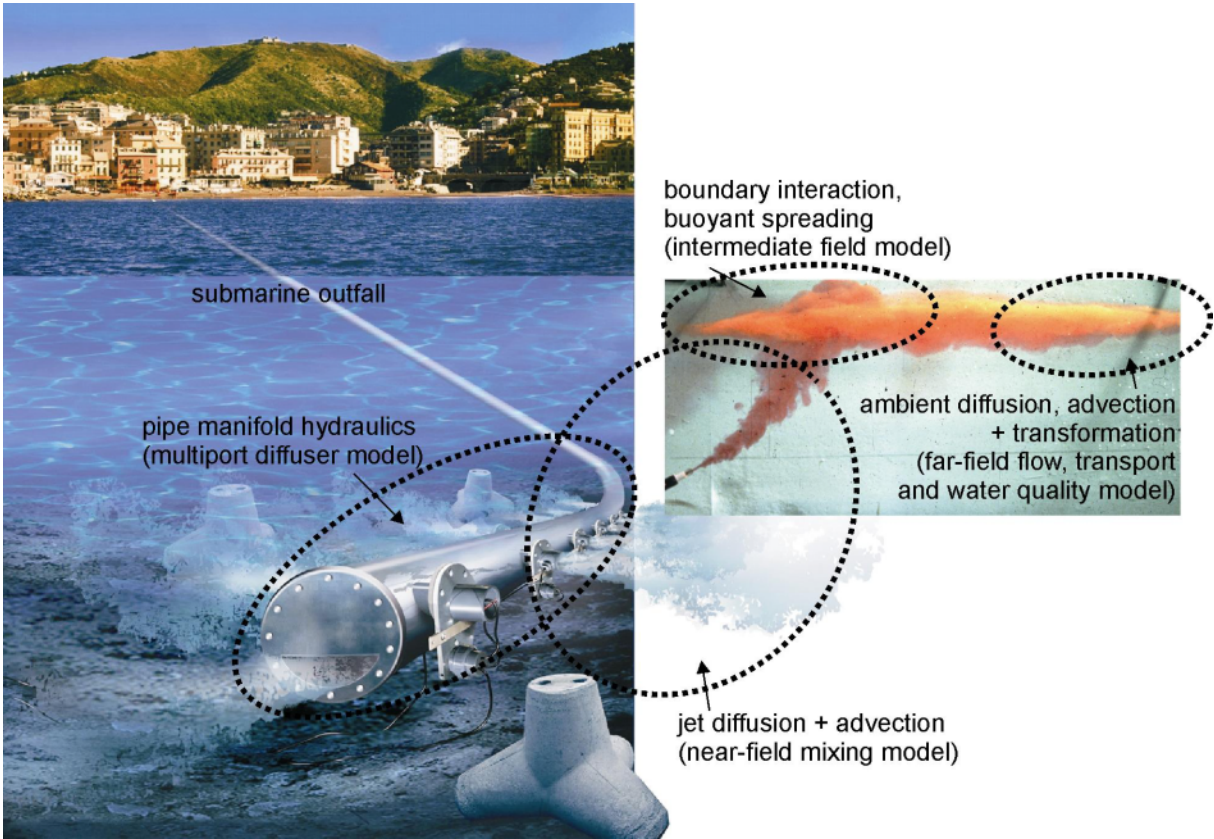
Universitätsverlag Karlsruhe 2007
Print on Demand

ISSN: 1439-4111
ISBN: 978-3-86644-160-6

Coupled 3D hydrodynamic models for submarine outfalls: Environmental hydraulic design and control of multiport diffusers

Doctoral thesis

*Tobias Bleninger
Institute for Hydromechanics, University Karlsruhe*



**Coupled 3D hydrodynamic models for submarine outfalls:
Environmental hydraulic design and control of multiport diffusers**

Zur Erlangung des akademischen Grades eines

DOKTOR - INGENIEURS

von der Fakultät für

Bauingenieur-, Geo- und Umweltwissenschaften
der Universität Fridericiana zu Karlsruhe (TH)

genehmigte

DISSERTATION

von

Dipl.-Ing. Tobias Bleninger
aus Marbach (Neckar)

Tag der mündlichen Prüfung: 19. Juli 2006

Hauptreferent: Prof. Gerhard H. Jirka, Ph.D.

Korreferenten: Prof. Dr.-Ing. E.h. Hermann H. Hahn, Ph.D.
Prof. Peter A. Davies, University of Dundee, UK

Karlsruhe 2006

Abstract

Long submarine outfalls with a multiport diffuser are an efficient discharge device avoiding pollutant accumulation and collapse of ecosystems by dispersing the treated effluents. This thesis describes the results of a project to raise the current level of hydraulic design and environmental impact prediction technologies for such installations. Focus are the hydrodynamic aspects approached by computer modeling techniques. First, a multiport diffuser design program was developed. Secondly, two model systems for discharge analysis, CORMIX for the near-field and intermediate-field and Delft3D for the far-field were coupled, and third a regulatory procedure is proposed to license and monitor outfall installations.

The multiport diffuser design program CorHyd calculates the flow distribution along the diffuser and the related pressure losses in the pipe system. It considers different pipe materials and geometric configurations, and releases restrictions of previous diffuser programs by considering flexible geometry specifications, high risers and variable area orifices, all with automatic definition of loss coefficients. Additional features regarding blocked ports, sensitivity analysis and performance evaluation for varying parameters guarantee proper diffuser operation and reduced costs for installation, operation and maintenance. Case studies show a strong sensitivity to the representation and formulation of local losses even for relatively simple riser/port configurations.

CORMIX was coupled to Delft3D for the prediction of the substance fate, especially for bacteria distributions. CORMIX includes a near-field buoyant jet model for the source induced turbulent mixing and additional modules to consider boundary interaction and buoyant spreading processes in the intermediate-field. Delft3D models the ambient flow hydrodynamics and water quality parameters. The coupling algorithm pays special attention to the intermediate-field modeling, where the CORMIX flow classification system is an important component for the modeling approach. The existing set of length scales as base for the flow classification has been extended by an additional unsteady length and time scale. These ascertain, whether buoyant spreading results as predicted by the steady intermediate-field model correlate with the unsteady motions in the receiving waters. The proposed coupling approach firstly classifies field-data and CORMIX time-series results for the near-field / intermediate-field and computes input and source files for both models according to the chosen far-field grid resolution and intermediate-field plume geometry and concentration. Secondly, the water quality model within Delft3D computes the substance concentrations. The algorithm is implemented and tested for the Cartagena outfall in Colombia. The study incorporated the ocean bathymetry and predicted ocean currents and density distributions through the water column that are generated by wind stresses and the appropriate boundary conditions. Results showed significant improvements compared to traditional design approaches.

Moreover, a proposal for improved water quality regulations and their implementation for discharge permits has been added to the engineering design approach. Especially the specification of where in the water body the environmental quality standards apply and how to predict and monitor has been considered. The proposal of a regulatory discharge zone in combination with a regulatory preservation zone promises to improve procedures regarding discharge licensing and monitoring. Its implementation with support of coupled hydrodynamic and water quality models are demonstrated for the Cartagena outfall.

Kurzfassung

Gekoppelte 3D hydrodynamische Modelle für Einleitungen in Küstengewässer:

Hydraulische Bemessung, Berechnung und Kontrolle der Auswirkungen von Einleitungen über mehrdüsig Diffusorbauwerke

Mehrdüsig Diffusorbauwerke, die über lange Rohrleitungen das gereinigte Abwasser einer Kläranlage in den Vorfluter einleiten, stellen hocheffiziente Systeme zur Vermeidung von Gewässerqualitätsproblemen dar. Die starke Durchmischung und Verteilung des behandelten Abwassers vermeidet die lokale Anhäufung von Schadstoffen und unterstützt somit natürliche Abbauprozesse. Die vorliegende Arbeit beschreibt das Resultat eines Projektes zur Verbesserung von Bemessungs- und Vorhersageinstrumenten für mehrdüsig Diffusorbauwerke in Küstengewässern. Im Mittelpunkt stehen die hydrodynamischen Aspekte der Umwelttechnologie, welche mit der Anpassung und Neukonzeption von Modellen untersucht werden. Als erstes wurde ein Bemessungsprogramm für Diffusorbauwerke entwickelt. Als zweites Programmmodul zur Kopplung des Nahfeld Misch- und Transportmodellsystems CORMIX mit dem Fernfeldmodell Delft3D entwickelt und als drittes Vorschläge ausgesprochen, um die Bewilligung und Überwachung einer Abwassereinleitung zu verbessern.

Das Bemessungsprogramm für Diffusorbauwerke, CorHyd, berechnet die Durchflussverteilung in einem mehrdüsig Rohrleitungssystem. Es beinhaltet die Berechnung von Druckverlusten infolge verschiedener Rohrmaterialien und geometrischer Konfigurationen, wie lange Steigrohre, aufgesetzte Verteilerrosetten und Ventile mit durchflussvariabler Öffnung. Zusätzliche Programmoptionen ermöglichen die Anpassung der notwendigen Betriebsdruckhöhe, auch für Betriebszustände, die sich stark von den Bemessungsbedingungen unterscheiden. Die erhöhte Leistungsfähigkeit der somit bemessenen Systeme garantiert des Weiteren einen niedrigeren Unterhaltungsaufwand und stabile Betriebsbedingungen. Die Programmtauglichkeit wurde anhand von zwei Fallstudien überprüft. Beide Studien zeigen eine starke Abhängigkeit von Definitionen zur Bestimmung lokaler Druckverluste.

Zur Prognose der Einleitungsauswirkungen auf das Gewässer und dessen Nutzungen, insbesondere von Bakterienkonzentrationsverteilungen wurde CORMIX, mit Delft3D gekoppelt. CORMIX berechnet die Ausbreitung von Auftriebsstrahlen sowie Interaktionen mit Berandungen und Dichteströmungen. Delft3D berechnet die Küstenströmung und den Schadstofftransport, dem noch zusätzliche Abbauprozesse obliegen. Der Kopplungsalgorithmus befasst sich insbesondere mit dem Übergangsbereich. Die CORMIX Strömungsklassifizierung wurde hierfür um eine instationäre Zeit- und Längenskala erweitert, um die dynamische Interaktion zwischen den Modellen korrekt zu erfassen. Hiermit ist es möglich die Ergebnisse einer stationären Berechnung bis zum Übergangsbereich mit der Instationarität der Küstenströmung zu vergleichen und gegebenenfalls die Kopplungsposition anzupassen. Zuerst werden Naturdaten und Zeitreihen der CORMIX Ergebnisse klassifiziert und Eingabedaten für Randbedingungen und Quellenterme für beide Programme CORMIX und Delft3D erzeugt. Die Ergebnisse beinhalten die Durchmischung, die Fahnenposition und Fahnengeometrie am Ende des Übergangsbereichs und Strömungsabhängige Kopplungsposition und Zeitpunkt. Die abschließende Anwendung des Fernfeldtransportmodells ergibt die Konzentrationsverteilungen. Der Algorithmus wurde in die Programmsysteme implementiert und am Beispiel des Einleitungsbauwerks für die Stadt Cartagena in Kolumbien getestet. Die Rechnungen beinhalteten die Berechnung des Strömungs- und Dichtefeldes unter zusätzlichem Einfluss von Wind. Ergebnisse zeigen, dass realistischere Resultate im Vergleich zu früheren Vorhersagemethoden erzielt wurden.

Neben der ingenieurmäßigen Bemessung und Standortbestimmung des Bauwerks wurde auch die gängige Praxis der Genehmigungsverfahren für solche Bauwerke erörtert. Es wurden zwei Konzepte vorgeschlagen, um vorhandene Defizite, insbesondere in neuen Richtlinien, zu beheben. Ersteres ist die Definition einer behördlichen Einleitungszone, die festlegt, an welcher Stelle im Gewässer die Umweltqualitätsnormen einzuhalten sind. Die bisherige Praxis hatte nicht berücksichtigt, dass Mischprozesse nur langsam und über lange Strecken ablaufen. Zweites ist die Definition einer behördlichen Schutz- bzw. Erhaltungszone. Diese soll Einleitungsauswirkungen auf Gewässerbereiche mit besonderer Nutzung, zum Beispiel als Badegewässer oder für Trinkwassernutzung, auf die gesetzlichen nutzungsspezifischen Grenzwerte reduzieren. Beide Ansätze wurden auf die Fallstudie für die Einleitung der Stadt Cartagena angewandt und verdeutlichen die Vorteile einer Erweiterung der gesetzlichen Richtlinien in diesem Sinne.

Preface and acknowledgements

This doctoral thesis was elaborated at the Institute for Hydromechanics at the University of Karlsruhe in Germany in parallel to the appointment as teaching and research assistant. The thesis works have been fully funded by the Institute. Complementary support was offered from Delft Hydraulics regarding the software license for the applied program suite Delft3D. Further support from the German Academic Exchange Service was related to the travel expenses for two research stays at the University of São Paulo, Brazil. The case has been supported by the World Bank, regarding travel expenses for two research stays at the Georgia Institute of Technology in the United States.

I would like to express my gratitude especially to my supervisor Gerhard Jirka for his every time friendly and open discussions and all the helpful ideas. I enjoyed listening to his lively and active visions and feeling his strong enthusiasm for teaching and researching environmental hydraulics. Thanks also to all colleagues from the Institute for Hydromechanics providing such a beautiful and nice working environment and support.

I thank very much Peter Davies from the University of Dundee, Herrmann Hahn, and Wolfgang Rodi from the University of Karlsruhe for contributing to my thesis offering their supervision as member of my committee and their helpful comments. Moreover, I appreciate the support from Arthur Mynett from Delft Hydraulics for providing a research license of the software Delft3D. The software system CORMIX has been offered by Rob Doneker from MixZon, which included an outstanding support and very friendly exchange of ideas.

Regarding my research stay in São Paulo, I thank Jayme Ortiz from the University of São Paulo for the kind hospitality and scientific exchange. I furthermore appreciate the assistance and friendship from Emilia Arasaki and Edward Brambilla. I am grateful to Paolo Rosman from the University of Rio de Janeiro and João Carvalho from the University of the Vale de Itajaí for sharing their data and ideas.

I am very glad that Phil Roberts from the Georgia Institute of Technology and Menahem Libhaber from the World Bank did believe in my ideas and supported my stay in Atlanta. It was a very efficient and most interesting practical application of research outcomes, what I kindly appreciate.

Thanks to RedValve Company and Elasto-Valve Rubber Products for providing their data regarding Duckbill valves. I also express my gratitude to the student assistants Martina Kurzke and Gudrun Hillebrand who contributed to the coding of the present programs. And thanks to Volker Weitbrecht and John Fenton for their patience in correcting my draft versions and keeping me laughing even in the last days before submitting the thesis.

Finally yet importantly, I thank my wife Katya and my children Vincent and Valentina for their love and understanding.

Karlsruhe, 12th June 2006
Tobias Bleninger

Contents

1	Introduction	1
1.1	Background and motivation - coastal water quality problems	2
1.2	Problem - wastewater discharges	3
1.3	Objectives and outline	5
2	Characteristics of coastal wastewater discharges.....	7
2.1	Coastal waters characteristics	7
2.1.1	Coastal circulation	8
2.1.2	Density stratifications	9
2.1.3	Natural purification.....	10
2.2	Wastewater sources and characteristics	11
2.3	Wastewater treatment technologies	13
2.3.1	Limitations of conventional treatment technologies.....	15
2.4	Discharge technologies - outfall characteristics	16
2.4.1	Discharge processes and their characteristics.....	19
2.4.2	Limitations of discharge technologies	24
2.5	Need for a discharge assessment - improved outfall design	24
2.5.1	Outfall design parameters - dilution characteristics.....	25
2.5.2	Outfall design tools - need for prediction models.....	27
3	Governing equations: assumptions and simplifications.....	29
3.1	General simplifications for coastal discharges	30
3.2	Simplifications regarding spatial scales	30
3.2.1	Effect of earth rotation.....	30
3.2.2	Shallow water approximation - hydrostatic assumption.....	31
3.2.3	Spatial averaging: 1, 2 or 3 dimensions	31
3.3	Simplifications regarding time scales	32
3.3.1	Steady flow	32
3.3.2	Time averaging - simplification of turbulent fluctuations	32
3.4	Simplifications regarding boundaries	33
3.4.1	Closed boundaries.....	34
3.4.2	Open boundaries	35
4	Multipoint diffuser design program - CorHyd.....	37
4.1	Multipoint diffuser configurations	38
4.2	Internal diffuser hydraulics - manifold processes	38
4.2.1	Governing equations for turbulent pipe flow.....	41
4.2.2	Friction losses - cross-sectional non-uniformities	42
4.2.3	Local losses - streamwise non-uniformities.....	43
4.2.4	Simplifications and modeling assumption.....	45
4.3	CorHyd model	49
4.3.1	Governing equations	49
4.3.2	Solving scheme	53
4.3.3	Data Input	55
4.3.4	Data Output.....	57
4.4	Diffuser design and optimization	57

4.4.1	Design constraints	57
4.4.2	Design and optimization steps	59
4.4.3	Sensitivity Analysis	62
4.4.4	Transients, saline intrusion and purging	63
4.4.5	Design rules	63
4.5	Case studies	64
4.5.1	Ipanema outfall - Rio de Janeiro - Brazil	64
4.5.2	Berazategui - Buenos Aires - Argentina	75
4.6	Discussion and recommendations	78
5	Coupled discharge and transport modeling - CorLink.....	81
5.1	Near-field processes and modeling applications	82
5.1.1	Governing equations for multiport buoyant jets	84
5.1.2	Dimensional analysis - empirical methods	88
5.1.3	Integral methods	94
5.1.4	Numerical methods	96
5.1.5	Near-field jet models.....	97
5.2	Intermediate-field processes and modeling applications	101
5.2.1	Near-field instability	101
5.2.2	Boundary interaction processes	102
5.2.3	Buoyant spreading processes	105
5.2.4	Intermediate field models	109
5.3	Far-field processes and modeling applications	111
5.3.1	Passive ambient mixing - empirical dilution equations	111
5.3.2	Governing equations for 3-D shallow water flows	114
5.3.3	Numerical methods - CFD	117
5.3.4	Far-field flow models - coastal circulation	120
5.3.5	Far-field transport models - transport and mixing	122
5.3.6	Water quality modeling - decay and transformation processes	125
5.4	Model coupling - approaches and algorithms	126
5.4.1	Review of coupling concepts	131
5.4.2	Coupling approach	132
5.4.3	Coupling algorithm and program modules	135
6	Regulatory discharge and preservation zone - CorZone	145
6.1	Water quality objectives	145
6.2	Regulatory water quality control measures	146
6.3	Regulatory discharge and preservation zone concept	150
6.3.1	Regulatory discharge zone specification	150
6.3.2	Regulatory preservation zone specification	152
6.4	Discharge licensing procedure	152
7	Case study - Cartagena outfall	155
7.1	Background and problem	155
7.1.1	Caribbean circulation	157
7.2	Data basis - CorField analysis	162
7.2.1	Bathymetry and shoreline	162
7.2.2	Wind.....	162

7.2.3	Currents.....	164
7.2.4	Tides.....	168
7.2.5	Density (Salinity and Temperature) profiles.....	168
7.3	Near-field baseline modeling - CorTime	170
7.4	Ambient hydrodynamics baseline modeling with Delft3D flow	174
7.4.1	Computational domain.....	175
7.4.2	Boundary and initial conditions.....	177
7.4.3	Hydrodynamic simulation.....	178
7.5	Source representation in far-field model - CorLink	183
7.6	Coupled water quality modeling	184
7.7	Regulatory consequences - CorZone	185
7.8	Discussion and recommendations	189
8	Conclusions.....	191
9	Outlook.....	193
	Annex A: Loss coefficients in CorHyd.....	195
	Annex B: Example of CorHyd report.....	205
	References.....	207
	Curriculum vitae.....	219

List of Figures

Fig. 1:	Pollutant sources and environmental objectives (underlined) in coastal waters. Water quality management needs to balance pollutant reduction and ecosystem response.	1
Fig. 2:	Aerial photograph of Santos Bay, Brazil showing Santos city (approx. 500,000 inhabitants) and Santos harbor (along the river). Visual contours of the waste plume (arrow) from the Santos outfall, 4 km offshore, show a plume impact with the city's most frequented beaches (courtesy of municipality of Praia Grande, Brazil).	4
Fig. 3:	Aerial view of the receiving waters of outfalls discharging in the Santos Bay, Brazil (<i>left</i> , courtesy of municipality of Praia Grande) and the São Sebastião channel, Brazil (<i>right</i> , Lamparelli, 2003).....	8
Fig. 4:	Aerial view of an outfall, discharging in the São Sebastião channel at two different time-steps, showing completely different dispersion patterns (Lamparelli, 2003).	9
Fig. 5:	Satellite image from Rio Magdalena (Colombia), showing the river plume (courtesy of Menahem Libhaber, World Bank).	10
Fig. 6:	Inactivation in seawater of echovirus 6 as a function of temperature (<i>left</i>) and E. coli as a function of solar radiation (<i>right</i>) (reproduced from Bitton, 1994)	11
Fig. 7:	Milliscreens for preliminary treatment (Huber technology)	14
Fig. 8:	Pictures from offshore, submerged, and positively buoyant wastewater discharges. <i>Left</i> : single port (www.cormix.info), <i>right</i> : multiport diffuser (Lamparelli, 2003)	17
Fig. 9:	Schematic view of submarine outfall with diffuser length L_D , port diameter D , port spacing ℓ , port and diffuser orientations β , γ , θ , effluent flowrate Q_o and density ρ_o , average depth of receiving water H with density ρ_a and velocity u_a (reproduced from Jirka et al., 1996).....	17
Fig. 10:	Antalya outfall (Turkey) during installation in 1997. <i>Top</i> : Diffuser section assembling on shore. <i>Down</i> : Feeder section ($L_F = 5$ km, HDPE pipe, $D = 1600$ mm) while sinking with attached concrete weights on the seabed (PipeLife Company).....	18
Fig. 11:	Boston outfall during installation in 1998. <i>Left</i> : View into tunnel section (16 km with 8 m diameter). <i>Right</i> : One out of 55 riser caps with eight outlets each in rosette like configuration (Roberts and Snyder, 1993).....	19
Fig. 12:	Schematic view of an operating multiport diffuser outfall merged with a laboratory picture of a trapped waste plume in stratified ambient (modified from Domenichini et al., 2002) 19	19
Fig. 13:	Typical temporal and spatial scales for transport and mixing processes related to coastal wastewater discharges (Jirka et al., 1976, Fischer et al., 1979)	21
Fig. 14:	Comparison of two wastewater systems and their impact on receiving waters as exceedance-frequency of ambient standards (i.e. beach water quality). <i>Left</i> : Secondary treatment plant with short outfall. <i>Right</i> : Preliminary treatment with long outfall and multiport diffuser.	22
Fig. 15:	Comparison of technical and natural contributions to pollutant concentration reductions. <i>Left</i> : Technically achievable concentration reductions for primary and secondary treatment. <i>Right</i> : Naturally occurring concentration reductions after discharging preliminary treated wastewater (reproduced from WRc, 1990).....	22
Fig. 16:	Replaced diffuser, blocked with sediment (courtesy of Eng. Pedro Campos, Chile)	37
Fig. 17:	Outfall configuration showing feeder pipe and diffuser from side view and top view, defining the pipelines and port/riser configurations.....	39
Fig. 18:	Pictures of multiport diffusers during construction (Bonnasabla.com)	39
Fig. 19:	<i>a</i>): standard diffuser; <i>b</i>): Y- or T-shaped diffuser configuration	39
Fig. 20:	<i>a</i>) Buried outfall with short riser; <i>b</i>) tunneled outfall with long riser and multiple ports; <i>c</i>) terrain following outfall laid on seabed (reproduced from Davies, 2003).....	40
Fig. 21:	<i>a</i>) simple port (courtesy of Carlo Avanzini); <i>b</i>) variable-area orifices ('duckbill valves', RedValve Company); <i>c</i>) riser/port configuration (Guarujá, Brazil); <i>d</i>) rosette like riser / port arrangement (Lee et al., 2001).....	40
Fig. 22:	Definition diagram for a general pipe flow (reproduced from Jirka, 2001).....	41
Fig. 23:	Shear-stress in pipe flows (reproduced from Jirka, 2001)	42

Fig. 24:	Examples for local pressure losses in pipe flows (Miller, 1990)	44
Fig. 25:	Picture of the headworks of a coastal outfall showing the inlet to the feeder pipe (courtesy of Carlo Avanzini)	44
Fig. 26:	Steady pipe flow with constant boundary conditions ($Q_{in,a} = const.$)	46
Fig. 27:	Pipe flow immediately after a relatively fast change of the water level elevation in the headworks tank ($Q_{in,b} > Q_{in,a}$).....	46
Fig. 28:	Pipe flow after the acceleration of the whole fluid in the outfall took place	47
Fig. 29:	Definition scheme for the port-to-port analysis: $p_{a,i}$ = ambient pressure, H = average ambient water level elevation, q_i = discharge through one riser/port configuration with velocity v_i at elevation $z_{j,i}$. $p_{d,i}$ = internal diffuser pipe pressure upstream a flow division (node) with diffuser pipe centerline elevation $z_{d,i}$ and horizontal pipe location $x_{d,i}$	50
Fig. 30:	The graphical user interface of CorHyd.....	55
Fig. 31:	Coordinate system used in CorHyd. Five pipe sections and two port/riser groups are shown in this example.....	56
Fig. 32:	Graphical output: bar charts showing the discharge per riser, the relative discharge deviation and port/riser headloss distribution, the discharge velocity at ports and in the final jet, the velocity in the diffuser pipe as well as port and diffuser diameter.	58
Fig. 33:	Graphical output: Energy and Hydraulic grade line of the whole system and the diffuser ..	59
Fig. 34:	Schematization of general diffuser design algorithm.....	59
Fig. 35:	Location map of the Ipanema outfall of the city Rio de Janeiro in Brazil (reproduced from Carvalho, 2003).....	65
Fig. 36:	Side view and cross section of the Ipanema outfall	66
Fig. 37:	Image from the construction site of the Ipanema outfall (reproduced from Grace, 1978)....	66
Fig. 38:	Flow characteristics for design flow. <i>Top-down</i> : Individual riser flow distribution along diffuser, riser flow deviation from mean, pressure losses in port/riser configurations (line), port and jet discharge velocities and diffuser pipe velocities, port and diffuser diameter (lines)	67
Fig. 39:	Riser flow deviation from mean flow, for a horizontal diffuser line (<i>top</i>) and a sloped diffuser line (3 m / 449 m, <i>down</i>). Pressure losses in port/riser configuration is shown as line. 68	68
Fig. 40:	Flow characteristics for different flowrates Q and sloped diffuser, showing riser flow deviation, port/riser headloss, jet discharge velocities, diffuser pipe velocities and total head H_t 69	69
Fig. 41:	Changes in total head for varying discharges vs. constant ambient water level.	69
Fig. 42:	Flow characteristics for different flowrates Q for tapered diffuser where diffuser diameter is reduced to 1.2 m for the end section. <i>Top-down</i> : riser flow deviation from mean, pressure losses in port/riser configurations, jet discharge velocities and diffuser pipe velocities	70
Fig. 43:	Side view and cross section of two design alternatives for the Ipanema outfall. <i>Left</i> : covered diffuser pipe and short risers, <i>right</i> : diffuser pipe laid in a refilled trench and short risers.....	71
Fig. 44:	Flow characteristics for: <i>top</i> : tapered diffuser covered or laid in a trench with additional short risers and two different riser diameters, <i>down</i> : tapered diffuser on piles without risers. 72	72
Fig. 45:	Side view and cross section of a constructional design alternative for the Ipanema outfall with a tunneled diffuser pipe, long risers, and rosette like port arrangements.....	73
Fig. 46:	Flow characteristics for: <i>top</i> : tapered tunneled diffuser with long riser and rosette like port arrangements, <i>down</i> : tapered diffuser on piles without risers	73
Fig. 47:	Flow characteristics for different discharges (Q), for a diffuser with additional Duckbill valves ($D = 200$ mm), showing the riser flow deviation, port/riser headloss, port and jet discharge velocities, diffuser pipe velocities and total head (H_t).....	74
Fig. 48:	Schematic view of diffuser longitudinal section of Berazategui outfall	75
Fig. 49:	Side and top view of riser/port configuration of diffuser.....	75
Fig. 50:	Top view of the Rio de la Plata delta showing the location of the Berazategui outfall and the ambient characteristics at its location (source: Nasa, 2005)	76

Fig. 51:	Flow characteristics for final design at maximum flow. <i>Top-down</i> : Individual riser flow distribution along diffuser, riser flow deviation from mean, pressure losses in port/riser configurations (line), port and jet discharge velocities and diffuser pipe velocities, port and diffuser diameter (lines).....	77
Fig. 52:	Flow characteristics for the final design and attached Duckbill valves (150 mm), for different discharges (Q), showing the riser flow deviation.....	78
Fig. 53:	Changes in total head for varying discharges	78
Fig. 54:	Instantaneous picture and long-term exposure picture of laboratory studies for pure single jets, showing entrainment motions diluting the effluent (source: G.H. Jirka).....	82
Fig. 55:	Schematized figures and visualizations from laboratory experiments showing different jet trajectories influenced by <i>a</i>) ambient density, <i>b</i>) ambient current u_a , and <i>c</i>) ambient stratification (Jirka, et al., 1996; pictures from G.H. Jirka; L. Fan).....	83
Fig. 56:	Schematization and visualization of laboratory experiment for merging of jets discharged unidirectional by multiport diffusers (reproduced from Jirka 2006)	83
Fig. 57:	Schematization of merging jets discharged by a multiport diffusers with an alternating port arrangement in stagnant conditions and in crossflow (reproduced from Jirka 2006)....	84
Fig. 58:	Definition diagram for a multiport diffuser (reproduced from Jirka et al., 1996).....	85
Fig. 59:	Definition diagram for the plane jet (reproduced from Jirka, 2006).....	86
Fig. 60:	3-dimensional horizontal buoyant jet trajectories for a single port discharge in stagnant ambient. Comparison between predictions and experimental data. <i>Left</i> : normalized with port diameter. <i>Right</i> : normalized with momentum length scale L_M (reproduced from Jirka, 2004)	90
Fig. 61:	Jet to plume transition length scale L_M for a single jet allows distinguishing between a jet like or plume like single jet behavior (reproduced from Jirka et al, 1996).....	90
Fig. 62:	Schematic illustration of the range of model applicability in Regulatory discharge zone analysis (source: www.cormix.info).....	101
Fig. 63:	Submerged buoyant slot jet discharging into stagnant water of finite depth (Jirka, 1982). <i>a</i>) Deep water discharge with stable discharge configuration, <i>b</i>) shallow water discharge with unstable recirculation zone (reproduced from Jirka et al., 1996).....	102
Fig. 64:	Diagram for selection of predictive models for submerged multiport diffusers with variable spacing and stability characteristics (reproduced from Jirka, 2006).....	103
Fig. 65:	Pictures of laboratory experiments showing boundary interactions with the surface, the bottom and the pycnocline (courtesy of G.H. Jirka, L. Fan, Keck Lab, CIT).....	103
Fig. 66:	Examples of boundary interactions for submerged jets in finite depth (reproduced from Jirka et al., 1996).....	104
Fig. 67:	Examples of <i>a</i>) wake attachment and <i>b</i>) Coanda attachment conditions for jets discharging near boundaries (reproduced from Jirka et al., 1996).....	104
Fig. 68:	Buoyant spreading processes after near-field region (upstream and lateral spreading), superimposed on the transport by ambient currents (reproduced from Jirka and Akar, 1991)	106
Fig. 69:	Buoyant surfacing plume. Boundary (surface) interaction and density difference cause slight upstream spreading of the plume against the ambient current (Source: I. Wood)	106
Fig. 70:	Definition diagram for surface spreading model for an unstratified ambient water body with uniform velocity (reproduced from Akar and Jirka, 1995).....	109
Fig. 71:	CORMIX flow classification tree for bottom attachment (reproduced from Jirka et al., 1996)	110
Fig. 72:	CORMIX flow classification tree for a buoyant multiport discharge into uniform ambient water (reproduced from Jirka et al., 1996).....	110
Fig. 73:	Flow classification tree within CORMIX, for a buoyant multiport discharge in stratified ambient waters (reproduced from Jirka et al., 1996).....	111
Fig. 74:	Passive ambient diffusion process with advection in the far-field (reproduced from Jirka et al., 1996)	112
Fig. 75:	Example showing far-field waste plume transport and dispersion. The transport is governed by the tidal current and mixing is governed by the wind shear stress (courtesy of Torben Larsen, Denmark).....	113
Fig. 76:	Unstructured finite element mesh for the Telemac model (www.telemacsystem.com)	117

Fig. 77:	Structured finite difference mesh for the Delft3D model, <i>top</i> : horizontal curvilinear, <i>down</i> : vertical σ -coordinate discretization (Delft Hydraulics, 2001).....	118
Fig. 78:	Nesting of a small-scale water quality model (Siu Lam Model) and a large-scale hydrodynamic model for Hong Kong waters using the Delft3D modeling system (Delft Hydraulics, 2005).....	124
Fig. 79:	Schematization of a zonal modeling approach for buoyant waste discharges and the related velocity and substance concentration fields. Hydrodynamic regions are the near-field (NF), the intermediate field (IF) and the far-field (FF).	129
Fig. 80:	Schematization of coupling approaches for zone models, either using boundary conditions (B.C.) or source definitions for the near-field representation in the far-field domain. 130	
Fig. 81:	Definition of source term locations for two different time steps, where ambient conditions changed considerably.	133
Fig. 82:	CORMIX schematization for vertical density profiles. CORMIX distinguishes between a uniform density distribution, a linear distribution (A), a two layer density distribution with constant densities (B), and a two layer system with constant surface density and linear bottom layer density separated with a jump (C) (reproduced from Jirka et al., 1996) 137	
Fig. 83:	Example for a CORMIX schematization applied on a measured vertical density profile (reproduced from Jirka et al., 1996).....	137
Fig. 84:	CORMIX schematization for ambient velocity and diffuser orientation. CORMIX only requires the input of a vertically and horizontally uniform, depth averaged ambient velocity, and its direction related to the diffuser orientation (reproduced from Jirka et al., 1996) 138	
Fig. 85:	CORMIX schematization of diffuser configurations (reproduced from Jirka et al., 1996) 140	
Fig. 86:	Example for a 2D CORMIX visualization of a surfacing waste plume discharged from a single port (www.mixzon.com) and contacting the shore after a short distance.	140
Fig. 87:	Example for a 3D CORMIX visualization of a surfacing waste plume discharged from a single port (www.mixzon.com) and contacting the shore after a short distance. The changing flow characteristics after surface interaction can clearly be seen. Blue dashed lines indicate where CORMIX switches to another module to compute the related flow class. 141	
Fig. 88:	Example of a CorJet prediction of a diffuser discharge into a stratified flowing environment with an oblique alignment angle ($\gamma = 45^\circ$) seen in the plan view, leading to an internally trapped plume, seen in the side view, resulting in a concentration profile along the plume centerline of an effluent concentration of 100%.	141
Fig. 89:	CORMIX schematization for the horizontal and vertical concentration distributions at one specific plume cross-section, depending on the dominant processes (reproduced from Jirka et al., 1996).....	143
Fig. 90:	Example of a CORMIX prediction of a diffuser discharge into a stratified flowing environment, leading to an internally trapped plume, seen in the side view. Superposed are far-field grid characteristics, where source characteristics may enter the far-field model. 144	
Fig. 91:	Overview of instruments improving water quality	146
Fig. 92:	Pollutant sources and water quality management in coastal waters: Compliance with emission limit values (ELV) for point-source discharges guarantees local protection at the outfall site, whereas compliance with environmental quality standards (EQS) outside a specified regulatory discharge zone (dashed line) guarantees water body usage and preservation (underlined items) partly based on ecological standards (ES).	147
Fig. 93:	Illustration of interpretations regarding the location where EQS-values apply	149
Fig. 94:	Definition of a numeric dimension for the regulatory discharge zone in relation to the average water depth H_{ave} and a factor N , and the regulatory preservation zone as a fixed distance from the preserved area (here the beaches).....	151
Fig. 95:	General map of studied area	155
Fig. 96:	Proposed outfall for Cartagena City, Colombia (Roberts, 2005).....	156

Fig. 97: Aerial views of Cartagena city. Left: prestigious beaches. Right: low-income neighborhoods (courtesy of M. Libhaber, World Bank).....	156
Fig. 98: Existing wastewater / drainage situation, where raw sewage flows in open canals or sewers to either the Bahía de Cartagena (40%) or the Ciénaga de Tesca (60%) causing considerable environmental and public health impacts (courtesy of M. Libhaber, World Bank) 157	
Fig. 99: ELCOM grid nodes in the numerical domain (Roberts and Villegas, 2006).....	158
Fig. 100: Schematic representation of the Southern Caribbean Coastal Undercurrent, including the Panama - Colombian gyre (reproduced from Andrade et al., 2003).....	158
Fig. 101: ELCOM prediction for the Panama-Colombian gyre. Rotating directions are not consistent with measurements or literature for half of the observed scenarios (Roberts and Villegas, 2006).....	159
Fig. 102: Large scale satellite picture of project region, showing the influence of the Magdalena river plume on the coast around Cartagena (courtesy of M. Libhaber, World Bank).....	159
Fig. 103: Comparison of modeled density differences over the vertical at the proposed outfall location for two different boundary conditions related to the inclusion or exclusion of the buoyant river discharge (Roberts and Villegas, 2006).....	160
Fig. 104: Comparison of modeled current velocities at two different depths at the proposed outfall location for two different boundary conditions related to the inclusion or exclusion of the buoyant river discharge (Roberts and Villegas, 2006).....	160
Fig. 105: Magnitudes of modeled velocities compared with measured ADCP data (Roberts and Villegas, 2006).....	161
Fig. 106: Polar scatter plots of modeled velocities for different depths and two different months (Roberts and Villegas, 2006).	161
Fig. 107: Wind angle definition diagram. A 45° wind is blowing from northeast to south-west.....	163
Fig. 108: Time-series feather plot of wind magnitudes and direction measured at the Cartagena airport for February 1998.....	163
Fig. 109: Histogram of wind velocity magnitudes (a) and direction (b), and a diagram for the cumulative distribution of the velocities (c) for the wind data measured at the Cartagena airport during February 1998.....	163
Fig. 110: Statistical analysis of wind directions and velocities for 1998-2000 (reproduced from Roberts, 2005).....	164
Fig. 111: Feather plots of measured current directions and velocities in different water depths (top is near surface and bottom near bed) for February 1998. Right column shows histograms of velocity magnitude in every layer.....	165
Fig. 112: CorField velocity profile analysis for all profiles of February 1998. Top: histogram of standard deviations of the velocities over the vertical, middle: histogram of standard deviations of the horizontal velocity angles to the depth-averaged mean, bottom: relative frequency of horizontal angles of the velocities compared to the dept-averaged mean, shown for every depth.....	166
Fig. 113: Feather plot of the depth averaged velocities at Punta Canoas, for February 1998.....	166
Fig. 114: Scatter plot, cumulative velocity, and histograms for depth averaged velocities and direction, measured from an ADCP moored at Punta Canoas for February 1998 (left) and November 1998 (right).....	167
Fig. 115: Tide gauge comparison for February 1998 at Punta Canoas and Boca Grande.....	168
Fig. 116: Temperature data at the planned outfall location showing temperature difference between 5.5 m and 17.4 m probes (Roberts and Villegas, 2006).....	169
Fig. 117: Typical density profile for maximum stratification. Results from measurements offshore Cartagena (Hazen & Sawyer, 1998)	169
Fig. 118: Assumed flow pattern for the effluent flow rate (Roberts and Carvalho, 2000).....	170
Fig. 119: Proposed design for the Cartagena outfall.....	170
Fig. 120: CORMIX flow classification tree for the basecase example calculation for the Cartagena outfall.....	172
Fig. 121: CORMIX plume visualization (side view) for the example basecase for the Cartagena outfall 172	

Fig. 122: CorTime output. Time-series of dilution, plume thickness and plume elevation at the end of the near-field / intermediate-field, as predicted by CORMIX for every single time-step out of 672 time-steps for February 1998 data.....	173
Fig. 123: CorTime histograms for parameters at the end of the near-field / intermediate field: dilution, downstream location, plume elevation, thickness and width and the cumulative travel time.	173
Fig. 124: Statistical analysis of the plume centerline dilution at 500 m downstream the diffuser. <i>Left</i> : Histogram of the relative frequency, <i>right</i> : cumulative distribution of frequencies...	174
Fig. 125: Model domains for ELCOM and Delft3D (Roberts and Villegas, 2006).....	175
Fig. 126: Delft3D model domain for the Cartagena coastal region. Grayscale indicates different depths. Boundary conditions (B.C.) are described at all open and closed boundaries.....	176
Fig. 127: Vertical cross section through model domain to visualize sigma-layers with high resolution at shallow regions. The diffuser is located at 2.8 km distance from the shore.	177
Fig. 128: Depth-averaged velocity field zoomed in to the outfall region at Punta Canoas.....	179
Fig. 129: Time-series of model and measured water levels at Punta Canoas (outfall location) for February 1998.....	180
Fig. 130: Time-series feather plot of depth averaged modeled (top) and measured (down) velocities at the planned outfall location for February 1998.....	180
Fig. 131: Time-series of modeled (dashed-line) and measured (continuous-line) depth averaged current components at planned outfall location for February 1998.....	181
Fig. 132: Scatter plot of measured (<i>left</i>) and modeled (<i>right</i>) depth averaged currents for February '98.	181
Fig. 133: Statistical comparison of measured (<i>left</i>) and modeled (<i>right</i>) depth averaged current magnitudes and directions for February 1998.....	181
Fig. 134: Comparison of modeled and measured 3-D visualizations of vertical velocity profiles at Punta Canoas for different time steps.....	182
Fig. 135: Histogram of the frequency of duration of periods where ambient velocities are below 0.1 m/s for November 1998.	184
Fig. 136: Modeled depth averaged concentration [MPN/m ³] of total coliforms at 21 st of February. Effluent concentration is $C_0 = 10^{11}$ MPN/m ³ . Bathing water standard is $C = 10^7$ MPN/m ³ = 10^3 MPN/100 ml (dashed line).....	185
Fig. 137: Positions, where concentration data is saved as time-series, shown in Fig. 138.....	186
Fig. 138: Time-series of modeled depth averaged concentration [MPN/m ³] of total coliforms at different locations (Fig. 137). The figure named "outfall" has an axis one magnitude larger than the others. Effluent concentration is $C_0 = 10^{11}$ MPN/m ³ . Bathing water standard is $C = 10^7$ MPN/m ³ = 10^3 MPN/100 ml (dashed line).....	186
Fig. 139: Exceedance frequency of total coliforms exceeding 1000 MPN/100 ml for the month February 1998. Effluent concentration is $C_0 = 10^{11}$ MPN/m ³	187
Fig. 140: Exceedance frequency of total coliforms exceeding 1000 MPN/100 ml for the month November 1998.....	188
Fig. 141: Frequency that total coliforms exceed 1000 MPN / 100 ml, <i>left</i> : for Feb. 1998 (Delft3D) and the whole year 1998 (Roberts, 2005), and <i>right</i> : for Nov. 1998. Contours in foreground are modeled with NRFIELD-FRFIELD (exceedance frequencies for 1%, 10% and 20%, reproduced from Roberts, 2005) compared with the final results of the 3-D coupled modeling (<i>background</i> , where exceedance frequencies are shown for 1%, 10%, 20% and 50%).	188
Fig. 142: Diagram for the coefficients to compute the loss coefficient for a flow division (reproduced from Idelchik, 1986).....	199
Fig. 143: Diagram for the coefficients to compute the loss coefficient for a flow division (reproduced from Idelchik, 1986).....	200
Fig. 144: Diagram for the coefficients to compute the loss coefficient for a flow division (reproduced from Idelchik, 1986).....	201
Fig. 145: Additional loss coefficients for orifices (reproduced from Idelchik, 1986).....	202
Fig. 146: Additional loss coefficients for orifices (reproduced from Idelchik, 1986).....	203
Fig. 147: Additional loss coefficients for orifices (reproduced from Idelchik, 1986).....	204

List of Tables

Table 1: Typical composition of untreated municipal wastewater (Lee, 2003; Maier et al., 2000)....	12
Table 2: Typical wastewater treatment techniques and residual disposal and effluent discharge	13
Table 3: Comparison of removal efficiencies for conventional primary treatment and chemically enhanced primary treatment (CEPT), (reproduced from National Research Council, 1992)	14
Table 4: Typical effluent changes depending on treatment (Lee, 2003; Maier et al., 2000)	15
Table 5: Overview of dominant processes for coastal submerged multiport discharges	20
Table 6: Typical effluent concentration reductions depending on applied treatment or discharge technology (Lee, 2003; Maier et al., 2000). nn: difficult to detect	21
Table 7: Required effluent dilution for different levels of treatment (modified from Wilkinson and Wareham, 1996).....	27
Table 8: Comparison of different turbulence modeling approaches (Rodi, 2004).....	33
Table 9: Outfall pipe materials and their related equivalent sand roughness values k_s (Idelchik, 1986)	43
Table 10: Step 1: Baseline calculation - for far future design conditions	60
Table 11: Step 2: Diffuser characteristics - diffuser performance calculations	61
Table 12: Step 3: Off-design calculation - near future design conditions.....	62
Table 13: Step 4: Sensitivity analysis - prediction accuracy.....	62
Table 14: Sensitivity of involved parameters on head loss, total head, and homogeneity of the discharge profile.....	63
Table 15: Comparison of constructional alternatives for Ipanema diffuser	75
Table 16: Scales and resolutions of different modeling techniques.....	81
Table 17: Comparison of typical flux quantities (modified from Jirka (1982), listing length and time scales for two typical discharges for a city with a population of 1 million people and a diffuser with length $L_D = 400$ m. The average ambient velocity is assumed to 0.1 m/s and 0.5 m/s (values in brackets), with a stratification defined by $\varepsilon = -(g/\rho_a)(d\rho_a/dz) = 0.0064$ 1/s ²	92
Table 18: Comparison of typical flow quantities at different hydrodynamic regions. Discharge characteristics are assumed for a population of 1 million people and a diffuser with length $L_D = 400$ m discharging at a depth of $H = 20$ m (modified from Jirka (1982). Considered discharge cases only differ in the total flow and density (e.g. wastewater and thermal). Ambient conditions differ only in velocity, where only the horizontal components of small and medium (in brackets) flows are considered (note that discharge velocities and momentum may act in orientations different to the horizontal).....	126
Table 19: Overview on modeling techniques regarding waste discharge modeling. Middle column adjusted characteristics denote the capability to model intermediate-field processes.	128
Table 20: Coupling step 1: Classification of measured ambient conditions - CorField.....	136
Table 21: Coupling step 2: Near-field baseline modeling - CorTime	139
Table 22: Coupling step 3: Ambient hydrodynamics baseline modeling with Delft3D flow	142
Table 23: Coupling step 4: Source representation in far-field model - CorLink	142
Table 24: Coupling step 5: Far field modeling with Delft3D Part/WAQ (mixing, transport, decay)	144
Table 25: Examples for emission limit values (ELV) and environmental quality standards (EQS) for two selected pollutants	147
Table 26: CORMIX sensitivity analysis for slow current velocities (u_a) and stratified or unstratified conditions. Results are for a plume location at 1000 m downstream. Values in brackets () are plume width results at 100 m downstream.	184

List of Symbols

Parameter	Dimension	Definition
A	m^2	pipe cross sectional area
B	m	equivalent slot width $B = A_p/\ell$
C_c	-	jet contraction coefficient
C	$mg/\ell, kg/m^3$	substance concentration
D	m	internal pipe diameter
E	m	energy head
F	-	densimetric Froude number
F_e	N	external Forces
g	m/s^2	gravitational acceleration
g'	m/s^2	reduced gravity, $g' = \Delta\rho/\rho g$
H	m	head above datum / water depth
i	-	numbering of port/riser configurations
j	-	numbering of local losses in ports, risers or the diffuser
j_o	m^3/s^2	buoyancy flux per diffuser length, $j_o = g' q_o$
J_o	m^4/s^3	buoyancy flux
k_s	m	equivalent sand roughness
ℓ	m	riser spacing
L	m	length of the considered pipe section
L_M	m	momentum length scale
ℓ_M	m	slot jet / plume transition length scale $\ell_M = m_o/j_o^{2/3}$
ℓ_m	m	crossflow length scale $\ell_m = m_o/u_a^2$
ℓ_m'	m	stratification length scale $\ell_m' = m_o^{1/3}/\epsilon^{1/3}$
ℓ_b'	m	stratification / plume length scale $\ell_b' = j_o^{1/3}/\epsilon^{1/2}$
ℓ_a	m	stratification / crossflow length scale $\ell_a = u_a/\epsilon^{1/2}$
m	m^3/s^2	momentum flux per diffuser length
M	m^4/s^2	momentum flux
n	-	total number of local losses j in between one pipe section
N	-	total number of port/riser locations i of diffuser
N_d	-	total number of diffuser sections (includes feeder)
N_g	-	total number of port/riser groups
N_{gp}	-	number of risers per group
N_p	-	number of ports per riser
p	$Pa = N/m^2$	pressure
Q	m^3/s	total flow through outfall system
q_i	m^3/s	individual discharge through a riser or port at position i
q	m^2/s	mass flux per diffuser length
R	m	radius of pipe bend
Re	-	Reynolds number $Re = VD/\nu$
S	-	dilution
t	s	time
t_M	s	jet / plume time scale $t_M = m_o/j_o$
t_m	s	jet / crossflow time scale $t_m = m_o/u_a^3 [s]$
T_{90}	h	the time taken for 90% of the bacteria to die-off
u, v, w	m/s	velocity
U, V, W	m/s	mean velocity
x, y, z	m	Cartesian coordinates

Greek symbols

α	-	Coriolis coefficient (kinetic energy correction coefficient)
α_i	-	1 / (number of ports at a riser at position i)
β	$^\circ$	angle of gradual expansion or contraction
ζ	-	dimensionless loss coefficient for local losses
λ	-	dimensionless friction coefficient
μ	Ns/m^2	dynamic viscosity
ν	m^2/s	kinematic viscosity
τ_b	N/m^2	bed-shear stress
τ_w	N/m^2	wind-shear stress

ε		stratification parameter, $\varepsilon = -(g/\rho_a)(d\rho_a/dz)$
ρ	kg/m ³	density $\Omega =$ earth rotation vector
Ω	1/s	earth rotation vector

Indices

<i>a</i>	ambient
<i>b</i>	background
<i>c</i>	centerline
<i>dec</i>	decay
<i>D</i>	diffuser
<i>e</i>	effluent
<i>F</i>	feeder
<i>ff</i>	far-field
<i>j</i>	jet
<i>lim</i>	limit
<i>min</i>	minimal
<i>nf</i>	near-field
<i>o</i>	initial quantity
<i>p</i>	port
<i>r</i>	riser
<i>tot</i>	total

1 Introduction

High child mortality and significant economic damages are frequent consequences of water quality problems (WHO, 2000). Waterborne diseases are directly related to deficiencies in wastewater systems (UNEP, 2002). Wastewater treatment is commonly seen as the only way to cope with water quality problems, although waste source and effluent discharge control play a considerable role especially for coastal environments. Optimized discharge systems as part of the wastewater system may substantially reduce investment costs still reaching the same environmental objectives as higher treatment levels without discharge control. Thus, there are a rapidly increasing number of long ocean outfall installations worldwide. These efficient mixing devices avoid pollutant accumulation and collapse of ecosystems by dispersing the treated effluents via long submarine pipelines with multiport diffuser, which are several openings at the end section of the pipeline (Fig. 1). Environmental monitoring campaigns show significant improvement on public health and economic growth for the entire beneficent communities, often directly related to good beach or fishing water quality. A major breakthrough for that development to continue is new environmental regulations emphasizing on the ecosystem rather than on water quality indicators alone. Plans for wastewater systems will have to concentrate on actions targeted at improving (at least not deteriorating) the state of ecosystem and not at emissions alone. Especially for poorer communities and developing countries even strongly biased solutions with pre-treated effluents and high-level discharge installations may considerably improve public health. Intensive monitoring studies of such outfalls show no evidence, that these may have deteriorating impacts on the ecosystem, provided design and siting is appropriate.

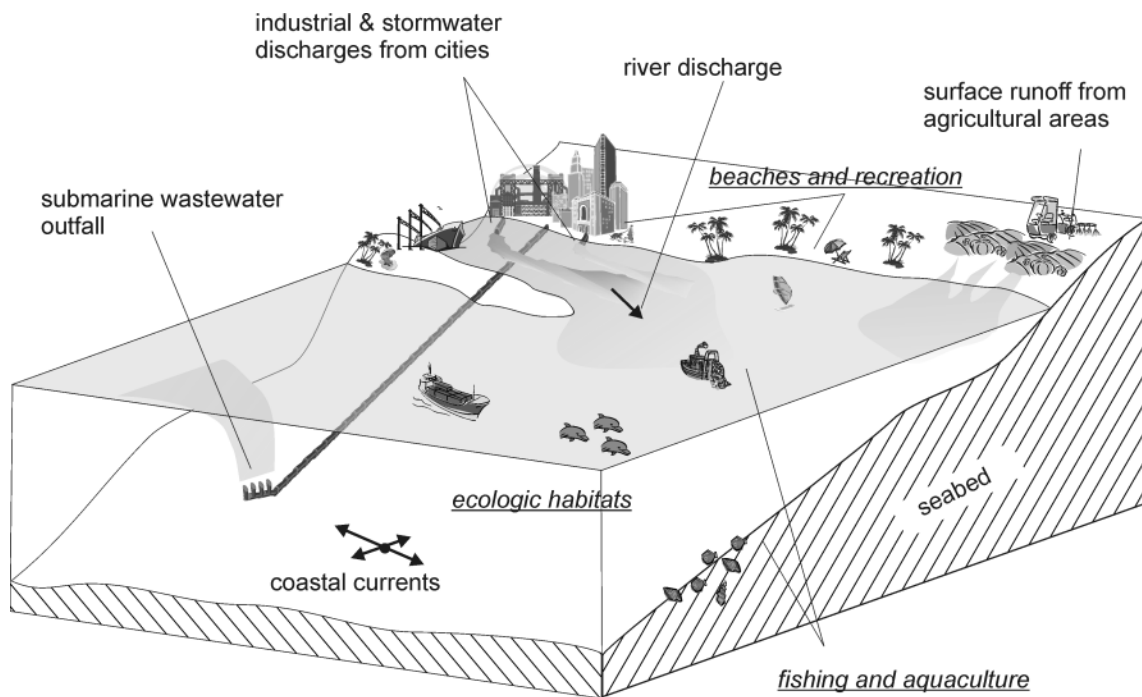


Fig. 1: Pollutant sources and environmental objectives (underlined) in coastal waters. Water quality management needs to balance pollutant reduction and ecosystem response.

1.1 Background and motivation - coastal water quality problems

Coastal waters, including estuaries, wetlands, mangrove forests, and bays represent enormous natural and economic importance for most of the countries in the world. These productive and diverse areas host a multitude of species important for nature and man. The coastal population is attracted by, and depends strongly on these values for their livelihood, food, health, recreation, and enjoyment. The areas within 100 km from the shoreline coastal areas occupy 18% of the earth's surface and host more than 60% of the human population (UNEP, 2004). Coastal cities grow faster than cities in the interior. This trend is expected to continue especially for developing countries creating additional environmental pressures. Beside the direct physical coastline alterations, coastal water quality is the most affected part (UNEP, 2002).

A major primary water quality issue is infectious diseases caused by pathogenic bacteria, viruses, protozoa or parasites, which are the most common and widespread health risks associated with water. Faecal contamination of water is responsible for many disease outbreaks (WHO, 1998), where marine contamination-related diseases are estimated to have an economic impact of 13 billion dollars worldwide and up to 2 million people, most of them children in developing countries die annually due to marine contamination-related diarrhoeal diseases (Shuval, 2000). Thus, badly managed wastewater systems are directly responsible for adverse health problems.

The second major water quality issue is environmental degradation. Excessive uses of coastal waters cause destruction of ecosystems and thus the living base of coastal communities. Major threats are again wastewater discharges exceeding the environmental capacities causing i) accumulation of harmful substances, where lethal or chronic concentrations affect fishery and shellfish or accumulate in benthic or aquatic resources, and ii) eutrophication due to nutrient inputs, where overloading leads to excessive vegetation and algal blooms and so far in low dissolved oxygen and high turbidity. Consequences are economic problems due to reduced fishing, recreational, and commercial activities.

Water quality problems, especially in urban coastal regions, often are directly related to badly or non-controlled *point-source* discharges originating from municipal and industrial wastewater systems and storm water overflows. This is especially true for all Mega cities (e.g. Rio de Janeiro, Istanbul, Mumbai, or Hong Kong), densely populated or touristic high-frequented regions (e.g. Spanish Mediterranean coast), or regions with poor infrastructure (e.g. developing countries). There, point source contributions to water quality problems may exceed 80% (IETC, 2000) causing considerable public health impacts and environmental degradation (UNEP, 2004). In these regions, pollution control is most efficient if improving engineering point-source control techniques (National Research Council, 1993), which will be described as follows. *Diffuse sources*, originating mainly from surface runoff, instead dominate water quality problems especially in rural and agricultural regions or environmentally sensitive regions with weak flushing characteristics of the receiving waters (e.g. mangrove forests at Paranaguá, Brazil or Wadden Sea at the northern German coast). Impacts are related mainly to ecosystem damages and only marginally to public health impacts (e.g. algal blooms and drinking water resource pollution). Controlling diffuse sources is still challenging and long-winded to control diffuse sources. Techniques strongly depend on long-term administrative control mechanisms rather than on engineering solutions. Therefore, the present approach will focus on the improvement of the point-source control techniques, but nonetheless considers diffuse source loads while analyzing the environmental response of receiving waters.

1.2 Problem - wastewater discharges

Water quality problems from point-source discharges arise once the capacity of the receiving waters to assimilate the introduced substances in their natural cycles is exceeded. Pollution is caused by exceeding critical assimilation time-scales (too many substances in a too short time), and assimilation length scales (too much substance mass at one location). Engineering action is then required to reduce substance concentrations by combinations of reducing the substance loads (wastewater treatment technology) and increasing the substance dispersion (effluent discharge technology). The engineering system therefore consists of a wastewater treatment plant and a discharge structure - the outfall. However, the misconception that treatment results in a “pure” and “clean” effluent lead to a strong under utilization of discharge technologies. On the other side, highly efficient discharges without treatment do not necessarily eliminate pollution because of their unchanged substance loads. Consequences are non-efficient or too expensive wastewater systems and ongoing water quality problems (UNEP, 2002).

Both systems, the treatment plant and the discharge structure are characterized by complex hydrodynamic and biodegradation processes. Treatment plants need to control these processes to operate efficiently, whereas discharge structures need to be designed to fit best to mostly uncontrollable natural dispersion and biodegradation processes within the receiving waters. Although discharge technologies are used and studied since decades, there is still a high uncertainty and standard solutions are not available for designing such systems. A large range of combinations regarding treatment level and outfall specifications is possible. There is high potential in improving such systems by optimizations of the discharge structure or siting in combination with appropriate treatment. The existing problems are illustrated in Fig. 2, which raises the partly unsolved (public) questions: “What is the bacterial concentration at Santos Beaches for that situation, and for the rest of the year?”, “Are the beaches safe for swimming?”, “Are beach closures related to this outfall plume or to other waste sources?”, “Are the fish safe to eat?”, “Is the environment being degraded?”, “How could the outfall design or siting be improved?”, “Is the level of treatment appropriate?”. A discharge assessment answers these questions by field studies (monitoring ocean currents, ocean and beach water quality, sediment and organisms quality) and modeling campaigns (mixing models and waste plume modeling) (CETESB, 2005). Although Fig. 2 suggests strong negative impacts on the city beaches, first results from these studies undertaken from the local environmental regulator (CETESB) do not show evidence that the outfall causes beach closures or significant environmental degradation. Near-shore creeks, harbor access dredging and industrial spills seem to be dominant pollutant sources for the actual water quality problems in this case.

Discharge assessment problems are summarized in four problem categories:

A) Strategic problem: Once recycling or reutilization is maximized there is no single concept to balance treatment technologies and discharge strategies. Historically only one-way approaches have been followed, either emission-based, reducing effluent concentrations as much as possible or feasible, or immission based, discharging as much as environmentally sound. Obviously, a two-way approach combines advantages of both and follows the principles of closing substance cycles. Public concerns on discharge technologies are often related to sustainability, often mixing up the differences of dumping harmful substances and disposing natural substances. The latter is related to the reintegration of substances into the biogeochemical cycle instead of removing them. It is therefore needed to extend and communicate engineering strategies on a more interdisciplinary level regarding the system-wide social and integral environmental impacts.

B) Regulatory control problem: Most of the recent water quality regulations (e.g. EC-Water framework directive, 2000; CONAMA, 2000) account for environmental values and already follow the two-way approach with two strategies in combination: limitations on pollutant releases at the source due to promulgation of emission limit values (“discharge regulations”) as well as the establishment of environmental quality standards (“environmental regulations”). However, actual implementation is vague and incomplete. In particular, the fact that most of the regulations do not state where and when precisely in the water body the environmental quality objective-values should be applied will lead to arbitrary and contradictory interpretations on part of water authorities (Jirka et. al, 2004; Ragas et al. 1997). A clear definition of a regulatory discharge and preservation zone approach is needed.



Fig. 2: Aerial photograph of Santos Bay, Brazil showing Santos city (approx. 500,000 inhabitants) and Santos harbor (along the river). Visual contours of the waste plume (arrow) from the Santos outfall, 4 km offshore, show a plume impact with the city's most frequented beaches (courtesy of municipality of Praia Grande, Brazil).

C) Outfall design problem: Outfall design requires on one hand an intensive analysis of the receiving water bodies, and on the other hand detailed predictions of possible impacts for the environment due to different discharge alternatives. Although prediction models exist for coastal environments and for multipoint diffusers there is neither a “complete model” including all important spatial and temporal scales of the dominant processes nor a standard procedure for the coupling of single models (IMPRESS, 2002). Therefore, a methodology for the linkage of predictive models especially for submerged wastewater discharges is needed.

D) Multipoint diffuser design problem: The constructional design and the operation of multipoint diffusers have to account for the dilution requirements, and particularly that the ports flow full and the discharge is distributed evenly along the diffuser. Existing design algorithms and diffuser programs do not comply with all of these demands. Furthermore, the construction itself is seldom checked and tested. There is a demand from engineers and planners for a more sophisticated internal diffuser hydraulics program.

1.3 Objectives and outline

Objectives are to provide supporting tools for the solution of previously listed major water quality problems with focus on public health impacts in less developed or densely populated regions. The approach is based on an increased, innovative, and efficient utilization and development of hydraulic modeling tools for design and control techniques for submerged multiport diffuser outfalls. Therefore new model developments are undertaken and existing models are coupled and integrated into a design scheme considering regulatory, constructional, and operational demands.

The following developments especially address the formulated needs from the Specialist Groups: “Wastewater Treatment Systems Utilizing Submarine Outfalls” at IWA (International Water Association) and “Sea outfalls” at TechWaRe (Technology for Water Resources) summarized in Burrows et al. (1998):

- Comprehensive *summary of technologies and governing processes* for coastal wastewater discharges to point up the fundamental basis for strategic decisions (chapter 2 and 3).
- *Development of a design and optimization program for internal diffuser hydraulics (CorHyd)* resulting in an improved engineering design of multiport diffuser pipe geometries and configurations for a balanced flow rate distribution along the diffuser, minimized total head and sufficient pipe velocities to prevent plugging due to sediments in the pipe under most operational conditions (chapter 4).
- *Development of a coupling routine for near-field and far-field models (CorLink)* resulting in improved modeling of short-term and long-term predictions for waste field characteristics. This allows optimally siting and designing planned discharges or modify existing ones satisfying water quality standards under given technological constraints (chapter 5)
- Critical analysis and improved regulatory control, permit and licensing using the regulatory discharge and preservation zone approach resulting in a *definition of numerical dimensions and statistical compliance assessment (CorZone)* for coastal discharges (chapter 6).

The contributions and developments are based on point-source discharges of municipal wastewater into coastal waters, focusing on submerged multiport diffuser installations. Diffuse source control, thermal discharges, surface discharge installations and discharges into rivers will not be covered in this thesis although several analogies allow for similar technologies and solutions.

Beneficiaries of these developments are directly entities that discharge wastewater into coastal water bodies and indirectly their customers and water body users.

2 Characteristics of coastal wastewater discharges

Coastal discharges of treated wastewater differ from inland discharges by their proximity to very large receiving waters, the oceans or seas. These have generally large assimilative capacities regarding the natural substances contained in municipal wastewater. Inland waters generally do have only limited assimilative capacities. Thus coastal pollution control demands for a good knowledge on the characteristics of the receiving waters as well as more comprehensive discharge assessments due to increased hydrodynamic complexity and an increased number of engineering alternatives.

Modern wastewater management offers a wide variety of solutions to avoid impacts of wastewater discharges on the receiving waters, human health, and the ecosystem. A keyword is sustainability, focusing on not only environmentally sound solutions, but also long-term, integrated, system wide approaches. The three following major approaches and their technological mechanisms should therefore be applied in strict hierarchical order:

- I. Development and implementation of *source control and recycling technologies* to reduce the amount of waste substances, to close the material cycles locally, and to ban persistent pollutants (e.g. highly oxidizing cleaning agents or detergents), which are neither decomposed in conventional treatment plants, nor in receiving waters. For example, washing agents have been the major source for phosphate in German municipal waste effluents. Long-term political and social efforts nowadays lead to the elimination of phosphate from washing agents, thus reducing the amount of phosphate in municipal wastewater significantly. Other examples are: using less detergents, substituting harmful substances with biodegradable ones, separating urine and feces, water re-use, etc.
- II. Installation of *treatment technologies* to remove harmful substances (i.e. non-degradables), to recycle resources (e.g. phosphorus as fertilizer for agriculture, wastewater re-use for irrigation, energy recovery from waste sludge), and to reduce the concentration or harmfulness of substances (e.g. nutrient reduction, or bacteria inactivation by disinfection). Treatment technologies reduce substance loads of the wastewater.
- III. Installation of *discharge technologies* to re-integrate substances into the natural cycles and to enhance natural processes in the receiving water body to minimize the harmfulness of substances by adequate siting and fast dilution to tolerable concentrations.

If feasible every step should be fully utilized before heading to the next step to obtain a sustainable wastewater management solution. The following considerations will focus on the technical solutions for and the trade-off between step II and III, but keeping in mind that step I is preferential, if feasible.

2.1 Coastal waters characteristics

Enormous quantities of organics and sediments are naturally carried to the oceans by rivers, as a result of natural processes within the water cycle. Man's contribution of wastes transported in the water cycle causes problems when concentrating waste products in rather restricted areas instead of dispersing them over larger areas where natural purifying processes can better act. Environmental engineering needs to analyze to what extent substances should be removed prior to the discharge, and what may be reasonably left for the receiving waters to absorb and disperse. Technologies reducing pressures or enhancing natural processes thus

should achieve the return without damage or undue changes of the ecosystem. It is therefore essential for planners and designers to understand not only coastal physical processes, but also the natural purification processes, which are described briefly as follows. Problems are their high temporal and spatial variability in combination with slow and weak mixing and flushing characteristics, thus vulnerable to local impacts related to substance accumulation.

2.1.1 Coastal circulation

The dispersive characteristics, especially the mixing and transport characteristics are directly related to the coastal currents, which themselves are strongly influenced by the coastline as lateral borders and the bed-forms as vertical borders (Fischer et al., 1979). Circulation patterns in bathymetrical complex regions (bays and inlets or channels) cause strongly irregular, non-uniform current features with scales even larger than the irregularity. Extreme but frequent situations are illustrated in Fig. 3, where discharges are dispersed in a shallow (10 m) enclosed coastal bay or a relatively deep (36 m) coastal channel. Lateral extensions are of the order of kilometers. The depth/width ratio clearly shows that coastal waters can generally be considered as shallow flows.



Fig. 3: Aerial view of the receiving waters of outfalls discharging in the Santos Bay, Brazil (*left*, courtesy of municipality of Praia Grande) and the São Sebastião channel, Brazil (*right*, Lamparelli, 2003)

Except for buoyancy driven zones (close to river outflows and estuaries), current systems in coastal regions used for outfall installations are dominated by the combined effects of surface wind forcing and tidal action resulting in non-uniform, unsteady flows. Winds cause surface waves and shear stress on the water surface leading to the establishment of a surface current. Estimates indicate that the surface current is typically about 3-4% of the wind speed at a reference height of 10 m above the water surface. Wind field characteristics are generally unsteady and non-uniform and are mainly influenced by the coastal topography. The wind induced surface current speed typically reduces with depth by a factor of 4-5 within the top 3 m of the water column (Davies, 2003). Tidally forced currents arise from the (astronomical) gravitational forcing of the water surface. The tide-generating force may be resolved into a series of harmonic components with as many as 60 of these components being required to make tidal elevation predictions with acceptable accuracy. The resulting tidal currents show more variability than tidal elevations because of local flow effects (bathymetry). Especially sensitive and touristically attractive regions generally have only weak currents (mainly wind dominated, e.g. Mediterranean) and low flushing characteristics (weak tides, e.g. Caribbean). Consequences of different circulation patterns on waste plumes are shown in Fig. 4.



Fig. 4: Aerial view of an outfall, discharging in the São Sebastião channel at two different time-steps, showing completely different dispersion patterns (Lamparelli, 2003).

Current data are best obtained by the use of both, Eulerian and Lagrangian measurements. For Eulerian field measurements a vertical profile with several moorings and at different locations near the diffuser location is preferred (Roberts, 2000). Sampling should cover at least one-year data (hourly or less values) to get seasonal changes. Fixed installed acoustic Doppler current profiler (ADCP) are good instruments to resolve entire vertical profiles. Lagrangian measurements in addition are necessary to analyze spatial variations of current directions. There are consequent difficulties with non-synchronicity and doubts that the measured values at one point can be correlated with those at another because the flow may have changed during the survey process (Davies, 2003). This is even more complex if correlations with measured temperature (thermistor string data) and salinity profiles (conductivity probes) are needed. Although numerous data and studies exist for the deep-sea oceanography (ocean circulation models), there are only limited approaches available for near coast oceanographical analysis. This because ocean studies have mainly been made for climate or weather forecast, rather than for waste dispersion studies (TetraTech, 2000). Engineers and oceanographers have to meet this challenge by approaching each other more than before.

2.1.2 Density stratifications

The density of coastal waters, if not uniform over depth is characterized by stratifications caused by salinity and/or temperature differences over the depth. In temperate climates, the existence of thermally derived stratification and a thermocline separating cold and hot water is seasonal (summer surface heating), while in low latitude waters the thermal stratification may be permanent. Salinity variations arise usually from significant freshwater flows into coastal waters, resulting from drainage of land joining the coastal region, primarily river outflows with seasonal variations (Fig. 5). Large rivers form distinct river plumes flowing along the coast and attaching to it (with the coast at left in the southern hemisphere, Fig. 5, Davies, 2003). These plumes are characterized by strong horizontal and vertical density gradients and convergence. Stratifications and the position and thickness of the transition halocline depend on the degree of the shear-induced interfacial mixing and diffusion processes between these layers. Velocities within river plume density currents may be comparable with those of tidal residual currents.

Generally, vertical density gradients in stratified waters inhibit vertical motion of fluid discharged into it. Under these circumstances, substances within the waste plume do not reach the surface of the water column but a subsurface equilibrium level where the mean density of the diluted effluent matches that of the surrounding fluid.



Fig. 5: Satellite image from Rio Magdalena (Colombia), showing the river plume (courtesy of Menahem Libhaber, World Bank).

2.1.3 Natural purification

In nature, waste materials are produced by living organisms (plants, animals, and people) and transformed by natural processes. These wastes are characterized by their *organic* nature consisting of carbon, nitrogen, phosphorus and other elements constituting organisms, as also described for wastewater in chapter 2.2. These constituents are continuously cycled in nature dominated by four cycles, the carbon, nitrogen, phosphorus and the water cycle (in detailed described in common textbooks). Biodegradation, an element of these biogeochemical cycles, is the transformation of organic substances into energy or when complete into minerals due to oxidation processes forming carbon dioxide and water. Most of the agricultural or industrial substances based on carbon (organic solvents, or petroleum based products) are also considered biodegradable because of their similarity to naturally occurring organic carbon. Basically, every man-made waste treatment technology is based on natural purification processes. A limitation of natural purification processes is that they can only handle naturally occurring wastes and *no toxic chemicals* that in addition may disturb the natural processes. Another limitation are physical-chemical parameters (temperature, salinity), as well as biological ones (number of microbes in the receiving waters) making natural purification a relatively slow process with limited capacities.

Large coastal cities affect the waste cycling by generation and discharge of large amounts of waste and in addition by removing or reducing large areas of natural ecosystem. Once waste discharges exceed the natural purification capacity, also called carrying capacities (Maier et al., 2000), a maximum of microbial activity is reached and environmental degradation occurs. Commonly degradation takes place by accumulation of organic materials, nitrogen, phosphorus, or other pollutants that cannot be absorbed any more by the ecosystem.

An additional problem of anthropogenic discharges are *pathogens*. Pathogens generally are inactivated (die-off), once the conditions outside their hosts are unfavorable or competition with naturally occurring microorganisms occurs. For example, for faecal bacteria, nutrient levels in coastal waters are generally too low to support their growth, except in highly polluted freshwaters in warm climates. Pathogen inactivation rates are highly sensitive to environmental parameters and their variations. Laboratory and field studies have shown, that for the marine environment mainly temperature and ultraviolet radiation from solar radiation are of major importance (Bitton, 1994 and Fig. 6). Due to small and transient variations in salin-

ity inactivation by salinity is unlikely to decrease mortality rates significantly (WRc, 1990). Reduced radiation intensities instead, for example due to light attenuation in few meters below the water surface, may reduce inactivation rates up to 90% of the value at the surface (WRc, 1990). In turbid waters, inactivation is even smaller. Thus, significant differences exist between daylight and night conditions. Variations in temperature do not have these drastic changes. Increases in temperature accelerate the rate of inactivation under dark conditions, but do not have significant effect in light over normal temperatures (WRc, 1990). Virus inactivation instead mainly depends on temperature. Adsorption to sediments is the most significant factor affecting virus survival. Viruses never grow. Nevertheless, inactivation rates are of the same order as for bacteria.

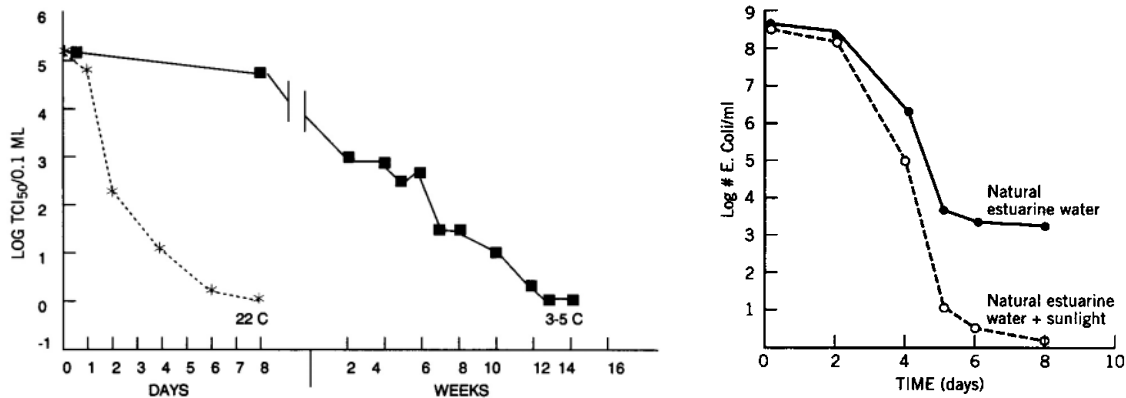


Fig. 6: Inactivation in seawater of echovirus 6 as a function of temperature (*left*) and *E. coli* as a function of solar radiation (*right*) (reproduced from Bitton, 1994)

All above mentioned variability and uncertainties in describing pathogen inactivation in unsteady, non-uniform and stratified flows indicate the difficulties in describing assimilative capacities and transport characteristics and their representative scales in general and for wastewater discharges into coastal waters in particular.

2.2 Wastewater sources and characteristics

Three kind of wastewater sources are generally considered, which characteristics may differ considerably: municipal wastewater originating from households, public facilities, and businesses; industrial wastewater from production facilities; and stormwater from roof, streets, places, and surface run-off. The raw wastewater is often transported away from the communities in open canals or pipe systems to the treatment facility, which is generally located near the discharge location of the receiving waters. Such waste conveyance systems are divided into separated and combined sewer systems, where the latter combines stormwater and municipal sewage. The flow of municipal wastewater is generally variable with peak flows coinciding with high household activities in the morning and evening, while in the night minimal flow occurs. An average measure is the water consumption, for example of around 200 l per person and per day (Brazilian raw average), resulting in a wastewater flow of 2.3 m³/s for a city of one million inhabitants. Seasonal changes in touristic coastal areas may influence design flows considerably. Stormwater is underlying high natural variability. Municipal wastewater is the dominant source of bacteria pollution and public health impacts. If sanitation coverage is poor, also stormwater run-off may contain significant pollutant loads. Industrial wastewater in many instances should be treated directly on the production site, resulting in effluent characteristics, which then should not differ significantly from municipal wastes consisting primarily of biodegradable organic substances. These industrial effluents are

commonly mixed with municipal wastewater or discharged separately. Therefore, the following discussion regarding especially public health impacts will focus on municipal wastewater characteristics only. Nonetheless slight modifications on effluent characteristics allow for consideration of stormwater and industrial wastewater too. Special industrial effluents, having physical characteristics which considerably differ from municipal wastewater (i.e. regarding temperature and salinity, e.g. originating from mining sites, desalination plants or power plants), will not be considered here because these follow other process scales.

Municipal wastewater consists of freshwater (99.9%) and substances added during the usage. Its density is equal to that of drinking water. Wastewater components are generally divided into biodegradable and other organic materials (e.g. detergents, pesticides, fat, and oil), microorganisms (i.e. pathogenic bacteria and virus), nutrients, metals, and other inorganic materials (e.g. acids, bases) (Henze et al., 2002). Pollutants may occur dissolved or suspended in water. The division of both is essential, as many of the treatment or dispersion processes are only effective for one of these (Henze et al., 2002). Copper for example is to 50% attached to particles and not dissolved, whereas Ammonia is 100% dissolved. Typical concentrations of raw wastewater components are listed in Table 1.

Constituent	Concentration [mg/ℓ]		
	Strong	Medium	Weak
Solids			
solids, total	1200	720	350
dissolved, total	850	500	250
suspended, total	350	220	100
settleable solids [mℓ/ℓ]	20	10	5
Organic material (nutrients)			
biochemical oxygen demand, BOD ₅	400	220	110
nitrogen (total as N)	85	40	20
phosphorus (total as P)	15	8	4
Bacteria			
total coliform [count/100ml]	10 ¹²	10 ⁸	10 ⁷
faecal coliforms [count/100ml]	10 ⁸	10 ⁷	10 ⁶
E. coli [count/100ml]	10 ⁸	10 ⁷	10 ⁶

Table 1: Typical composition of untreated municipal wastewater (Lee, 2003; Maier et al., 2000)

Difficulties exist describing concentrations for organics or microorganisms, because it is impossible to consider each of the existing thousands organic compounds or microorganisms. Thus, organic matter commonly is described by BOD₅, the biochemical oxygen demand in 5 days. This and other methods like the chemical oxygen demand (COD), total oxygen demand (TOD) or the total organic carbon (TOC) are described in detail in Henze et al., 2002.

Microorganisms instead are quantified by indicator microorganisms that are easier to sample. There is no interest in knowing all microorganisms, but especially in those related to human health or treatment plant efficiency. Typical indicators are coliform bacteria indicating the probability of the existence of pathogens. Coliform bacteria also occur in faeces of warm-blooded animals, thus their concentrations are roughly proportional to the degree of faecal pollution (WHO, 2000). They are none pathogenic organisms, which are easy to isolate and to quantify. Many countries adopted coliform bacteria as indicator of faecal contamination. Decades of experience with these indicators show, that waterborne disease outbreaks are directly related to bacteria in drinking water (Maier et al., 2000). Nowadays not only total coliforms, but also especially faecal coliforms are measured to distinguish between faecal and other origin. However, this does still not allow distinguishing between human or animal origin. For example, sheep produce almost 10 times more total coliforms but the same amount

of *E. coli* than humans do. *Escherichia coli* (*E. coli*) are a widely used faecal coliform species, which occurs in high numbers in faeces. In addition, its inactivation rates are similar to enteric bacteria. However, it has been observed, especially in the tropics, that inactivation rates of coliform bacteria are highly dependent on the environmental conditions (Paul, 2001). Therefore new standards not only measure coliform bacteria, but also include Enterococci (a faecal bacteria), but they also do not allow to distinguish between human or animal origin. Their advantage against coliform bacteria is their very slow inactivation rates, thus allowing for better evidence of past pollutions. Enterococci are also much more resistant against disinfection using chlorine, thus useful for examination of such treated waters. Disadvantages of indicator organisms in general are deficiencies relating high indicator concentrations to health threats on one hand or to pollution sources (man-made, animal based) on the other hand. Paul (2001) therefore summarizes that there will be no unique indicator in future and highly recommends the testing of indicators at the observed region.

2.3 Wastewater treatment technologies

Wastewater treatment technologies aim for removal of harmful substances and transformation into effluents or residuals acceptable for re-use or discharge. General treatment techniques are classified in Table 2. Important extensions or special details of each technique will briefly be described as follows. Detailed descriptions on the processes involved are described in various textbooks, for example in Henze et al. (2002).

Type	technique	purpose	residuals	residual disposal	effluent discharge
Preliminary	screening	remove solid waste, avoid clogging and damage of pipes and pumps	rubbish, wood, paper	landfill	long outfall, high carrying capacities
Primary	sedimentation and grit chambers	remove settleable and floatable matter, primary sludge formation and removal	sand, fat, sludge	landfill and/or incineration	long outfall, high carrying capacities
Secondary	biological oxidation	remove BOD	large amounts of sludge	landfill, incineration, agriculture	short outfall, low carrying capacities
Tertiary	disinfection, filtration, flocculation, settling	remove nitrogen, phosphorous and bacteria	very large amounts of sludge	landfill incineration, agriculture	very short outfall

Table 2: Typical wastewater treatment techniques and residual disposal and effluent discharge

Preliminary treatment is commonly done with milli screening (Fig. 7) or fine screening using screen bar distances of 0.25 - 5 mm, or 5-15 mm respectively. Details are described for example in (Huber et al. 1995), where removal efficiencies for a grid with 1 mm are given to: 90% for floatable solids, 10% for suspended solids, 30% for total oil and grease, 70% for floatable oil and grease and 20% regarding BOD₅. If preliminary treatment is applied alone, effluent disinfection may be needed.

Conventional *primary treatment* consists of sedimentation tanks and grit chambers aiming for the removal of suspended solids (SS). Besides the conventional primary treatment, new technologies have been developed especially for discharges into sensitive receiving waters using long sea outfalls (National Research council, 1992). A prominent example is the chemically enhanced primary treatment (CEPT, Harleman and Murcott, 1999, Table 3), because of its successful installation and operation for the Hong Kong wastewater treatment. Preliminary and primary treatment is of main importance if sediment deposition in the receiving waters is

possible and metals or toxics are contained in the wastewater (attached to particles). Primary treatment may considerably reduce ecotoxicological impacts (Abessa et al., 2005).

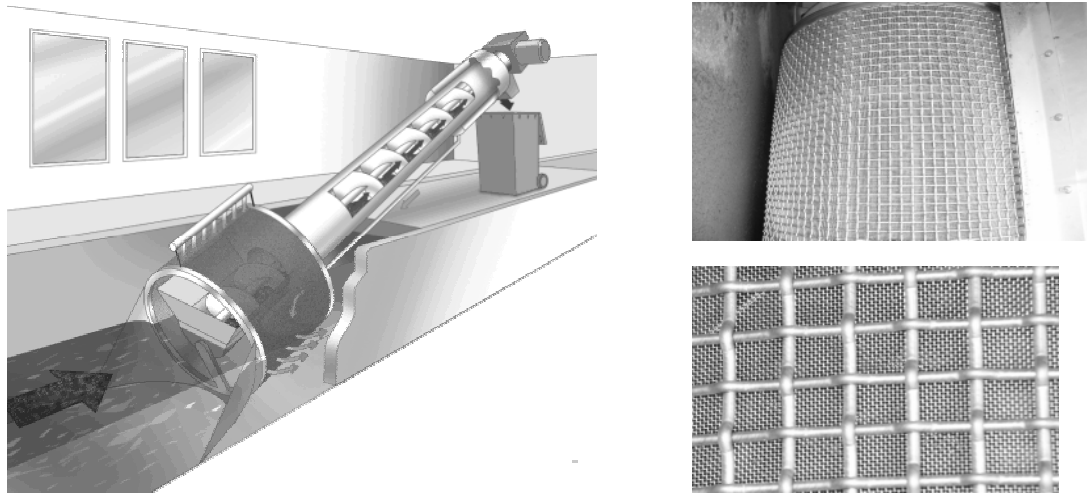


Fig. 7: Milliscreens for preliminary treatment (Huber technology)

	Total suspended solids [%]	BOD ₅ [%]	Total Phosphorus [%]	Total Nitrogen [%]
Conventional primary treatment	55	35	20	15
Conv. primary + secondary treatment	91	85	30	31
CEPT	85	57	85	37

Table 3: Comparison of removal efficiencies for conventional primary treatment and chemically enhanced primary treatment (CEPT), (reproduced from National Research Council, 1992)

Conventional *secondary treatment* consists traditionally of installations reducing the wastewater's biological oxygen demand (BOD). Removal of SS and BOD produces sludge, and the sludge has to be treated prior to reuse or disposal. These processes usually are expensive to operate due to the large energy, skilled labor, infrastructure, and maintenance requirements. The costs of treatment of sludge are generally of the same order as the costs of removing the sludge from the wastewater. Heavy metals and other pollutants are not generally a problem unless the sewerage system receives industrial discharges. In this case, treatment of industrial wastes prior to discharge to the sewerage system is the solution.

Tertiary treatments must be added to the process to effectively reduce pathogen and nutrient levels (Table 4). Nutrient removal is realized by flocculation and sedimentation processes adding chemical substances. Separate or additional disinfection is applied for destruction of microorganisms. Heat, chemicals, filtration or radiation are the most common techniques of disinfection. Widespread, because cheapest is chlorine used as chemical disinfectant. Its efficiency depends especially on water temperature and reaction time. Alfredini and Roma (1999) showed that disinfection of preliminary treated effluents with chlorine reduces total coliform concentration by the order of 95%. Examples from the Sao Paulo coast, where chlorine disinfection of preliminary effluents is commonly applied showed a reduction from 10^7 counts / 100 ml to $6 \cdot 10^5$ counts / 100 ml after a chlorine addition 0.5-1.5 mg/l and a contact time of 30 min. (Alfredini and Roma, 1999). However, effluent chlorination is generally considered as harmful due to the possible generation of halogenated hydrocarbons, which are cancer-causing (Lattemann and Höpner, 2003). Therefore, in several regions (e.g. California

(USA) or Rio de Janeiro (Brazil)) chlorine is not permitted for discharge. Interim solutions are dechlorination and/or further treatment to neutralize chlorine. Addition of further treatment steps however, significantly increases the cost and complexity of the process.

A summary of general removal efficiencies of the different techniques is listed in Table 4.

Constituent	Concentration reduction [%]		
	Primary	Primary + Secondary	Primary + Secondary + Tertiary
Solids, suspended, total	60	85	95
Biochemical oxygen demand (BOD, 5d, 20°C)	20	85	95
Nitrogen (total as N)	3	10	95
Phosphorus (total as P)	3	10	95
Total coliform [count/100ml]	95	96	98

Table 4: Typical effluent changes depending on treatment (Lee, 2003; Maier et al., 2000)

2.3.1 Limitations of conventional treatment technologies

The inherent problem of treatment technologies is its focus on removal efficiency thus process engineering instead of also considering the ecosystem response, thus the wastewater management efficiency. Though especially hydromechanical aspects are fundamental for all treatment processes and for water pollution control in general, these are still under-represented in most wastewater system designs.

Treatment technologies are expensive technologies regarding their investment costs but also their high operational demands. Maintenance demands increase strongly with increasing removal characteristics. Therefore theoretical treatment plant efficiencies (Table 4) strongly depend on proper operation, which is still not guaranteed for an alarmingly high number of treatment plants worldwide (UNEP, 2002, 2004). In developing countries, estimates suggest that only about 5% of all sewage is treated before discharge (World Resources Institute, 1998). Despite more investment in water and sanitation projects in the last decades, the total number of people without access to water and sanitation services remains high, particularly in urban and peri-urban areas (WHO, 1997). In addition, even industrialized countries still need to improve wastewater management. About 20% of the surface water resources in the European Union are considered heavily contaminated (EU-Commission, 2002) and major European rivers are characterized by steadily increasing average coliform levels (Meybeck et al., 1990). The European environmental agency shows that the percentage of the population served by wastewater treatment varies from about 50% in the Southern to about 80% in the Northern and Western European countries. It concludes that wastewater treatment and disposal has improved in many countries during the past 10 to 15 years, especially in the South of Europe where the backlog was large. However, most of the new eastern European countries cannot afford these large investments in future.

Consequently, World Bank and World Health Organization studies indicate that past investments regarding wastewater treatment have been excessive compared to their practical efficiency on one hand and society/ecosystem needs on the other hand. Given that there will be very large investments in wastewater infrastructures in the next decades in developing, but also in industrialized countries, wastewater system management improvements may considerably affect the environment and society.

For example, the history of Sanitation in Latin America has shown that only the main centers of the most important cities benefited from conventional wastewater treatment (IETC, 2000). These small gains in sanitation on a Regional scale are attributed firstly to the diversion of most of the resources generated from sewerage tariffs to improve the financial situation of the existing water systems and secondly because conventional sewerage, at least under the design codes prevailing in almost all the countries of the Region, is in itself too expensive (Ludwig, 1988, Arasaki, 2004). As a result, the sewerage coverage in the Region has been disastrous (IETC, 2000). The experience in the Latin America Region to date has been to copy, without adaptation, prevailing urban patterns of American sewerage design codes. This may be correct if stable population areas are assumed, as happen to occur in the developed world cities. However, for a typical Latin American city whose estimated population in the next 25 years is expected to be 4 times present population the adoption of developed world codes is not efficient. In addition there are also in Europe several examples where upgrades of treatment plants did not show any significant environmental difference (Neves, 2003; Larsen, 2004). Following studies considering ecosystem response showed instead, that for these cases investments would have been much more efficient if put into other infrastructural elements like polluted storm water overflows or other waste sources.

Another fundamental problem of treatment technologies is their centralized structure. Conventional treatment is usually carried out at the point of discharge, also called 'end of pipe' treatment. The sewage collection systems needed are the most expensive part of such a wastewater management solution with up to 80 % of the whole investment costs of a sanitation system. However, there are actually numerous ongoing activities and first technical solutions available for alternative and de-centralized treatment systems to approach that problem.

Thus integrated wastewater management technologies will allow improving infrastructural efficiencies even without significant increases of planned budgets. Environmental hydraulic engineering design should therefore not only focus on treatment technologies, which are efficient for single processes, but especially on the hydrodynamically dominated eco-system response processes for the integrated system. Such approaches are also the major design instrument to show and improve efficiencies of alternative and de-centralized solutions.

2.4 Discharge technologies - outfall characteristics

Discharge technologies aim for *enhanced effluent dispersion* in the receiving environment and *adequate discharge siting* to avoid pollutant accumulation, to protect sensitive regions and to utilize natural purification processes. General discharge techniques are outfalls designed as efficient mixing devices installed at locations with high transport and purification capacities.

An outfall is the facility where (treated) wastewater is discharged into the receiving water body. Commonly this is the outlet, canal, or pipeline from the municipal or industrial wastewater treatment plant or drainage system discharging into a water body (Fig. 8).

Ocean outfalls are classified according their location (onshore surface discharges / offshore submerged discharges), their mixing features (single port / multiport) and their effluent characteristics (positive buoyant, e.g. treated sewage or cooling water, or negatively buoyant, e.g. desalination brine or dredging material). In the following only submerged multiport diffuser outfalls for positively buoyant effluents (i.e. municipal wastewater) are considered. They consist of three components (Fig. 9): the onshore headworks (e.g. gravity or pumping basin); the feeder pipeline that conveys the effluent to the discharge area; and the diffuser section where a set of ports releases and disperses the effluent into the environment.

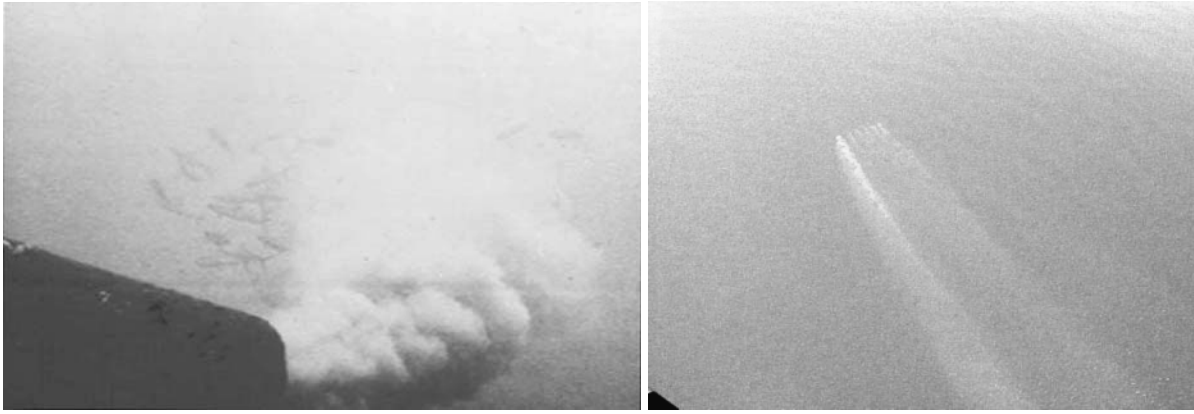


Fig. 8: Pictures from offshore, submerged, and positively buoyant wastewater discharges. *Left*: single port (www.cormix.info), *right*: multiport diffuser (Lamparelli, 2003)

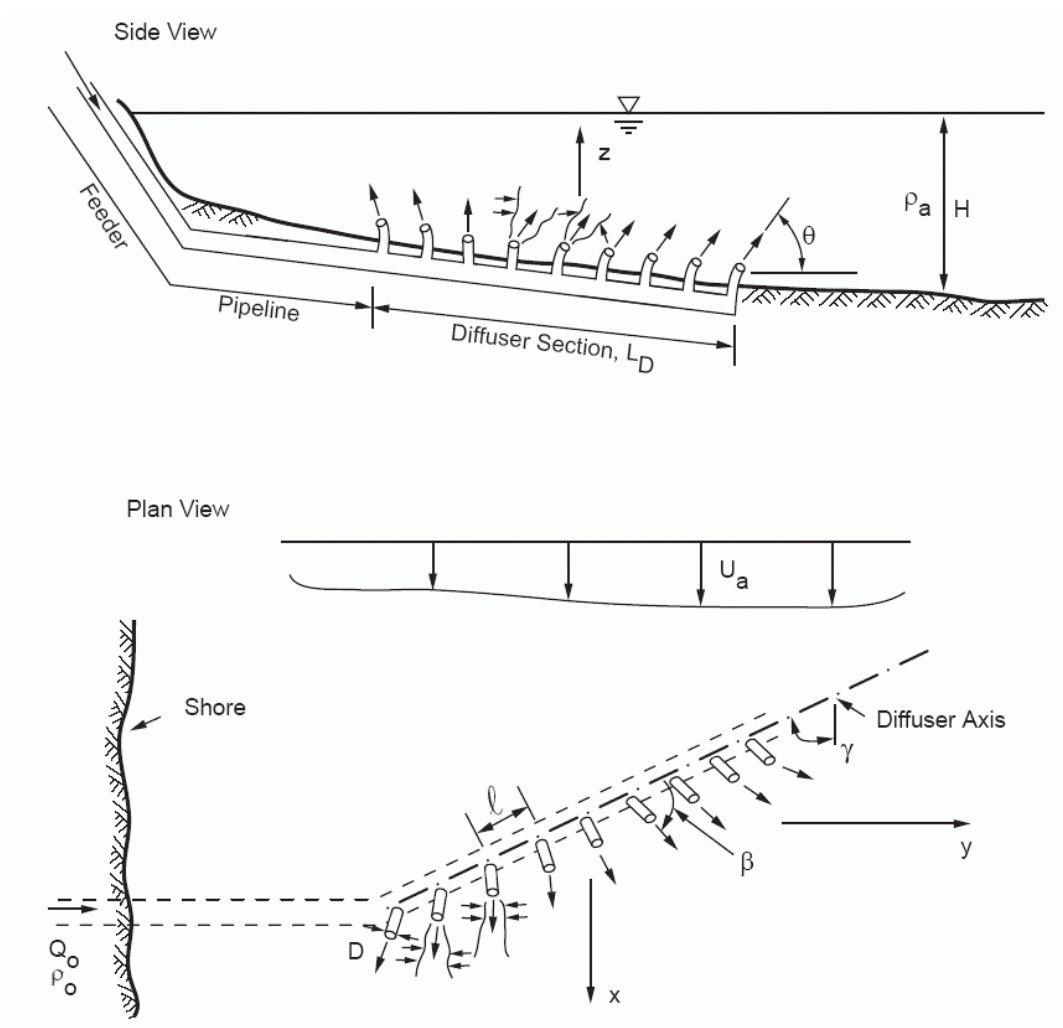


Fig. 9: Schematic view of submarine outfall with diffuser length L_D , port diameter D , port spacing l , port and diffuser orientations β , γ , θ , effluent flowrate Q_o and density ρ_o , average depth of receiving water H with density ρ_a and velocity u_a (reproduced from Jirka et al., 1996)

Outfall dimensions may vary considerably, mainly depending on available construction techniques. A literature survey (i.e. Salas (1994), Neves and Neves (1992), Grace (1978), www.mwwd.org, www.emisarios.unican.es) contacts with pipe companies (i.e. Sweco, Her-

renknecht and others) and an online database with voluntary input (Bleninger and Jirka, 2002) resulted in a table containing about 200 large wastewater and industrial outfalls worldwide (<http://outfalls.ifh.uni-karlsruhe.de>). The following compilation of average characteristics and minimum - maximum values (in brackets) is intended to exemplify the dimension of outfall projects. Images from the medium size Antalya outfall (Turkey) and the large size Boston outfall (USA) illustrate these values (Fig. 10 and Fig. 11):

- Investment costs: 7 million US\$ (2 to 3,500 million US\$)
- Half of all systems are connected to the drainage system, thus conveying also rainwater
- More than 60% of all systems have preliminary treatment only
- Maximum flow rates: $Q_o = 1.5 \text{ m}^3/\text{s}$ (0.1 to 55 m^3/s)
- Feeder pipe diameters: $D_F = 1 \text{ m}$ (0.1 to 8 m)
- Pipe materials changed according to new available technologies:
 - 1950 - 1980: carbon steel or cast iron
 - 1970 - 2000: reinforced concrete
 - 1990 - now: high density polyethylene or tunnels
- Diffuser length: $L_D = 100 \text{ m}$ (10 to 1000 m), around 60% with decreasing diameter
- Outfall lengths: $L = L_F + L_D = 1300 \text{ m}$ (100 to 16,000 m)
- Port diameters: $D = 100 \text{ mm}$ (10 to 300 mm), almost 10% with attached Duckbill valves and 2% with rosette like discharge arrangements
- Discharge depth: $H = 10 \text{ m}$ (4 to 60 m)



Fig. 10: Antalya outfall (Turkey) during installation in 1997. *Top*: Diffuser section assembling on shore. *Down*: Feeder section ($L_F = 5 \text{ km}$, HDPE pipe, $D = 1600 \text{ mm}$) while sinking with attached concrete weights on the seabed (PipeLife Company)



Fig. 11: Boston outfall during installation in 1998. *Left:* View into tunnel section (16 km with 8 m diameter). *Right:* One out of 55 riser caps with eight outlets each in rosette like configuration (Roberts and Snyder, 1993)

2.4.1 Discharge processes and their characteristics

Discharge processes are an interplay of ambient conditions (see chapter 2.1) and the outfall configuration. Different hydrodynamic processes drive and control the system. Most processes are running simultaneously, but with very clear dominance in different temporal and spatial regions, according to their predominant flow characteristics, schematized in Fig. 12:

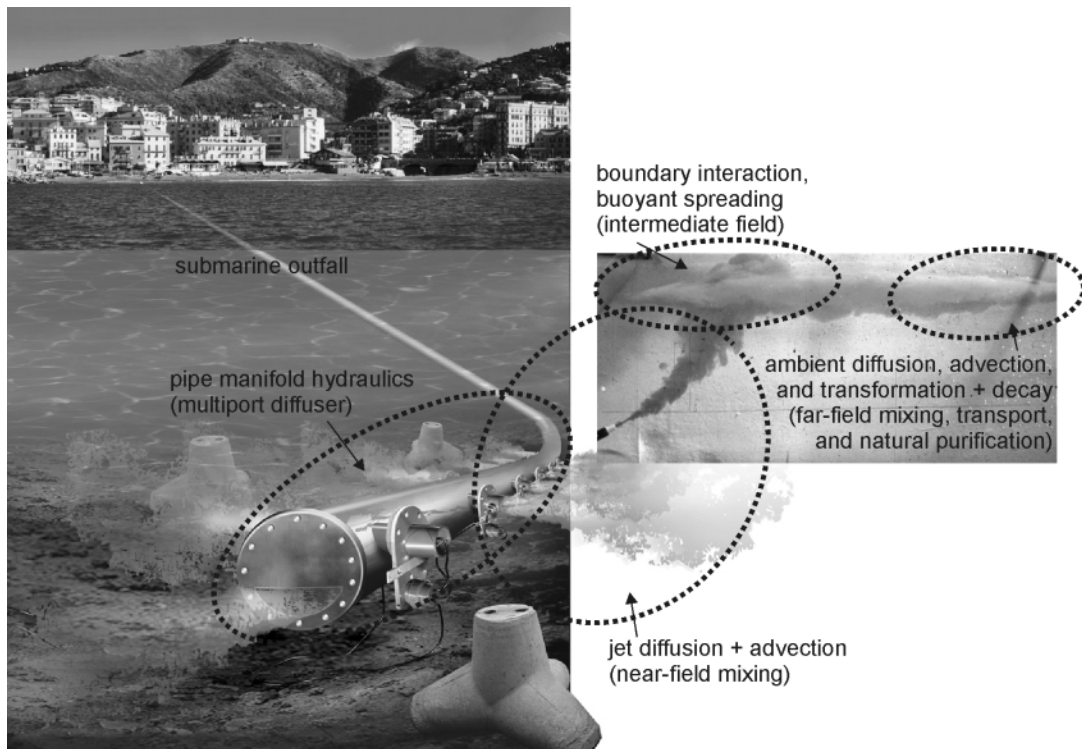


Fig. 12: Schematic view of an operating multiport diffuser outfall merged with a laboratory picture of a trapped waste plume in stratified ambient (modified from Domenichini et al., 2002)

The first region is the outfall pipe system, conceptualized as an *internal hydraulic manifold*. It does not change effluent characteristics, but considerably contributes to the subsequent dispersion processes by conveying the effluent to adequate discharge locations and spatially distributing the effluent in the discharge region. The flow is driven by the pressure difference between the headworks and the receiving waters as well as the density difference between the

effluent and the ambient water. Manipulations of manifold geometries have direct implications on the flow distribution and the pressures losses.

In the second region, the "*near-field*" (also called active dispersal region or initial mixing region), the initial jet characteristics of momentum flux, buoyancy flux, and outfall configuration (orientations and geometries) influence the effluent trajectory and degree of mixing. Source induced turbulence entrains ambient fluid and dilutes the effluent. Though ambient characteristics affect the discharge once the effluent left the diffuser openings, they are still only of minor importance until any bottom or terminal layer interaction occurs. This characterizes the transition to the intermediate field.

The "*intermediate field*" (or zone of wastefield establishment (Ridge, 2002)) is characterized by the impact of the turbulent plume with boundaries and the transition from the vertically rising plume/jet characteristics to a horizontal motion generated by the gravitational collapse of the pollutant cloud. Source characteristics become less important. Generally, a pool of initially diluted wastewater is formed either at the surface or at the level of submergence under stratification conditions (shown in Fig. 12). Vertical and horizontal boundary conditions will control trajectory and dilution in the intermediate field through buoyant spreading motions and passive diffusion due to interfacial mixing. Intermediate field processes have often been neglected in practical applications (i.e. model formulations), because focus has been given to either the near-field or the far-field processes and not their combination. In addition, only few lab and field studies examined these processes in more detail (Jirka & Lee, 1994; Akar and Jirka, 1995). Although these works generally confirm negligible scales of intermediate field effects for discharges into reasonable strong turbulent current fields, they clearly show their importance in either stagnant or shallow waters, where large spreading processes or instabilities occur.

After the wastefield establishment ambient conditions will control trajectory and dilution of the turbulent plume in the "*far-field*" (also called passive dispersal region), through passive diffusion due to ambient turbulence, and passive advection by the often time-varying, non-uniform, ambient velocity field. The flow is forced by tides and large-scale currents, wind stress at the surface, pressure gradients due to free surface gradients (barotropic) or density gradients (baroclinic), and the effect of the Earth's rotation (Coriolis force). Dynamic discharge related effects are unimportant in that region. Vertical mixing in stratified water bodies is damped by buoyancy, so dilution is mainly due to horizontal mixing by turbulent eddies (Zielke & Mayerle, 1999). Concentration reductions in the far-field are related to natural dispersion but also significantly to natural purification processes.

An overview of the physical processes is given in Table 5, and an example for their characteristic length and time scales for large discharges in the coastal environment in Fig. 13.

	manifold	near-field	intermediate-field	far-field
dominant forcing	pressure difference	momentum and buoyancy flux	buoyancy flux and boundary resistance	tidal, baroclinic, barotropic and wind
dominant advection	mean pipe velocity	jet/plume induced velocity field	density current or ambient velocity	ambient velocity field
dominant mixing	fully mixed	strong shear induced turbulence	frontal mixing at plume borders	bed and wind shear induced turbulence
temporal variance	steady	quasi steady	unsteady	highly unsteady
spatial variance	uniform	non-uniform	non-uniform	non-uniform

Table 5: Overview of dominant processes for coastal submerged multipoint discharges

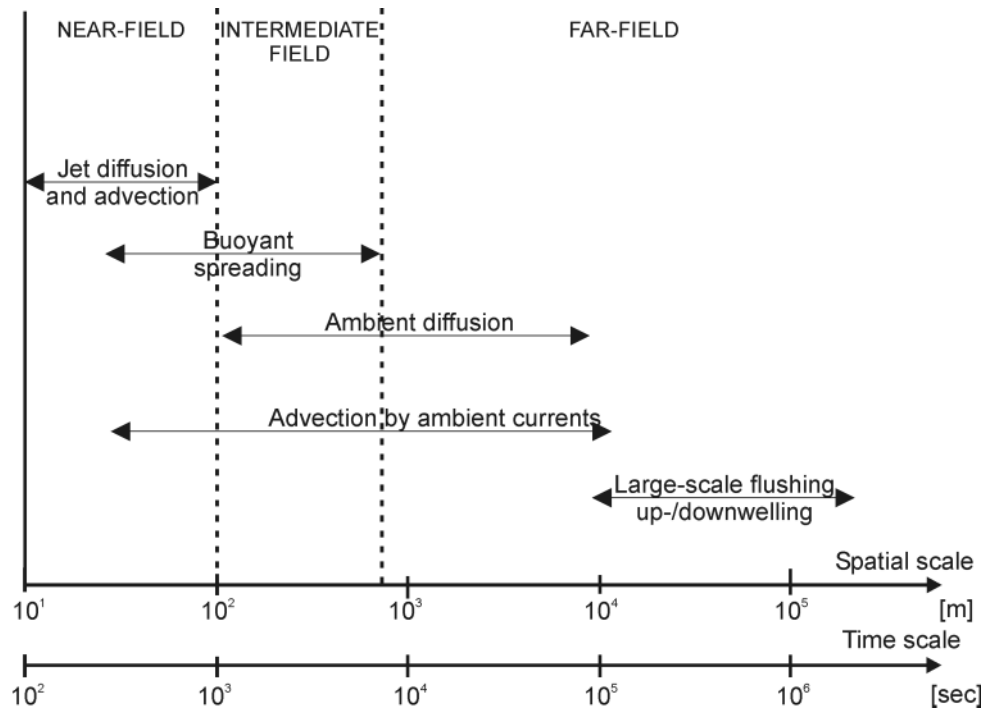


Fig. 13: Typical temporal and spatial scales for transport and mixing processes related to coastal wastewater discharges (Jirka et al., 1976, Fischer et al., 1979)

The combination of strong initial mixing induced by a multiport diffuser installation and adequate siting regarding high ambient mixing, transport and natural purification capacities reduces concentrations significantly. The theoretical comparison between treatment and discharge technologies qualitatively illustrated in Fig. 14 and quantitatively described in Table 6 and Fig. 15 shows that without proper consideration of water quality response and without proper outfall design even secondary treated effluents may cause ambient concentrations which fail environmental standards. This because of i) an improper discharge siting at a location where coastal conditions near the coastline (shallow, slow currents, poor flushing) do not allow for sufficient substance dispersion and transformation, and ii) an insufficient treatment regarding the environmental objectives defined for the receiving waters. Thus conventional short outfall solutions, though connected to high-level treatment plants do often not guarantee sufficient protection of the sensitive coastline ecosystems, nor public health. Well designed and sited outfalls instead may guarantee that protection and in addition may require less treatment, thus not only saving investment and operating costs (Harleman and Murcott, 1999; Arasaki, 2004), but also allowing for the reduction of environmental pressures on-shore due to reduced sludge production.

Constituent	Concentration reduction [% of raw sewage concentration]				
	primary	primary + secondary	primary + secondary + tertiary	preliminary WWTP, long outfall, 1h after discharge	preliminary WWTP, long outfall, 6h after discharge
Solids, suspended, total	60	85	95	99	nn
Biochemical oxygen demand (BOD ₅)	20	85	95	99	nn
Nitrogen (total as N)	3	10	95	99	99
Phosphorus (total as P)	3	10	95	99	99
Total coliform [count/100ml]	95	96	98	99	99,9

Table 6: Typical effluent concentration reductions depending on applied treatment or discharge technology (Lee, 2003; Maier et al., 2000). nn: difficult to detect

- Coastal wastewater discharges -

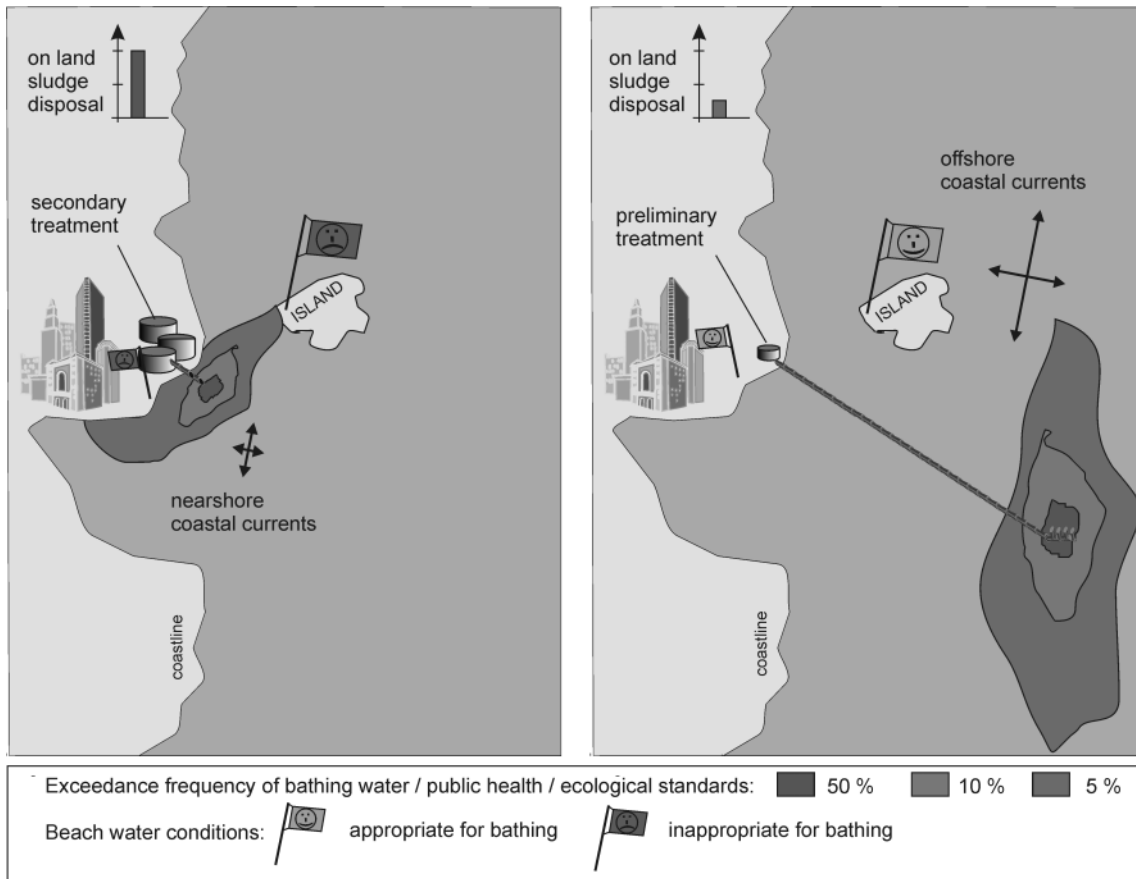


Fig. 14: Comparison of two wastewater systems and their impact on receiving waters as exceedance-frequency of ambient standards (i.e. beach water quality). *Left*: Secondary treatment plant with short outfall. *Right*: Preliminary treatment with long outfall and multipoint diffuser.

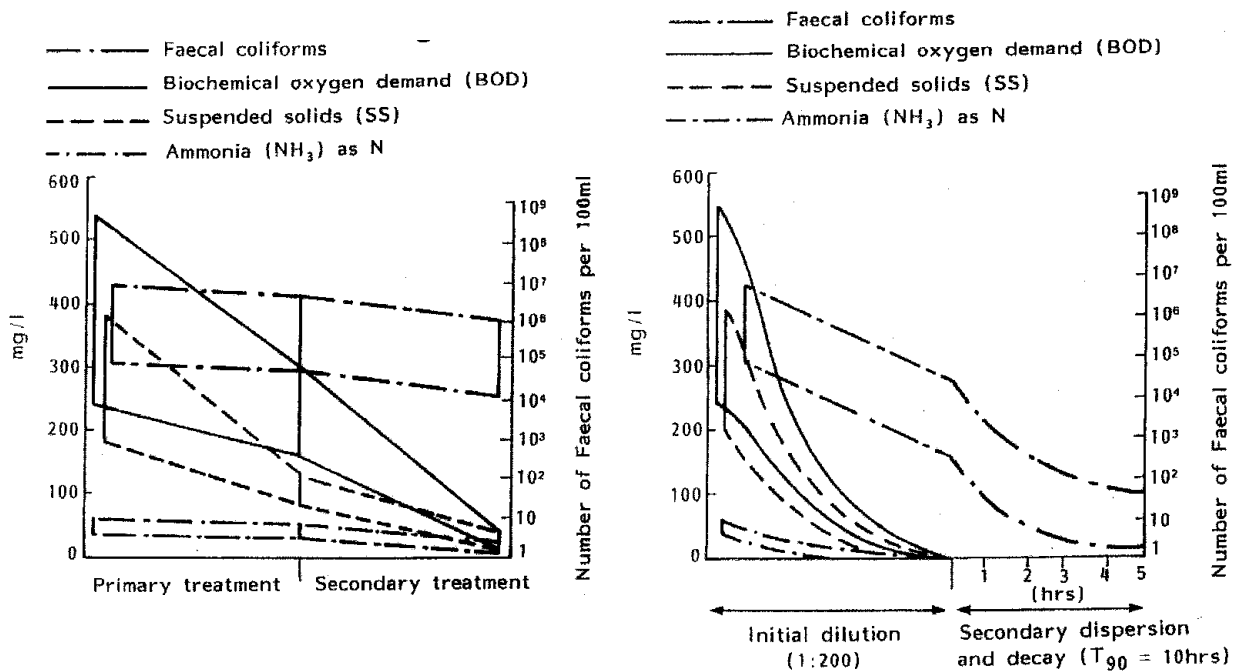


Fig. 15: Comparison of technical and natural contributions to pollutant concentration reductions. *Left*: Technically achievable concentration reductions for primary and secondary treatment. *Right*: Naturally occurring concentration reductions after discharging preliminary treated wastewater (reproduced from WRc, 1990)

Even though pure discharge solutions seem to be clearly competitive with treatment technologies they do reduce concentrations by dilution and do not reduce substance loads. This has to be considered carefully regarding long-term impacts. Regarding sustainable solutions discharge technologies furthermore should neither head for the replacement, nor for a competition with treatment technologies, but should be understood as an important tool for improving water quality in combination with treatment technologies.

However, the lack of co-ordination between the selection of treatment technologies and discharge technologies has led to suboptimal solution in the past (Wilkinson and Wareham, 1996). For example, regarding minimal health risks associated with bathing waters there is no reason to suggest that health risks from preliminary treated long sea outfall discharges will be different to those from high level treatment plants and short outfalls provided the schemes are designed to produce a similar microbial quality in the bathing waters (e.g. by meeting the bacteria standards in the bathing water regulations). It can hereby be shown, that regarding pathogen removal conventional treatment technologies generally need additional disinfection of their effluents, if discharged directly at a bathing shoreline. Even activated sludge, the most efficient biological treatment technology for bacteria pollution, does not guarantee effluent concentrations in compliance with bathing water regulations (compare Table 6 and Fig. 15). Moreover, because variations in inflow concentrations and treatment plant performance still cause significant bacteria concentrations in treatment plant effluents (Maier et al., 2000). Where short-term exposures to pathogens may result in significant risk, the issue of reliability is of major importance. WHO guidelines state that an effective outfall preceded by preliminary treatment has low risk of human health impacts. WRc (1990) further summarizes, that regarding capital costs preliminary treatment plants with a long sea outfall are most cost effective because of less plant requirements to treat, and smaller area of land. Operating costs for preliminary treated ocean outfalls are generally around one third of a secondary treatment plant operating costs (WRc, 1990). Investment costs are about the same, whereas up to 40% is related to the analysis of receiving waters for outfalls (Water Research Centre, 1990). The implementation of new discharge adopted treatment technologies like the chemically enhanced primary treatment will cause less environmental impacts with cheaper solutions (National Research Council, 1998). This or similar options should be considered especially for regions with strongly increasing sanitation coverage (UNEP, 2004, 2002).

New environmental philosophies and adopted technology approaches confirm the need for efficient integrated approaches including strong discharge technologies. This explains the worldwide increasing utilization of submarine outfalls. Positive examples with detailed monitoring programs of the receiving waters have been reported recently, showing no adverse effects of outfalls on the environment: Sydney Australia (Philip and Pritchard, 1996), Boston, USA (Signell et al., 2000), Lisbon, Portugal (Silva et al., 2004), Santos, Brazil (Berzin, 1992 and Braga et al., 2000), Rio de Janeiro, Brazil (Roldão et al, 2001), Hong Kong (Lee et al., 2002), Huntington Beach, California, USA (USGS, 2004). There are six out of seven outfalls along the Sao Paulo coast which operate well (Cetesb, 2005), Northern Spain (Revilla et al., 2002), Chile (Galindo and Simpson, 2003), Montevideo, Uruguay (Crosignani et al., 2002). The Pan American Health organization (PAHO) states generally that over 100 outfalls are in operation in Latin American countries with no problem. Numerous publications during the conference series "Marine Waste Water Discharges - MWW" (www.mwwd.org) are related to discharge impacts and give a positive image.

2.4.2 Limitations of discharge technologies

The inherent problem of discharge technologies is their focus on the ecosystem response instead of also considering load reductions thus foreseeing more sustainable solutions including alternative treatment technologies. This is also important considering the accumulation of non-biodegradable substances, which eventually could have been removed by treatment technologies or source control.

Technical limitations of discharge technologies are related to difficult and complex design procedures, which need an interdisciplinary approach, because of the need to understand the interaction of the discharge with the receiving waters. Problems with projects handling wastewater discharges have been mainly related to a poor understanding of what measures need to be taken to protect the environmental values of receiving waters. Measures to ensure bathing water quality may be different to those ensuring fishing water quality.

Another drawback of discharge technologies is little public acceptance which is directly related to the previously stated little understanding and poor scientific communication. There is the prevalent misconception that the discharge of less treated effluents is dumping wastes into the environment, although there is indeed a clear difference between discharge “re-enter substance into bio-geochemical cycle, forcing the ambient to react” and disposal “final disposition, isolating substance from bio-geochemical cycle, avoiding any further reaction.” The poor public acceptance is further facilitated by prevailing post-installation pollution suspected those to be a result of malfunctioning or improper designed outfalls. However, it has been shown, that most of these problems are related to other waste sources (often illegal discharges or surface run-off (USGS, 2004 or Berzin, 1992) or uncontrolled industrial sources (Braga et al., 2000) or nearby treatment plants with inappropriate discharge systems (Garber, 1998) and not to the outfall discharges. In polluted regions often very little is discussed regarding the adequate sewage treatment and discharge option that may restore environmental conditions now damaged by uncontrolled wastes discharges. An example for better public involvement is given in Garber (1998) for Victoria, B.C. in Canada.

Such limitations mainly show the need for a better understanding and control of discharge processes. The additional advantage of studies based on the ecosystem-response on the installation of discharge technologies is their capability to detect the critical pollution sources, thus providing tools for a more efficient wastewater management (USGS, 2004).

2.5 Need for a discharge assessment - improved outfall design

The failure to properly manage and dispose wastewater has enormous financial implications. The economic damage due to medical treatment and loss of productivity associated with diseases caused by exposure to contaminated food and water are high but difficult to estimate (IETC, 2000). However, Esrey et al. (1991) found that when well-designed basic water, sanitation, and hygiene interventions were implemented at the community level, sickness from Diarrhoea was reduced by 25 - 33%, Schistosomiasis was reduced by 77%, trachoma was reduced by 25%, and overall child mortality was reduced by 60%. The World Bank (1993) estimated 40% reductions for both Diarrhoea and intestinal worm infections using similar interventions. The consequent loss in costs is estimated in a few examples: In the US water-borne diseases cost the country between 3 and 22 billion dollars per year in medical bills and lost productivity (Bennett et al., 1987; Murphy, 1999). Illnesses related to water contaminated by untreated wastewater in China cost the country almost 4 billion dollars per year (World Bank, 1997).

In addition coastal regions are often rich in touristic resources, thus depending on intact and clean ecosystems. Closed beaches have enormous implications on the local economy. For example, the beach closures of Huntington Beach, California, strongly affected regional tourism industry with an annual budget of 80 million US \$ and five million visitors each summer (USGS, 2004). Costs for proper treatment and discharge installations are small compared to these implications.

The balancing approach to decide on an appropriate discharge technology and the compatible treatment technology is analyzed in discharge assessments. Different design alternatives are hereby compared and evaluated regarding environmental impacts, investment costs, and operational demands. These assessments nowadays play an important role not only for the final discharge permit or for permit prolongation, but also especially for investors and politicians. Wastewater systems are fundamental infrastructural investments and generally so big, that safe and sustainable financing is essential. Financers are development banks (e.g. the World Bank) if projects for poorer communities are planned or private banks or even large companies (i.e. water related multinational groups). Both financing lines nowadays demand financially safe, thus sustainable, environmentally sound, and socio-economically adopted and economically stimulating investments. Projects hereby have to pass challenging and comprehensive pre-planning investigations. A well-elaborated discharge assessment is substantial for the approval. Further extensions of such assessments are subsequent steps to the final planning, public communication, and permit approval. Even the regular monitoring can be based on the outcomes of the previous assessment, for example the existing models.

The main question in discharge assessments are pollutant plume concentrations, locations, and geometries. A good example of such an assessment for a coastal water quality problem is described in Connolly et al. (1999) for the Mamala Bay (Hawaii) outfall, showing the importance of an efficiently designed outfall. This thesis provides solutions to improve the modeling techniques for such outfall designs.

2.5.1 Outfall design parameters - dilution characteristics

Outfall design includes the evaluation of alternatives for different treatment technologies, outfall locations (siting options) and constructional alternatives (outfall lengths, diffuser geometries and orientations). The design criteria are resulting distributions of pollutant concentrations C in the receiving waters:

$$C = \text{substance mass per unit volume [mg/l, ppm, ppb, bacteria - counts, etc.]} \quad (2.1)$$

Outfall design aims for avoiding temporally or spatially concentration peak stresses and substance accumulation by reducing local concentrations due to mixing, transport, decay and transformation processes (Jirka and Bleninger, 2004). As a measure for the concentration reduction generally a reciprocal volume fraction of effluent in a sample defined as dilution S (Fischer et al., 1979) is used:

$$S = \text{total volume of sample / volume of effluent in sample} \quad (2.2)$$

Though the term dilution is generally associated with a pure physical mixing process only, strictly speaking, processes leading to dilution (or concentration reductions) are:

- physical mixing: reducing substance concentration by increasing the volume of the carrier medium, e.g. adding water to a concentrated fluid and mixing, to reduce its strength

- transformation and decay, decreasing dissolved substance mass, e.g. bacteria inactivation
- boundary interaction processes, reducing a constituents concentration by removing it from the carrier medium (e.g. particle settling or adsorption processes at the bed)

These processes naturally occur in receiving waters, however over huge temporal and spatial scales. Diffusers are designed to enhance the naturally slow mixing by strong initial-dilutions. Thus, initial concentration peaks are reduced to comply with ambient standards outside a Regulatory discharge zone around the outfall and a proper siting allows natural processes to further dilute the effluent to comply with public health standards at the Regulatory preservation zone (i.e. beaches, see also chapter 6 and Jirka et al, 2004).

Therefore, it is commonly distinguished between dilutions related to different processes or design steps. In the following S is used for the pure hydrodynamic dilution describing the mixing of the effluent with the ambient and $S_{tot} = S_{dec} S$ for the total dilution including transformation and decay processes and marginally also the boundary interaction processes. Regarding different design steps it is often distinguished between a discharge induced initial or near-field dilution S_{nf} , generally not including decay processes, and an ambient flow induced far-field dilution S_{ff} that occasionally includes bacterial decay, depending on the analyzed parameter. For the total dilution S_{tot} then follows:

$$S_{tot} = S_{nf} S_{ff} S_{dec} = S S_{dec} \quad (2.3)$$

With a background ambient concentration C_b the pollutant concentration can be calculated by

$$C = C_b + (C_e - C_b) / S_{tot} \quad (2.4)$$

Ecological effects are often related to lethal or chronic concentrations, thus discharge permits generally demand ambient pollutant concentrations not exceeding critical values defined as ambient concentration limits $C_{a,lim}$. Permit compliance requires $C < C_{a,lim}$, which can be achieved by varying the design parameters C_e and S . The design optimum is the cheapest solution achieving permit compliance, generally a combination of maximized dilution and minimized effluent concentration. Design limitations are technological limits for the minimization of C_e and limits regarding the assimilative capacity of receiving waters for the maximization of S_{tot} .

Design optimization for discharges into sensitive water bodies are limited, because achievable dilutions in those waters are generally small and temporally and spatially approximately constant values (e.g. for rivers $S_{tot} \approx 10 - 30$). In addition, often pre-defined effluent concentration limits $C_{e,lim}$ are specified from authorities. Thus, the design equation results in the minimum necessary treatment technology (effluent concentration C_e) dominating the total costs, with slight variations in discharge structure optimizations:

$$\min [C_e = C_b + S_{tot}(C_{a,lim} - C_b) ; C_{e,lim}] \quad (2.5)$$

Coastal discharges instead are generally characterized by high and strongly variant achievable dilutions (e.g. from 100 to 10,000 depending on location and time) in combination with weak or non-existing effluent concentration limits. A typical design approach thus compares alternatives for different treatment technologies (preliminary, primary, secondary, or tertiary treatment, $C_{e,pre}$, $C_{e,1}$, $C_{e,2}$, $C_{e,3}$) regarding their required dilution:

$$S_{tot,min,i} = (C_{e,i} - C_b) / (C_{a,lim} - C_b) \quad (2.6)$$

For example the ambient concentration limits of the Brazilian bathing water standards regarding *E. coli* bacteria counts are $C_{a,lim} = 1000 / 100$ ml (CONAMA, 2000). An application of equation (2.6) results in dilution requirements for different treatment technologies and zero background concentrations as summarized in Table 7. Results indicate that only treatment plant effluents, which passed primary and secondary treatment together with disinfection are allowed to discharge directly in bathing waters, provided that there is no background concentration and no concentration built-up. Discharges from treatment plants with lower treatment levels have to be located a sufficient distance away from the bathing water zone to allow dilution processes to occur before reaching the bathing waters. Long distances (long outfalls) and high dilutions (i.e. multipoint diffusers) allow for reduced treatment. Required concentration reductions thus can be achieved by several combinations of treatment and discharge techniques. The optimal solution is the cheapest technology combination.

Treatment	Effluent concentration C_e : E. coli [counts / 100 ml]	Required dilution $S = C_e / C_{a,lim}$
Untreated	10^7	10^4
Primary treatment	10^6	10^3
Primary and secondary treatment	10^5	10^2
Primary and secondary treatment and disinfection	10	0

Table 7: Required effluent dilution for different levels of treatment (modified from Wilkinson and Wareham, 1996)

2.5.2 Outfall design tools - need for prediction models

Whereas the prediction of C_e is a standard application including uncertainty and variation mainly as a function of technological processes within the treatment plant, there is a large degree of uncertainty related to the prediction of S_{tot} , where the determination of pollutant concentrations as a function of natural processes within the receiving waters poses the major problem. Thus, discharge assessment is mainly related to the prediction of the dilution. Historically only conservative estimates on initial dilution have been used to design and control outfalls. These worst-case scenarios based for example on the Cederwall equation (Wood et al., 1993) or simply using still water conditions (WRc, 1990) resulted in under-estimations of real initial dilutions and did not allow for considerations of far-field dilution values for example at beaches. Advancements have been made regarding additional processes summarized in empirical dilution equations and design procedures, outfall guidelines and books (Jirka and Lee, 1994; Wood et. al, 1993; Water Research Centre, 1990; Williams, 1985; UNEP, 1996; Grace, 1978; National Research Council, 1993; Telford, 1989 and proceedings from the conference series “Marine Waste Water Discharges - MWWD, www.mwwd.org). However, these techniques are still unreliable for outfalls where receiving water conditions depart significantly from the idealized cases (Davies, 2003). Therefore submarine outfalls generally discharging into highly unsteady, non-uniform coastal waters are still challenging design cases.

Traditional designs are mostly based on measured parameters (currents, densities, tracer tests, etc.). Such measurements are costly, spatially limited to a few locations and temporally limited to short time periods. Therefore, modeling techniques are needed to receive spatial data over longer time-scales. Appropriate combination with field studies allow the definition of missing boundary conditions, model calibration and model validation. Simplest models “just”

interpolate or extrapolate field data for example to infer currents between meter locations or measurement periods. However, field data extrapolation is limited to relatively small spatial scales and cannot predict changes due to planned installations. Furthermore, interpolation models do not necessarily allow for dynamic representations and understanding. A waste plume generally cannot be tracked or resolved by a few point measurements and interpolation.

Hydraulic laboratory model studies are quite reliable if certain conditions on minimum scales are met as has been demonstrated in the past. Nevertheless, just like field tests, they are costly to perform and inefficient for examining a range of possible ambient/discharge conditions and long time-scales. Therefore, hydrodynamic mathematical models are needed.

Larsen (2000) summarizes that there are excellent computer packages available for the general diffuser design (e.g. CORMIX), also confirmed by measurements (e.g. Carvalho et al., 2002), whereas the procedure for outfall siting on one hand and optimization of outfall hydraulics on the other hand is much more complex and troublesome. He recommends that predictions of bathing water quality should have highest priority in the design of an outfall including reasonable safety factors. The question of initial dilution should only have a secondary priority in balance with a reliable engineering design. Nonetheless the strong interaction of these processes makes a proper model coupling necessary. A discussion of these issues and an example of predicting dispersion from the Boston Harbor outfall is given by Blumberg et al. (1993), Zhang and Adams (1999), Tetratex (2000), Zhang (1995). This thesis aims for an improved discharge assessment linking simple dilution equations for continuous discharges in steady environments (e.g. Fischer et al., 1979, Jirka and Lee, 1994) with complex expert systems (Jirka et al., 1996) up to high resolved 3D, unsteady hydrodynamic models for time variant discharges. Contributions are related especially to three hydraulic regions according to the occurring physical processes: the hydraulic constructional design, the hydrodynamic mixing induced by the outfall (defined as near-field) and the transport and dispersion due to natural processes (defined as far-field):

- Environmental design (far-field):
Analysis and optimization of different alternatives regarding outfall location (siting) and the necessary treatment options according to an improved interaction with assimilative capacities of receiving waters. These analyses are mainly focused on large scales for long periods, where natural far-field processes dominate with partially overlaying intermediate-field processes.
- Hydrodynamic design of discharge structure (near-field):
Optimization of main outfall characteristics (geometries and configuration) to improve the outfall induced mixing efficiency. These analyses are focused on smaller scales and shorter periods, where outfall induced near-field processes dominate with partially overlaying intermediate-field processes.
- Hydraulic design of discharge structure:
Optimization of the diffuser characteristics and features to improve the internal hydraulic performance and operational demands. This analysis is based on pipe hydraulics, where manifold processes dominate.

The design and the extraordinary construction conditions for submarine installations will not be covered here, though also mainly derived from hydraulic models for the analysis of wave and current resistance loadings and further risks (scour, anchor, earthquakes, and tsunamis).

3 Governing equations: assumptions and simplifications

Effluent flow and effluent mixing follows conservation principles. The governing equations are generally derived for an infinitesimal control volume in a Cartesian coordinate system and are valid everywhere. The governing equations are the continuity equation, the Navier-Stokes equation and the transport equation (Ferziger and Peric, 2002):

Continuity equation - conservation of mass

$$\frac{\partial \rho}{\partial t} + \frac{\partial(\rho u_i)}{\partial x_i} = 0 \quad (3.1)$$

where ρ = density, t = time, u_i = velocity vector, x_i = location vector.

Momentum equation - conservation of forces and momentum

$$\underbrace{\frac{\partial(\rho u_i)}{\partial t}}_{\text{local acceleration}} + \underbrace{\frac{\partial(\rho u_j u_i)}{\partial x_j}}_{\text{advective acceleration}} + \underbrace{\rho 2\Omega_i \times u_i}_{\text{Coriolis acceleration}} = - \underbrace{\frac{\partial p}{\partial x_i}}_{\text{pressure force}} - \underbrace{\rho g_z}_{\text{gravitational force (hydrostatic)}} + \underbrace{\mu \frac{\partial^2 u_i}{\partial x_j^2}}_{\text{viscous stress}} + \underbrace{F_{i,e}}_{\text{external forces}} \quad (3.2)$$

where Ω = earth rotation vector, p = pressure, g_z = gravitational acceleration acting against the vertical, μ = dynamic viscosity, $F_{i,e}$ = external forces. The equation follows from Newton's second law, $F = ma$, where the left-hand side of equation (3.2) consists of acceleration terms per unit volume (if the density is factored out) and the right-hand side of force terms per unit volume.

Transport equation - conservation of dissolved substance

$$\frac{\partial c}{\partial t} + \frac{\partial(cu_i)}{\partial x_i} = D_m \frac{\partial^2 c}{\partial x_i^2} + kc \quad (3.3)$$

where c = substance concentration, D_m = molecular diffusion coefficient and k = decay or growth function.

For most of the hydrodynamic problems and especially for discharge processes, it is not possible to solve these exact equations. However, engineering design does not necessarily demand exact solutions, but safe and reliable approximations. Additional safety factors furthermore account for inaccuracies in constructional techniques (there is no exact construction) and for uncertainties of the interaction with the environment of the installation, (nature cannot be predicted exactly). Therefore, scale analysis is used to make assumptions and approximations based on characteristic scales occurring in the problem (Ferziger and Peric, 2002). Results are simplified equations, which can be solved either numerically or, in rare instances analytically. However, the definition or finding of characteristic scales is strongly problem or

process dependent. There is no unique characteristic scale for waste discharges, but there are characteristic scales for each hydrodynamic region dominated by distinct processes. Therefore, one could try to find a common denominator heading for a final unique equation set, or one could try to develop as much equation sets, as hydrodynamic regions exist. The result then will not be a unique equation set, but as much equations sets as hydrodynamic regions exist. There is still a scientific and engineering controversy, if a unique equation set based on one common characteristic scaling can be solved with sufficient accuracy or if different coupled equation sets may solve the problem in equal or even better accuracy. Both approaches will be discussed here.

3.1 General simplifications for coastal discharges

The following simplifications are valid for all hydrodynamic regions of waste discharges considered in this text:

Single-phase flow: This thesis will not cover multi-phase flows (e.g. air-water or particle-water), thus only describe the liquid phase.

Incompressible fluids: Waste discharges occur in hydrodynamic regimes where fluids can be considered as incompressible. This means that the density ρ is constant along a streamline. This approximation is valid for velocities and pressures occurring in environmental flows, provided that the Mach number is below 0.3 (Ferziger and Peric, 2002). The only exception is water-hammer in artificial pipe-systems, which will be discussed separately.

Newtonian fluids: Water (even when heated and with typical seawater or wastewater properties) is a Newtonian fluid. Therefore, approximations for the viscous terms of the momentum equation can be used. An example for a non-Newtonian fluid would be mudflow processes, where other approximations have to be used. Furthermore the dynamic viscosity can be approximated as a constant if temperature differences are not exceeding $\Delta T = 100^\circ\text{C}$, which is clearly the case in this study.

Boussinesq approximation: Density variations ρ' in natural flows are generally small compared to the average density $\bar{\rho}$, thus $\rho'/\bar{\rho} \ll 1$. Therefore, it is only necessary to retain density differences, thus simplifying the equations for decomposed parameters.

Spatial and temporal approximations: Reducing the dimensionality of a problem and/or increasing the time scales, probably have the strongest implications on simplifying and accelerating problem solutions. However, these are also related to crucial changes of accuracy. Therefore, both simplifications are discussed in more detail as follows.

3.2 Simplifications regarding spatial scales

3.2.1 Effect of earth rotation

For very large scales, forcing due to earth rotation (Coriolis force) may have significant influence on the flow and transport characteristics. The Rossby Number

$$Ro = \Omega L / (2\pi \bar{u}) \quad (3.4)$$

where $\Omega = 7.29\text{E-}05 \text{ 1/s}$ = earth rotation speed, L = characteristic length scale, \bar{u} = average characteristic velocity, allows distinguishing between flows where rotation is important or not. If the Rossby number is of the order of one, rotation has to be considered.

For example, if a characteristic average velocity of approximately 0.1 m/s is assumed for ocean currents, earth's rotation is important if scales larger than $L > 8.6 \text{ km}$ are considered. Therefore, in accordance with typical scales of waste discharges (Fig. 13) the earth's rotation is only important for the far-field region. Near-field and intermediate-field equation sets can be simplified neglecting effects of earth rotation.

3.2.2 Shallow water approximation - hydrostatic assumption

If the water depth H is much smaller than the characteristic horizontal length scale L , $H/L \ll 1$, vertical accelerations are dominated by gravitational accelerations and other contributions of accelerations can be neglected. This results in the so-called hydrostatic assumption reducing the governing equations significantly, i.e. the vertical components, thus leaving only the term $\partial p / \partial x_3 = -\rho g$. One may even eliminate the pressure variable writing it as a function of the water surface elevation z_s (assuming constant density, DVWK, 1999),

$$\frac{\partial p}{\partial x_i} = -\rho g \frac{\partial z_s}{\partial x_i}, \quad (3.5)$$

using in addition a depth averaged continuity equation for the unknown water level elevation. The vertical velocity then results from the continuity equation. Thus, immediate effects of buoyancy on the vertical flow cannot be considered. Vertical density differences only affect horizontal pressure gradients. Therefore small-scale convective mixing, occurring when less dense water ascends through the water column (a typical near-field process), cannot be resolved with that assumption.

Assuming an average characteristic depth for waste discharges to be from 10 - 50 m and the water body to be shallow for $H/L < 0.2$ the hydrostatic assumption is only valid for characteristic problem scales L larger than approximately 200 - 1000 m. Therefore, in accordance with typical scales of waste discharges (Fig. 13) hydrostatic assumptions are only valid for the far-field region. For the near-field region instead, or problems related to steep vertical gradients (bathymetrical slopes $> 1:8$, DVWK, 1999) or strong internal waves this assumption is not valid.

3.2.3 Spatial averaging: 1, 2 or 3 dimensions

If flows are even more constrained than described for shallow flows (chapter 3.2.2) and accelerations and forces are dominated by one or two components, the accelerations and forces of the other components can be neglected as a whole. In analogy to shallow flows, characteristic length scales are used to distinguish if these rather strong simplifications are valid.

Manifold flows are generally described with 1-D equation sets only. This can be justified assuming a characteristic length of an outfall pipe to be in the order of $L \approx 100\text{s}$ of meters and a diameter of $D \approx 1 \text{ m}$ resulting in $D/L \ll 1$.

Near-field flows are generally dominated by fully 3-D motions, only very simple cases can be described by one or 2-D equation sets (e.g. 1-D description valid for a single, non-buoyant

turbulent jet discharging in infinite uniform and stagnant environment and a 2-D description for multipoint diffuser plumes after merging, discharged into a steady, uniform environment).

Far-field flows in receiving waters are characterized by two-dimensional (2D, depth-averaged) or three-dimensional (3D) unsteady flow and transport phenomena resulting from tidal and meteorological forcing, including the effect of density differences due to a non-uniform temperature and salinity distribution (density-driven flow). A depth-averaged approach (2D) is thus only appropriate, if the fluid is vertically homogeneous. Examples in which the two-dimensional, depth-averaged flow equations can be applied are tidal waves, storm surges, tsunamis, harbor oscillations (seiches) and transport of pollutants in vertically well-mixed flow regimes. Three-dimensional modeling is of particular interest in transport problems where the horizontal flow field shows significant variation in the vertical direction. This variation may be generated by wind forcing, bed stress, Coriolis force, and bed topography or density differences. Examples are dispersion of waste or cooling water in lakes and coastal areas, upwelling and downwelling of nutrients, salt intrusion in estuaries, fresh water river discharges in bays, thermal stratification in lakes, seas, and strong wind shear.

3.3 Simplifications regarding time scales

3.3.1 Steady flow

If the flow does not change with time, or only very slowly, derivations related to time are negligible $\partial/\partial t = 0$, thus allowing for considerable simplifications of the governing equations. A measure to distinguish if unsteady effects are important is the comparison of typical time scales of changes at the boundaries and time scales of the system to react (accelerate or decelerate). If the latter are small compared to the former unsteady effects are negligible.

Manifold flows are generally described as steady. This can be justified assuming that outfall inflow changes and receiving water level changes are in the order of minutes to hours and times to accelerate or decelerate pipe flows are in the order of seconds to minutes (see detailed discussion in 4.2.4.1).

Similar assumptions apply for near-field flows and partly also for intermediate flows, for considerable ambient flow. However, for still water conditions or quiescent ambient time scales of intermediate field motions to accelerate or decelerate (i.e. buoyant spreading) may be considerably larger than the changes of the flow. Thus, the simplification of steady flow conditions should only be applied for the equation sets regarding the near-field region.

The far-field region is generally highly transient, notably tidally influenced flows, and no simplification applies.

3.3.2 Time averaging - simplification of turbulent fluctuations

Regarding the small-scale temporal variations, it is still very difficult to resolve up to the turbulence scales (Kolmogorov scale) and very often, there is no need for, because only temporal averaged values are needed. Therefore techniques to decompose the velocity in average values \overline{u}_i and turbulent fluctuations u_i' are used. The flow is hereby assumed stationary over the integral time scale t_I and the "Reynolds Average" equations are obtained by substituting the Reynolds decomposition $u_i(t) = \overline{u}_i + u_i'(t)$ and averaging over t_I . Thus, decomposition tech-

niques apply if the average velocities \overline{u}_i are changing in time scales bigger than the integral time scale t_i . The resulting simplified equations still need further approximations for the turbulence closure, before being solved numerically.

Regarding the characteristic scales of all hydrodynamic regions of waste discharges, Reynolds averaging using above decomposition in the governing equations theoretically applies for all regions. However, problems exist describing appropriate turbulence closures, thus limiting these solutions to flow conditions where available turbulence models exist and apply. There is no standard closure and the choice of the turbulence closure is strongly oriented to the application. Most experience exists for the classical statistical eddy-viscosity models, but nowadays also computationally more demanding approaches like the Large-Eddy-Simulation or Reynolds-stress models are used (Rosman, 1987, DVWK, 1999, Rodi, 2004). These approaches are still considered as research approaches but are indeed necessary for extreme complex geometries, high buoyancy effects, or swirling flows, which might occur in near-field regions. However, the far-field region generally does not require these approaches. This is because far-field waste discharges analysis does still not require analysis of vortex shedding frequencies or flow separation zones, which would demand these model types. An overview of existing approaches and their performance related to specific problems is given in Table 8. Details of the $k-\varepsilon$ model are described for the far-field modeling in chapter 5.3.2.1.

performance	eddy-viscosity ($k-\varepsilon$)	eddy-viscosity ($k-\omega$)	large-eddy (LES)	Reynolds-stress (RS)
well for...	<ul style="list-style-type: none"> local equilibrium of turbulence structure, e.g. free flow turbulence 	<ul style="list-style-type: none"> adverse pressure gradients (i.e. near walls) 	<ul style="list-style-type: none"> external unsteadiness (vortex shedding) unsteady forces 	<ul style="list-style-type: none"> non-equilibrium turbulent structures (swirling flows, high buoyancy, geometrical complexity)
bad for...	<ul style="list-style-type: none"> adverse pressure gradients (i.e. near walls) curved flows non-isotropic turbulence low Re 	<ul style="list-style-type: none"> free flow turbulence (far-field) strong buoyant processes (cause bad mixing characteristics in near-field) 	<ul style="list-style-type: none"> difficult boundary conditions (insufficient vortex information) near walls 	<ul style="list-style-type: none"> difficult boundary conditions (needed for each stress component)
problems	<ul style="list-style-type: none"> excessive turbulence production in stagnation points 	<ul style="list-style-type: none"> limited experience for practical applications 	<ul style="list-style-type: none"> expensive only few models available and still under development, but promising for future applications 	<ul style="list-style-type: none"> expensive available models still not universal enough to compete with eddy-viscosity in practical applications

Table 8: Comparison of different turbulence modeling approaches (Rodi, 2004)

3.4 Simplifications regarding boundaries

Waste discharge problems are spatially limited regarding the process scales, but also regarding the region of interest. Thus, the problem domain for the equations sets is constrained by natural and artificial boundaries. The former are defined as closed boundaries, where no flow across the boundary is assumed. The latter are boundaries limiting the region of interest, but without any physical meaning (i.e. allowing the flow to pass). The solution of the governing

equations (regardless of their simplification) requires the definition of boundary conditions at all boundaries.

3.4.1 Closed boundaries

Closed boundaries are defined by the pipe walls, the known shoreline, the bathymetry, and the free water surface, where the flow through the boundary is set to zero. The vertical diffusive flux through the free surface and bed is also set to zero except for the heat flux through the free surface.

Shear stresses act on all closed boundaries. However, for the far-field region often only the bed shear is important, whereas the influence of the lateral shear stresses along the lateral boundaries may be neglected. Latter approximation applies generally for shallow flows, where a so-called free slip boundary condition is set at all lateral boundaries. Approximations related to the bed shear formulation, like

$$\tau_b = \rho \nu \frac{\partial u}{\partial z} \quad (3.6)$$

with τ_b = bed-shear stress, ν = kinematic viscosity, may be useful, if the bed shear stress cannot be resolved near boundaries. This because strong velocity gradients occur in relatively short distances from the wall and laminar regions exist, where standard turbulence models, like the k - ϵ turbulence model fail due to a wrong turbulence damping. In these cases or in cases where universal velocity distributions apply (i.e. in pipe flows) wall-functions simplify the problem. Common wall functions relate the bed shear stress to the current just above the bed and universal velocity distributions at the wall are used (i.e. the Newton-Taylor approach (DVWK, 1999)):

$$\tau_b = \rho r \overline{u_i} \left| \overline{u} \right| \quad (3.7)$$

where r = dimensionless roughness coefficient. For $r = \lambda/8$ this results in the Darcy-Weisbach equation with λ defined after Colebrook-White depending on the Reynolds number Re and the equivalent sand roughness. The definition of λ will be discussed in detail in chapter 4.2.2.

Regarding wind-shear at the free surface a formulation analogous to bed-shear is

$$\tau_w = \rho_a c_d W_i |W| \quad (3.8)$$

where W = wind velocity in 10 height above the surface, ρ_a = density of air, c_d = wind drag coefficient.

The free surface in addition is influenced by waves. Flow contributions from wave-induced flows (e.g. Stokes-waves or due to asymmetry of waves) are generally negligible in all hydrodynamic regions. Nevertheless, waves can have considerable effect near the bed or in the surf-zone, which is especially important if particle settling is of interest. Neves (2003) described that deposition of fine matter might be prevented by wave motions, thus identifying waves as an important process for predictions of benthic impacts. This is not the objective of this study, thus the equation sets do not need to resolve short waves and can be simplified.

3.4.2 Open boundaries

Open boundaries are boundaries in the mathematical model with no physical meaning. In nature, waves can cross these boundaries unhampered and without reflections. In a mathematical model, this property must be included in the open boundary conditions. If the incoming characteristic at an open boundary is not prescribed exactly, the outgoing characteristic will reflect at the boundary and propagate as a disturbance into the area (Courant and Hilbert, 1962). Unfortunately this information is not available and consequently the incoming characteristic not known. It is therefore almost impossible to represent the open boundaries in an accurate way. Nonetheless influences of inaccurate boundary conditions can be minimized by choosing them as far away from the observed project region and choosing a location where flows are easier to describe. Thus, subcritical flows and perpendicular flows are a good modeling practice.

- Governing equations -

4 Multiport diffuser design program - CorHyd

Good outfall design must consider the hydraulics outside and inside a diffuser. External hydraulics affects the effluent mixing with the ambient fluid. Given dilution requirements hereby result in major choices for the riser/port spacing and diameter and a minimum diffuser length. Internal hydraulics affects the flow partitioning and related pressure losses in the manifold resulting in a discharge profile along the diffuser. The computer program developed in the course of this work, CorHyd, covers the internal diffuser hydraulics, predicting velocities, pressures losses, and flow distribution for varying discharge and ambient conditions. The integration of CorHyd into the mixing zone expert system CORMIX (Jirka et. al, 1996) will provide a direct linkage to subsequent waste plume modeling. This will allow for evaluations of design alternatives regarding a cost effective internal hydraulics design, environmental sound solutions, and operational feasible systems.

Recent monitoring of diffuser installations showed that inadequate attention to the internal diffuser hydraulics often lead to hydraulic problems like partial blockage (Fig. 16), high pressure losses, uneven flow distribution and salt water intrusion (Bleninger et al., 2003, Domenichini et al., 2002, Neville-Jones and Chitty, 1996a, b). Consequences are higher energy demands on one hand but also increased public health and environmental risks due to reduced effluent dilutions. A simple estimate of effects from a distorted discharge profile is a comparison of the centerline dilution for two different volume fluxes. A 10% discharge variation along the diffuser line results in a dilution difference of 7%. Neither laboratory studies nor field studies exist for that phenomena, though for example Faisst et al. (1990) proposed strongly inclined diffusers as source for observed parallel plume layers at different depths for the Vancouver outfall.



Fig. 16: Replaced diffuser, blocked with sediment (courtesy of Eng. Pedro Campos, Chile)

Internal diffuser hydraulics design objectives are:

- *uniform discharge distribution along the diffuser* in order to meet dilution requirements and to prevent operational problems (e.g. intrusion of ambient water through ports with low flow). Exceptions should avoid near-shore impacts by keeping the seaward discharge higher.
- *minimized investment and operation and maintenance costs* using simple, flow optimized manifold geometries causing small pressure losses

- *prevention of off-design operational problems* like particle deposition or salt-water intrusion in the pipe system. This requires full flowing pipe sections and reasonably high velocities.
- *robustness to unsteady operation conditions* in order to reach steady flow condition after short purging during start-up periods, optimized intermittent pumping cycles and considerations of wave induced circulations and transients.

These conflicting design parameters require compromises, in many cases not sufficiently resolved (Bleninger et al., 2004). Existing diffuser hydraulic programs (Fischer et al., 1979, implemented as code PLUMEHYD; and Wood et al., 1993, implemented as DIFF) have deficiencies for diffuser designs other than pipes with simple ports in the wall. They only consider short risers with negligible friction and local pressure losses and lack the implementation of long risers (like in deep-tunneled outfalls) with significant frictional and local pressure losses, Y-shaped diffusers, complex port/riser configurations like rosette like arrangements, multiple ports on one riser, duckbill valves or other port pressure losses. In addition, available design rules regarding velocity ratios (Fischer et al., 1979) or loss ratios (Weitbrecht et al., 2002) for diffuser sections and downstream ports are only applicable for simple and uniform geometries (i.e. no geometrical changes along the diffuser). For others, unnecessarily conservative designs are achieved, because velocities and pressure losses may change in an irregular manner along the diffuser line in actual diffuser installations.

4.1 Multiport diffuser configurations

An outfall is a pipe system between the dry land and the receiving water. It consists of three major components (Fig. 17): the *onshore headworks* (e.g. gravity or pumping basin); the *feeder pipeline* that conveys the effluent to the discharge area; and the *diffuser section* (Fig. 18), where a set of openings releases and disperses the effluent into the water body. The diffuser section can be a single branched or double branched system (T- or Y-shaped, Fig. 19), buried, tunneled or laid on the seabed (Fig. 20). If the diffuser section is installed open on the seabed it consists of port orifices in the wall of the diffuser pipe (simple port configuration, Fig. 21a), which may carry additional elements like elastic, variable area orifices (duckbill valves, Fig. 21b). If diffusers are covered with ballast, laid in a trench or even tunneled in the ocean floor, vertical risers (riser/port configuration, Fig. 21c) are connected to the diffuser to convey the effluent to the water body. For deep-tunneled solutions often rosette-like port arrangements (similar to a gas burner device, Fig. 21d) are used to save the number of costly riser installations. In addition, risers may carry duckbill valves, which change their effective open port area related to the pressure difference between inside and outside the valve. They avoid salt-water intrusion during low flow periods and allow high discharges during peak flow periods.

4.2 Internal diffuser hydraulics - manifold processes

The flow in multiport diffusers is a turbulent pipe flow controlled by two boundaries: first, the entrance boundary (flow rate or head), and, second, the ambient/discharge boundary, where the effluent properties differ from the ambient fluid. Both conditions vary in time due to discharge variations (diurnal changes, storm water events and long-term changes due to increased sanitation coverage) and ambient pressure variations caused by density and/or water level variations (tides or waves). However manifold flow time-scales are considerably smaller than the time-scales of boundary condition variations, thus a steady-state approach can be justified (a brief example on unsteady effects is shown in chapter 4.2.4.1).

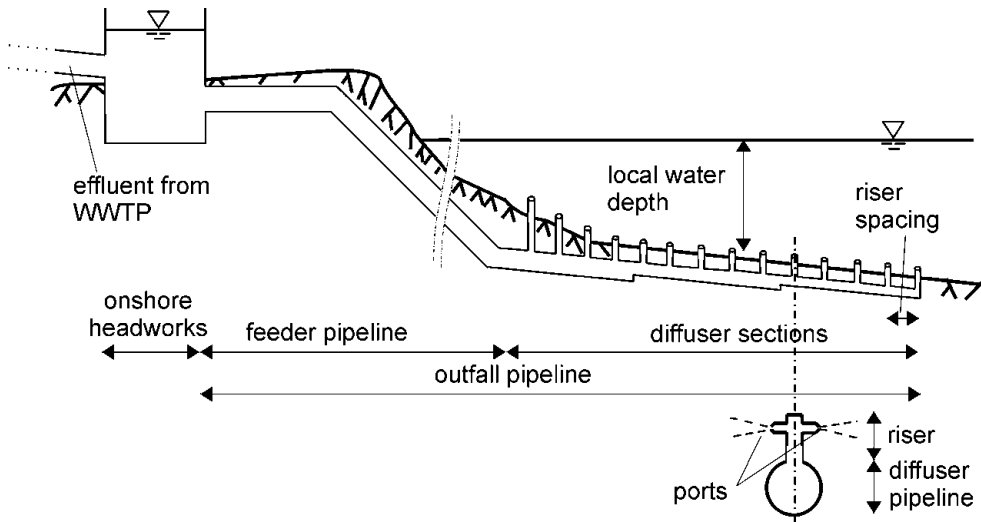


Fig. 17: Outfall configuration showing feeder pipe and diffuser from side view and top view, defining the pipelines and port/riser configurations



Fig. 18: Pictures of multiport diffusers during construction (Bonnasabla.com)

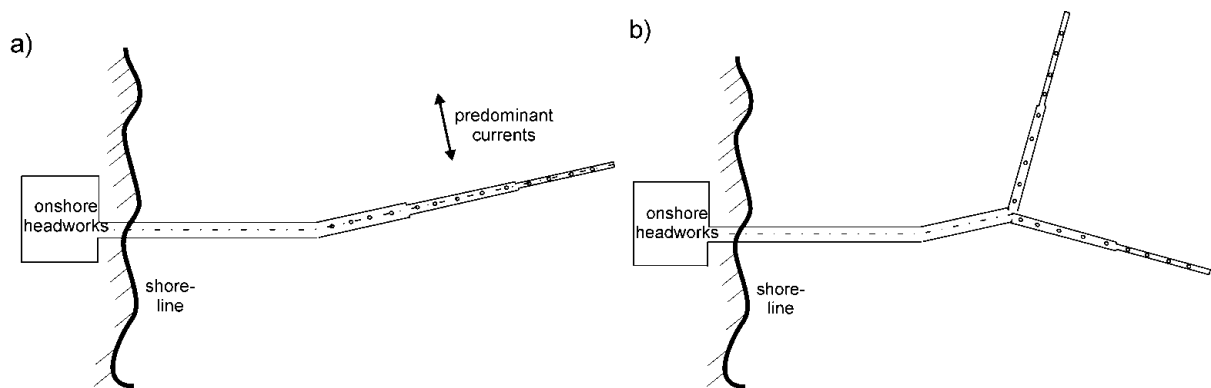


Fig. 19: a): standard diffuser; b): Y- or T-shaped diffuser configuration

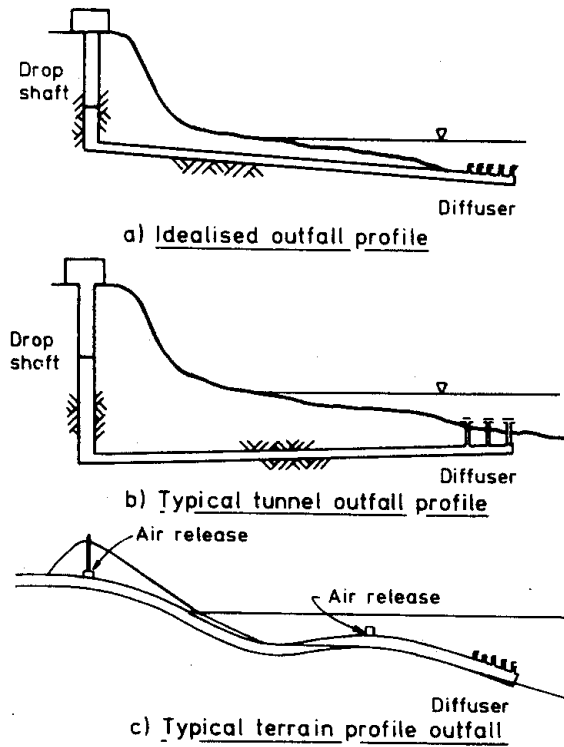


Fig. 20: a) Buried outfall with short riser; b) tunneled outfall with long riser and multiple ports; c) terrain following outfall laid on seabed (reproduced from Davies, 2003)

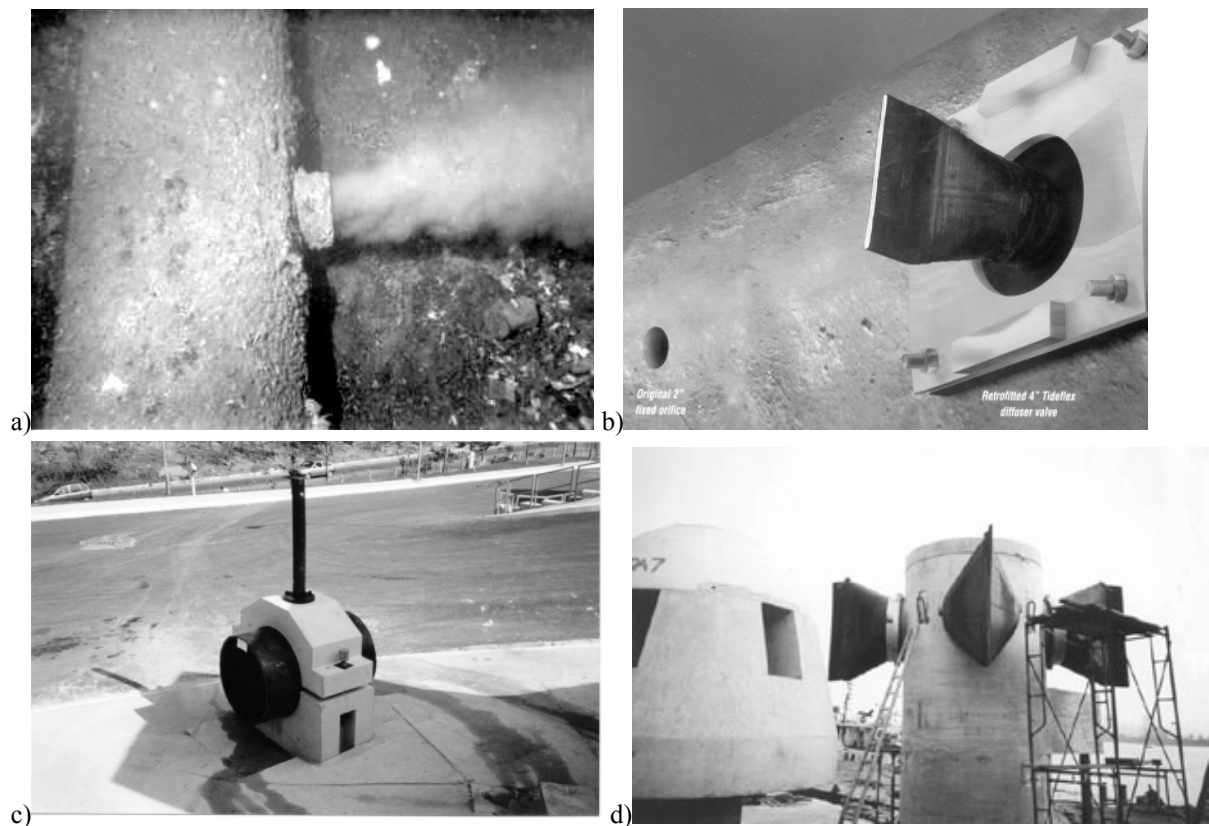


Fig. 21: a) simple port (courtesy of Carlo Avanzini); b) variable-area orifices ('duckbill valves', RedValve Company); c) riser/port configuration (Guarujá, Brazil); d) rosette like riser / port arrangement (Lee et al., 2001)

4.2.1 Governing equations for turbulent pipe flow

The definition diagram for a general steady pipe flow is shown in Fig. 22, for a pipe in a Cartesian coordinate system. For means of scale analysis and measurement techniques (piezometer tubes), it is convenient to define pipe flow parameters in length scales (heads). There is the diameter D , the geodetic head z , the pressure head p/γ_e with the internal pressure p and the effluent specific weight γ_e , the velocity head $V^2/2g$ with the mean pipe flow velocity V . The sum of the geodetic and the velocity head is called the hydraulic head, whereas the sum of the hydraulic head and the velocity head is defined as the energy head. The description of the hydraulic and the energy head along the streamwise coordinate s are called hydraulic grade line (hgl) or energy grade line (egl), respectively. Consequently, the difference of energy heads between two locations 1 and 2 is defined as the headloss h_ℓ .

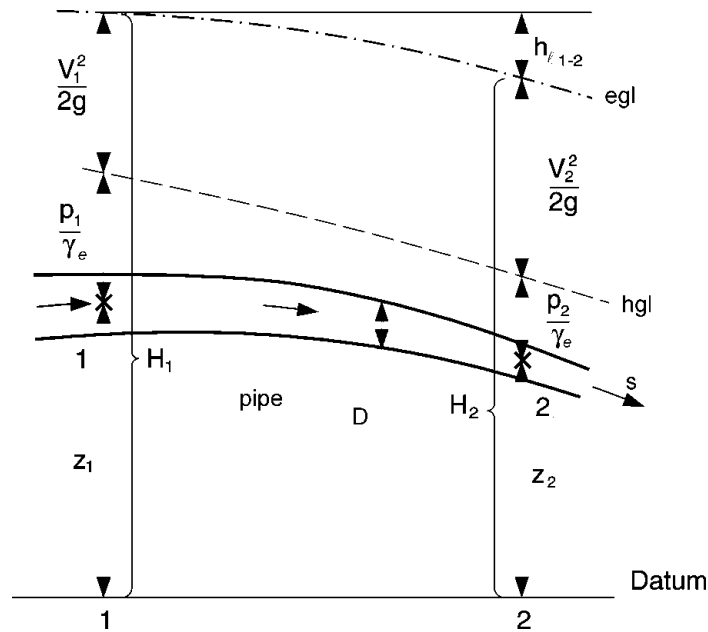


Fig. 22: Definition diagram for a general pipe flow (reproduced from Jirka, 2001)

Flows in pipe systems can be classified into laminar and turbulent flows by the pipe Reynolds number $Re = VD/v_e$ with the kinematic viscosity of the effluent v_e . Pipe flows with Reynolds numbers above a critical Reynolds number $Re_{crit} \approx 2000$, are considered as turbulent flows, which is essentially the case for wastewater pipe systems.

The governing equations for such a pipe system can either be derived from the Navier-Stokes equations (equations 3.1 and 3.2) for a 1-D flow, by integrating the shear-stresses over the wall surfaces) or by using energy conservation principles together with mass conservation. The latter is probably more convenient because of better parameterization means for the turbulent fluctuations. The derivation of the so-called work-energy equation is described in Jirka (2001) in the dimensions of length (energy heads):

$$\alpha_1 \frac{V_1^2}{2g} + z_1 + \frac{p_1}{\gamma_e} + h_p = \alpha_2 \frac{V_2^2}{2g} + z_2 + \frac{p_2}{\gamma_e} + h_t + h_\ell \quad (4.1)$$

where h_p is an energy head input into the system, generally caused by mechanical energy inputs of pumps. h_t is an energy extraction head, generally from turbines. α_1 and α_2 denote coefficients related to the non-uniformity of velocity profiles while using mean velocities only:

$$\alpha = \frac{1}{A} \int_A \left(\frac{V}{\bar{V}} \right)^3 dA \quad (4.2)$$

Uniform velocity profiles would result in $\alpha = 1$, whereas typical non-uniform turbulent pipe flow profiles result in $\alpha = 1.05$. The definition of h_ℓ can be seen as the turbulence closure for pipe flow hydraulics. The dissipation of turbulent kinetic energy causes heat losses in the system. This energy loss is compensated by decreasing pressure. Pressure losses in pipe flows are classified according the source of turbulence production in continuous pressure losses due to wall friction and local pressure losses due to geometrical changes. Wall friction causes cross-sectional flow non-uniformities, whereas geometrical changes cause streamwise flow non-uniformities.

Mass conservation results in the continuity equation:

$$Q_1 = Q_2 \Leftrightarrow V_1 A_1 = V_2 A_2, \quad (4.3)$$

where A denotes the pipe cross-sectional area.

4.2.2 Friction losses - cross-sectional non-uniformities

Pipe flows are axisymmetrical with a linear shear-stress distribution (Fig. 23). Therefore, universal definitions for the velocity and shear-stress distributions apply. The velocity distribution can be approximated by a logarithmical profile, in practice often simplified with power laws in the form of $V/V_{max} = (y/r_o)^m$, where V_{max} defines the maximum velocity, y the transversal coordinate, r_o the pipe radius and m the power (e.g. $m = 1/7$ for $Re = 10^5$ (Jirka, 2001)).

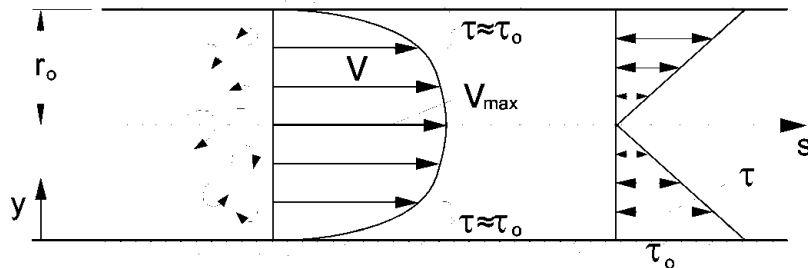


Fig. 23: Shear-stress in pipe flows (reproduced from Jirka, 2001)

Using the wall function from equation (3.7) results in a definition for the wall-shear stress τ_o :

$$\tau_o = \frac{\lambda}{4} \rho \frac{V^2}{2} \quad (4.4)$$

or in terms of a friction headloss in the so-called Darcy-Weisbach equation:

$$h_{\ell,f} = \lambda \frac{L V^2}{D 2g} \quad (4.5)$$

where L = the length of the considered pipe section and λ = the friction coefficient defined by the Colebrook-White equation.

The friction coefficient λ describes the relative influence of fluid viscosity and wall roughness by the dimensionless parameters k_s/D with the equivalent sand roughness k_s (after Nikuradse) and the Reynolds number Re . For laminar flows it is possible to derive λ analytically to $\lambda = 64/Re$ (for $Re < 2000$). However, for turbulent flows only empirical values from experimental studies exist. For computer applications, an explicit formulation after Swamee and Jain (1976) is used λ :

$$\lambda = \frac{0.25}{\left(\lg\left(\frac{k_s}{3.7D} + \frac{5.74}{Re^{0.9}}\right)\right)^2}, \quad (4.6)$$

which is valid for $10^{-6} < k_s/D < 10^{-2}$ and $10^3 < Re < 10^8$

Values of k_s for different pipe materials and surface conditions of use are listed in Table 9. Further materials and conditions are listed in almost all hydraulics textbooks or are available from pipe manufacturers. A comprehensive summary is given in Idelchik (1986).

material	condition	k_s [mm]
steel		
HDPE (high density polyethylene)	new	0.0015 - 0.0070
	used	0.2 - 0.5
cast iron	new	0.25 - 1
	used (corroded)	1 - 1.5
	old (heavily corroded)	3 - 4.5
	with deposits	2 - 4
reinforced concrete	new (smoothed)	0.3 - 0.8
	new (average)	2 - 3
	with joints	2

Table 9: Outfall pipe materials and their related equivalent sand roughness values k_s (Idelchik, 1986)

If only Manning's n values are known from literature or pipe manufacturers a conversion to k_s can be done by:

$$k_s = (n \cdot 5.87 \cdot (2g)^{0.5})^6 \quad (4.7)$$

4.2.3 Local losses - streamwise non-uniformities

Streamwise changes of the pipe system cause non-uniform streamwise velocities. Even gradual changes may hereby cause internal flow detachment processes, reverse currents in dead-zones, locally increased accelerations or decelerations and overall increased turbulence. This increase is associated with additional energy, thus pressure losses. Typical geometrical differences occurring between one cross-sectional area and the adjacent one are inlets at the headworks (Fig. 24) or orifices at the outlet ports, pipe diameter expansions, contractions, bends, or combining and dividing flows (Fig. 24).

Local pressure losses $h_{\ell,\ell}$ are generally parameterized as:

$$h_{\ell,\ell} = \zeta \frac{V^2}{2g} \quad (4.8)$$

where ζ denotes the dimensionless loss coefficient.

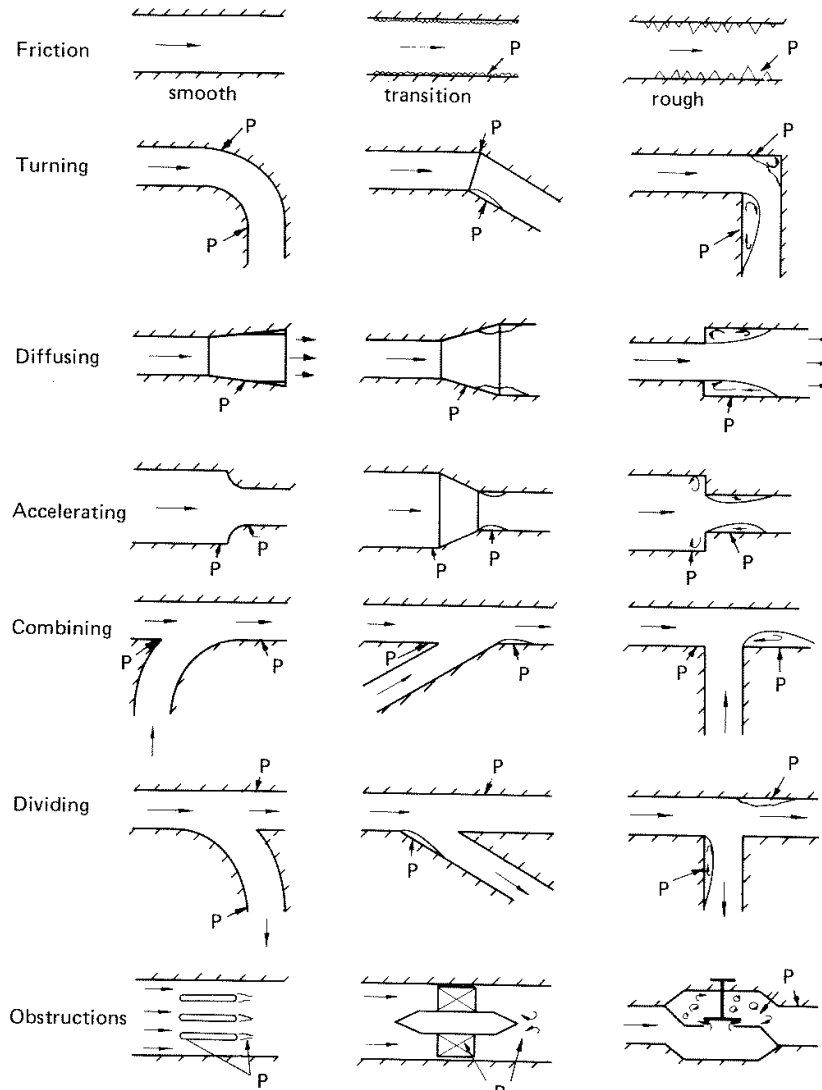


Fig. 24: Examples for local pressure losses in pipe flows (Miller, 1990)



Fig. 25: Picture of the headworks of a coastal outfall showing the inlet to the feeder pipe (courtesy of Carlo Avanzini)

ζ depends on the geometrical configuration (diameter ratios, angles and radii of bends, gradual or immediate (rounded or sharp edged) changes), and the Reynolds number. For combining and dividing flows additional consideration of the flow ratios have to be included. Again mainly empirical values are available, which have been obtained in laboratory studies. There

are numerous publications defining local loss coefficients ζ for a large number of different geometries under different flow conditions. Comparisons between some of these publications showed considerable discrepancies even for simple geometries. The most accurate works stem from Idelchik (1986) and Miller (1990), which have been chosen for this study. The few analytical solutions (e.g. for sudden expansions) are also included.

Annex A gives an overview of implemented local loss coefficients ζ . These coefficients assume reasonably high Reynolds numbers (above 10^4) and reasonable geometrical distance between the changes ($> 5D$) to avoid interaction of pressure losses. If needed, modification of the listed formulations can be found in Idelchik (1986). Furthermore, additional optional pressure losses, which are not considered here (e.g. obstructions due to valves or monitoring instruments), can be added manually. Examples for non-conventional nozzles or flanged orifices are therefore given in the Annex A.

Loss coefficients can be combined to reduce the amount of computation. The bulk loss coefficient is the sum of all coefficients, providing that the reference velocity is the same. Thus, all loss coefficients are being modified to refer to the same reference velocity V_{ref} . However, the velocity is an unknown quantity, but the flow rate Q in one pipe section does not change. The modified loss coefficient ζ_{mod} is obtained by:

$$\zeta_{mod} = \zeta \frac{V^2}{V_{ref}^2} = \zeta \left(\frac{Q/A}{Q/A_{ref}} \right)^2 = \zeta \left(\frac{A}{A_{ref}} \right)^2 \quad (4.9)$$

with A_{ref} being the cross-sectional area of the reference section.

4.2.4 Simplifications and modeling assumption

The whole pipe system is assumed as flowing full under all conditions. A two-phase flow due to air entrance at the inlet or a stratified flow due to saltwater intrusion at the outlets will not be considered here. However, CorHyd allows specifying the hydraulic conditions down to which flowrate a full flowing system can be guaranteed. Air entrance at the inlet is avoided by keeping the top pipe invert under the minimum sea level or using backpressure valves or deaeration chambers. Saltwater intrusion can be avoided by keeping the port densimetric Froude number larger than unity (Wilkinson, 1988):

$$F_p = \frac{V_p}{\sqrt{g \frac{\Delta\rho}{\rho} D_p}} > 1 \quad (4.10)$$

where V_p and D_p denote the port exit velocity and the port diameter respectively and $g\Delta\rho/\rho = g'$ the reduced gravity with the density difference $\Delta\rho$ at the port orifice between the effluent and the ambient water. This condition can be achieved by designing either small enough port diameters or using variable area orifices.

4.2.4.1 Steady flow assumption

Real manifold flow is an unsteady flow, where the driving head difference between the headworks and the ambient water level is changing continuously due to discharge variations and water level variations (i.e. tides). However, time scales of these variations are generally larger than time scales of the outfall and diffuser flow. It is therefore assumed, that unsteady

flow effects can be neglected in the calculation of the manifold flow, which is discussed in the following example:

For a steady inflow $Q_{in,a}$ into the headworks and a steady ambient water level H a steady water level elevation z_a is obtained in the headworks. The flow in a single port diffuser pipe is $Q = Q_{in,a}$ with velocity V_a (Fig. 26). Now an unsteady motion is assumed by increasing the inflow into the headworks ($Q_{in,b} > Q_{in,a}$) during the time Δt . This causes the water level in the headworks to rise to $z_b = z_a + \Delta z$. For short time-scales (e.g. pump switched on immediately) fast water level rises $\Delta z/\Delta t > 1$ may cause pressure waves including water hammer effects in the pipe system. These transients should be prevented by operational means (e.g. gradual pump start-up) keeping $\Delta z/\Delta t \ll 1$. For the latter case, the pressure waves are of small amplitudes and dissipate after a very short time (order of seconds) due to pipe elasticity and friction. A new pressure difference with higher headworks water level elevation z_b and unchanged ambient water level is developed (Fig. 27). However fluid inertia prevents the pipe flow to react immediately to increase from $Q_{in,a}$ to $Q_{in,b}$. The whole pipe flow needs time to accelerate. During that time the internal pressure in the outfall is generally higher than that for both flow rates $Q_{in,a}$ and $Q_{in,b}$. This additional pressure is needed to accelerate the fluid until equilibrium is reached. However, accelerations do not stop immediately at the equilibrium point and overshoot causing oscillations until steady conditions prevail again (Fig. 28).

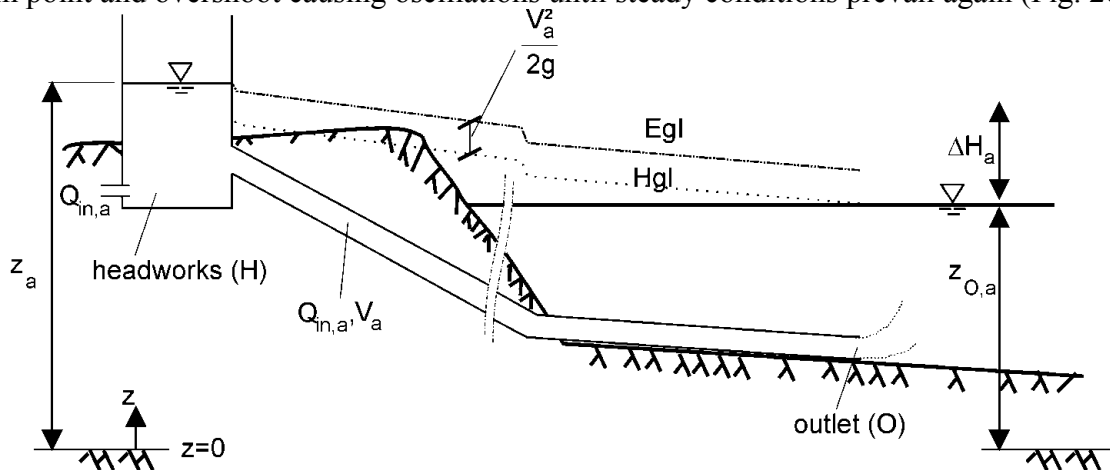


Fig. 26: Steady pipe flow with constant boundary conditions ($Q_{in,a} = const.$)

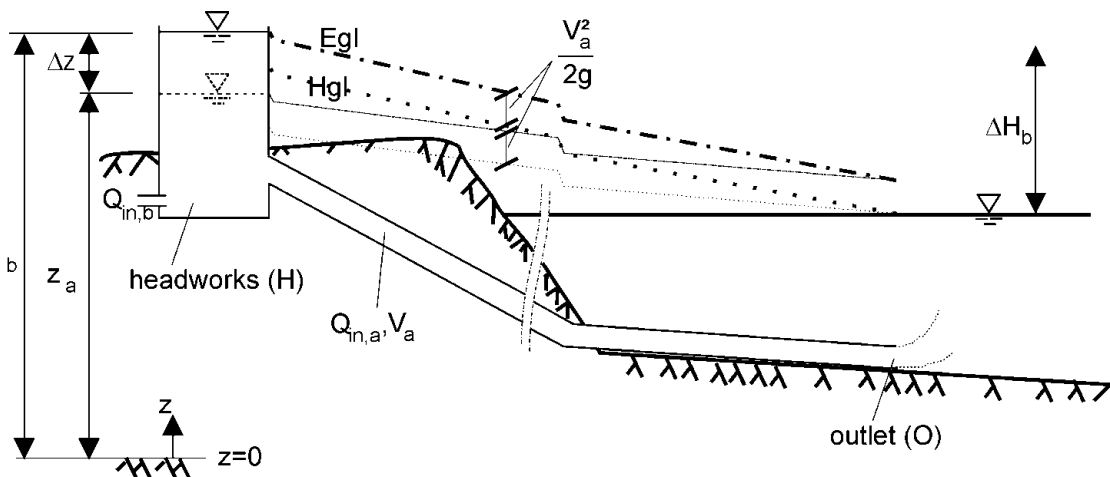


Fig. 27: Pipe flow immediately after a relatively fast change of the water level elevation in the headworks tank ($Q_{in,b} > Q_{in,a}$)

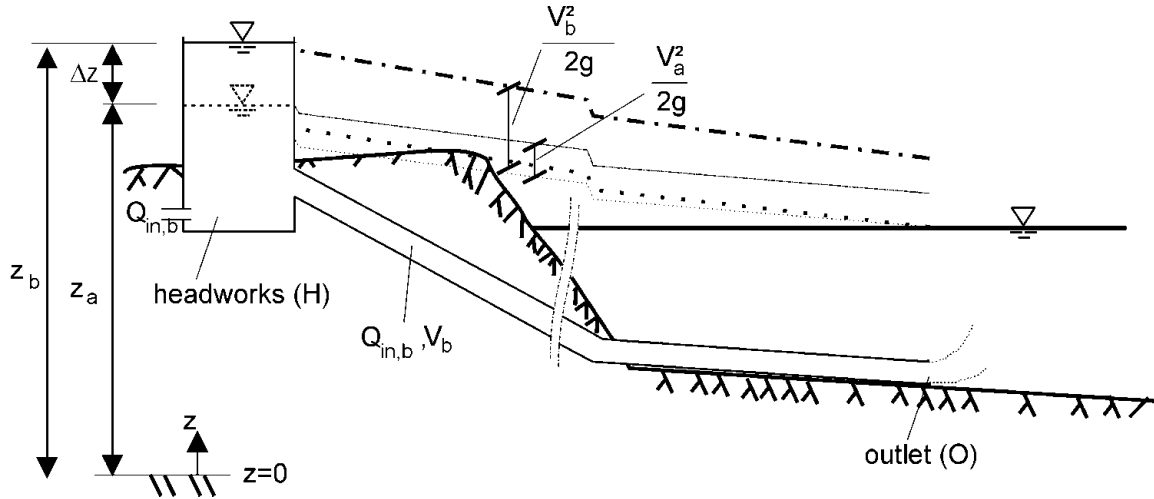


Fig. 28: Pipe flow after the acceleration of the whole fluid in the outfall took place

The time t during that accelerations take place is estimated by using the unsteady, but incompressible pipe flow equations along the coordinate s following a streamline:

$$\frac{1}{g} \frac{\partial v}{\partial t} + \frac{\partial E}{\partial s} = 0, \quad (4.11)$$

where E denotes the energy head.

Mass conservation for an incompressible fluid ($\partial \rho / \partial t = 0$) in an non-deformable pipe ($\partial A / \partial t = 0$) gives

$$\frac{\partial(\rho v A)}{\partial s} + \frac{\partial(\rho A)}{\partial t} = 0 \rightarrow \frac{\partial Q}{\partial s} = 0 \quad (4.12)$$

Assuming a pipeline with constant cross section A and length L the first term of equation (4.11) results in

$$\frac{1}{g} \frac{\partial v}{\partial t} = \frac{1}{g} \frac{dQ}{dt} \int_{s(H)}^{s(O)} \frac{1}{A} ds = \frac{1}{g} \frac{dQ}{dt} \frac{L}{A} = \frac{L}{g} \frac{dv}{dt}$$

moreover, the second term is

$$\frac{\partial E}{\partial s} = E_O - E_H + h_{l,f},$$

where E_H , the energy head at the headworks water level

$$E_H = \left(\frac{v_H^2}{2g} + \frac{p_H}{\gamma_e} + z_H \right) = z_a + \Delta z = z_b \quad (4.13)$$

and E_O , the energy head at the outlet related water level surface

$$E_O = \left(\frac{v^2}{2g} + \frac{p_O}{\gamma} + z_O \right) = \frac{v^2}{2g} + z_{O,a} \quad (4.14)$$

and $h_{\ell,f}$ the headloss due to friction is

$$h_{\ell,f} = r \left(\frac{v^2}{2g} \right) \quad \text{where } r = \lambda L/D \text{ and } \lambda \text{ the friction coefficient,} \quad (4.15)$$

all at the time right after the water level rise in the headworks, but before acceleration took place.

Substituting equations (4.13), (4.14) and (4.15) in (4.11) gives

$$\frac{L}{g} \frac{dv}{dt} + \frac{v^2}{2g} + z_{O,a} - z_b + r \left(\frac{v^2}{2g} \right) = 0. \quad (4.16)$$

Additionally, the terminal velocity v_b is defined as

$$z_{O,a} - z_b = -(1+r) \left(\frac{v_b^2}{2g} \right) \quad (4.17)$$

Substituting equation (4.17) solved for r in equation (4.16) and assuming a hydraulic rough regime, where λ is independent of the flow velocity gives

$$\frac{L}{g} \frac{dv}{dt} + \frac{v^2}{2g} + z_{O,a} - z_b - \left(\frac{(z_{O,a} - z_b)2g}{v_b^2} + 1 \right) \frac{v^2}{2g} = 0$$

$$\frac{L}{g} \frac{dv}{dt} + z_{O,a} - z_b - \frac{(z_{O,a} - z_b)v^2}{v_b^2} = 0$$

$$\frac{L}{g} \frac{dv}{dt} + (z_{O,a} - z_b) \left(1 - \frac{v^2}{v_b^2} \right) = 0$$

$$dt = \frac{L}{-g(z_{O,a} - z_b)} \frac{v_b^2}{v_b^2 - v^2} dv$$

$$\int_{t_a}^{t_c} dt = \frac{L}{-g(z_{O,a} - z_b)} \int_{v_a}^{v_c} \frac{v_b^2}{v_b^2 - v^2} dv,$$

$$t_c - t_a = \frac{Lv_b}{-g(z_{O,a} - z_b)} \left(\operatorname{arccoth} \left(\frac{v_c}{v_b} \right) - \operatorname{arccoth} \left(\frac{v_a}{v_b} \right) \right)$$

where $v_c = c v_b$, when the velocity ratio of the prevailing velocity v_c and the terminal steady velocity v_b is c .

For $t_a = 0$, t_c is the time needed to reach the velocity $v_c = c v_b$:

$$t_c = \frac{Lv_b}{-g(z_{O,a} - z_b)} \left(\operatorname{arccoth} \left(\frac{v_c}{v_b} \right) - \operatorname{arccoth} \left(\frac{v_a}{v_b} \right) \right)$$

or using $z_{O,a} - z_b = -(1+r) \left(\frac{v_b^2}{2g} \right)$ it is

$$t_c = \frac{2L}{(1+r)v_b} \left(\operatorname{arccoth}\left(\frac{v_c}{v_b}\right) - \operatorname{arccoth}\left(\frac{v_a}{v_b}\right) \right) \quad (4.18)$$

For example applying equation (4.18) for $c = 0.99$ and a 4 km long outfall an acceleration from $v_a = 0.6$ m/s to $v_c = 0.99 \cdot 1.2$ m/s takes approx. $t_c = 2$ min. until reaching a velocity 1% smaller than the terminal steady flow velocity $v_b = 1.2$ m/s. Thus, the order of t_c is relatively small compared to the order of time-scales of tidal water level variations at the outlet or in-flow variations at the inlet. It is therefore justified to assume steady flow conditions for the calculation of pressures, velocities and the discharge flow distributions of the diffuser manifold. The additional pressure during acceleration periods is hereby expected to be not available for changing local parameters (e.g. discharge at one specific port) because inertia of the whole water mass prevents especially those accelerations which are not directly related to the general flow changes.

However, extreme conditions during start-up or shutdown have to be considered in the headworks design, where sufficient storage capacities are needed for water level changes increasing faster than the fluid in the outfall accelerates. Decreasing discharges furthermore may lead to a situation, where moving fluid in the outfall sucks the effluent from the headworks even beyond the equilibrium level, and swinging back once the flow is entirely shut down, sucking seawater in the outfall (Burrows, 2001). Besides the necessity of subsequent outfall purging the latter has critical impacts on valves mounted on discharge ports.

Another critical situation might be related to wave motions in the ambient water, changing ambient pressure along the diffuser (wave crest above one riser and wave trough above other). These pressure differences can have effects on the flowrate distribution, if the fluid volume in the riser/port configuration is relatively small, compared to additional forcing (Mort, 1989).

4.3 CorHyd model

Three methodologies for the analysis of the internal hydraulics have been adopted by various authors. The first involves a 1-D pipe flow port-to-port analysis (Fischer et al., 1979, Wood et al., 1993) the second discretizes a fictitious porous conduit (French, 1972) while the third is based on solving the 2 or 3-D field equations on an Eulerian grid for every point of the diffuser (Shannon, 2002, Mort, 1989). The latter two have the advantage that unsteady, stratified flow (i.e. saltwater intrusion) calculations are easier to implement than into the port-to-port analysis. However, they have the disadvantage in defining appropriate local loss formulations for common or complex geometries. Besides numerical grid based calculations are very time consuming. This study focuses on a steady state pipe flow analysis without considerations of salt water purging or intrusion processes, which are covered elsewhere (Wilkinson, 1984, 1985; Wood et al. 1993, pp. 122, pp. 326; Wilkinson und Nittim, 1992; Burrows, 2001). The assumption of steady flows has been discussed in the previous chapter, justifying the choice of using a port-to-port analysis for CorHyd.

4.3.1 Governing equations

Manifold hydraulics is characterized especially by several flow separations, where local pressure losses not only depend on geometrical relations but also on the discharge ratios. For wastewater diffuser manifolds, discharge ratios furthermore are influenced by the pressure difference between the effluent and the ambient.

The governing equations are continuity equations (4.3) at each flow division and the work-energy equation (4.1) along pipe segments with constant or known flowrate (Fig. 29). Re-

quired input data are the geometries of the discharge structure with sets of diffuser pipe segment locations x, y, z , riser/port segment geometries (i.e. cross-sections A , riser/port number and allocation, and roughness k_s). Pipe lengths L and pipe joint configurations are calculated automatically out of these parameters. Indices used are 'd' for diffuser pipe sections, 'r' for riser sections, 'p' for port sections and 'j' for jet properties at the vena contracta of the discharging jet. The ambient fluid is described by its density distribution $\rho_a(z)$ and the average water level elevation H resulting in different external hydrostatic pressures $p_{a,i}$ at the vertical location of the jet centerline at the vena contracta at each i position along the diffuser pipe, where risers or ports are attached. The effluent is described by its fluid density ρ_e and either the total flowrate Q_o or the total available water level at the headworks (total head H_i).

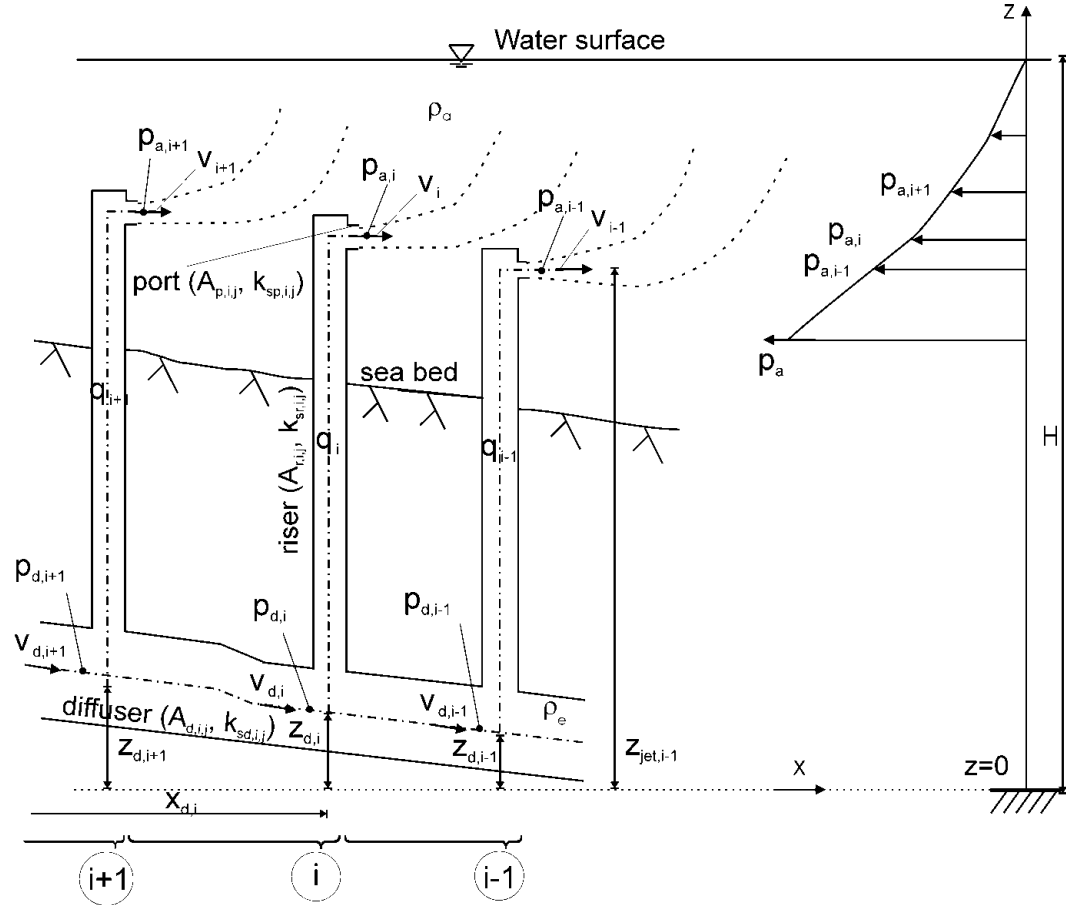


Fig. 29: Definition scheme for the port-to-port analysis: $p_{a,i}$ = ambient pressure, H = average ambient water level elevation, q_i = discharge through one riser/port configuration with velocity v_i at elevation $z_{j,i}$. $p_{d,i}$ = internal diffuser pipe pressure upstream a flow division (node) with diffuser pipe centerline elevation $z_{d,i}$ and horizontal pipe location $x_{d,i}$

Optional input fields are foreseen in the computer model to allow specifying more detailed information on unusual local pressure losses ζ_i , T- or Y-shaped diffuser configurations or the denomination of clogged or temporary closed ports. Implemented are all common local pressure losses, which are listed in Annex A. Therefore $\zeta_{p,i,j}$, $\zeta_{r,i,j}$, $\zeta_{d,i,j}$ denote the local loss coefficients for each j -component of the total number $n_{p,i}$ of pressure losses in a port, $n_{r,i}$ in a riser or $n_{d,i}$ in the diffuser pipe with pipe cross-sectional areas $A_{p,i,j}$, $A_{r,i,j}$ and $A_{d,i,j}$ respectively. $\lambda_{p,i,j}$, $\lambda_{r,i,j}$ and $\lambda_{d,i,j}$ denote the friction coefficients for related pipe components with length $L_{p,i,j}$, $L_{r,i,j}$ and $L_{d,i,j}$ diameter $D_{p,i,j}$, $D_{r,i,j}$ $D_{d,i,j}$ equivalent pipe roughness $k_{sp,i,j}$, $k_{sr,i,j}$, $k_{sd,i,j}$ respectively for either port, riser or diffuser component j . For each port or riser, the local and friction loss coefficients are determined iteratively, since they depend on the discharge.

To calculate the individual riser discharge q_i of such a system at the position i (Fig. 29) following considerations are in order:

- 1) The work energy equation (equation 4.1) is applied along a streamline following the diffuser pipe centerline. This results in equation (4.19). It equals the diffuser pressure $p_{d,i}$ directly upstream the port/riser branch with the known downstream diffuser pressure $p_{d,i-1}$ plus the known static pressure difference due to the elevation difference, plus the dynamic pressure difference plus the known pressure losses occurring in the main diffuser pipe. The pressure losses are divided into friction losses and local pressure losses like bends and diameter changes or the passage of a branch opening:

$$p_{d,i} = p_{d,i-1} + \rho_e g(z_{d,i-1} - z_{d,i}) + \frac{\rho_e}{2} v_{d,i-1}^2 - \frac{\rho_e}{2} v_d^2 + p_{\ell,d,i}, \quad (4.19)$$

where pressure losses $p_{\ell,d,i} = \frac{\rho_e}{2} v_{d,i-1}^2 \sum_{j=1}^{n_{d,i-1}} \left(\zeta_{d,i-1,j} + \lambda_{d,i-1,j} \frac{L_{d,i-1,j}}{D_{d,i-1,j}} \right)$, with loss coefficients related to the reference velocity $v_{d,i-1}$ (compare with chapter 4.2.3).

- 2) The continuity equation (equation 4.3) between i and $i-1$ allows specifying the velocities:

$$v_{d,i-1}^2 = \frac{1}{A_{d,i-1}^2} \left(\sum_{k=1}^{i-1} q_k \right)^2$$

$$v_d^2 = \frac{1}{A_{d,i}^2} \left(\sum_{k=1}^i q_k \right)^2$$

- 3) The work energy equation (equation 4.1) applied along a streamline following the branch pipe and leaving the diffuser through the orifice results in equation (4.20). It equals the upstream diffuser pressure $p_{d,i}$ with the ambient pressure $p_{a,i}$ plus the static pressure difference due to the elevation difference between diffuser centerline and jet centerline, plus dynamic pressure difference between the diffuser and one single jet plus the pressure losses occurring in all pipe segments between these points:

$$p_{d,i} = p_{a,i} + \rho_e g(z_{jet,i} - z_{d,i}) + \frac{\rho_e}{2} v_{p,i}^2 - \frac{\rho_e}{2} v_d^2 + p_{\ell,i}, \quad (4.20)$$

where pressure losses $p_{\ell,i} = \frac{\rho_e}{2} v_{p,i}^2 \left(\sum_{j=1}^{n_{p,i}} \left(\zeta_{p,i,j} + \frac{\lambda_{p,i,j} L_{p,i,j}}{D_{p,i,j}} \right) \right) + \frac{\rho_e}{2} v_{r,i}^2 \left(\sum_{j=1}^{n_{r,i}} \left(\zeta_{r,i,j} + \frac{\lambda_{r,i,j} L_{r,i,j}}{D_{r,i,j}} \right) \right)$, with loss coefficients related to the reference velocity $v_{r,i-1}$ (compare with 4.2.3).

- 4) The continuity equation (equation 4.3) between the diffuser and the port at position i allows specifying the velocities:

$$v_{p,i}^2 = \frac{\rho_e}{2(C_{c,i} A_{p,i})^2} (\alpha_i q_i)^2$$

$$v_{r,i}^2 = q_i / A_{r,i},$$

where the individual jet discharge for more than one port at a riser is defined as $q_{jet,i} = \alpha_i q_i$ with $\alpha_i = 1/(\text{number of ports at a riser at position } i)$, thus assuming that the discharge through one specific riser with multiple ports is homogeneously distributed among these ports. This is valid for ports with similar geometry at this diffuser position that are

mounted at the same elevation, what is common practice for multiport risers. Equation (4.20) therefore applies for multiple ports at one diffuser position or on the riser, but not for multiple risers at one location on the diffuser pipe, because constructional impractical. In addition $C_{c,i}$ defines the jet contraction coefficient either given by the user or calculated iteratively if Duckbill Valves are applied using $C_{c,i,DBV} = \alpha_i q_i / (V_{DBV,i} A_{p,i})$ with $V_{DBV,i}$ = the duckbill jet velocity, which itself depends on the discharge individual port discharge αq_i .

- 5) For the calculation of the pressure outside the diffuser p_a , namely at the port orifice location, it is important to consider the exact elevation z_{jet} , a vertical density distribution $\rho_a = f(z)$ and the elevation of the water level $z_o = H$.

$$\int_{p_o}^{p_a} dp = - \int_{z_o}^{z_{jet}} \gamma_a(z) dz, \quad (4.21)$$

where $\gamma_a(z) = g\rho_a(z)$ and p_o the reference pressure at the water surface, thus

$$p_a = - \int_{z_o}^{z_{jet}} \gamma_a(z) dz + p_o \quad (4.22)$$

- 6) The individual discharge q_i is then given by solving equation (4.19) and (4.20) for q_i :

$$q_i = \sqrt{\frac{\frac{2}{\rho_e} (p_{d,i-1} - p_{a,i}) + 2g(z_{d,i-1} - z_{jet,i}) + \left(\sum_{k=1}^{i-1} q_k \right)^2 \left[\frac{1}{A_{d,i-1}^2} + \sum_{j=1}^{n_{d,i-1}} \frac{1}{A_{d,i-1,j}^2} \left(\zeta_{d,i-1,j} + \lambda_{d,i-1,j} \frac{L_{d,i-1,j}}{D_{d,i-1,j}} \right) \right]}{\frac{\alpha_i^2}{(C_{c,i} A_{p,i})^2} + \sum_{j=1}^{n_{p,i}} \left(\frac{\alpha_i}{A_{p,i,j}} \right)^2 \left(\zeta_{p,i,j} + \frac{\lambda_{p,i,j} L_{p,i,j}}{D_{p,i,j}} \right) + \sum_{j=1}^{n_{r,i}} \left(\frac{1}{A_{r,i,j}} \right)^2 \left(\zeta_{r,i,j} + \frac{\lambda_{r,i,j} L_{r,i,j}}{D_{r,i,j}} \right)}}} \quad (4.23)$$

For simple diffusers equation (4.23) reduces to equation (4.24) if no risers and no port configurations are applied and the diffuser is just represented by simple holes in the pipe wall. Equation (4.24) is the one presented in Fischer et al. (1979) which has been used for simple diffuser calculations.

$$q_i = C_{c,i} A_{p,i} \sqrt{\frac{2}{\rho_e} (p_{d,i-1} - p_{a,i}) + \left(\sum_{k=1}^{i-1} q_k \right)^2 \left[\frac{1}{A_{d,i-1}^2} + \sum_{j=1}^{n_{d,i-1}} \frac{1}{A_{d,i-1,j}^2} \left(\zeta_{d,i-1,j} + \lambda_{d,i-1,j} \frac{L_{d,i-1,j}}{D_{d,i-1,j}} \right) \right]} \quad (4.24)$$

Fischer et al. (1979) furthermore defined a bulk loss coefficient $C_{c,i}$ for example for sharp-edged entrances:

$$C_{c,i} = 0.63 - \frac{0.58}{2g} \left(\left(\sum_{k=1}^{i-1} q_k \right)^2 \left[\frac{1}{A_{d,i-1}^2} \right] \left(\frac{2}{\rho_e} (p_{d,i-1} - p_{a,i}) + \left(\sum_{k=1}^{i-1} q_k \right)^2 \left[\frac{1}{A_{d,i-1}^2} \right] \right)^{-1} \right) \quad (4.25)$$

in addition, for bell-mouthed ports:

$$C_{c,i} = 0.975 \left(1 - \frac{1}{2g} \left(\sum_{k=1}^{i-1} q_k \right)^2 \left[\frac{1}{A_{d,i-1}^2} \right] \left(\frac{2}{\rho_e} (p_{d,i-1} - p_{a,i}) + \left(\sum_{k=1}^{i-1} q_k \right)^2 \left[\frac{1}{A_{d,i-1}^2} \right] \right)^{-1} \right)^{3/8} \quad (4.26)$$

The latter two equations are limited for the application of Duckbill valves and extensions with other loss coefficients.

4.3.2 Solving scheme

The pre-processor of CorHyd is used to calculate geometrical relations (i.e. lengths of pipe sections, horizontal and vertical angles between pipe axis and diameter ratios) and pre-defining necessary formulations for the calculation of loss coefficients according to the specified input data (chapter 4.3.1). CorHyd then solves for either the total head or the total flow together with the discharge distribution along the diffuser line. The post-processor allows for graphical visualization and saves the results additionally in an ASCII file for further coupling or external analysis. Additional program features allow for design optimization and off-design analysis.

To allow for an easy input procedure and fast calculations, CorHyd consist of different modules. Depending on the input details, CorHyd chooses automatically the applicable modules without user interaction. The available modules are

1. one diffuser (simple setup)
2. two diffuser (T or Y setup), where two diffuser calculations are coupled with one feeder pipe calculation
3. both modules 1 and 2 are furthermore subdivided into a module for diffusers without risers or ports (just holes in the wall) and those with risers
4. all calculations can be done either for a given total discharge and solving for the individual discharges and the total head or for a given total head and solving for the individual discharges and the total discharge

4.3.2.1 Algorithm for given bulk discharge: solving for total head

Probably the typical application is related to the problem, where a total discharge Q_o is given (e.g. treatment plant flow rate). For existing diffuser geometry and given boundary conditions (i.e. ambient pressure and/or ambient water level and density distribution) the governing equations can then be solved for the individual discharges and the total head (bulk head) at the headworks necessary to drive the system.

The solving scheme then starts with an estimate (initial condition) of the initial discharge q_1 at the first port/riser on the seaward side ($i = 1$). CorHyd already implemented this estimate using $q_1 = Q_o/N$ with $N =$ total number of risers. Equation (4.20) then gives the first internal pressure of the diffuser $p_{d,1}$. Subsequent discharges q_2 until q_N are then calculated by equation

(4.23). The total discharge is $Q_{c(s)} = \sum_{k=1}^N q_k$. The error compared to the planned total discharge

is $e_{(s)} = Q_o - Q_{c(s)}$. Further iterations (numbering s) are performed with modified initial conditions $q_{1,m(s)}$ until sufficient accuracy is achieved (CorHyd uses the default stop condition $e_{(s)} < Q_o/10,000$). To achieve fast convergence the algorithm in equation (4.27) has been implemented to calculate $q_{1,m(s)}$:

$$q_{1,m(1)} = q_1 \sqrt{\frac{Q_o}{Q_{c(1)}}}, q_{1,m(2)} = q_1 \frac{e_{(2)} - q_{1,m(1)}e_{(2)} - e_{(1)}}{e_{(2)} - e_{(1)}}, \dots$$

$$q_{1,m(s)} = q_{1,m(s)}e_{(s)} - q_{1,m(s-1)} \frac{e_{(s-1)}}{e_{(s)} - e_{(s-1)}} \text{ for } s > 2 \quad (4.27)$$

A final application of equation (4.19) gives the total pressure $p_{d,N+1}$ at the headworks. The total head H_t is defined as $H_t = p_{d,N+1}/\gamma_e$ for example if the water level elevation of a gravity driven system or the necessary pump head has to be defined.

4.3.2.2 Algorithm for given total head: solving for total flow

The solution method changes for cases where the total head is limited, for example if gravity discharge is desired and treatment plant operation results in a given water level elevation H_t . For existing diffuser geometry and given boundary conditions (i.e. ambient pressure and/or ambient water level and density distribution) the governing equations can be solved for the individual discharges and the total flow (bulk flow) which is possible for those conditions.

The solving scheme then starts with an estimate (initial condition) of the initial internal pressure $p_{d,1}$ at the first port/riser location on the seaward side. CorHyd already implemented this estimate using $p_{d,1} = H_t \gamma_e/N + p_{a,1} + \gamma_e(z_{jet,i} - z_{d,i})$. Equation (4.20) then gives the first discharge q_1 . Subsequent discharges q_2 until q_N are then calculated by equation (4.23). Equation (4.19) gives the total pressure $p_{d,N+1}$ at the headworks. The total head is $H_{t,c(s)} = p_{d,N+1}/\gamma_e$. The error compared to the planned total head is $e_{(s)} = H_t - H_{t,c(s)}$. Further iterations (numbering s) are performed with modified initial conditions $p_{d,1,m(s)}$ until sufficient accuracy is achieved (CorHyd uses the default stop condition $e_{(s)} < H_t/10,000$). To achieve faster convergence the algorithm in equation (4.28) has been implemented to calculate $p_{d,1,m(s)}$:

$$p_{d,1,m(1)} = p_{d,1} \sqrt{\frac{H_t}{H_{t,c(1)}}}, \quad p_{d,1,m(2)} = p_{d,1,m(1)} e_{(2)} - p_{d,1,m(2)} \frac{e_{(1)}}{e_{(2)} - e_{(1)}}, \dots$$

$$p_{d,1,m(s)} = p_{d,1,m(s)} e_{(s)} - p_{d,1,m(s-1)} \frac{e_{(s-1)}}{e_{(s)} - e_{(s-1)}} \quad \text{for } s > 2 \quad (4.28)$$

The total discharge is $Q_o = \sum_{k=1}^N q_k$.

4.3.2.3 Program coding and structure

The CorHyd algorithm (chapters 4.3.2.1 and 4.3.2.2) has been coded within the commercial software MatLab[®] Release 14 from the company Mathworks[®]. The code includes a graphical user interface, allows using all additional MatLab facility functions for graphics, analysis, and facilitates further modifications. CorHyd is no self-executable and needs MatLab[®] to be installed. Also open source software like Scilab (<http://scilabsoft.inria.fr/>) or Octave (<http://www.octave.org>) usual allow importing and executing MatLab based CorHyd files, though some debugging is needed in these cases. CorHyd is an open source code and allows for easy modifications. Downloads of the code and a manual, as well as further information is available under <http://www.cormix.de/corhyd.htm>.

An additional version is under development, which will be embedded into CORMIX (Cornell Mixing Zone Expert System from MixZon, www.cormix.info). It is based on the same algorithm and includes the same loss formulations, but will be accessed and linked via the CORMIX interface, thus allowing for easy data transfer between an external hydraulics calculation with CORMIX and the internal hydraulics calculation with CorHyd. Publications from Bleninger et al., 2002, 2004, and 2005 describe the code development and demonstrate comparisons and validation.

For easier understanding of the code as well as to reduce the number of repeated lines, the program consists of several short subprograms (so called m-files). Subprogram definitions and structure, as well as code elements are described in the user manual (Bleninger, 2004).

4.3.3 Data Input

The graphical user interface (GUI, Fig. 30) consists of five tabs: ambient data, effluent data, diffuser/feeder pipe data, port/riser data, and output. The input can be done either by typing the data directly into the designated spaces or by importing an existing text file. In addition, a help system is available.

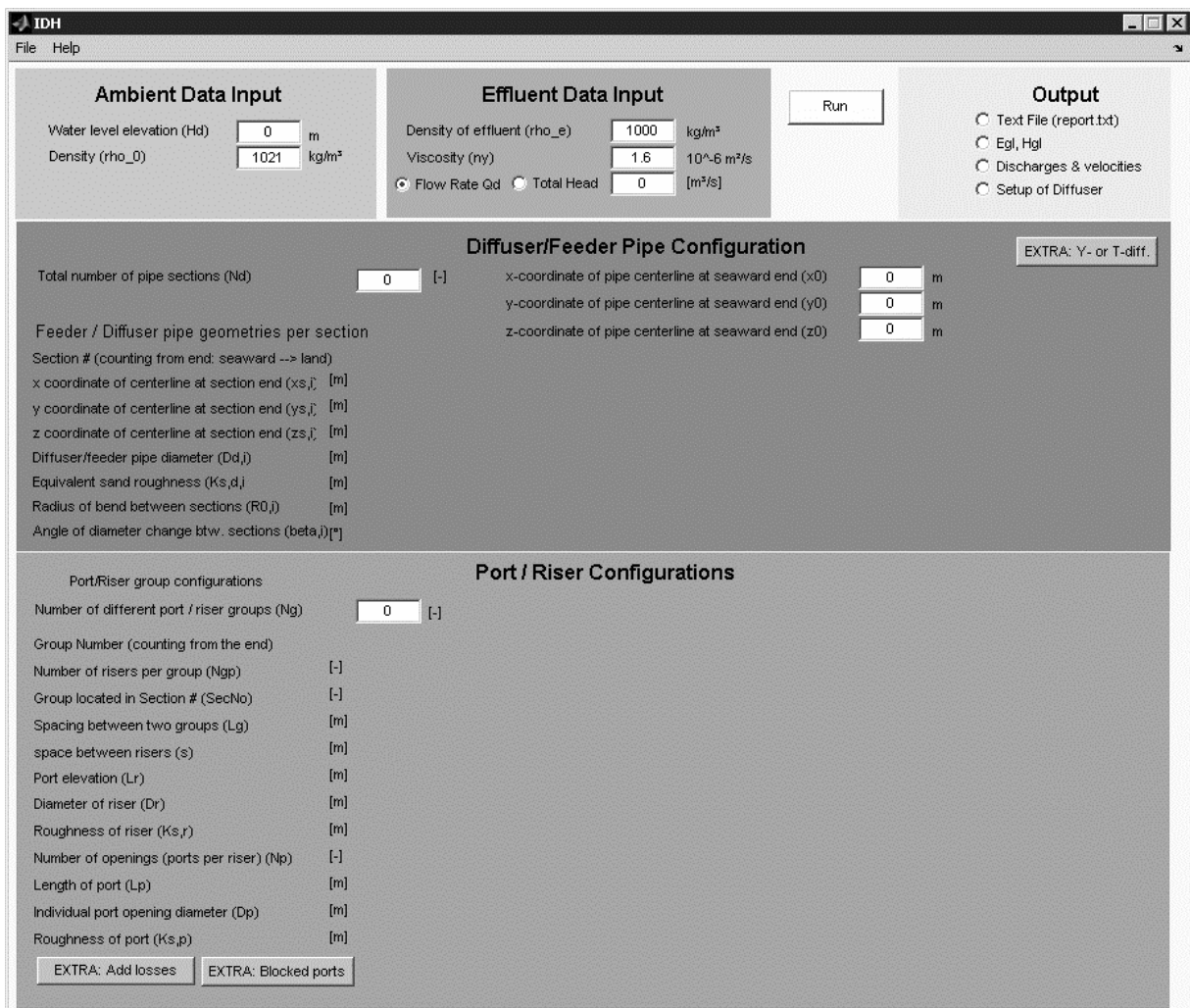


Fig. 30: The graphical user interface of CorHyd

The definition diagram for the input parameters is shown in Fig. 31. The input methodology was based on the concept of grouping similar diffuser, and riser/port sections (Delft Hydraulics, 1995). This reduces the number of datasets to be defined, which is especially important for large diffusers with more than hundreds of ports. Diffuser and feeder pipe sections are defined by their start and end point coordinates x_s , y_s , z_s , the diameter D_d and the roughness $k_{s,d}$. The number of used feeder/diffuser sections is N_d . Section limits are generally defined at locations where either bends or diameter changes or roughness changes occur. Input on section transition configurations are necessary for bends or gradual changes, where the radius R

(typical $R = 3D_d$) for a bend or an angle β (typical $90^\circ - 180^\circ$) for gradual diameter changes have to be specified, respectively. Diffuser/feeder sections can be chosen independently of the port/riser configurations. If two (different) diffusers are connected to one feeder (T- or Y-shape configuration), the diffuser joint location has to be specified in addition to both diffuser configurations. The input for each diffuser is analogue to the input for single diffuser outfalls.

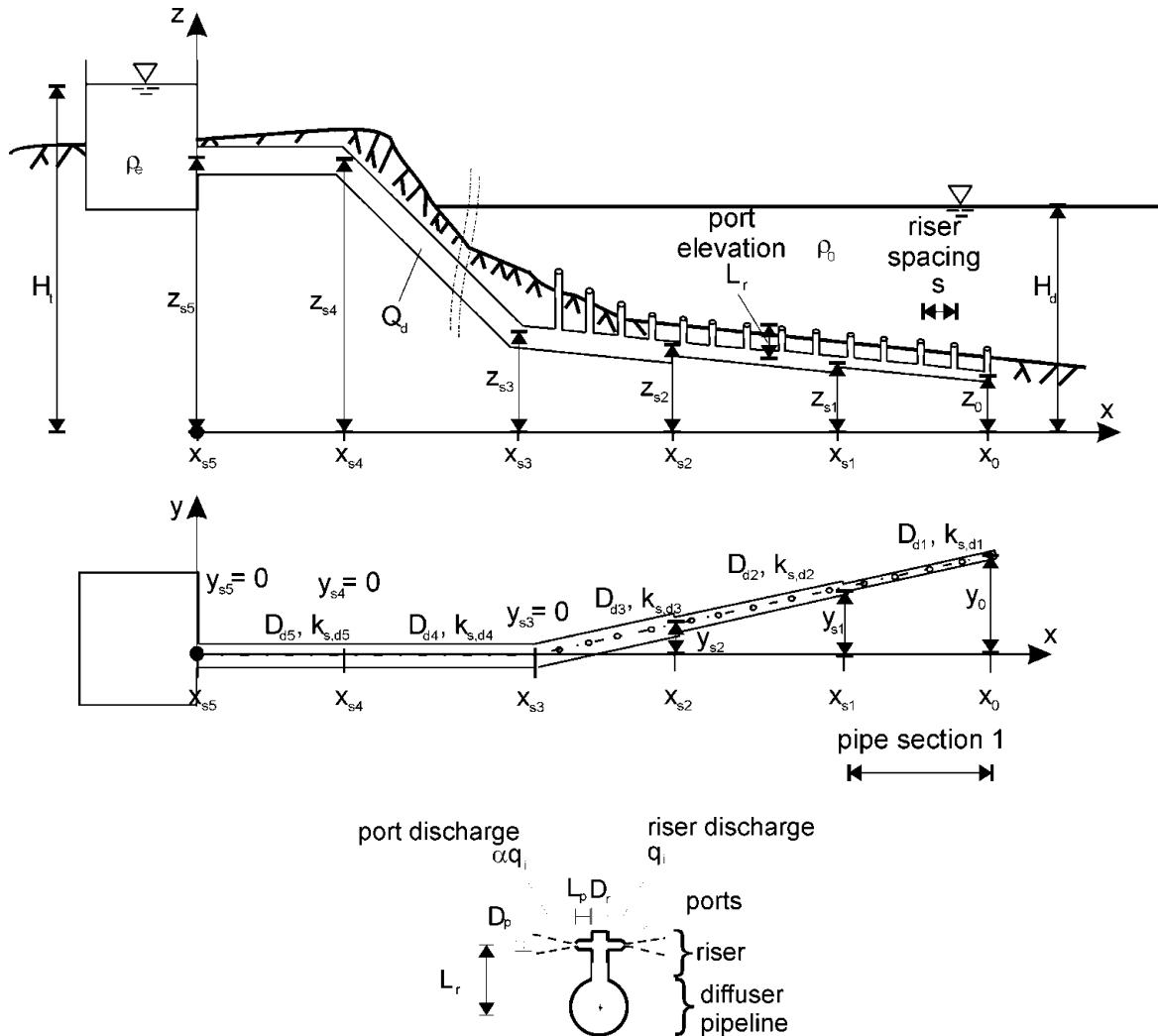


Fig. 31: Coordinate system used in CorHyd. Five pipe sections and two port/riser groups are shown in this example.

Port/riser configurations are also defined in groups. The total number of different groups is N_g . The number of risers in each group is N_{gp} . Different port/riser groups can be assigned to one diffuser group, but should fit into one diffuser group. Thus there have to be at least as many port/riser groups as diffuser groups. The spacing between two groups L_g and between each riser S in a group has to be defined. Finally, port elevations L_r above the diffuser centerline, port and riser diameters D_r , D_p and the roughness $k_{s,r}$ have to be specified. If more than one port is located at one position or at one riser the number of ports, N_p is needed. If ports consist of little attached pipes their length L_p and related roughness $k_{s,p}$ should be given. Design variations and performance evaluations can be analyzed by specifying blocked ports.

4.3.3.1 Automatic implementation of loss formulations

CorHyd automatically applies the necessary local loss formulations for the user given geometrical inputs. For example, calculations for risers with more than one port already include loss formulations for a T-shape flow diversion (assuming that the flow is distributed evenly among the attached ports). Following loss formulations are included:

Local feeder losses: inlet loss at headworks, horizontal and vertical bends, contractions/expansions along the feeder pipe, flow separation, if several diffusers are mounted on one feeder

Diffuser manifold pressure losses: pressure losses at the division of flow for the diffuser pipe passing a riser, horizontal or vertical bends, contractions/expansions along the diffuser pipe

Port - riser branch pressure losses: the division of flow from the diffuser pipe into a riser, optional: bends or additional pressure losses in the riser, the transition or division of flow from riser to port(s), optional: additional pressure losses in the port or at the orifice, contraction of jet, duckbill valves at the port orifices

For special and unusual configurations, which need more detailed specifications of geometries or loss formulations, optional input facilities are foreseen (marked as optional in previous listing). These include input for additional loss coefficients ζ (related to the port exit velocity) jet contraction ratios C_c and duckbill valve nominal diameters. The applied formulations and coefficients are summarized in Annex A.

4.3.4 Data Output

The CorHyd post-processor includes a visualization of the input parameters, a detailed report (ASCII file, see example in Annex B), and graphics for the results. The latter shows the output parameters along the diffuser line: absolute and relative discharges and the port/riser head-loss (first and second bar chart in Fig. 32), port and jet velocities and the related diameters (third chart in Fig. 32), velocities in the diffuser and the related diameters (fourth chart in Fig. 32). Fig. 33 shows the results as energy and hydraulic grade lines.

4.4 Diffuser design and optimization

4.4.1 Design constraints

The feeder diameter design is constrained by a maximum diameter to allow scouring of sediments during low flow periods. The near future design discharge Q_{nf} (daily maximum) should therefore result in feeder velocities $v_{f,nf} > 0.5$ m/s (DIN EN 1671, ATV-DVWK-A 110 (2001) and ATV-DVWK-A 116 (2005)). This corresponds to a maximum feeder pipe diameter of $D_{d,max} = (Q_{nf}8/\pi)^{0.5} \approx 1,6 Q_{nf}^{0.5}$. The feeder velocity for the far future design flowrate Q_{ff} and the same diameter results then in $v_{f,ff} = v_{f,nf}Q_{ff}/Q_{nf}$. Generally, flow rates do not more than double or triple during the lifetime of an outfall, so far field feeder velocities are from 1 to 2 m/s, what is clearly acceptable in terms of operational viewpoints considering the related pressure losses.

The same considerations apply for the diffuser pipe, though that the flow decreases with every riser. Theoretically this would result in a continuously decreasing diffuser pipe diameter, but

practical solutions include only very few of these tapers. This because tapered diffusers are more expensive to install (about 20% more expensive than single diameter diffuser) and maintain (i.e. cleaning).

Port diameters are constrained by operational restrictions, where a 50 mm minimum port size for secondary- or tertiary-level treated effluent and storm water inflow to the sewage system was suggested by Wilkinson and Wareham (1996), to avoiding the risk of blockage. A minimum port size of 70 to 100 mm was specified for primary treatment plants (just screening and settling tank).

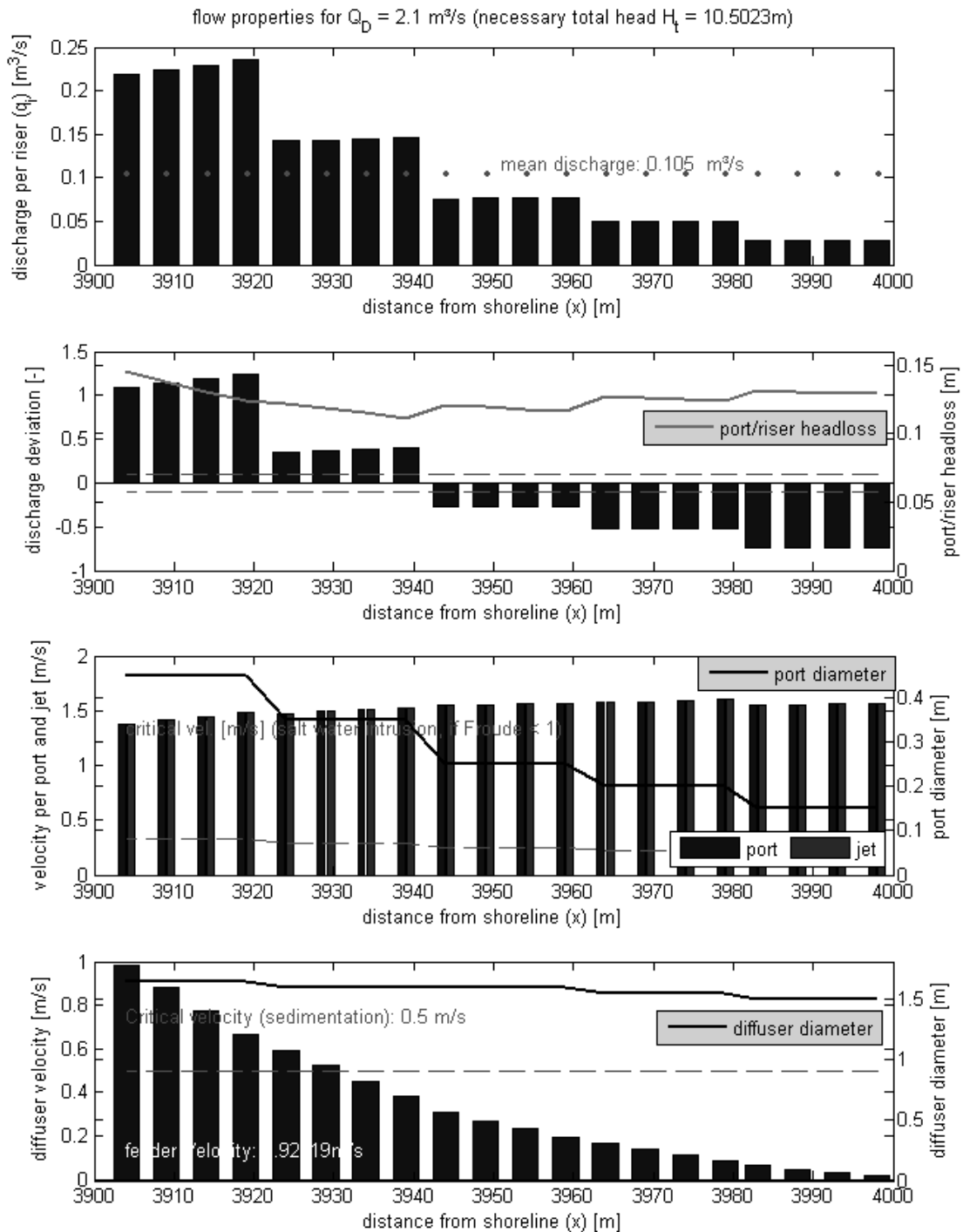


Fig. 32: Graphical output: bar charts showing the discharge per riser, the relative discharge deviation and port/riser headloss distribution, the discharge velocity at ports and in the final jet, the velocity in the diffuser pipe as well as port and diffuser diameter.

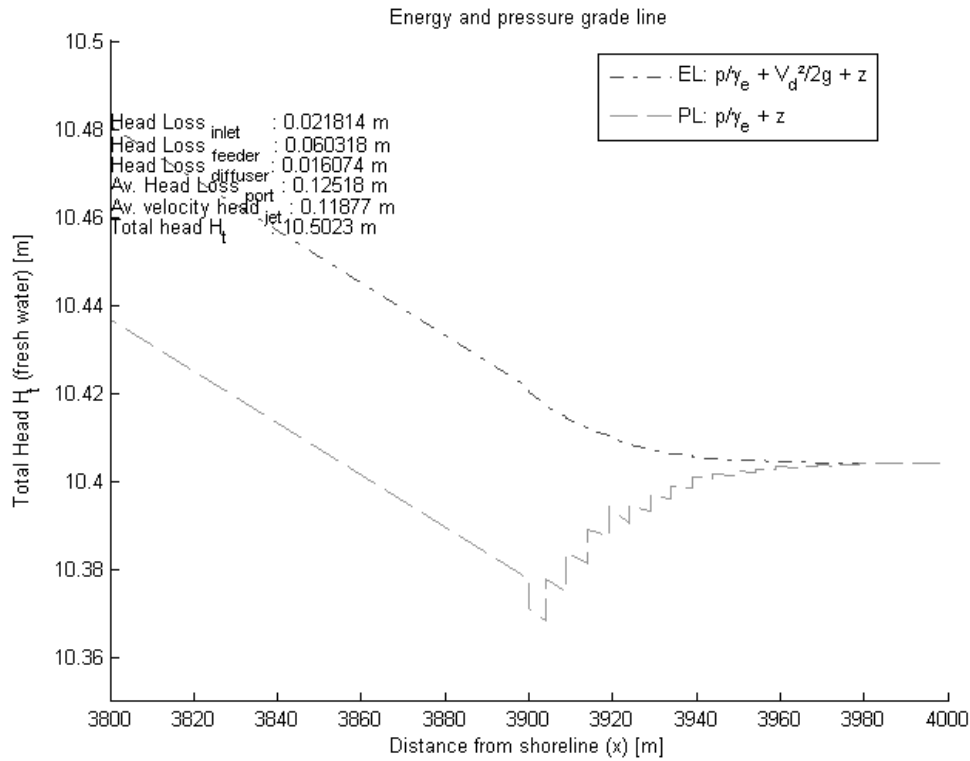


Fig. 33: Graphical output: Energy and Hydraulic grade line of the whole system and the diffuser

4.4.2 Design and optimization steps

The design of multiport diffusers depends on several interacting parameters. The general approach is schematized in Fig. 34, which converges to an optimized system.

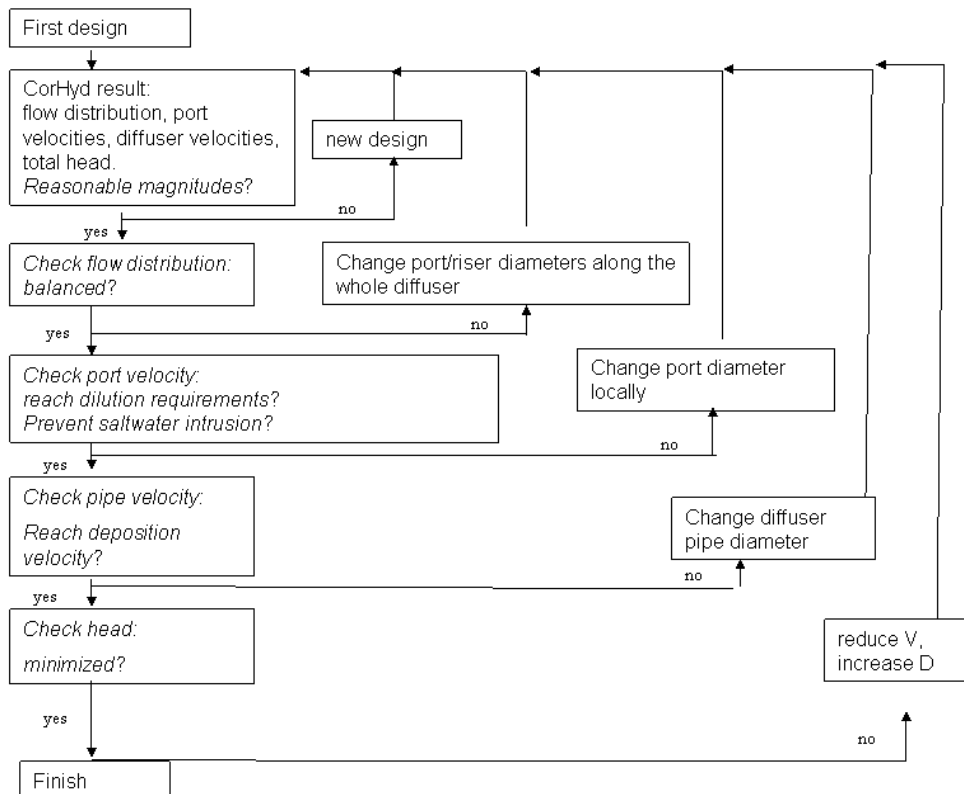


Fig. 34: Schematization of general diffuser design algorithm

The first design flow rate should be the maximum foreseen at the end of design life. Generally there is a headworks basin (or the treatment plant itself) with sufficient capacity to accept daily peaks and storm waters. The ratio of the peak rate of flow to the average rate of flow might hereby range from 6 for small areas down to 1.5 for larger areas. For large ratios commonly additional storm water outfalls are foreseen. In the former cases, the design can be made on the average daily maximum flow at life end. For installations without storage facilities the design flowrate is the daily peak flow either including or excluding the stormwater peak discharges. The latter design discharge does not occur on a daily basis; therefore, optimization procedures for non-design discharges are even more important than for the other cases. The first internal hydraulics design step described in Table 10 uses the resulting geometries for a baseline calculation regarding the maximum design flow.

Step 1: Baseline calculation - for far future design conditions
<ul style="list-style-type: none"> - The data from the first successful mixing calculations is used as first design alternative for the internal hydraulics <ul style="list-style-type: none"> ⇒ run CorHyd with very few diffuser and port/riser sections and plot results - Pipe velocities: Diffuser, riser and port velocities should be in between reasonable ranges, otherwise the diameters have to be increased or decreased generally for all sections and/or groups ($V_d < V_r < V_p < V_j$) <ul style="list-style-type: none"> ⇒ modify feeder/diffuser diameter to obtain operable velocities ($0.5 \text{ m/s} < V_d < 5 \text{ m/s}$) ⇒ modify riser diameters to obtain operable velocities ($0.5 \text{ m/s} < V_r < 5 \text{ m/s}$) ⇒ modify port diameters to obtain operable velocities ($0.5 \text{ m/s} < V_p < 12 \text{ m/s}$) at least at the majority of port/riser configurations ⇒ port diameters should not be less than 100 mm to avoid possible problems of blockage - Total head: The necessary total Head or the final flow should be in the desired order of magnitude, otherwise velocities and/or locations of high pressure losses should be reduced <ul style="list-style-type: none"> ⇒ simplify geometries and/or increase diameters to reduce the total head - Flow distribution: <ul style="list-style-type: none"> ⇒ check whether the flow distribution lies in between reasonable limits ($q_{min} = -0.1q_i/N < q_i < 0.1q_i/N = q_{max}$) for at least the majority of port/riser configurations ⇒ modify riser diameters for the whole diffuser to obtain a more homogeneous distribution of the riser inlet pressure losses ⇒ modify port diameters for the whole diffuser to obtain a more homogeneous distribution of the port pressure losses (i.e. if Duckbills are applied) - Check external hydraulics with modified diffuser - If either the external hydraulics or even the modified internal hydraulics does not fulfill the general requirements listed above, the user should try to do a re-design of the main diffuser characteristics. Else, proceed to the optimization in step 2.

Table 10: Step 1: Baseline calculation - for far future design conditions

However, diffusers are generally operated under varying flow conditions due to diurnal or seasonal changes. CorHyd does include an automatic routine for diffuser analysis of varying effluent flow or varying total head respectively in combination with varying ambient water level elevations (still steady state). Varying inflows hereby affect the discharge distribution

for diffusers, which are not horizontal. Under low-discharge conditions, diffusers are furthermore confronted with issues of sediment deposition and/or intrusion of seawater. Seawater intrusion can seldom be avoided for all discharges. Duckbill valves and small diameter pipes prevent those problems, but lead to additional pumping costs or higher headworks storage buildings. Intrusion can be prevented if the port densimetric Froude number (equation 4.10) is bigger than one (Wilkinson, 1988). Particle deposition can be avoided by achieving pipe velocities bigger than critical velocity (≈ 0.5 m/s) at least once a day. Thus, the second design step (Table 11) considers the diffuser performance for varying conditions and improves the design mainly by local changes along the diffuser line.

Step 2: Diffuser characteristics - diffuser performance calculations
<ul style="list-style-type: none"> - Analyze diffuser performance for intermediate flows <ul style="list-style-type: none"> ⇒ run CorHyd time-series for varying discharges and plot results - Pipe velocities: time-series results allow to denote diffuser sections, where scouring velocities are too low for most of the flow rates and/or where port Froude numbers are below or near unity. <ul style="list-style-type: none"> ⇒ create additional diffuser sections at positions, where scouring velocities are not obtained for discharges which occur once a day ⇒ create additional port/riser groups for added diffuser sections (starting with the same geometry). ⇒ modify diffuser section diameters locally (tapering) to obtain scouring velocities - Flow distribution: check whether the flow distribution lies in between reasonable limits ($q_{min} = -0.1q_i/N < q_i < 0.1q_i/N = q_{max}$) for at least the majority of port/riser configurations <ul style="list-style-type: none"> ⇒ modify the riser group diameters locally ⇒ modify port group diameters locally ⇒ introduce additional port/riser groups if necessary and repeat local modifying - Check external hydraulics with modified diffuser - If either the external hydraulics or even the modified internal hydraulics do not fulfill the general requirements as listed above the user should try to do a re-design of the main diffuser characteristics. Else, proceed to the optimization in step 3.

Table 11: Step 2: Diffuser characteristics - diffuser performance calculations

Additional analysis is needed, once the diffuser flows at startup differ considerably from those of the final design. A common technique to overcome the problem of initial malfunctions is “expanding diffusers” (Avanzini, 2003). These are designed to meet the initial and final requirements by either closing initially a certain number of ports (with fixed closures, welded duckbills or backpressure regulations, where former have to be removed manually and the latter open autonomous if enough discharge enters the system) or modifying port diameters using replaceable flanged orifices (Bleninger et al., 2004). Furthermore, it is often easier and cheaper to operate the diffuser under these optimized conditions than operating the final diffuser with low flows.

CorHyd allows analyzing the diffuser performance for these scenarios by simply closing the ports or modifying the configurations. This routine may also be used for the analysis of acci-

dents like port/riser ruptures due to anchor collisions, earthquakes, or structural failures. Step 3 (Table 12) thus considers off-design analysis and optimization.

Step 3: Off-design calculation - near future design conditions
<ul style="list-style-type: none"> - Near-future mixing calculations are used to figure out the number of necessary ports for low flow discharges. <ul style="list-style-type: none"> ⇒ run CorHyd with clogged ports and plot results - Analyze pipe velocities, and the flow distribution, if the final diffuser configuration with clogged ports allows discharging near-future flows under reasonable conditions. <ul style="list-style-type: none"> ⇒ modify the number and the location of the clogged ports to optimize near-future flow conditions - Check external hydraulics with modified diffuser - If either the external hydraulics or even the modified internal hydraulics do not fulfill the general requirements as listed above the user should try to do a re-design of the main diffuser characteristics. Else, proceed to the optimization in step 4.

Table 12: Step 3: Off-design calculation - near future design conditions

4.4.3 Sensitivity Analysis

Multiport diffuser installations are complex and large constructions submerged in coastal waters. Besides the previously discussed varying environmental conditions, further uncertainties regarding constructional imprecision and deterioration have to be analyzed. In addition the governing equations are based on certain simplifications (i.e. empirical loss coefficients), which contain another source of inaccuracy. It is therefore strongly recommended to elaborate sensitivity analysis by varying critical parameters and comparing the consequences on the design parameters (total head and discharge distribution). This is especially important for the local loss coefficients and pipe roughness. Examples for that analysis are given in Wood et al. (1993, p. 133) and WRc (1990). Once considerable differences are obtained, it is recommended to perform laboratory studies for more accurate definitions of the coefficients.

Step 4: Sensitivity analysis - prediction accuracy
<ul style="list-style-type: none"> - Final diffuser design under maximum discharge conditions <ul style="list-style-type: none"> ⇒ run CorHyd with additional port pressure losses to check influences of loss formulations on final result ⇒ vary geometrical details to check influences of construction imprecision on final result ⇒ add additional pressure losses on whole pipe-system to account for imprecision ⇒ vary material properties, roughness to check influences of deterioration - Check external hydraulics with modified diffuser

Table 13: Step 4: Sensitivity analysis - prediction accuracy

Table 14 summarizes the results of a sensitivity analysis performed with CorHyd. It is hereby distinguished between horizontal and sloped diffusers where the port elevations are either at constant depth or varying along the diffuser.

Increasing the ... :	leads to ... of the total head or the discharge distribution resp.	
	Total Head	Uniformity
Total discharge (no slope)	↑↑	0
- " - (with slope)	↑↑	↓↓ or ↑↑
Ambient water depth (no slope)	↑↑	0
- " - (with slope)	↑↑	↓ or ↑
Density difference (no slope)	↑	↑
- " - (with slope)	↑	↓ or ↑
Feeder length	↑	0
Diffuser length (constant total length)	↓↓	↓
Diffuser pipe diameter	↓↓	↓ or ↑
Pipe roughness	↑	0
Number of risers (constant diffuser length)	↓	0
Riser spacing (variable diffuser length)	↓↓	↓
Riser height	↑	0
Ports per riser	↓	↓
Port diameter	↓	↓↓
Flexible valves	↑↑	↑↑

↑ / ↓	=	moderate in- / decrease
↑↑ / ↓↓	=	strong in- / decrease
0	=	neutral or small changes

Table 14: Sensitivity of involved parameters on head loss, total head, and homogeneity of the discharge profile.

4.4.4 Transients, saline intrusion and purging

Extraordinary conditions, like very short pumping cycles (order of minutes), full shutdown of flow, purging of a saline wedge during start-up or water-hammer issues cannot be analyzed with CorHyd due to its steady state assumption. Any of these conditions should be avoided by using duckbill valves, slowly closing valves, or pumps, sufficiently large headworks reservoirs allowing for long pumping cycles or flushing periods.

For the analysis of saline wedge purging usually laboratory or numerical studies are performed. Saline wedge purging can be guaranteed, for example, by using some velocity criterion (Wilkinson, 1984) or a plug flow system, where one half of the outfall volume is accumulated in the headworks storage and then pumped at high velocities (e.g. 1.5m/s proposed by Wood et al. (1993, pp. 122, pp. 326)). The time required to reach steady state once purging was initiated must also be determined (see Wilkinson und Nittim, 1992). Furthermore, flow accelerations during pump start-up could lead to oscillations (WRC 1990, p. 212). Wave-induced oscillations occur if large waves are passing over a diffuser section in shallow water (Grace, 1978, p. 302). Resonance effects and internal density-induced circulations are possible (Wilkinson, 1985).

4.4.5 Design rules

A design rule that is often mentioned in literature (Grace 1978), recommends to keep the ratio between the cumulative port areas downstream a diffuser pipe $\sum_{k=1}^N A_{p,k}$ and the cross sec-

tional area of the diffuser pipe $A_{d,N}$ smaller than one. This is explained by the justification that *"it is impossible to make a diffuser flow full if the aggregate jet area exceeds the pipe cross-section area, since that would mean that the average velocity of discharge would have to be less than the velocity of flow in the pipe"* (Fischer et al. 1979, p.419). A further suggestion taken from Fischer et al. (1979, p.419) resumes that the best ratio *"is usually between 1/3 and 2/3"*, $1/3 < \sum_{k=1}^i (A_{p,k}/A_{d,i}) < 2/3$. These criteria work fine for simple and uniform geometries without risers and for horizontal laid diffusers or for first estimates. However, they can be unnecessarily conservative if no further optimization is done. For example, sloped diffusers (following the sloped bathymetry) may equalize the distortion of the discharge profile resulting from an area ratio bigger than one. First estimates for non-uniform riser systems can be done by replacing the port cross-sectional area in the mentioned criteria with the riser cross-sectional area and applying these criteria for each section separately.

Nevertheless, for changing geometries along the diffuser the previous criteria are not applicable in general. This, because 1) the diffuser velocities generally decrease along the diffuser or change considerably if tapering is applied, 2) the port/riser velocities may change if port/riser diameters are varied along the diffuser line causing a variation of C_c and 3) the flow distribution depends also on the pressure losses along the diffuser, causing a variation of ζ_{dr} . For example, pressure losses along the diffuser are considerably different for systems with same area ratio, but different number of openings.

Design rules regarding general loss ratios (Weitbrecht et al., 2002) for diffuser sections and downstream ports are also only applicable for simple geometries (no changes along the diffuser). For others, they are either unnecessarily conservative or not applicable, because pressure losses are changing drastically along actual diffuser installations and cannot be summarized for the whole diffuser construction.

Therefore a design rule for non-uniform systems or for uniform sections and groups of a non-uniform system has to come out of a combination of a loss ratio (buoyancy and riser inlet (or port outlet) and a velocity ratio (diffuser velocity and branch velocity (port or riser)). Furthermore, sections and groups of a non-uniform system have to be balanced in between each other to achieve an overall uniform diffuser performance. The optimal procedure to organize these modifications also under different flow conditions and further design criteria is described in the following chapters.

4.5 Case studies

Two case studies have been chosen to demonstrate CorHyd capabilities: the Ipanema outfall in Rio de Janeiro, Brazil, which has been operating since 1975 and the planned Berazategui outfall in Buenos Aires, Argentina.

4.5.1 Ipanema outfall - Rio de Janeiro - Brazil

To demonstrate CorHyd capabilities the outfall from Ipanema in Rio de Janeiro, Brazil, has been chosen as base case. The outfall design is herein compared with typical other constructional configurations as they would be applied in actual designs.

The Ipanema outfall in Rio de Janeiro, Brazil, is operating since 1975 and discharges actually about 6 m³/s (+/- 1 m³/s daily variation, from 2.1 million people) coarse screened municipal sewage from the southern part of the city into the coastal waters of the Atlantic ocean (Fig. 35, Carvalho, 2003). The outfall was designed for an average discharge of 8 m³/s (equivalent

4.0 million people) with peak discharges up to $12 \text{ m}^3/\text{s}$. The outfall is made of a 4326 m long concrete pipe with a diameter of 2.4 m including a 449 m long diffuser section with 90 ports on each side of the pipe, each with a nominal diameter of 0.17 m, a spacing of 5 m and pointing downwards with an angle of 45° to the horizontal (Carvalho et al., 2002, Fig. 36 and Fig. 37). The diffuser is in a depth of about 27 m. The slope of the diffuser line could not be found in literature. The Ipanema outfall is one of the few outfalls, which have been monitored in detail, with special emphasize on mixing characteristics (Carvalho et al., 2002). These monitoring studies showed in general good mixing characteristics. At commissioning 59 of the 180 ports were closed on purpose to achieve reasonable flow conditions until design flow was reached. Since 1996, all ports have been discharging. The constructional design itself is unusual, with a concrete diffuser line fixed on piles above the seabed. The piles proved to be the weak point of the construction, where pile breaks lead to a major rupture in year 2000. Today simpler and cheaper laying methods are available (e.g. HDPE pipes with weights or laid in a trench), which promise to be more resistant to dynamic wave forcing and currents.

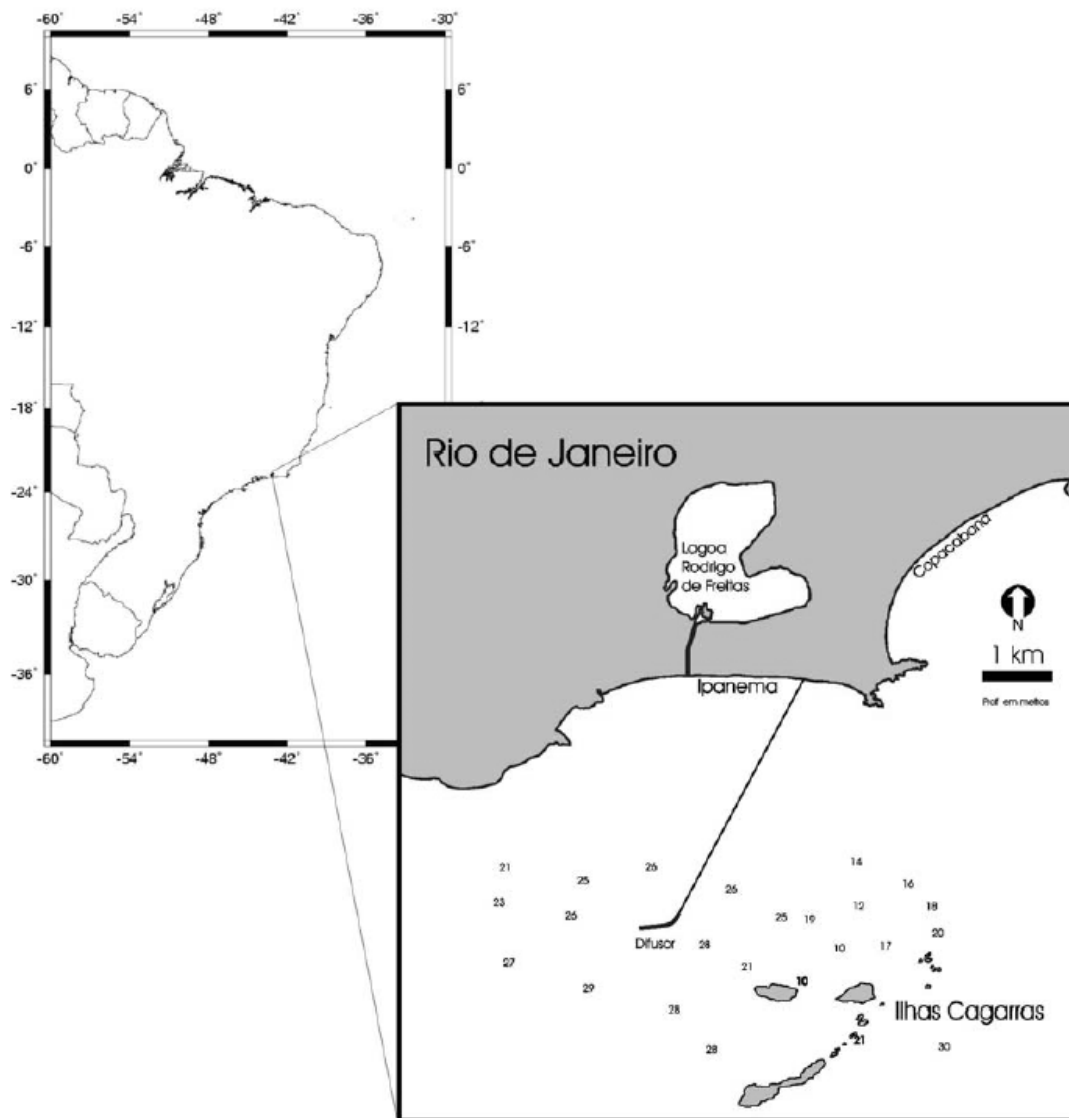


Fig. 35: Location map of the Ipanema outfall of the city Rio de Janeiro in Brazil (reproduced from Carvalho, 2003).

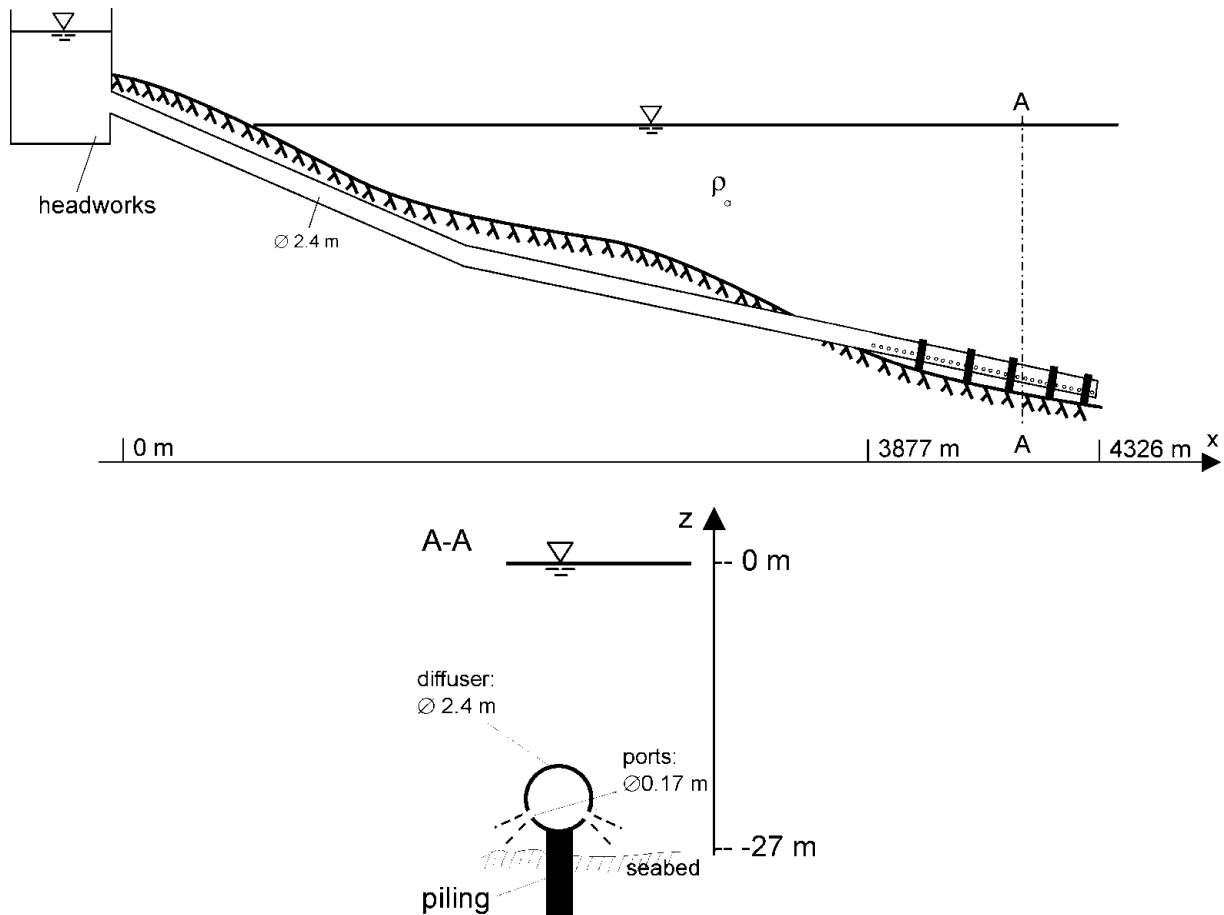


Fig. 36: Side view and cross section of the Ipanema outfall.

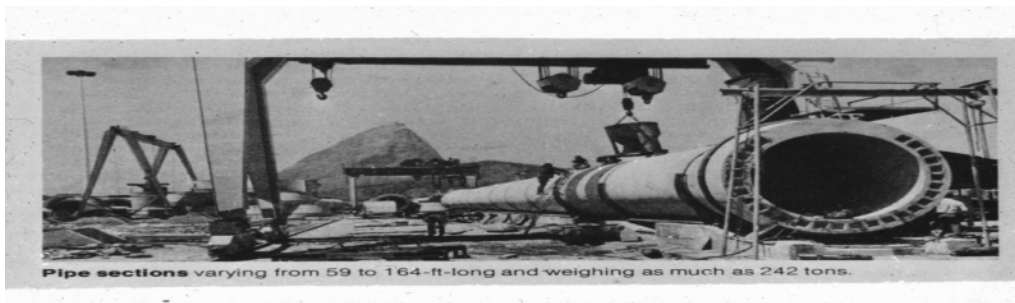


Fig. 37: Image from the construction site of the Ipanema outfall (reproduced from Grace, 1978)

The calculated internal flow characteristics are summarized in Fig. 38 for design flow $Q_d = 8 \text{ m}^3/\text{s}$ and a horizontal diffuser line. A reasonably good discharge distribution along the diffuser (first bar-chart, Fig. 38) with maximum deviations from the mean discharge of not more than 5% of the mean discharge (second bar-chart, Fig. 38) is obtained. Due to different pressure losses along the diffuser pipe and the port/riser configurations (line in second bar-chart, Fig. 38) the discharge is increasing here to the seaward end. Usually diffuser cannot be laid horizontally as assumed here, because of the sloping bathymetries. Therefore another calculation is shown in Fig. 39 (second chart), with a sloped diffuser with an assumed elevation difference of 3 m along the diffuser length of 449 m ($= 6.7\%$). The discharge deviation in this case is almost negligible, which is due to a higher pressure difference between the sewage in the diffuser pipe and the heavier ambient water especially in deeper waters at the seaward diffuser end.

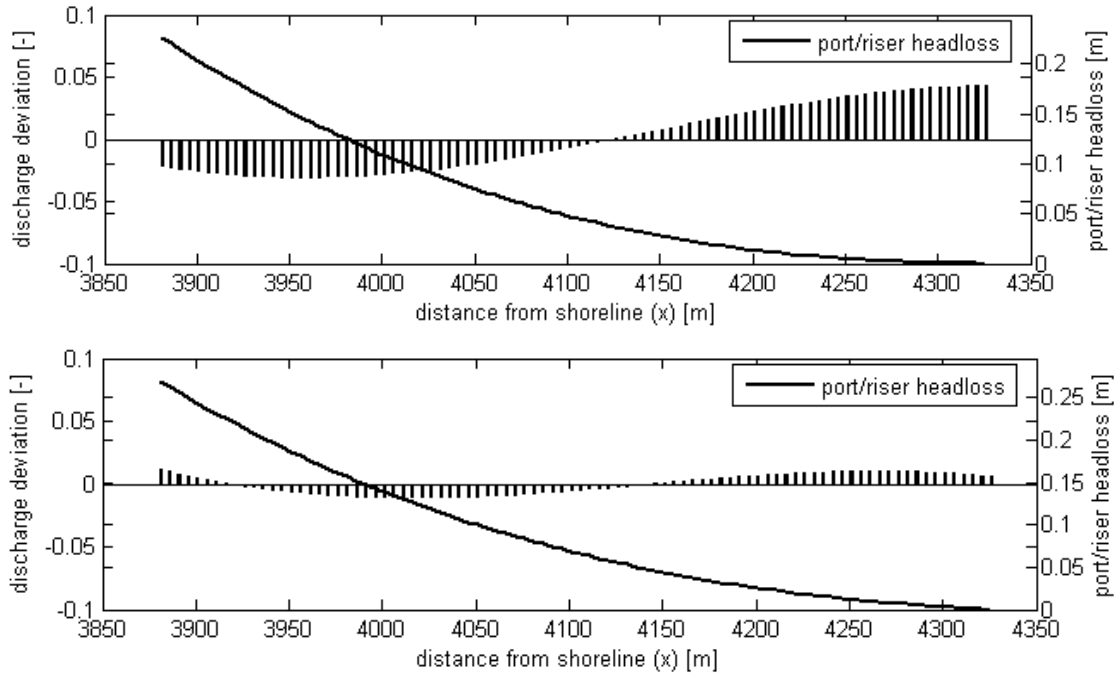


Fig. 39: Riser flow deviation from mean flow, for a horizontal diffuser line (*top*) and a sloped diffuser line (3 m / 449 m, *down*). Pressure losses in port/riser configuration is shown as line.

Fig. 40 shows the flow characteristics for several intermediate flow rates and the sloped diffuser. A slight variation of the discharge distribution can be observed for these flow variations, and only for the sloped diffuser. The changes of the total head for increasing discharges are shown in Fig. 41. Changes in the ambient water level do not have any effect on the flow characteristics but increase the total head. To prevent intrusion of ambient water (including sediments), especially during low flow, the port densimetric Froude number should be bigger than unity. This gives a critical port velocity $V_{p,crit} = (\Delta\rho/\rho g D_p)^{0.5} = 0.041$ m/s for Ipanema outfall. All port and jet exit velocities (third bar-chart, Fig. 40) are considerably higher for all applied flow rates. However, the most critical point stays the low scouring velocity, which affects almost 40% of the diffuser (169 m and about 60 ports) for the flowrate of 6 m³/s, which is presently the average flow.

4.5.1.1 Diffuser optimization

Scouring velocities

The present geometry does not allow for scouring velocities in the end part of the diffuser. The maximal flow, which occurs actually once a day, is 7 m³/s. The last 150 m of the diffuser do have too low velocities under this condition. Therefore, as an example a taper is introduced at exactly this position and the diameter reduced from 2.4 m to 1.2 m. Results shown in Fig. 42 indicate that the pipe section with velocities lower than 0.5 m/s are only the last 25 m (10 ports) of the diffuser. Furthermore, under peak design discharge (12 m³/s), there are only the last 10 m (4 ports) of the diffuser where velocities are lower than 0.5 m/s. Negative consequences of the taper are a higher head (5% increase of the relative head) and a more distorted discharge distribution (Fig. 42).

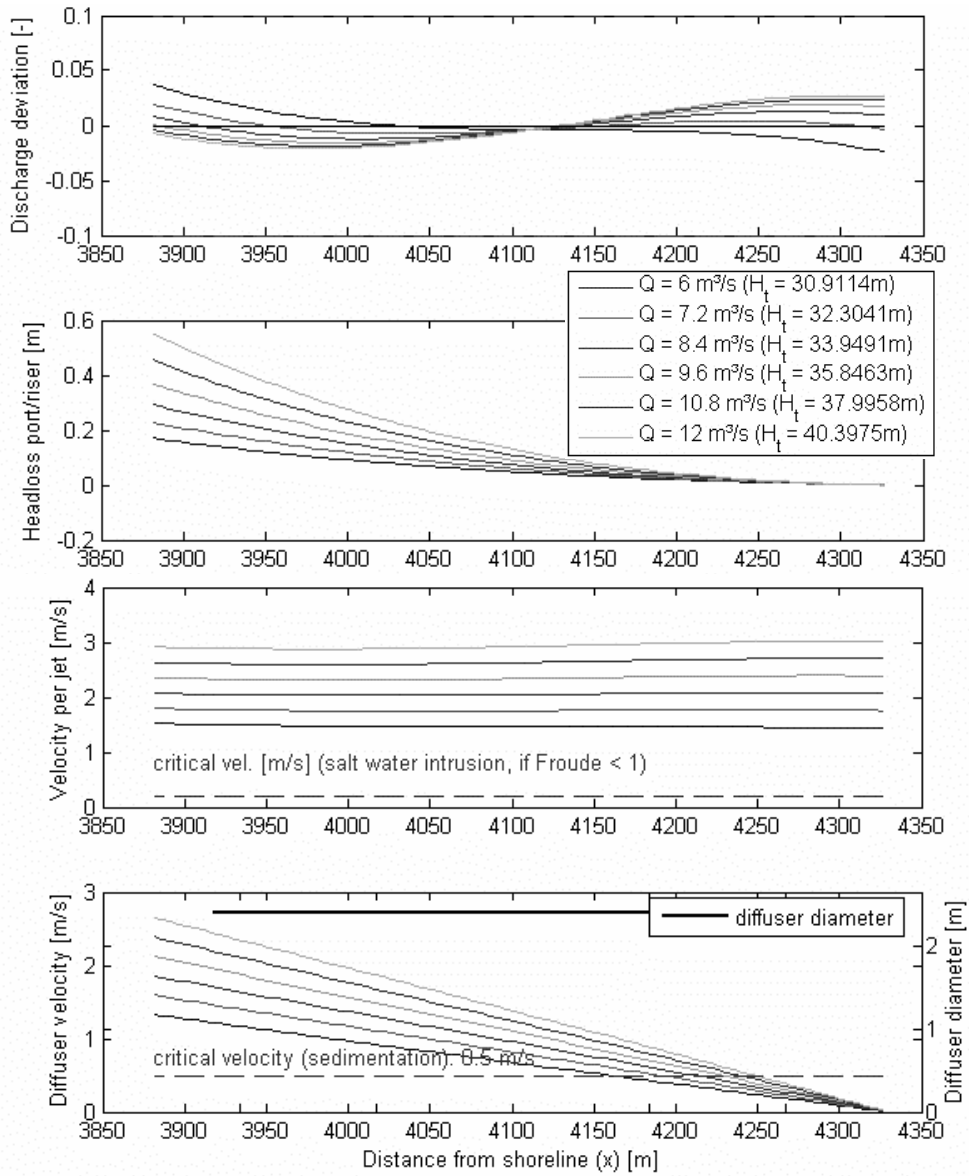


Fig. 40: Flow characteristics for different flowrates Q and sloped diffuser, showing riser flow deviation, port/riser headloss, jet discharge velocities, diffuser pipe velocities and total head H_t

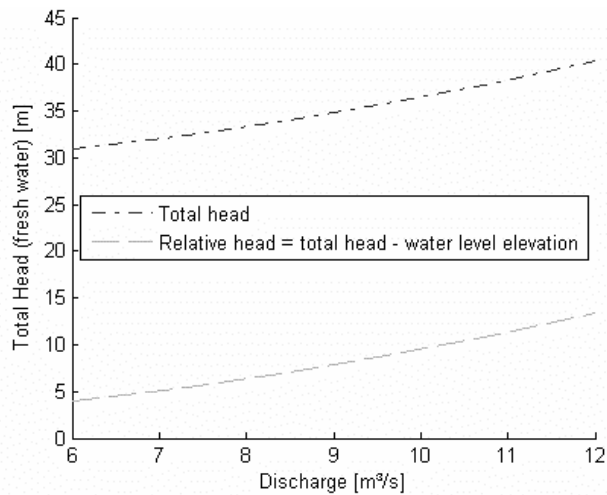


Fig. 41: Changes in total head for varying discharges vs. constant ambient water level.

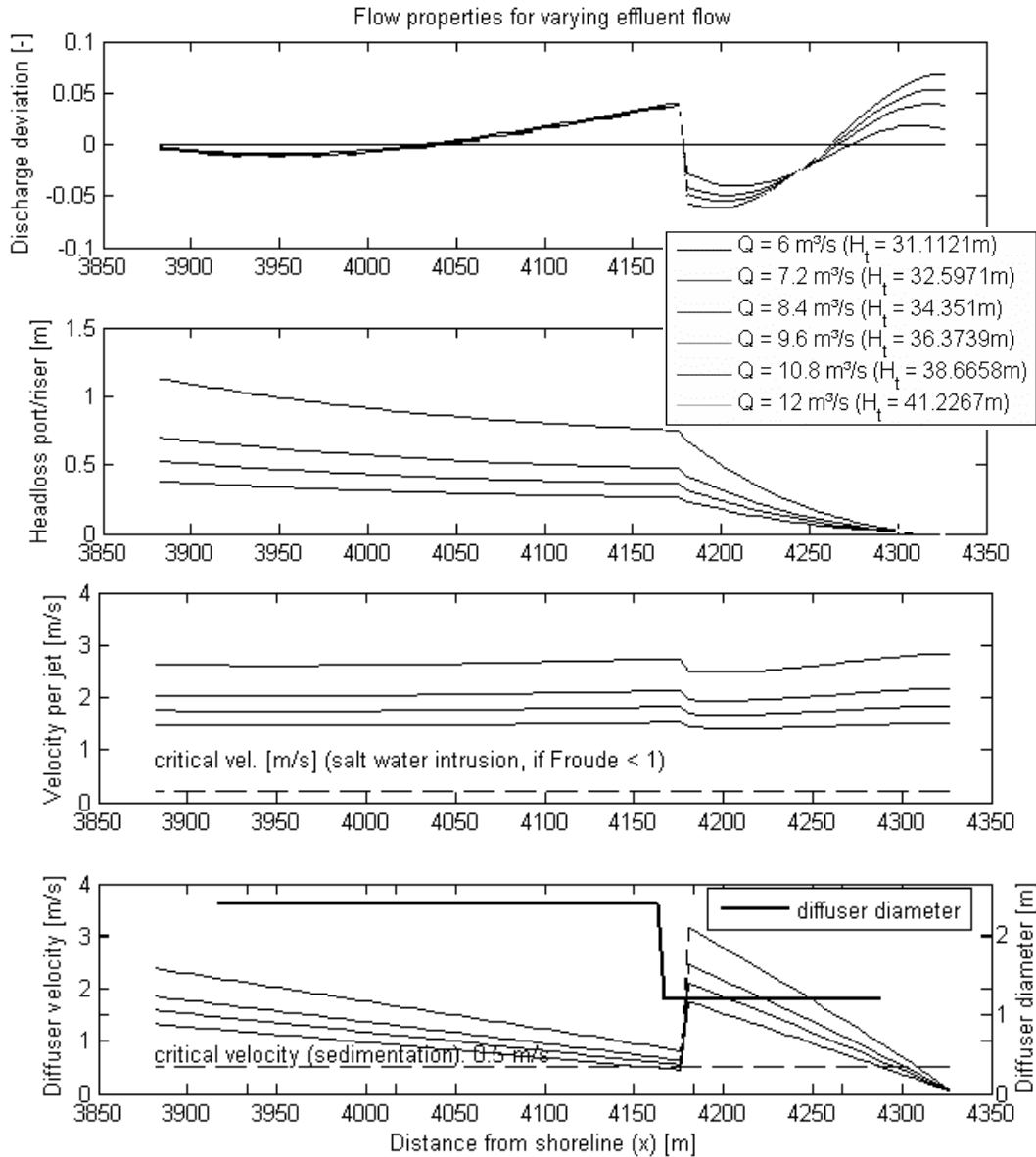


Fig. 42: Flow characteristics for different flowrates Q for tapered diffuser where diffuser diameter is reduced to 1.2 m for the end section. *Top-down*: riser flow deviation from mean, pressure losses in port/riser configurations, jet discharge velocities and diffuser pipe velocities

Constructional alternatives

The piling of the diffuser pipe caused problems due to broken piles and therefore leakage at diffuser pipe joints. Contemporary constructional design alternatives would try to avoid these problems by using a HDPE pipe with concrete weights fixing the diffuser on the ground. The internal hydraulics would be affected only by minor differences in roughness.

i. Covered diffuser or in trench - short risers

If wave forcing, sediment transport or navigation and fishing activities are a major problem for the diffuser pipe, it also can be covered or laid in a trench (Fig. 43). In both cases, short risers have to be used to connect the buried pipe with the ambient water. The riser pipes with the two attached ports are causing additional pressure losses and therefore distort the discharge profile. Changing riser diameters within the diffuser sections allows equilibrating these additional changes, because the additional separation pressure losses depend on the diameter ratio between diffuser pipe and riser pipe. Fig. 44 shows an improved discharge dis-

tribution for riser diameters of 0.3 m at the end section and 0.2 m at the near-shore section of the diffuser. This solution increases the total head of about 4% compared to the tapered diffuser with no risers and 10% compared to the basecase. These differences especially caused by the local pressure losses of the flow entering a riser and further additional loss formulations would not result out of existing diffuser programs (e.g. Fischer et al., 1979, implemented as code PLUMEHYD; and Wood et al., 1993, implemented as DIFF). The design and the important optimization of the riser diameters, is not possible in other programs, although influences on design parameters are huge.

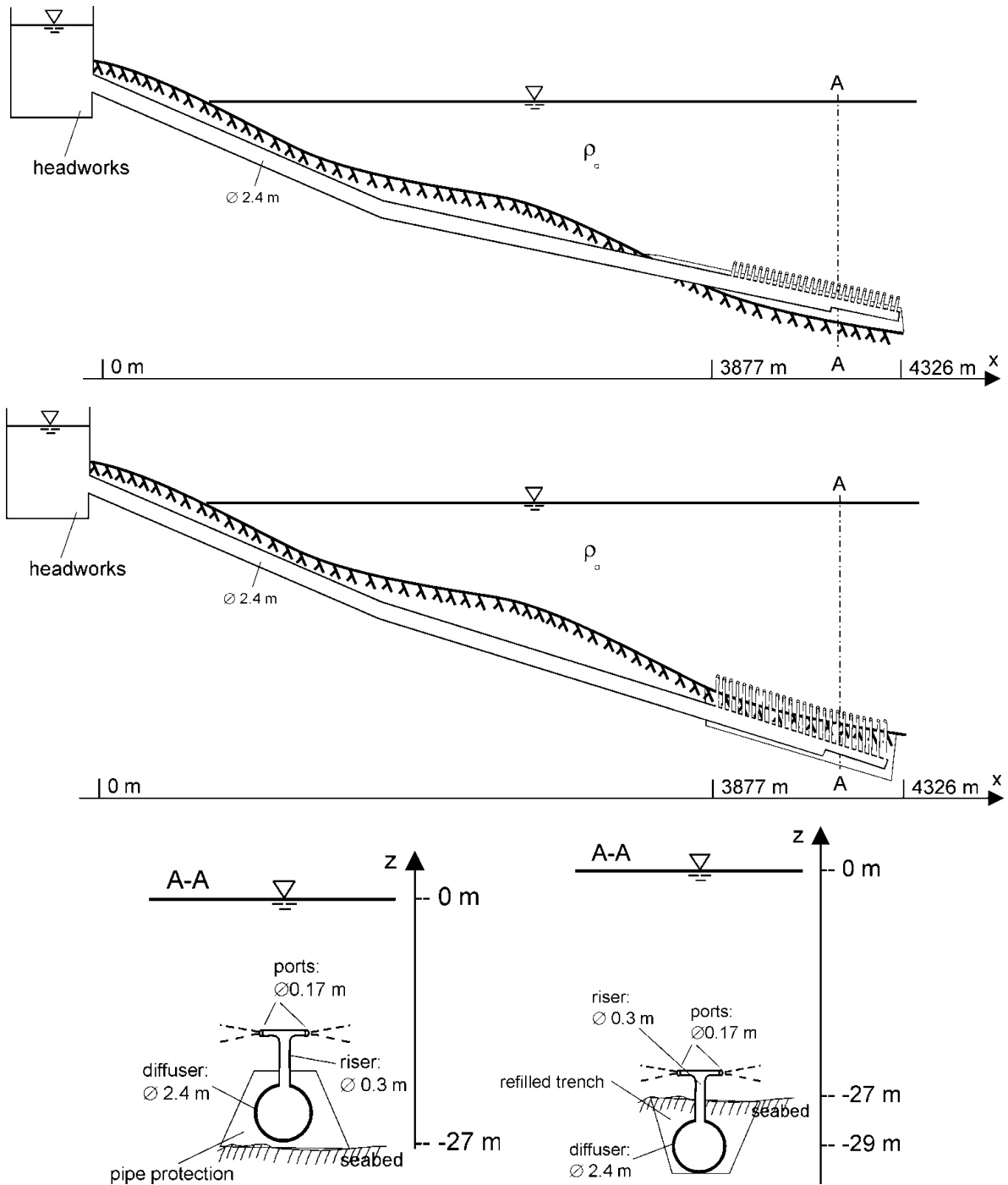


Fig. 43: Side view and cross section of two design alternatives for the Ipanema outfall. *Left*: covered diffuser pipe and short risers, *right*: diffuser pipe laid in a refilled trench and short risers

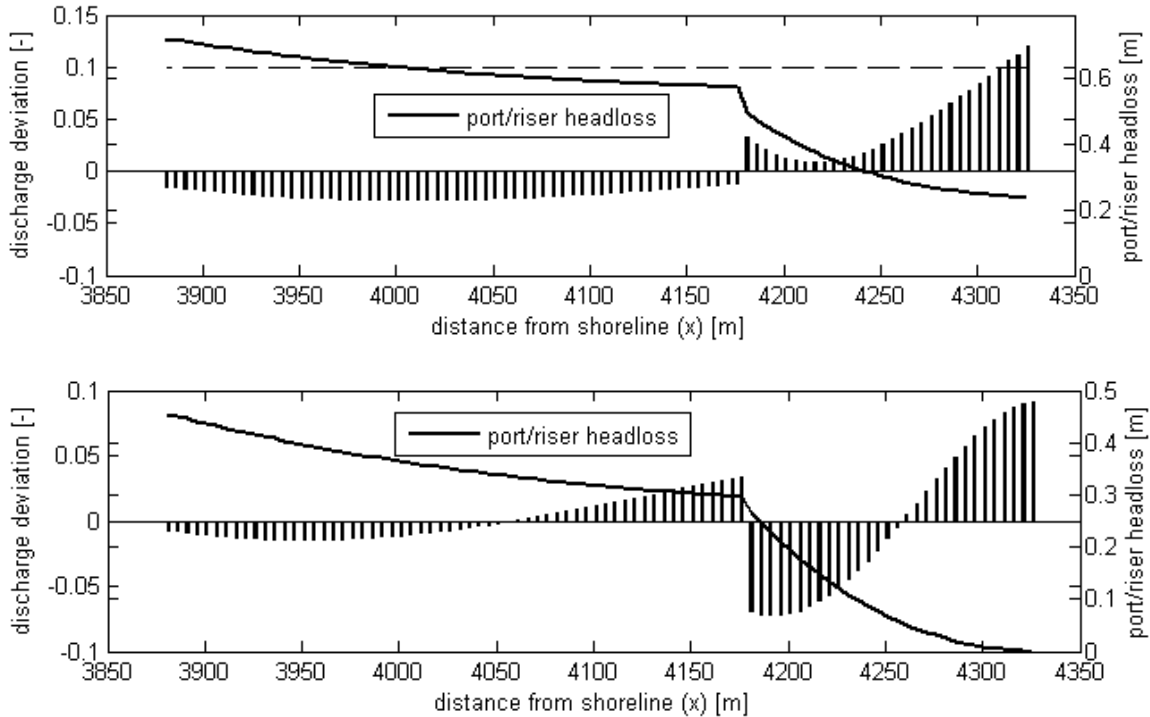


Fig. 44: Flow characteristics for: *top*: tapered diffuser covered or laid in a trench with additional short risers and two different riser diameters, *down*: tapered diffuser on piles without risers.

ii. Tunneled diffuser - long risers and rosette like port arrangements

Nowadays tunneled outfalls are affordable in some cases. Often long risers have been used in these circumstances. It is furthermore tried to reduce the number of risers, because drilling operations are quite expensive. Instead of many risers, a few large risers with rosette like port arrangements at the top are constructed (Fig. 45). The flow changes in flow distribution for the tapered tunneled diffuser with long risers and a rosette like port arrangement, using half of the risers and having four ports discharging at every rosette are shown in Fig. 46. The riser diameters have been increased to 0.6 m at the tapered diffuser section and 0.35 m at the near-shore section to cope with the increased riser flowrate.

However, it has to be considered, that the application of few rosettes compared to many risers does have a considerable effect on the external hydraulics. A detailed mixing calculation should be analyzed to study this drastic change of the diffuser geometry.

iii. Duckbill valves - variable area orifices

Existing diffusers may also be modified by attaching variable area orifices (Duckbill valves, DBV) to avoid intrusion of saltwater, debris or sediment as well as to make the discharge distribution more homogeneous during low flows. Fig. 47 shows results for different flowrates for a system with duckbill valves compared to a system without. Improvements regarding the discharge profile are especially seen for low flows, and even more effective for sloped diffusers. Beside the additional costs for Duckbill valves, also an increased total head has to be considered (11% increase compared to same system without duckbills and 14% compared to basecase).

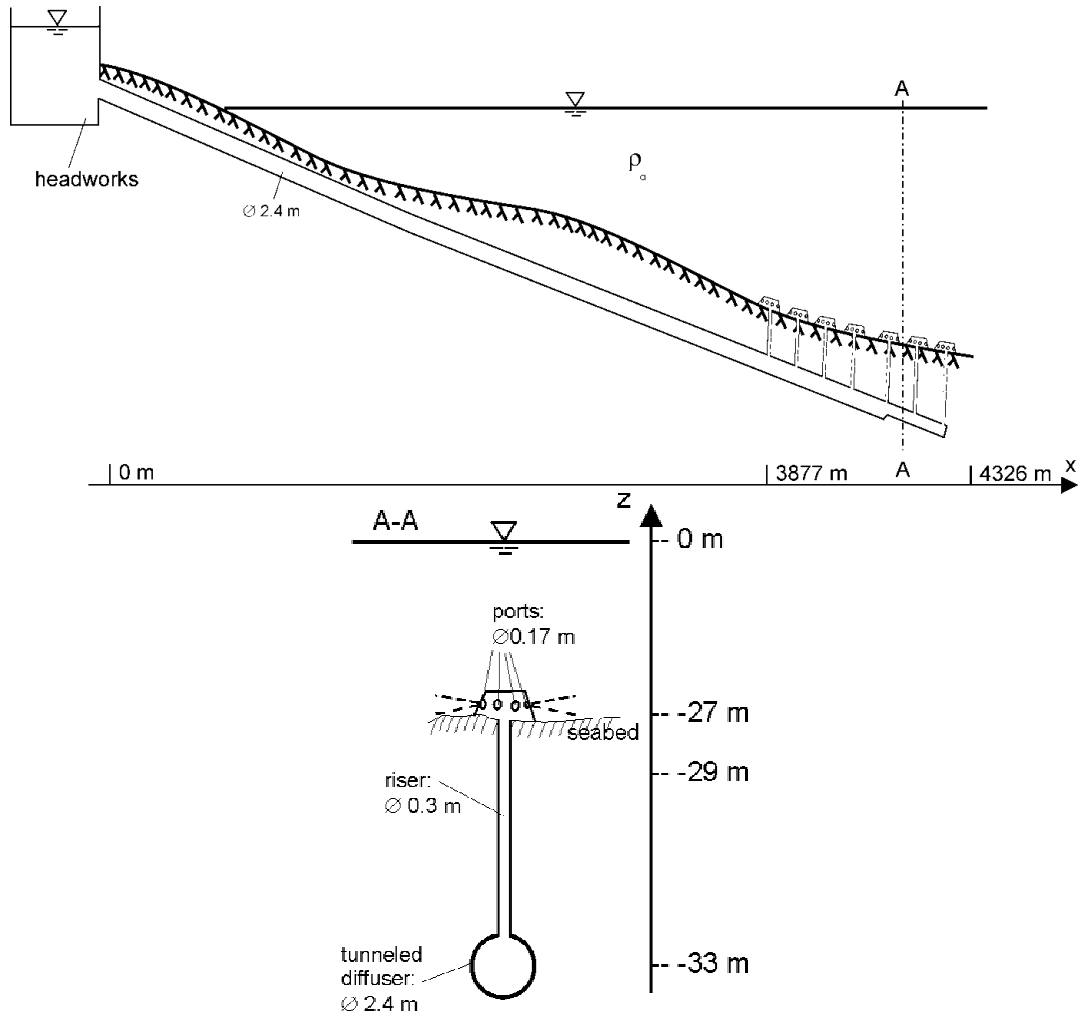


Fig. 45: Side view and cross section of a constructional design alternative for the Ipanema outfall with a tunneled diffuser pipe, long risers, and rosette like port arrangements.

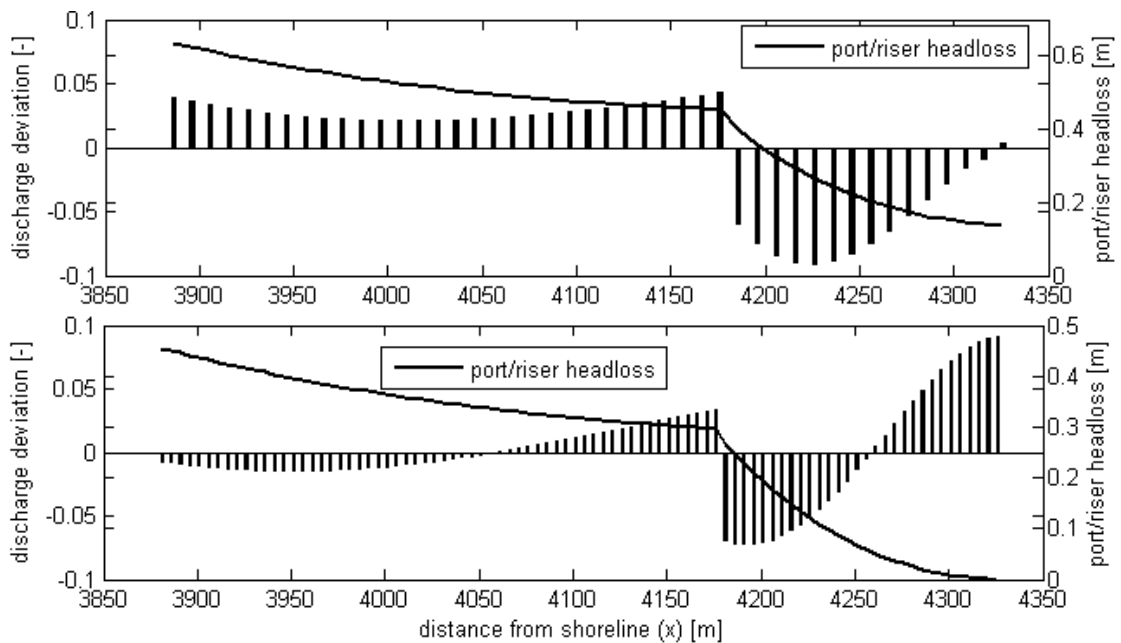


Fig. 46: Flow characteristics for: *top*: tapered tunneled diffuser with long riser and rosette like port arrangements, *down*: tapered diffuser on piles without risers

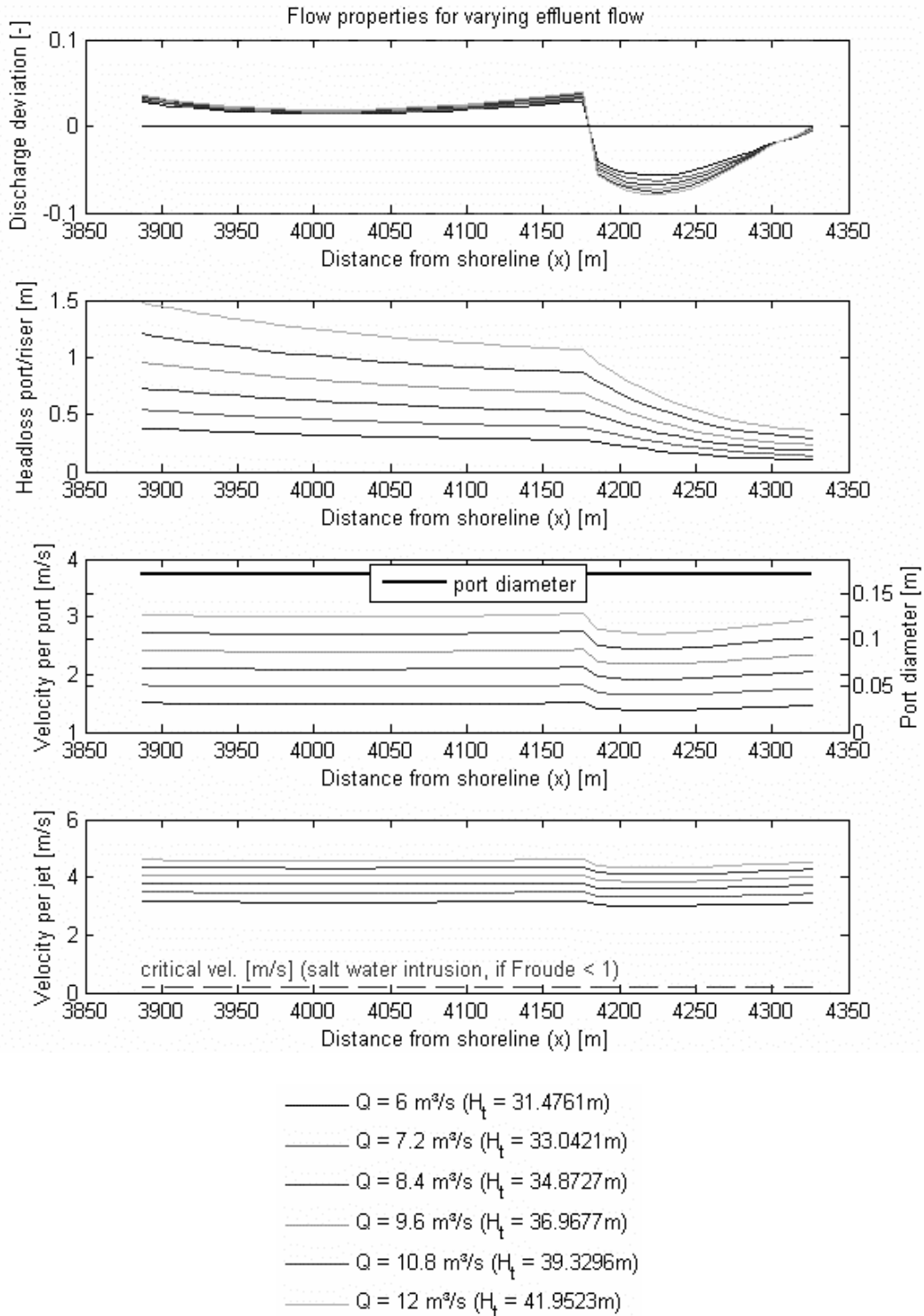


Fig. 47: Flow characteristics for different discharges (Q), for a diffuser with additional Duckbill valves ($D = 200$ mm), showing the riser flow deviation, port/riser headloss, port and jet discharge velocities, diffuser pipe velocities and total head (H_t)

Table 15 shows the comparison between the different alternatives listed above. An optimized diffuser design often results in an increased total head. Maximum values here are a 15% increase. However, even cheaper solutions in the order of 5% allow for very good diffuser performance and result in lesser maintenance necessities, better dilution characteristics, and therefore cheaper operation.

name	total head / relative head [m]	difference in total head to basecase [m / %]	discharge distribution [%]	no scouring [m] / [no. of ports] (L _d = 449, 180 ports)
basecase (build)	33.32 / 6.32	0 / 0	+/- 5	125 m / 50
taper	33.69 / 6.69	0.37 / 6	+/- 8	20 m / 8
taper short riser	33.92 / 6.92	0.60 / 9.5	+/- 8	20 m / 8
taper long riser rosettes	33.72 / 6.42	0.4 / 6.2	+/- 8	20 m / 12
taper DBV 200	34.23 / 7.23	0.91 / 14.4	+/- 6	20 m / 12

Table 15: Comparison of constructional alternatives for Ipanema diffuser

4.5.2 Berazategui - Buenos Aires - Argentina

The Berazategui outfall is planned to discharge the treated effluents of a wastewater treatment plant to be constructed for the city of Buenos Aires. The sewer-system is separated from the storm-water sewer and is designed for an average effluent flowrate of about 25 m³/s with a maximum peak discharge of 33.5 m³/s. The outfall starts at the pumping basin on the onshore headworks, from where a 4500 m long feeder tunnel conveys the effluent to the 3000 m long diffuser in the discharge area (Fig. 48). The diffuser is composed of vertical risers carrying four ports in a rosette-like arrangement (Fig. 49).

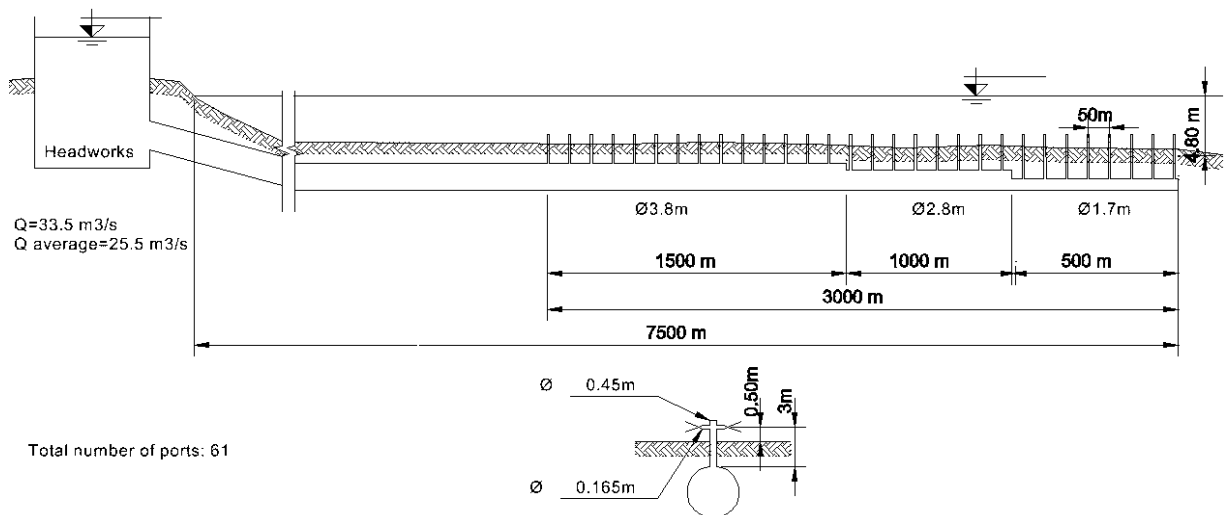


Fig. 48: Schematic view of diffuser longitudinal section of Berazategui outfall

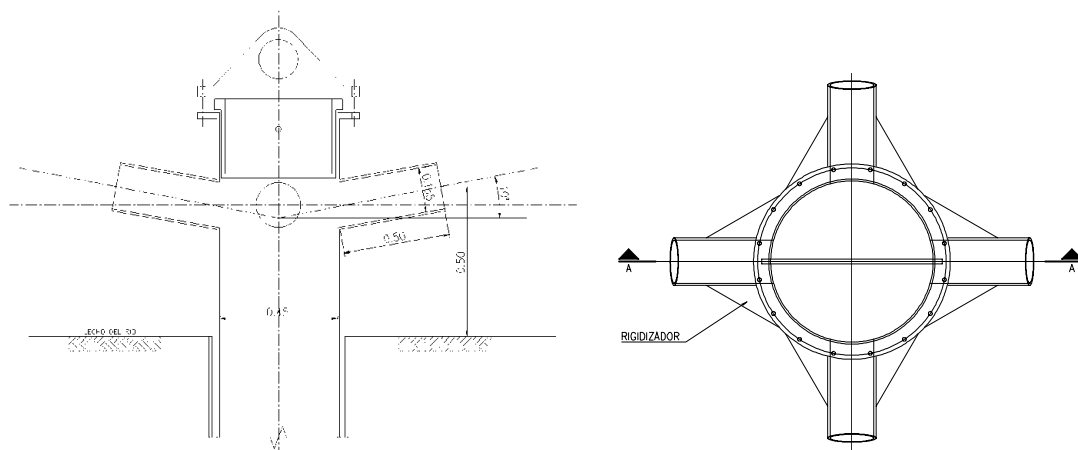


Fig. 49: Side and top view of riser/port configuration of diffuser

The receiving water body is the Rio de la Plata estuary of the rivers Paraná and Uruguay (average annual fresh water discharge: 23,000 m³/s). The width of the estuary at the outfall location is about 50 km with a depth varying from 4 to 7 m (Fig. 50). Tidal currents, including temporal density stratifications dominate the velocity field (average local velocity: $u_a = 0.04$ m/s, maximum velocities during tidal cycle $u_{a,max} = 0.3$ m/s).



Fig. 50: Top view of the Rio de la Plata delta showing the location of the Berazategui outfall and the ambient characteristics at its location (source: Nasa, 2005)

The calculated internal flow characteristics of the diffuser are summarized in Fig. 51 for maximum flow $Q_{max} = 33.5$ m³/s. A reasonably good discharge distribution along the diffuser (first bar-chart Fig. 51) with maximum deviations from the mean discharge of not more than 10% of the mean discharge (second bar-chart, Fig. 51) could be obtained to an equal dilution requirement along the diffuser. Due to different pressure losses along the diffuser pipe and the port/riser configurations (line in second bar-chart, Fig. 51) the discharge is decreasing typically to the seaward end, which can be prevented by modifying the geometries along the diffuser. In this case by reducing the main diffuser diameter to the seaward end, which also improves the diffuser velocities at the end sections (fourth bar-chart, Fig. 51).

The use of duckbill valves with a nominal diameter of 150 mm provides a more homogeneous flow distribution especially for low flows (Fig. 52). Without duckbills the flow distribution is unaffected by changing the total flow due to negligible density differences between the effluent and the ambient and the almost horizontal installation of the diffuser. However, the total head (H_t) necessary to drive the system is higher with duckbill valves (Fig. 52, legend). Larger duckbills (200 mm) reduce the total head almost to the level without duckbills, but decrease also the effects on the discharge distributions to negligible levels. Changes in the ambient water level do not have any effect on the flow characteristics but increase the total head.

To prevent intrusion of ambient water (including sediments), especially during low flow, the port densimetric Froude number should be bigger than unity. This gives a critical port velocity $V_{p,crit} = (\Delta\rho/\rho g D_p)^{0.5} = 0.041$ m/s for Berazategui. All port and jet exit velocities are considerably higher for all applied flow rates. Duckbill valves cause additionally a homogenization of the jet exit velocities.

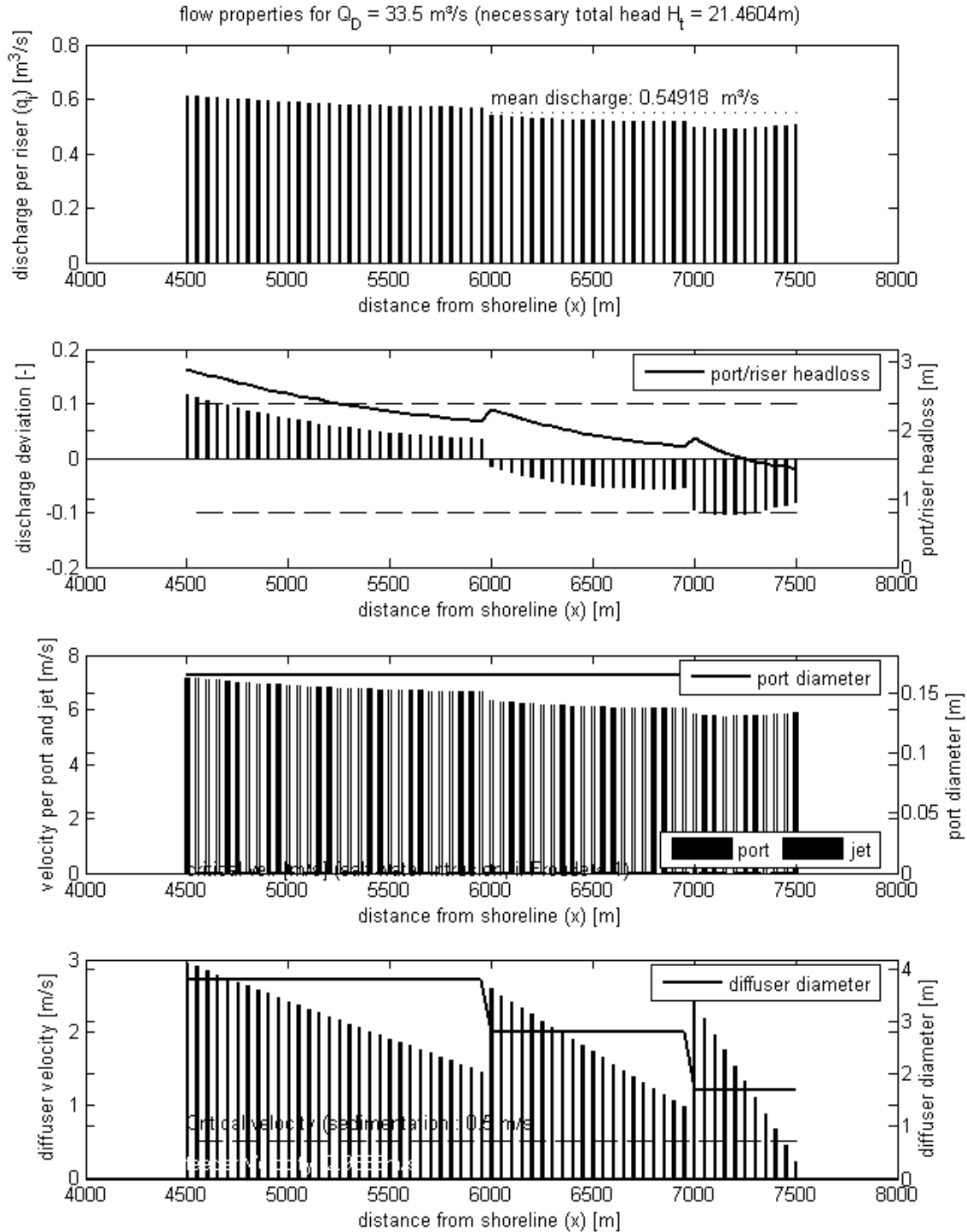


Fig. 51: Flow characteristics for final design at maximum flow. *Top-down*: Individual riser flow distribution along diffuser, riser flow deviation from mean, pressure losses in port/riser configurations (line), port and jet discharge velocities and diffuser pipe velocities, port and diffuser diameter (lines).

An increasing inflow or increasing ambient water level mainly increases the total head (Fig. 53). Headworks storage tanks should be capable of managing these changes. For slowly increasing future flows, an extension of storage tanks can be done only when necessary, saving investment costs for the commissioning.

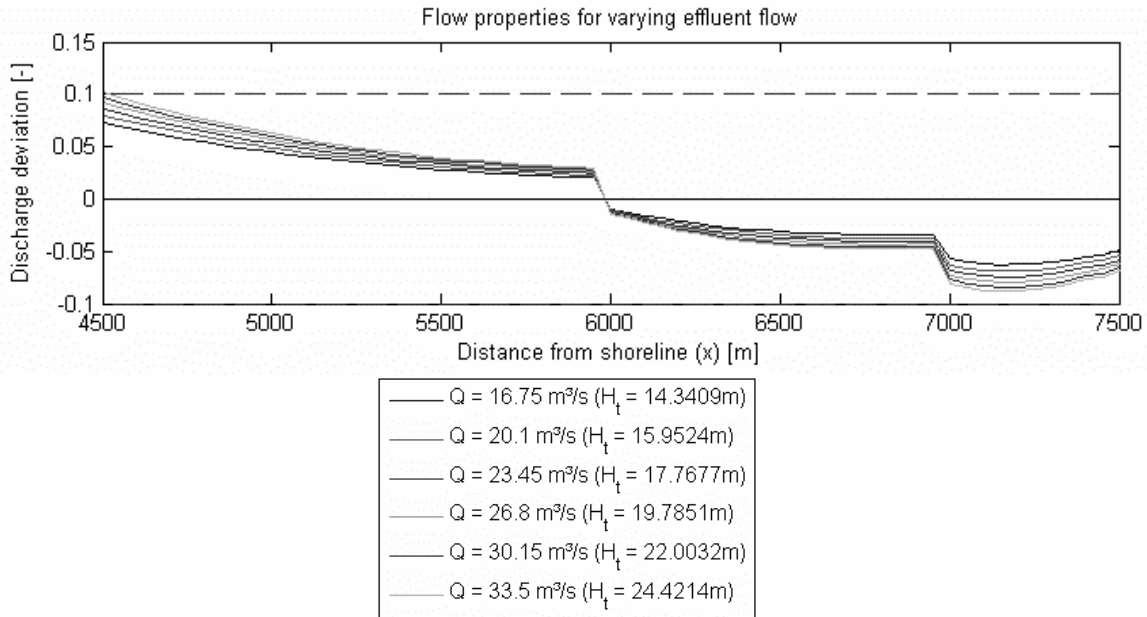


Fig. 52: Flow characteristics for the final design and attached Duckbill valves (150 mm), for different discharges (Q), showing the riser flow deviation

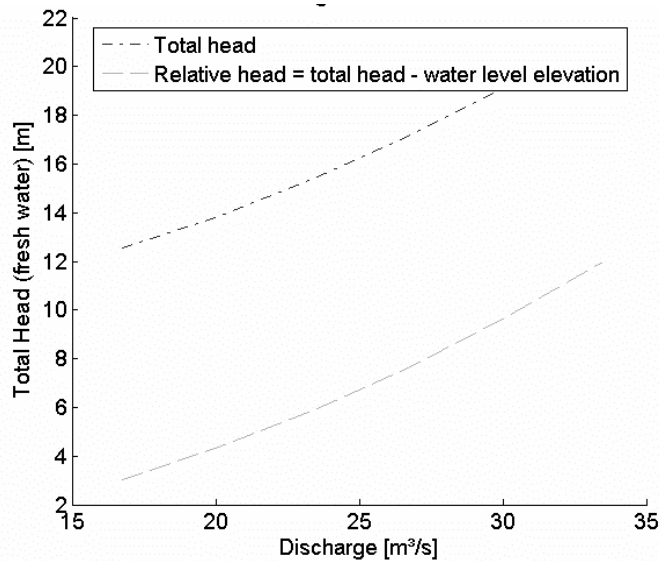


Fig. 53: Changes in total head for varying discharges

4.6 Discussion and recommendations

The computer program developed, CorHyd, releases restrictions of previous ‘diffuser programs’ by considering flexible geometry specifications with high risers and variable area orifices, all with automatic definition of loss coefficients. Additional design features regarding blocked ports, sensitivity analysis and performance evaluation for varying parameters guarantee proper diffuser operation and reduced costs for installation, operation and maintenance.

CorHyd capabilities are demonstrated within a case study for the Ipanema outfall in Rio de Janeiro, Brazil. The application of a large number of design alternatives shows sensitivities on design parameters regarding the total head at the headworks, the discharge distribution and

diffuser performance regarding particle deposition during low flows. Further optimization procedures indicate potential for improvements.

Detailed calculations for the internal manifold hydraulics in the 3 km exceptionally long diffuser of the Berazategui (Buenos Aires) sewage outfall show a strong sensitivity on the representation and formulation of local losses even for relatively simple riser/port configurations. Special attention is necessary to account for all these losses in multiport diffuser design, a fact that is often neglected in common programs. Diameter reductions in long diffusers allow maintaining scouring velocities, but change the discharge distribution. An optimization methodology accounted for a homogeneous discharge distribution along the diffuser, minimization of the total head and prevention of sedimentation or ambient water intrusion in the diffuser under varying inflow and ambient conditions. The additional application of Duckbill valves cause higher velocities and achieve only slightly more uniform distribution for low flows, but higher total head and additional costs. The final design achieves more economic and appropriate solutions for material use and operation as well as the minimization of environmental impacts and operational stability for off-design conditions.

General CorHyd design recommendations thus improve diffuser performance, and prevent hydraulic problems (partial blockage, high head losses, uneven flow distribution, salt water intrusion and poor dilution) often observed in diffusers with inadequate design. The utilization of CorHyd in combination with outfall performance monitoring would furthermore allow revealing such defects at an early stage (Bleninger et al., 2004). However, reality shows, that for example until 1990 only 30% of the UK outfalls incorporate some form of flow monitoring. In the Brazilian State of São Paulo only one out of 8 submarine outfalls has a flow monitoring device (Arasaki, 2004). Furthermore, beside the possibilities of pre-emptive remedial action before problems become acute a good knowledge of the flows is valuable for the environmental monitoring, permit and augmentation works.

The combination of CorHyd with CORMIX allows optimizing the internal hydraulics design (cost effective) resulting in environmental sound solutions.

- Multiport diffuser design program CorHyd -

5 Coupled discharge and transport modeling - CorLink

Offshore, submerged, multiport discharges of municipal wastewater in coastal waters pose a challenge for pollutant modeling because of the following dilemmas:

- *Offshore*: The discharge area and associated near-field lies in the inner part of the observed region which – in contrast to shoreline discharges – makes it more difficult to specify boundary or matching conditions for modeling approaches.
- *Submerged*: The buoyant waste water discharge flow is introduced near the bottom of the salt water column and after completion of the near-field motions including interaction with a potential coastal ambient stratification the transition conditions to the far-field may range anywhere from layered flow near the surface to terminal layer flow within the water column to vertically fully mixed flow. This is another major uncertainty in handling transition conditions to the far-field.
- *Multiport discharges*: The discharge geometries and orientations are rather small compared to the resulting plume sizes, though having major significance for the important initial dilution processes. Correct scaling in a computational sense is an inherent problem with modeling issues.
- *Municipal wastewater*: Wastewater discharges show considerable diurnal variation and change with population changes. These effects are amplified if stormwater is connected to the sewer system. Though flows are small compared to ambient flows, density differences cause buoyant processes changing near-field ambient characteristics. In addition, municipal wastewater contains non-conservative substances, like nutrients or pathogens which transformation processes and interactions need to be addressed. Considerations of large time-scales are therefore necessary.
- *Coastal waters*: As distinct from river discharges or discharges in lakes and reservoirs, coastal discharges are highly unsteady and three-dimensional, including further density stratification and tidal variations.

At present, different types of computer models exist for either predicting near-field or far-field characteristics of the effluent discharged into a water-body over different time and space scales (Table 16).

Model	Scale	Typical Grid Resolution
Ocean Circulation	Ocean wide	10 - 100 of km
Coastal Circulation (far-field)	Coastal Zones, Estuaries	0,1 - 1 km
Discharge Mixing Models (near-field)	Local (scale of outfall)	no grid; predictions for 100 m - 5 km

Table 16: Scales and resolutions of different modeling techniques

Several massive developments in this scientific area resulted in numerous improvements regarding numerical stability and computational performance. Anybody with reasonable computer knowledge can nowadays solve complex three-dimensional fluid mechanical problems by applying computational fluid dynamic (CFD) codes. However, substantial deficits remain regarding the basic understanding or practical implementation. Faulty designs do not necessarily originate from faulty models, but from either using the wrong model or the wrong modeling perception. This work therefore concentrates on problem schematization and model choice for practical solutions. First, a review of existing process descriptions and modeling

approaches is given for all hydrodynamic regions, and second a coupling algorithm is developed, which finally is applied to a case study for the Cartagena outfall (Colombia).

5.1 Near-field processes and modeling applications

Waste discharges originate either from pipes or from channels entering the receiving waters at the shoreline, through the water surface or from the inside through a submerged installation. Resulting hydrodynamic features are generally defined as jets, because the effluent flow from the port provides a velocity discontinuity between the discharged fluid and the ambient fluid causing an intense shearing action (Jirka et al., 1996). Then jets are further distinguished regarding the source of the velocity discontinuity into “jets” if the momentum flux or “plumes” if the buoyancy flux dominates (Jirka et al., 1996). One speaks of pure jets or pure plumes or also pure puffs, wakes or thermals if special asymptotic cases are considered (Jirka, 2004). There are large databases and literature resources for these asymptotic regimes and exact theoretical solutions and reasonably, specification of the closure coefficients can be given. However, the actual feature will be a combination generally called a buoyant jet. Furthermore buoyant jets are distinguished regarding their discharge configuration into “surface jets”, “wall jets”, “single port,” or “multiport jets.”

In the following, attention is restricted to turbulent buoyant jet flows resulting from submerged multiport diffuser installations. Buoyancy resulting from the density difference of the freshwater like waste effluent and the salty seawater cause the plume to rise. The shear region at the interface between the jet and the ambient increases rapidly by incorporating ("entraining") ambient fluid. Thus jet characteristics (e.g. fluid momentum or pollutants) become diluted by the entrainment of ambient water (Jirka et al., 1996), illustrated in Fig. 54.

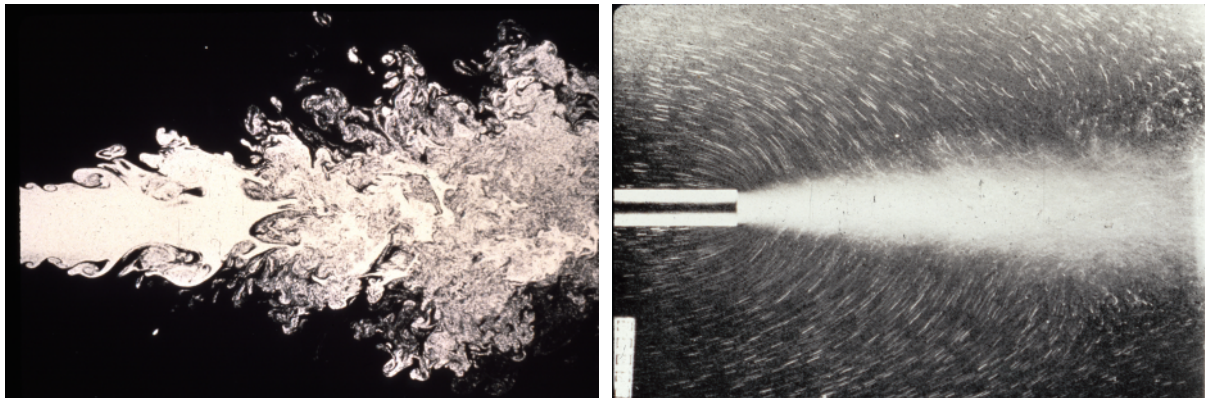


Fig. 54: Instantaneous picture and long-term exposure picture of laboratory studies for pure single jets, showing entrainment motions diluting the effluent (source: G.H. Jirka)

Discharge orientation, ambient currents, and densities influence the jet trajectories shown in Fig. 55 for the example of single buoyant jets. Consequences are generally higher dilutions for ambient velocity induced jet deflections and lower dilutions due to density induced dampening of vertical motions for trapped plumes. Multiport jets are additionally influenced by the merging processes of individual jets, forming a two-dimensional buoyant jet plane with its own characteristics, as illustrated in Fig. 56 and Fig. 57. A general review of these processes has been given by Fischer et al. (1979), Wood et al. (1993), Roberts (1990, 1996) or Jirka and Lee (1994).

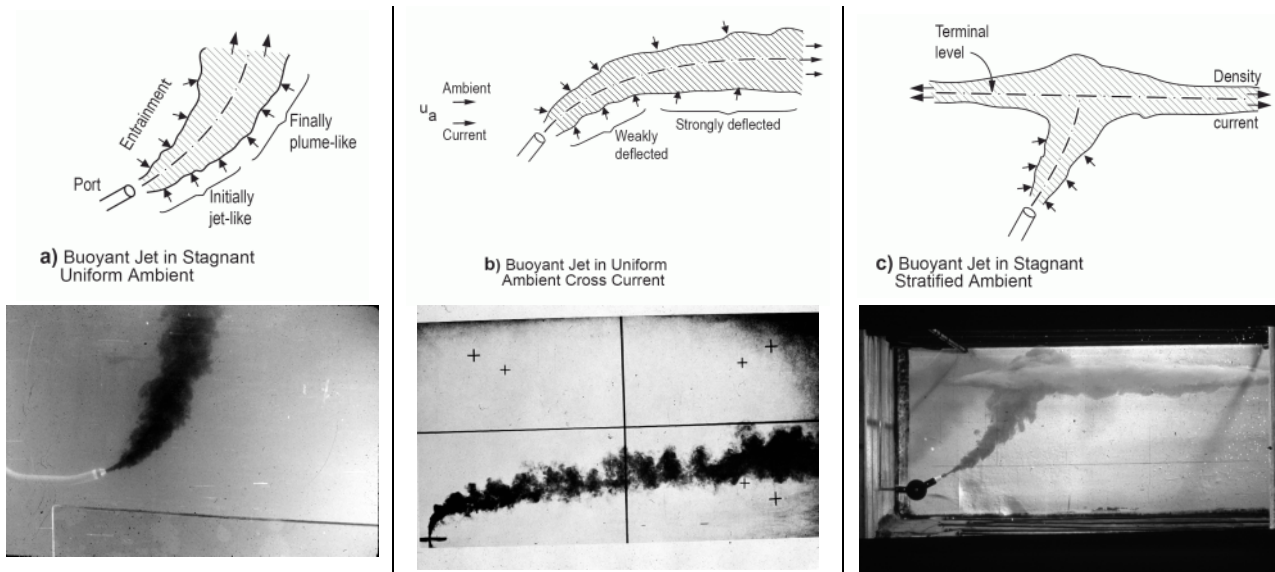


Fig. 55: Schematized figures and visualizations from laboratory experiments showing different jet trajectories influenced by *a)* ambient density, *b)* ambient current u_a , and *c)* ambient stratification (Jirka, et al., 1996; pictures from G.H. Jirka; L. Fan)

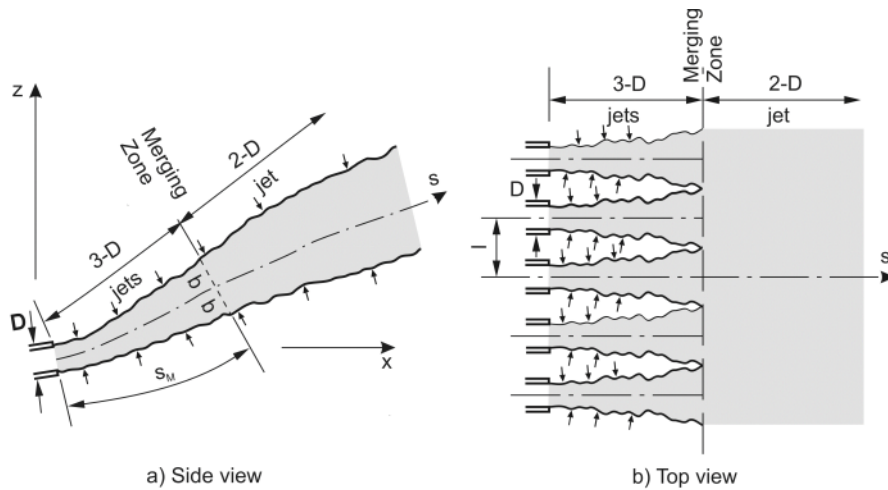


Fig. 56: Schematization and visualization of laboratory experiment for merging of jets discharged unidirectional by multiport diffusers (reproduced from Jirka 2006)

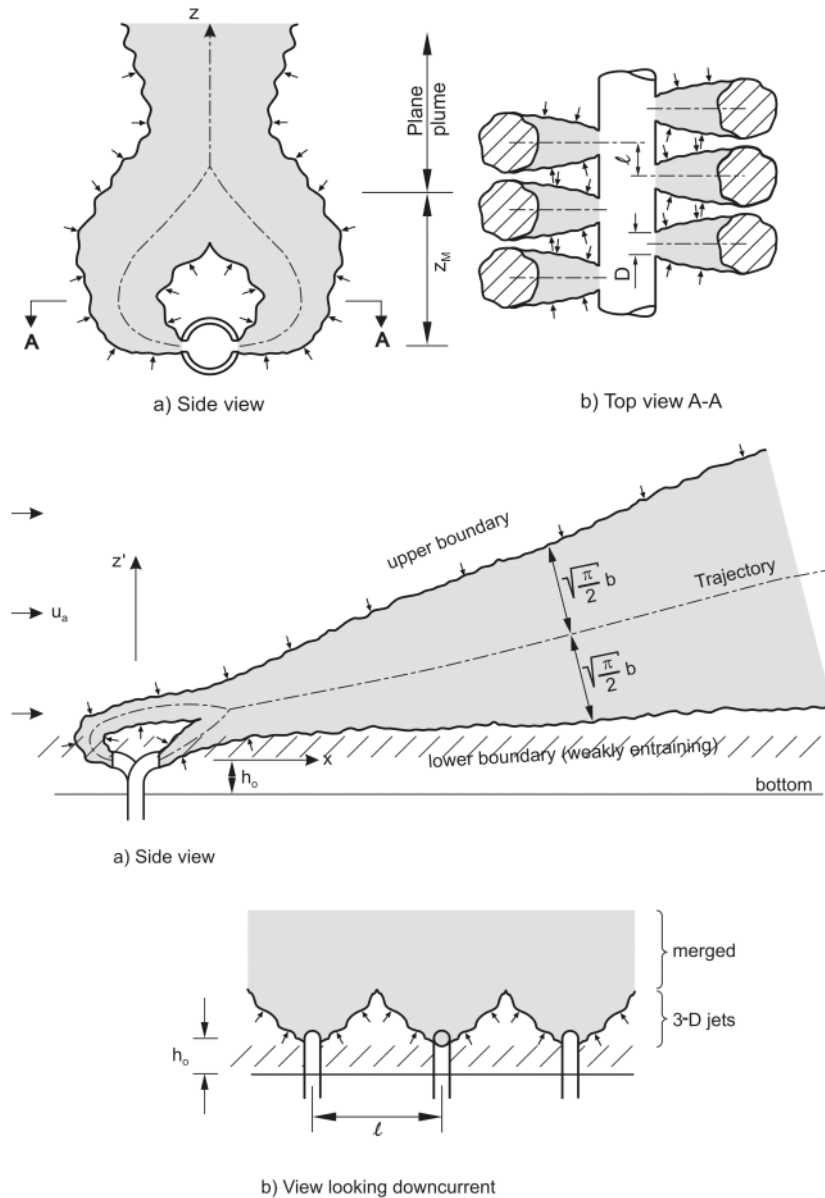


Fig. 57: Schematization of merging jets discharged by a multiport diffusers with an alternating port arrangement in stagnant conditions and in crossflow (reproduced from Jirka 2006)

5.1.1 Governing equations for multiport buoyant jets

Buoyant jet equations are all based on the simplifications explained in chapter 3 regarding the near-field region. This means steady-state in the mean, unbounded ambient environments (until the intermediate field) with stable density stratification and steady ambient current conditions. These are justified in many cases because time scales for the near-field mixing processes are usually of the order of minutes up to perhaps one hour. A review of single buoyant jet studies is given in Jirka (2004). The extension to plane jets and multiport jets is described in Jirka (2006), which will be summarized here. Multiport diffuser parameters are schematized in Fig. 58 and defined as the diffuser length L_D , the individual port diameter D , individual port cross-sectional area $A_o = \pi D^2/4$, port spacing ℓ , port and diffuser orientations β , γ , θ , port exit velocity U_o , effluent density ρ_o and concentration c_o , average depth of receiving water H with stable vertical density distribution $\rho_a(z)$ and a vertically sheared, steady velocity profile $u_a(z)$.

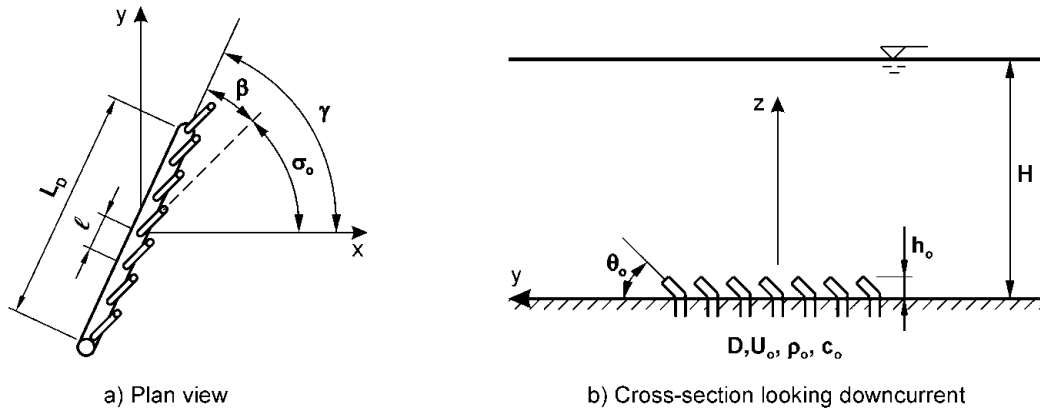


Fig. 58: Definition diagram for a multiport diffuser (reproduced from Jirka et al., 1996)

The extension of single buoyant jet theories to multiport jets is based on another major assumption regarding the so-called equivalent slot concept. Here a series of round jets from a multiport diffuser are idealized as a single two-dimensional plane jet, with similar characteristics after merging takes place (Fig. 56b, and Fig. 57b). The slot dimensions are hereby chosen as the diffuser length L_D for the total width and the equivalent slot width B calculated to achieve diffuser flux quantities equal to those caused by the individual multiport jets (see equations 5.1 - 5.4). This assumption is generally valid for most of the existing closely spaced multiport diffuser installations, where merging takes place after reasonable distances and in a rather uniform manner (Jirka, 2006, Roberts, 1996, Tian et al., 2004). However, two main limitations need to be considered:

- i) *Complex discharge configurations*: In recent years, more tunneled outfalls with buried diffusers have been built. These are often equipped with only few largely spaced long risers and rosette like port arrangements. Individual jet quantities are then not any more the right measure for calculating the equivalent slot width. Additional hydrodynamic considerations have to amplify the equivalent slot width concept, which are currently under development (Kwon and Seo, 2005, or Jirka, 2006). Experiments from Kwon and Seo (2005) hereby showed a strong dynamic regime between the individual jets, however this hold only for stagnant ambient. In strong ambient crossflows, these effects probably are reduced. The proposed equivalent slot jet concept calculating an equivalent port diameter (Jirka, 2006) followed by the application of the equivalent slot concept looks promising and straightforward. Another issue shown by Roberts and Snyder (1993) indicates that there are quite large regions of insensitivity of dilution on riser spacing.
- ii) *Non-uniform distribution of jet quantities along diffuser*: The assumption that an average of all individual jet quantities along the diffuser suffices to describe the mean plane jet quantities may be too general. It has been shown in chapter 4, that significant variations of jet quantities might occur along the diffuser line, though designs clearly should aim for nearly uniform distributions. A stepping of the whole slot into several different slots might be proposed here, though neglecting interaction between two resulting plane jets.

Thus buoyant plane jet parameters can be specified according the definition diagram in Fig. 59, where the slot is located in the horizontal plane and aligned, in general, at an oblique angle to the ambient current. Definitions are conform Jirka (2006) with the discharge slot located at the height h_0 above the x - y plane and obliquely aligned with an angle γ relative to the

x -axis and a vertical angle θ_0 above horizontal and a horizontal angle σ_0 between the vertical projection of the jet and the x axis.

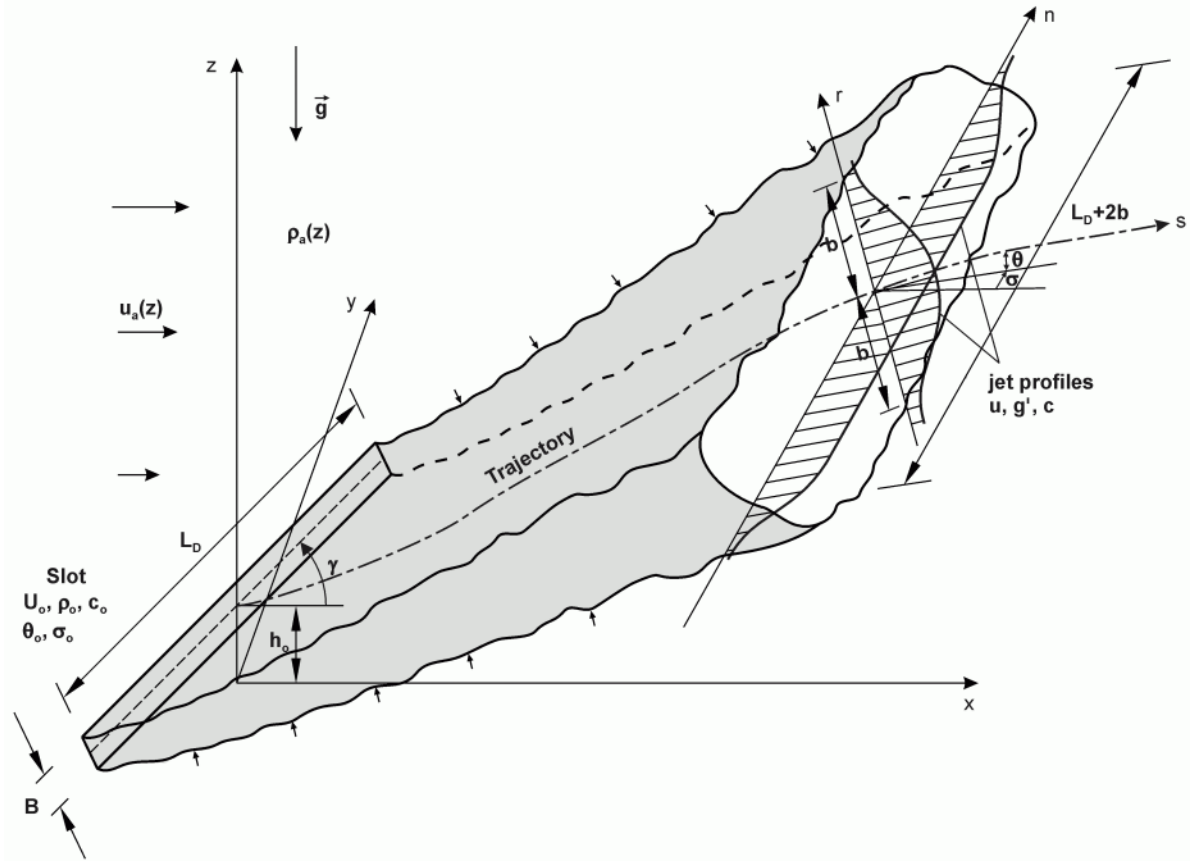


Fig. 59: Definition diagram for the plane jet (reproduced from Jirka, 2006)

The jet discharges through the cross-sectional area $a_o = BL_D$ with a steady top-hat velocity profile U_o . The initial fluxes for the individual buoyant jets (with index i) and the idealized plane jet are:

The initial volume flux

$$Q_o = \sum Q_{o,i} = \sum U_{o,i} A_{o,i} = U_o a_o \quad (5.1)$$

The initial mass flux

$$Q_{co} = \sum Q_{co,i} = \sum U_{o,i} C_{o,i} A_{o,i} = U_o c_o a_o \quad (5.2)$$

The jet is forced by two dominant dynamic quantities, the initial momentum flux

$$M_o = \overline{M_{o,i}} = \overline{U_{o,i}} (\sum U_{o,i} A_{o,i}) = U_o^2 a_o \quad (5.3)$$

and the initial buoyancy flux

$$J_o = \overline{J_{o,i}} = \overline{g_{o,i}'} (\sum U_{o,i} A_{o,i}) = U_o g_o' a_o \quad (5.4)$$

where $g_{o,i}' = g(\rho_a(h_{o,i}) - \rho_o)/\rho_{ref}$ defines the initial buoyant acceleration with a constant reference density ρ_{ref} .

Buoyant plane jets from waste discharges are generally considered as fully turbulent, because of sufficiently high values of the slot Reynolds number $Re_o = U_o B / \nu$ in which ν is the kinematic viscosity. Laboratory experiments show that its critical value is $Re_o \approx 1000$ (Jirka, 2006). Jet analysis is based on an Eulerian description of the centerline trajectory s as a function of the Cartesian coordinates x, y, z with superimposed Lagrangian type description of the evolution of the jet quantities $Q, M,$ and J along that centerline trajectory (Fig. 59). Turbulent fluctuations caused by turbulence shearing mechanisms lead to a gradual growth of the characteristic jet thickness $2b$ and characteristic width $L_D + 2b$. The parameter b is a measure typically defined where the excess velocity is e^{-1} (37%) of the centerline value. The relatively large diffuser lengths compared to plume thickness $L_D / (2b) \gg 1$ generally allow neglecting the entrainment at the lateral plume ends. Plane plume growth thus is dominated by two-dimensional processes (Jirka, 2006) and quantities per unit jet length can be described for the initial fluxes (Jirka, 2006):

$$q_o = Q_o / L_D = U_o B \quad (5.5)$$

$$q_{co} = Q_{co} / L_D = U_o c_o B \quad (5.6)$$

$$m_o = M_o / L_D = U_o^2 B \quad (5.7)$$

$$j_o = J_o / L_D = U_o g_o' B \quad (5.8)$$

Main interest in buoyant jet analysis is the development of the plane jet fluxes q, m and j along the centerline. These depend on the unknown distributions of jet parameters $u, v,$ and c in a coordinate system with axial distance s and transverse distance r inclined with the local horizontal angle θ and horizontal angle σ (Fig. 59) and are defined as:

$$q = \frac{1}{L_D} \int_r u \, dr \quad (5.9)$$

$$q_c = \frac{1}{L_D} \int_r uc \, dr \quad (5.10)$$

$$m = \frac{1}{L_D} \int_r u^2 \, dr \quad (5.11)$$

$$j = \frac{1}{L_D} \int_r ug' \, dr \quad (5.12)$$

The governing equations for the distribution functions then result from the Navier-Stokes equations described in chapter 3 with simplifications regarding a steady (time averaged) 2-D flow along the jet centerline (for the steady velocity u and v the averaging bar will not be used for simplicity reasons). Approximations from the boundary layer type of flow ($b/s \ll 1$) allow the assumption that $\partial/\partial r \ll \partial/\partial s$. Furthermore the jet internal pressure will be equal to the ambient pressure field (here assumed to be constant) thus $\partial p/\partial r = \partial p/\partial s = 0$, giving:

Continuity equation

$$\frac{\partial u}{\partial s} + \frac{1}{r} \frac{\partial rv}{\partial r} = 0 \quad (5.13)$$

Momentum equation

$$u \frac{\partial u}{\partial s} + v \frac{\partial u}{\partial r} = \frac{1}{r} \frac{\partial}{\partial r} (r \overline{u'v'}) - g' \sin \theta \quad (5.14)$$

Transport equation

$$u \frac{\partial c}{\partial s} + v \frac{\partial c}{\partial r} = \frac{1}{r} \frac{\partial}{\partial r} (r \overline{c'v'}) \quad (5.15)$$

And three additional equations to solve for the 3-D jet trajectory (Jirka, 2006):

$$\frac{dx}{ds} = \cos\theta \cos\sigma \quad (5.16)$$

$$\frac{dy}{ds} = \cos\theta \sin\sigma \quad (5.17)$$

$$\frac{dz}{ds} = \sin\theta \quad (5.18)$$

For the initial conditions it follows for $s = 0$ that $u = U_o$, $c = C_o$ and $v = 0$. The boundary conditions for $r \rightarrow \infty$ can be prescribed as $u \rightarrow 0$, $c \rightarrow 0$, $\overline{u'v'} \rightarrow 0$ and $\overline{c'v'} \rightarrow 0$. Different methods have been used to solve these equations:

- i) *Empirical methods*: For simple geometries and flows considerable simplifications of the governing partial differential equations, allow solving these problems analytically. Under these conditions, a zero equation turbulence closure can be assumed with a constant eddy viscosity ν_t calibrated with laboratory experiments. Results of empirical models often are only related to final dilution values.
- ii) *Integral methods*: Self-similarity approaches allow defining jet-cross-sectional distribution functions a priori thus converting the governing partial differential equations into ordinary differential equations, which are easier and faster to solve. Integral models are the standard type of models for jet analysis. Results of integral models generally are dilutions and trajectories of the resulting plume in an infinite water body, thus without any boundary interaction.
- iii) *Numerical methods*: For more complex geometries and flows numerical solution of the partial differential equations are needed. Furthermore an advanced (at least two equation) turbulence closure, e.g. the k- ϵ model, Reynolds-stress or Large Eddy simulation model is necessary. These solutions are difficult, demanding, and not yet practical. Results of numerical models are complete, giving dilutions and trajectories in limited water bodies.

5.1.2 Dimensional analysis - empirical methods

Flow parameterization and scaling of flow conditions allows classifying and analysis of different flows. Dimensional analysis is extremely useful for analytical studies and the flow classification, where dominant processes can be determined for the subsequent modeling and minor processes excluded. This is especially important for consideration regarding the asymptotic regimes (e.g. pure jet). However, for complex flows (i.e. unsteady non-uniform flows) the finding and definition of (steady) characteristic scales becomes difficult. Nonetheless, equations resulting from dimensional analysis then still provide a helpful tool for an “order of magnitude analysis” and means of flow classification.

5.1.2.1 Velocity and concentration distributions - dimensionless parameters

Unknowns (dependent variables) of the present problem are the jet velocities u and v , the concentrations c and the trajectory locations s . Considering now for example the asymptotic case

of a horizontal plane jet in stagnant, uniform ambient. Characteristic quantities are the width $b = f_1(x, m_o, a_o, v, \dots)$ and the centerline velocity $u_c = f_2(x, m_o, a_o, v, \dots)$, both as a function of independent parameters. Dimensional analysis then results in dimensionless parameters:

$$\frac{b}{x} = \text{const.} \quad (5.19)$$

$$\frac{u_c \sqrt{x}}{\sqrt{m_o}} = \text{const.} \quad (5.20)$$

Thus, the width development follows a linear function with the proportionality factor k_1 (e.g. from experiments $k_1 = 0.14$ (Jirka, 2006)):

$$b = k_1 x, \quad (5.21)$$

and the centerline velocity decays inversely with the distance with the proportionality factor k_2 (from experiments $k_2 = 3.36$ (Jirka, 2006))

$$\frac{u_c}{U_o} = k_2 \sqrt{\frac{B}{x}} \quad (5.22)$$

For the centerline concentration c_c , mass flux conservation results in

$$q_{co} = c_o U_o B \approx c_c u_c 2b \quad (5.23)$$

$$\Leftrightarrow \frac{c_c}{c_o} \approx \frac{U_o B}{u_c 2b} = \frac{1}{k_2 k_1} \sqrt{\frac{B}{x}} \quad (5.24)$$

Any buoyant jet property can theoretically be described in analogy to the previous examples. However, with increasing complexity, the number of independent parameters increases and difficulties arise in defining consistent relations on one hand and elaborating necessary laboratory studies on the other. Thus dimensional analysis is restricted to steady asymptotic cases with some slight extensions.

5.1.2.2 Plume dynamics and trajectories - length scales and flow classification

Another application of dimensional analysis is not directly related to the aim of developing dilution equations or characteristic profile distributions, but to distinguish between different flow regimes, namely a flow classification. Whereas velocities and concentrations have been successfully normalized by their initial values the results for the trajectories historically normalized by the individual jet diameter showed large scatter, for example for single buoyant jets in the left diagram of Fig. 60. Numerous different solutions have hereby been obtained for different initial densimetric Froude numbers:

$$F_o = \frac{U_o}{\sqrt{g' B}} \quad (4.25)$$

Another parameter combination based on the flux definitions instead resulted in the correct scaling (Fig. 60, right) using the so called momentum length scale, here for a single jet, $L_M = M_o^{3/4} / J_o^{1/2}$ (Jirka, 2004). This length scale allows distinguishing between dominating jet flow regions, thus classifying the flow, as illustrated in Fig. 61.

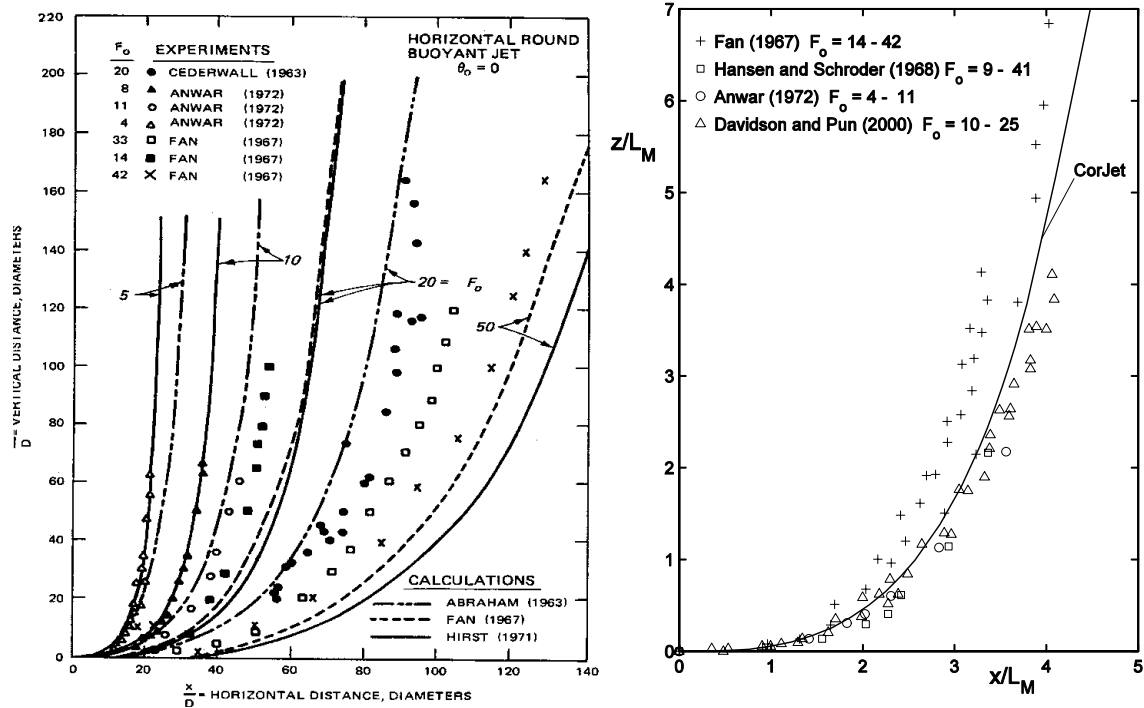


Fig. 60: 3-dimensional horizontal buoyant jet trajectories for a single port discharge in stagnant ambient. Comparison between predictions and experimental data. *Left*: normalized with port diameter. *Right*: normalized with momentum length scale L_M (reproduced from Jirka, 2004)

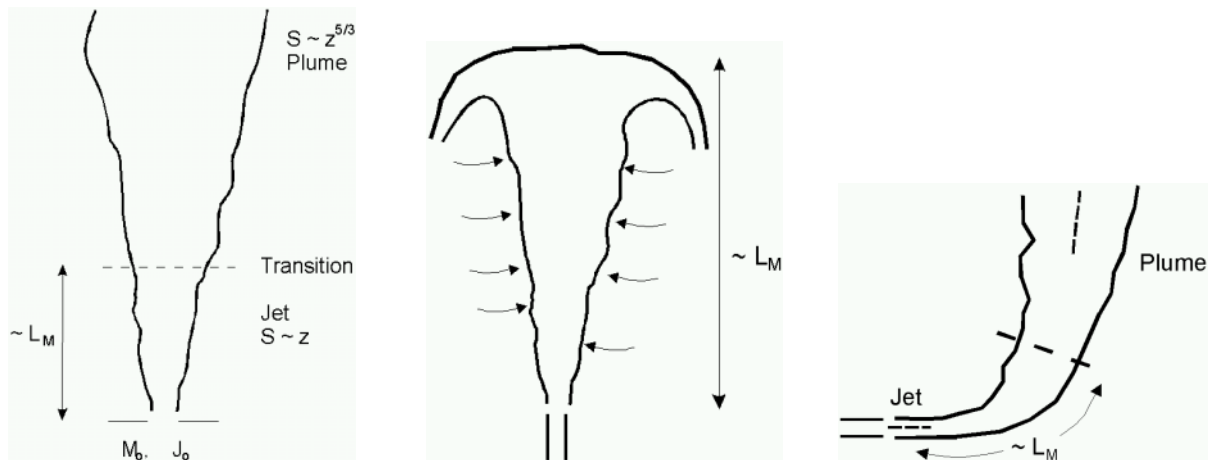


Fig. 61: Jet to plume transition length scale L_M for a single jet allows distinguishing between a jet like or plume like single jet behavior (reproduced from Jirka et al, 1996)

A consistent length scale based categorization of the different buoyant jet regimes in the presence of crossflow and/or stratification is summarized in Fischer et al. (1979) and modified for plane jets by Jirka and Akar (1991) resulting in the following length scales:

The discharge length scale, which denotes a scaling for the region over which the discharge slot geometry has a strong influence on the flow. This scale is generally very small ($\ell_Q = B$) and therefore relatively unimportant.

$$\ell_Q = \frac{g_0^2}{m_0} \tag{5.26}$$

The slot jet / plume transition length scale, which denotes a scaling for the transition from jet to plume behavior in a stagnant ambient (note that the ratio of ℓ_M and ℓ_Q gives F_o):

$$\ell_M = \frac{m_o}{j_o^{2/3}} \quad (5.27)$$

The slot jet / crossflow length scale, which denotes a scaling for the distance of transverse jet penetration beyond which strong deflection by the crossflow occurs:

$$\ell_m = \frac{m_o}{u_a^2} \quad (5.28)$$

The slot jet / stratification length scale, which denotes a scaling for the distance at which the jet becomes strongly affected by the stratification (defined by $\varepsilon = -(g/\rho_a)(d\rho_a/dz)$, the ambient buoyancy gradient), leading to terminal layer formation and horizontally spreading in a stagnant linearly stratified ambient:

$$\ell_m' = \frac{m_o^{1/3}}{\varepsilon^{1/3}} \quad (5.29)$$

The slot plume / crossflow length scale, which denotes the distance at which a plume becomes strongly affected by the crossflow, leading to less lateral spreading:

$$\ell_b = \frac{j_o^{1/3}}{\varepsilon^{1/2}} \quad (5.30)$$

The slot plume / stratification length scale, which denotes the distance at which a plume becomes strongly affected by the stratification, leading to terminal layer formation and horizontally spreading in a stagnant linearly stratified ambient:

$$\ell_b' = \frac{j_o^{1/3}}{\varepsilon^{1/2}} \quad (5.31)$$

The crossflow / stratification length, which denotes a scaling for the vertical flotation beyond a plume, becomes strongly affected by the stratification:

$$\ell_a = \frac{u_a}{\varepsilon^{1/2}} \quad (5.32)$$

In addition, time scales regarding some of the above length scales have been described by Nash (1995) and Nash and Jirka (1996): The slot jet / plume transition time scale, which denotes a scaling for the time until turbulent jet mixing dominates before buoyant mixing takes over in a stagnant ambient:

$$t_M = \frac{m_o}{j_o} \quad (5.33)$$

The slot jet / crossflow time scale, which denotes a scaling for the time required after that the ambient flow dominates:

$$t_m = \frac{m_o}{u_a^3} \quad (5.34)$$

An example for the magnitude of these scales is given for two typical discharges (medium and large flowrates) and two typical ambient conditions (medium and small velocities) as summarized in Table 17 (compare with Fig. 13, p. 21). This shows that near-field plume development occurs in regions of the order of one to tens of meters and time scales of the order of minutes. A comparison with typical ambient conditions, where time scales are of the order of hours and days, and water depths are of the order of tens of meters, confirms the steady state, unlimited ambient approach for the near-field region. Nonetheless, extreme cases (large discharges into slow and shallow waters) indicate, that additional considerations, beyond this simplified approach are necessary.

Variable	small discharge (I) (e.g. wastewater)	large discharge (II) (e.g. thermal discharges)	ratio (I/II)
initial velocity U_o , [m/s]	5	5	1
initial total volume flux Q_o [m ³ /s]	8	80	0.1
initial volume flux $q_o = Q_o/L_D$ [m ² /s]	0.02	0.2	0.1
initial momentum flux $m_o = U_o q_o$ [m ³ /s ²]	0.1	1	0.1
density difference $\Delta\rho/\rho$ [kg/m ³]	0.025 (freshwater)	0.0025 (heated salt-water)	10
initial buoyancy flux $j_o = q_o g_o'$ [m ³ /s ²]	0.005	0.005	1
momentum length scale $\ell_M = m_o/j_o^{2/3}$ [m]	3.4	34	0.1
crossflow length scale $\ell_m = m_o/u_a^2$ [m]	0.4 (10)	4 (100)	0.1
stratification length scale $\ell_m' = m_o^{1/3}/\varepsilon^{1/3}$ [m]	2.5	5.4	0.5
stratification / plume $\ell_b' = j_o^{1/3}/\varepsilon^{1/2}$ [m]	2.1	2.1	1
stratification / crossflow $\ell_a = u_a/\varepsilon^{1/2}$ [m]	6.25 (1.25)	6.25 (1.25)	1
jet / plume time scale $t_M = m_o/j_o$ [s]	20	200	0.1
jet / crossflow time scale $t_M = m_o/u_a^3$ [s]	0.8 (100)	8 (1000)	0.1

Table 17: Comparison of typical flux quantities (modified from Jirka (1982), listing length and time scales for two typical discharges for a city with a population of 1 million people and a diffuser with length $L_D = 400$ m. The average ambient velocity is assumed to 0.1 m/s and 0.5 m/s (values in brackets), with a stratification defined by $\varepsilon = -(g/\rho_a)(d\rho_a/dz) = 0.0064$ 1/s².

5.1.2.3 Empirical dilution equations

The principles and scaling described above have been applied to wastewater dispersion analysis already in the beginnings of environmental related research. Major contributions are from Brooks (1960, 1965, 1980, 1984, 1988), and by Koh (1988). Comprehensive reviews are given in Fischer et al. (1979), Wood et al. (1983) and Jirka and Lee (1994). Detailed discussion on buoyant jets were presented by Jirka (1979, 1994), Roberts (1980, 1986) Roberts et al. (1989a,b,c), Lee and Jirka (1981) and Lee and Neville Jones (1987). The resulting equations are all based on the near-field assumption stated in chapter 5.1.1 and trying to calculate the minimum jet centerline dilution $S_c = c_o/c_c$ at the end of the near-field, i.e. after surface contact or at the terminal layer for trapped plumes. However as stated previously limitations exist regarding mostly near asymptotic regimes.

One of the key equations is the equation for a line plume in a stagnant unstratified ocean (Rouse et al., 1952):

$$S_c = 0.38 \frac{j_o^{1/3} H}{q_o} \quad (5.35)$$

For a given flow Q_o , the unit discharge q_o and unit buoyancy flux j are inversely proportional to the diffuser length L_D , and equation 5.35 suggests that a higher dilution is obtained by increasing the length of the diffuser. For a line plume, the minimum dilution can be multiplied by a factor of $2^{1/2}$ to give the average dilution.

It has been demonstrated both theoretically and experimentally (Fischer et al., 1979) that maximum mixing can be achieved with closely spaced ports that allow some interference of adjacent jets. In relatively shallow coastal waters of typical depth 5 – 15 m, however, it is often the case that, given practical considerations (e.g. in order to maintain a minimum jet velocity and minimum diameter), multiport diffusers are designed to minimize interference of adjacent plumes. In such cases, the required spacing is about $H/3$.

In case of a linearly stratified ambient with a density gradient $d\rho_a/dz$ the maximum height of rise z_{max} to the terminal level and corresponding dilution S_c are given by

$$z_{max} = 2.84 j_o^{1/3} \left(-\frac{g d\rho_a}{\rho_a dz} \right)^{-1/2} = 2.84 \ell_b' \quad (5.36)$$

$$S_c = 0.31 \frac{j_o^{1/3} z_{max}}{q_o} \quad (5.37)$$

In a linearly stratified ambient, the spreading layer is found to occupy about 40 – 50% of the rise height. For computing bulk dilutions, one must allow for the thickness of the wastewater field. Simple models to account for blocking in the presence of an ambient current can be found in Fischer et al. (1979).

Roberts (1979, 1980) studied the mixing of a line source of buoyancy in an ambient current, and found that the shape of the flow field and the dilution are determined by the ambient Froude number $F = u_a^3/j_o$. F measures the ratio of the ambient current velocity to the buoyancy-induced velocity. For $F < 0.1$, the minimum surface dilution S_m is little affected by the current and is given by:

$$S_m = 0.27 \frac{j_o^{1/3} H}{q_o} \quad (5.38)$$

Compared with equation 5.35, the smaller dilution coefficient reflects the effect of blocking of the surface layer. For higher crossflow, $F > 0.1$, however, the entrainment is dominated by the crossflow, and the alignment angle γ between the diffuser line and the current direction is important. Higher dilution results for a perpendicular alignment, $\gamma = 90^\circ$, in which the maximum amount of flow is intercepted while the parallel alignment, $\gamma = 0^\circ$, gives the lowest dilution. For $F \approx 100$, the perpendicular alignment results in a dilution

$$S_m = 0.6 \frac{u_a H}{q_o} \quad (5.39)$$

that is proportional to volumetric mixing between ambient (velocity u_a) and discharge flow, but with a reduced coefficient 0.6. For parallel alignment, the dilution is lower by a factor of about four. Experiments by Mendez-Diaz and Jirka (1996) have examined the different plume trajectories for various crossflow strengths.

The simple dilution equations given in the foregoing are useful for initial design screening of alternatives. They are limited to simplified ambient conditions. For final design evaluations and for more general and complex ambient oceanographic conditions models that are more comprehensive must be employed.

5.1.3 Integral methods

The following description of the integral method applied to buoyant plane jets is a brief summary of the detailed considerations from Jirka (2006). Integral methods are based on the approach that distribution functions for jet velocities or concentrations can be defined a priori. Chapter 5.1.2 and comparisons of extensive laboratory (e.g. in Fig. 60) studies showed, that jet trajectories, but also jet cross-sectional distributions of velocity and density are self-similar. Transverse distribution functions are commonly described with Gaussian functions (Jirka, 2006):

$$u = u_c e^{-r^2/b^2} + u_a \cos \sigma \cos \theta \quad (5.40)$$

$$g' = g_c' e^{-r^2/(\lambda b)^2} \quad (5.41)$$

$$c = c_c e^{-r^2/(\lambda b)^2} \quad (5.42)$$

$$X_i = X_{ic} e^{-r^2/(\lambda b)^2} + X_{ia}(z) \quad (5.43)$$

where u_c is the excess axial velocity, $g_c' = (\rho_a(z) - \rho_c)g/\rho_{ref}$ the buoyancy, ρ_c the density, X_{ic} the excess value of the state parameters on the jet centerline and $\lambda > 1$ a plane jet/plume dispersion ratio as the observed width of the scalar distribution is larger than for the velocity (turbulent Schmidt number).

The plane jet integral method proceeds by making use of the boundary-layer nature of the flow and by integrating all terms of the governing turbulent Reynolds equations of motion (equations 5.13 to 5.15) across the cross-sectional plane per unit width. Jet bulk variables for the total volume flux q , the axial momentum flux m , the buoyancy flux j , the flux of excess state parameter q_{xi} and tracer mass flux q_c (equations 5.44 to 5.48) result from the cross-sectional integration of the transverse distributions functions (equations 5.40 to 5.43) between the integration limits $-b_j$ and b_j . These limits are understood according to the boundary-layer theory as the “edge of the jet” at which boundary conditions can be clearly specified or, alternatively, beyond which no further contributions to the integration should arise (Jirka, 2006).

The bulk fluxes are:

$$q = \int_{-b_j}^{+b_j} u dr = \sqrt{\pi} b (u_c + \sqrt{2} u_a \cos \theta \cos \sigma) \quad (5.44)$$

$$m = \int_{-b_j}^{+b_j} u^2 dr = \sqrt{\frac{\pi}{2}} b (u_c + \sqrt{2} u_a \cos \theta \cos \sigma)^2 \quad (5.45)$$

$$j = \int_{-b_j}^{+b_j} u g' dr = \sqrt{\pi} b \left(u_c \frac{\lambda_s}{\sqrt{1 + \lambda_s^2}} + \lambda_s u_a \cos \theta \cos \sigma \right) g_c' \quad (5.46)$$

$$q_{X_i} = 2\pi \int_{-b_j}^{b_j} u (X_i - X_{ia}) dr = \sqrt{\pi} b \left(u_c \frac{\lambda_s}{\sqrt{1 + \lambda_s^2}} + \lambda_s u_a \cos \theta \cos \sigma \right) X_{ic} \quad (5.47)$$

$$q_c = \int_{-b_j}^{b_j} u c dr = \sqrt{\pi} b \left(u_c \frac{\lambda_s}{\sqrt{1 + \lambda_s^2}} + \lambda_s u_a \cos \theta \cos \sigma \right) c_c \quad (5.48)$$

Conservation principles for volume (continuity), momentum components in the global directions x , y and z , state parameters, and scalar mass lead to the following equations formulated for a jet element of differential length ds and unit width located on the trajectory (Jirka, 2006).

$$\frac{dq}{ds} = e \quad (5.49)$$

$$\frac{d}{ds} (m \cos \theta \cos \sigma) = e u_a + f_D \sqrt{1 - \cos^2 \theta \cos^2 \sigma} \quad (5.50)$$

$$\frac{d}{ds} (m \cos \theta \sin \sigma) = -f_D \frac{\cos^2 \theta \sin \sigma \cos \sigma}{\sqrt{1 - \cos^2 \theta \cos^2 \sigma}} \quad (5.51)$$

$$\frac{d}{ds} (m \sin \theta) = \sqrt{\pi} \lambda_s b g_c' - f_D \frac{\sin \theta \cos \theta \cos \sigma}{\sqrt{1 - \cos^2 \theta \cos^2 \sigma}} \quad (5.52)$$

$$\frac{dq_{X_i}}{ds} = -Q \frac{dX_{ia}}{dz} \sin \theta \quad (5.53)$$

$$\frac{dq_c}{ds} = 0 \quad (5.54)$$

Furthermore, the geometry of the trajectory is defined by (Jirka, 2006)

$$\frac{dx}{ds} = \cos \theta \cos \sigma, \quad \frac{dy}{ds} = \cos \theta \sin \sigma, \quad \frac{dz}{ds} = \sin \theta \quad (5.55)$$

and the centerline density ρ_c contained in the definition of centerline buoyancy g_c' is given by the equation of state

$$\rho_c = \rho_c (X_{ic}) \quad (5.56)$$

Definitions for the “turbulence closure coefficients” e , the specific entrainment rate and f_D , an ambient pressure force, are given by Jirka (2006):

$$e = 2u_c \left(\alpha_{1s} + \alpha_{2s} \frac{\sin \theta}{F_\ell^2} + \alpha_{3s} \frac{u_a \cos \theta \cos \sigma}{u_c + u_a} \right) + u_a \sqrt{1 - \cos^2 \theta \cos^2 \sigma} \left(\alpha_{4s} + \alpha_{5s} \left| \frac{\tan \theta_{eq}}{\tan \theta} \right| \right) |\cos \theta \cos \sigma| \quad (5.57)$$

$$f_D = c_{Ds} u_a^2 (1 - \cos^2 \theta \cos^2 \sigma) |\sin \gamma|$$

where coefficients are α_{1s} for the pure jet, α_{2s} for the pure plume and α_{3s} for the pure wake, c_{Ds} for the blocking effect of the plane jet relative to the oncoming flow. Jirka (2006) proposed the set of coefficients:

$$\begin{aligned} \alpha_{1s} = 0.0625, \quad \alpha_{2s} = 0.815, \quad \alpha_{3s} = 0.031, \quad \alpha_{4s} = 0.5, \quad \alpha_{5s} = 1.0 \\ \lambda = 1.30, \quad c_{Ds} = 15.0 \end{aligned} \quad (5.59)$$

5.1.4 Numerical methods

Nowadays comprehensive and easy to use numerical flow models, so-called computational fluid dynamic codes (CFD) are available (e.g. Ansys - CFX, Fluent, and Flow3D). CFD models solve the governing field equations (5.13 - 5.15) numerically on a fixed predefined grid (see chapter 5.3.2 for details). As distinct from the previously discussed approaches, they need to calculate all flow characteristics at every point of the flow domain, thus they need to resolve the entire jet induced velocity field and its interaction with the surrounding fluid. A dynamically coupled solution together with the transport equation is necessary, due to strong buoyancy effects. In addition, especially jet like motions require specialized turbulence models, where only a Reynolds stress model or a realizable k - ϵ model and second order accurate convection schemes apply (Zhu and Shih, 1994). Thus, grid generation and computations are time-consuming, limiting its applicability. Furthermore, uncertainties exist in prescribing appropriate boundary conditions for the ambient flow. Calibration is needed, limiting the predictive capabilities of these models. Recently, research approaches have been discussed where either one single model is used in different modes (e.g. a hydrostatic mode and a non-hydrostatic mode) or resolutions (model-nesting), or models of the same type are blended (e.g. a k - ϵ turbulence model with a k - ω model) in transitional regions. However, even if the increasing computational speed and memory of modern computers is considered, these approaches do not appear feasible for present-day engineering practice. Therefore it is not expected, that CFD models will be applied for practical problems regarding the near-field region. Nonetheless, CFD models are helpful for the analysis of special cases, where either experiments are too difficult or too expensive and integral models do not apply. Examples are described in Law et al. (2002).

Disregarding all above limitations, there have been efforts in the past to use even simplified CFD models attempting to represent major near-field characteristics. Studies by Blumberg et al. (1996) and Zhang and Adams (1999) have shown that in a stratified environment the near-field dilution levels can be predicted “surprisingly well” even if a coarse grid and hydrostatic far-field ocean circulation model (ECOM) is used. Zhang et al (1999) attributed the success to three factors: (1) the total dilution is partly due to large scale density exchange flow that the far field model can resolve; (2) the strong pycnocline provides a natural ceiling for the plume; (3) there is beneficial feedback such that if the entrainment is overpredicted, the trap height will be underpredicted and less total dilution will occur. However, their agreement is strongly dependent on intensive calibration of the turbulence model used. Field data is generally not available for that purpose so they use near-field model results, which in conclusion does not necessarily imply physical process representations. Predictions beyond these tuned/calibrated regimes thus have to be treated carefully. Furthermore tuned far-field models strongly depend on grid resolutions, thus major deviations regarding trapping height and terminal layer thickness occur.

However, successful examples are shown in the literature for simple and large-scale discharges, like a river discharge. This can be explained by the less complex near-field proc-

esses within large-scale surface discharge in comparison with the small-scale submerged multipoint discharge. Furthermore, most ocean circulation models are developed for large-scale processes and their turbulence closure and boundary interactions normally do not include the necessary detail for near-field processes, dominated by shear stresses within jets. For example the k - ϵ model (Rodi, 1993), which is a standard model in coastal circulation models and i.e. important for far-field processes does not perform well in flows with adverse pressure gradients or strong buoyant processes which might occur in near-field regions (Rodi, 2004). Besides the shallow water approximation (hydrostatic assumption), this limitation of far-field models regarding near-field processes probably has the strongest implications.

5.1.5 Near-field jet models

The near-field region of wastewater discharges is governed by the initial mixing processes. Most important among these is the buoyant jet mixing process. For buoyant jet flows, it is convenient to apply the integral technique. A large number of buoyant jet integral models can be found in the literature, with many variations. Most prominent models for outfall analysis are CorJet (part of the CORMIX system), NRFIELD (former RSB model, part of the Visual Plumes system) and JetLag (part of the VisJet system), which are briefly reviewed in the following.

5.1.5.1 CorJet (CORMIX system)

The CORMIX system (Doneker and Jirka, 1990; Jirka and Akar, 1991; Jirka et al., 1996) addresses the full range of discharge geometries and ambient conditions, and predicts flow configurations ranging from internally trapped plumes, buoyant plumes in uniform density layers with or without shallow water instabilities, and sinking (negatively-buoyant) plumes. Boundary interaction, upstream intrusion, buoyant spreading, and passive diffusion in the far field are also considered. A flow classification system based on hydrodynamic criteria using length scale analysis and empirical knowledge from laboratory and field experiments provides a rigorous and robust expert knowledge base that distinguishes among the many hydrodynamic flow patterns that may occur. For every flow class, CORMIX assembles and executes a sequence of appropriate hydrodynamic simulation modules. The modules are based on buoyant jet similarity theory, buoyant jet integral models, ambient diffusion theory, and stratified flow theory, and on simple dimensional analysis. The basic tenet of the simulation methodology is to arrange a sequence of relatively simple simulation modules which, when executed together, predict the trajectory and dilution characteristics of a complex flow.

Additional features are contemporary 3D plume and diffuser visualizations, comprehensive documentation and help system, GIS linkage, benchmarking analysis and validation database, far-field locator post-processor, sensitivity analysis, batch running mode and time-series, all fully linked within the expert-system interface. CORMIX results include design recommendations, flow class descriptions and reporting oriented on discharge zone analysis.

At the heart of CORMIX is the integral jet model CorJet which is based on the equations described in chapter 5.1.3 developed by Jirka (2004, 2006). The model formulation includes the significant three-dimensional effects that arise from the complex geometric details that distinguish actual diffuser installations in the water environment. Local three-dimensional effects deal with the merging process to form the plane buoyant jet. A simple flux-preserving merging transition that considers geometric contact between adjacent individual jets is found to be sufficiently accurate for simple port arrangements with like orientation. For complex port arrangements with opposing or rosette-like orientation the highly complicated merging proc-

ess is not considered in detail and a buoyancy flux-preserving equivalent slot jet assumption is made for the zone of flow establishment. A variable drag force formulation is introduced to provide an accurate representation of the merging and jet bending process under crossflow conditions. Finally, proximity effects due to the presence of a horizontal bottom boundary near the level of the efflux are included in CorJet. These are related to a "leakage factor" that measures the combined affect of port height and spacing in allowing the ambient flow to pass through the diffuser line in order to provide sufficient entrainment flow for the mixing downstream from the diffuser. Multiport diffuser discharges with small leakage factors are thus predicted to have reduced plume rise trajectories in the crossflow. The model has been validated intensively and the range of applicability of the integral model has been carefully evaluated where a number of spatial limitations have been proposed beyond which the integral model necessarily becomes invalid. Whenever horizontal or lateral boundaries exist in the flow domain, e.g. the free surface or bottom of a water body, complex flow interactions may occur. Such resulting phenomena as jet impingement, attachment, internal hydraulic jumps, instabilities, and recirculation are of course beyond the predictive powers of a simple integral model. In these instances, additional techniques for flow classification and prediction must be used, embedded in the CORMIX expert system structure.

5.1.5.2 NRFIELD (Visual Plumes package)

Visual Plumes (Frick et al., 2001) is a collection of initial dilution models that simulate single and merging submerged plumes in arbitrarily stratified ambient flow and buoyant surface discharges. Predictions include dilution, rise, diameter, and other plume variables. Visual Plumes models are: UM3, a Lagrangian entrainment model, NRFIELD and FRFIELD (former RSB) using semi-empirical formulations based on laboratory experiments for the near-field (Roberts, 1999a) and the Brooks equations for the far-field, DKHW that is based on UDKHDEN (Muellenhoff et al., 1985), and PDS, a surface discharge model (Davis, 1999).

Additional features are a conservative tidal background-pollutant build-up capability, a sensitivity analysis capability, and a multi-stressor pathogen decay model that predicts coliform bacteria mortality based on temperature, salinity, solar insolation, and water column light absorption. The FRFIELD model estimates the long-term distribution of pollutants in the vicinity of the outfall. This model is based on the two-dimensional "visitation-frequency" model.

Out of these models NRFIELD is probably the most used model from this compilation. It is an empirical model for multiport diffusers based on the experimental studies on multiport diffusers in stratified currents described in Roberts, Snyder, and Baumgartner (1989, a, b, c) and subsequent experimental works. NRFIELD is based on experiments using T-risers, each having two ports, so at least four ports must be specified for it to apply. An important assumption is that the diffuser may be represented by a line source. NRFIELD is restricted to predictions regarding the strict near-field. No information on trajectory or boundaries is included.

Visual Plumes models are separated and the user has to choose the one desired. In this way, it promotes the idea that in the future modeling consistency will be achieved by recommending particular models in selected flow categories. Visual Plumes models may be run consecutively and compared graphically to help verify their performance.

5.1.5.3 JetLag (VisJet system)

VISJET (Lee and Cheung, 1990) is a general predictive, flow visualization tool to portray the evolution and interaction of multiple buoyant jets discharged at different angles to the ambient tidal current. VISJET can be used to study the impact of either a single or a group of inclined buoyant jets in three-dimensional space.

Special features are computer graphics techniques to trace the path and mixing characteristics of a group of arbitrarily inclined jets in three-dimensional space, in a uniform or density-stratified crossflow.

The Lagrangian buoyant jet model JETLAG (Lee and Cheung, 1990) is part of the model VISJET and predicts the mixing of buoyant jets with three-dimensional trajectories. The model, strictly speaking, does not solve the usual Eulerian governing differential equations of fluid motion and mass transport. Instead, the model simulates the key physical processes expressed by the governing equations. The unknown jet trajectory is viewed as a series of non-interfering “plume-elements” which increase in mass as a result of shear-induced entrainment (due to the jet discharge) and vortex-entrainment (due to the crossflow) - while rising by buoyant acceleration. The model tracks the evolution of the average properties of a plume element at each step by conservation of horizontal and vertical momentum, conservation of mass accounting for entrainment, and conservation of tracer mass/heat. The vortex entrainment is determined by a heuristic Projected-Area Entrainment (PAE) hypothesis for buoyant jets with 2D trajectories, while pressure drag is ignored. Predictions of the model have compared well with basic laboratory experimental data; the model also predicts correctly the asymptotic behavior of pure jets and plumes, and advected line puffs and thermals.

5.1.5.4 Model comparison and model choice

However, all three jet models, CorJet, JetLag, and NRFIELD are embedded in major mixing zone models, all packages allow for separate applications. Comparison for strict near-field applications, thus the prediction of the minimum dilution at the end of the near-field with related near-field location and plume dimension shows, that all models perform well and give reasonable results. This is confirmed by comprehensive peer-reviewed validations of each of these models. However comparing usability, range of application, physical process simulation, and modeling, philosophy differences are identified:

- CorJet and JetLag give results on trajectories, centerline dilution, flow, and entrainment characteristics, whereas NRFIELD only gives the final minimum near-field dilution and related near-field location and plume dimensions.
- CorJet applies for arbitrary, i.e. non-uniform, multi-directional velocity profiles, which are not covered in JetLag or NRFIELD
- CorJet deals with significant three-dimensional effects regarding the merging process to form the plane buoyant jet and/or the bending process under crossflow. It allows defining merging positions and characteristics. VisJet instead neglects these effects and uses superposition principles, whereas NRFIELD includes these processes as aggregated effects only
- CorJet includes proximity effects due to the presence of a horizontal bottom boundary near the level of the efflux. Both JetLag and NRFIELD do not consider those.
- CorJet includes clear statements of spatial limitations beyond which the integral model necessarily becomes invalid. JetLag and NRFIELD lack such clear statements.

Model differences might be considerably amplified when comparing performance of the jet models within their system. Though all three model suites pretend to be optimum for mixing analysis of wastewater discharges into coastal waters their system capabilities are quite different, which are summarized as follows:

A first difficulty is the different definition for the end of the near-field. Controversy exists especially regarding the question whether the near-field includes buoyant spreading, upstream spreading, or other boundary interaction processes or if they are already related to the far-field. This becomes critical once discharge permits are related to a minimal near-field dilution and different models lead to inconsistent implementations of regulations (Tetrattech, 2000). Nonetheless Visual Plumes and CORMIX are both US EPA (Environmental protection agency) approved models for Regulatory discharge zone analysis.

Major differences of the model systems are regarding model extensions beyond the buoyant jet model. There are a number of other mixing processes that occur in the near-field of the discharge depending on a given situation, such as boundary/surface interaction, internal hydraulic jumps and unstable mixing, stratified exchange flow, and buoyant spreading processes. The CORMIX model is, in fact, a collection of zone models for all these sub-processes. These models are invoked through a length-scale based classification scheme that first predicts the discharge flow behavior (so-called flow classes) and then consecutively links (couples) the appropriate zone models (so-called modules) to provide a prediction. PLUMES and VISJET do not address the effects of vertical or horizontal boundaries on mixing or on discharge stability. They simply assume the ambient water body is infinite. However, PLUMES allows for a coupling of NRFIELD results to FRFIELD an empirical ambient dispersion model. VISJET does not account for any processes beyond the near-field region.

All jet models have been validated with a wide range of fundamental laboratory data sources. The amount of comprehensive and reliable field data for actually operating diffusers that can be used for model validation is still limited at present. The field survey of Carvalho et al. (2002) for the Ipanema outfall in Rio de Janeiro has provided a highly satisfactory validation for all models regarding the near-field predictions and additionally for CORMIX as regards its predictive ability and accuracy not only for the immediate near-field but also the transition to the far-field in form of the buoyant spreading of the internally or surface-trapped plume (see Jirka and Doneker, 2003). The other models are clearly limited in that regard.

Reasons for these model differences are not necessarily failures or inconsistencies. They should also be seen in the context, that VISJET and CORMIX are commercial models with order of magnitudes difference in pricing (VISJET prices for a commercial/academic license are 300 / 150 US \$, whereas CORMIX prices are 5200 / 1500 US \$). The CORMIX system includes a high-level quality assurance, professional support and detailed documentation (Jirka et al., 1996), help system and bug fixing. VISJET is at the beginning in that regard, whereas the mostly academically oriented Visual Plumes system, which can be downloaded for free does not include any of these.

In summary, situations where PLUMES and VISJET can be applied would typically be deep ocean outfalls (e.g. sewage outfalls) and if near-field mixing is of interest only and there is no possibility of dynamic bottom attachments and surface interaction is unimportant. However, if discharge zone information after the near-field is desired, then the possibility of a density current in the far-field must be considered (compare Fig. 62).

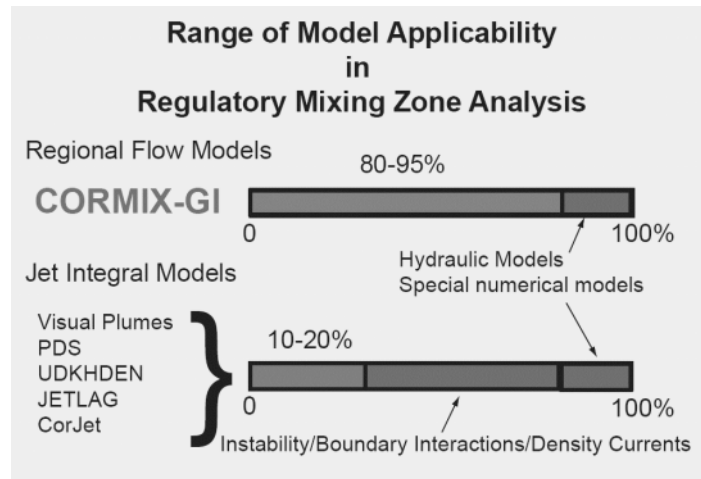


Fig. 62: Schematic illustration of the range of model applicability in Regulatory discharge zone analysis (source: www.cormix.info)

The CORMIX model system has been chosen for this study, because of its additional capabilities and the expert system approach allowing especially for design optimization and Regulatory discharge zone analysis.

5.2 Intermediate-field processes and modeling applications

Near-field jet models assume unlimited and steady ambient conditions. This assumption holds until the plume reaches vertical boundaries or the shallowness of a water body prevents the development of a stable jet regime. The intermediate field thus starts at the end of the jet regime (region (1) in Fig. 63a) and is classified according to three main processes: the boundary interaction, where the vertical boundaries inhibit any vertical motion (region (2) in Fig. 63a), the buoyant spreading, where the wastefield establishes horizontally (part of region (3) in Fig. 63a) and the near-field instability (Fig. 63b). Once these processes are of minor order compared to far-field transport and dispersion processes, the far-field is attained (region (4) in Fig. 63). For weak ambient flows or quiescent ambient the intermediate-field may extend over distances that are substantially greater than the water depth (Jirka, 1982), however, for strong ambient motions its effects are often negligible.

The classification of these hydrodynamic regimes is facilitated by the utilization of non-dimensional parameters, in particular ratios of the previously defined length scales (Jirka et al., 1996, see chapter 5.1.2.2), which provide assistance in the parameterization.

5.2.1 Near-field instability

Near-field instability is defined as the situation when discharge induced motions considerably influence the ambient motions in the near-field region (Jirka, 1982, 2006). Large recirculation zones or vertically mixed currents that laterally entrain ambient water are typical examples for an unstable near-field (Fig. 63b).

Jirka (2006) summarized the criterion to predict the occurrence of stable configurations as:

$$\frac{\ell_M}{H} (1 + \cos^2 \theta_o)^2 + \frac{\ell_M}{\ell_m} \sin \gamma_o - 0.1 \frac{h_o + \ell}{\ell_m} \sin \gamma_o \leq 0.54. \quad (5.60)$$

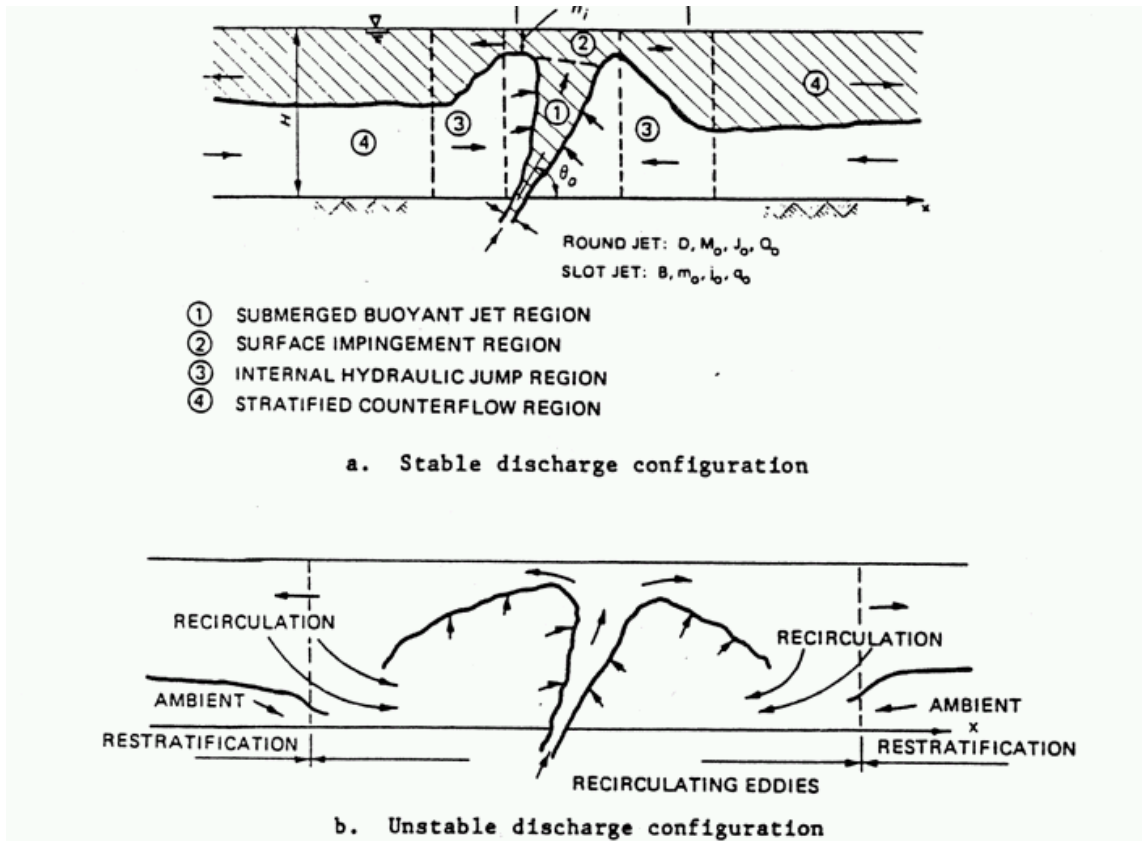


Fig. 63: Submerged buoyant slot jet discharging into stagnant water of finite depth (Jirka, 1982). *a*) Deep water discharge with stable discharge configuration, *b*) shallow water discharge with unstable recirculation zone (reproduced from Jirka et al., 1996)

The combination of hydrodynamic length scales hereby provides means for a general classification scheme (schematized in Fig. 64), which is also implemented in the CORMIX flow classification system (see Fig. 72, p. 110 for details). "Stable discharge" conditions, usually occurring for a combination of strong buoyancy, weak momentum, and deep water, are often referred to as "deep water" conditions. "Unstable discharge" conditions, on the other hand, may be considered synonymous with "shallow water" conditions, when a multiport diffuser represents a large source of momentum with a relatively weak buoyancy effect (i.e. for thermal plumes). Technical discussions on discharge stability are presented elsewhere (Jirka, 1982; Holley & Jirka, 1986).

5.2.2 Boundary interaction processes

Boundary interactions have strong implications on waste discharge assessments, because location and concentration of plumes when hitting either the surface or the shoreline are important project criteria. Boundary interaction processes are classified into interaction with vertical boundaries (surface, bed, or pycnocline) and horizontal boundaries (shoreline), as illustrated in Fig. 65 and Fig. 66.

For large ambient velocities the boundary interaction can simply be conceptualized as a gradual transition of a bent-over plume to a far-field surface layer flow (Fig. 66a). However, boundary interaction processes become important for weak ambient currents. The almost vertically rising plume motions are either stopped suddenly by surface impingement or overshoot and fall down back on the terminal layer for pycnocline impacts. Both plumes conse-

quently experience rapid horizontal spread in all directions. Additional mixing is referred to this impact and spreading motions, where so-called upstream spreading may extend considerably (Fig. 66b). Shallow conditions may furthermore lead to local recirculation (Fig. 66c,d).

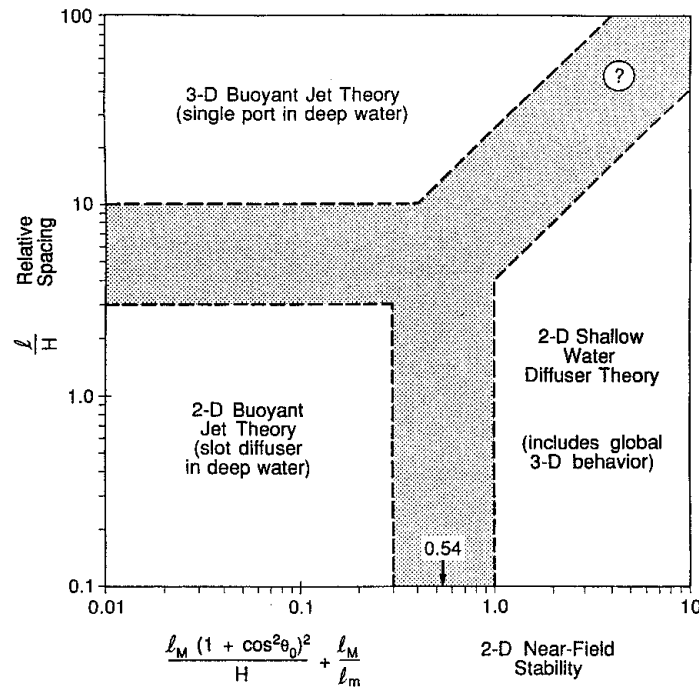


Fig. 64: Diagram for selection of predictive models for submerged multiport diffusers with variable spacing and stability characteristics (reproduced from Jirka, 2006)



Fig. 65: Pictures of laboratory experiments showing boundary interactions with the surface, the bottom and the pycnocline (courtesy of G.H. Jirka, L. Fan, Keck Lab, CIT)

Another type of interaction process concerns submerged buoyant jets discharging in the vicinity of the water bottom into a stagnant or flowing ambient. Two types of dynamic interaction processes can occur that lead to rapid attachment of the effluent plume to the water bottom as illustrated in Fig. 67. These are wake attachment forced by the receiving water's cross flow or Coanda attachment forced by the entrainment demand of the effluent jet itself. The latter is due to low-pressure effects as the jet periphery is close to the water bottom.

Jirka et al. (1996) described criteria for the prediction of boundary interactions, which are mainly based on dimensionless numbers, parameterized out of ratios of the geometrical length scales (e.g. port elevation, water depth, distance to shore) and the hydrodynamic length scales (Jirka et al., 1996, and chapter 5.1.2.2). These criteria are implemented in the CORMIX classification scheme regarding boundary interactions (see Fig. 71, p. 110 for details).

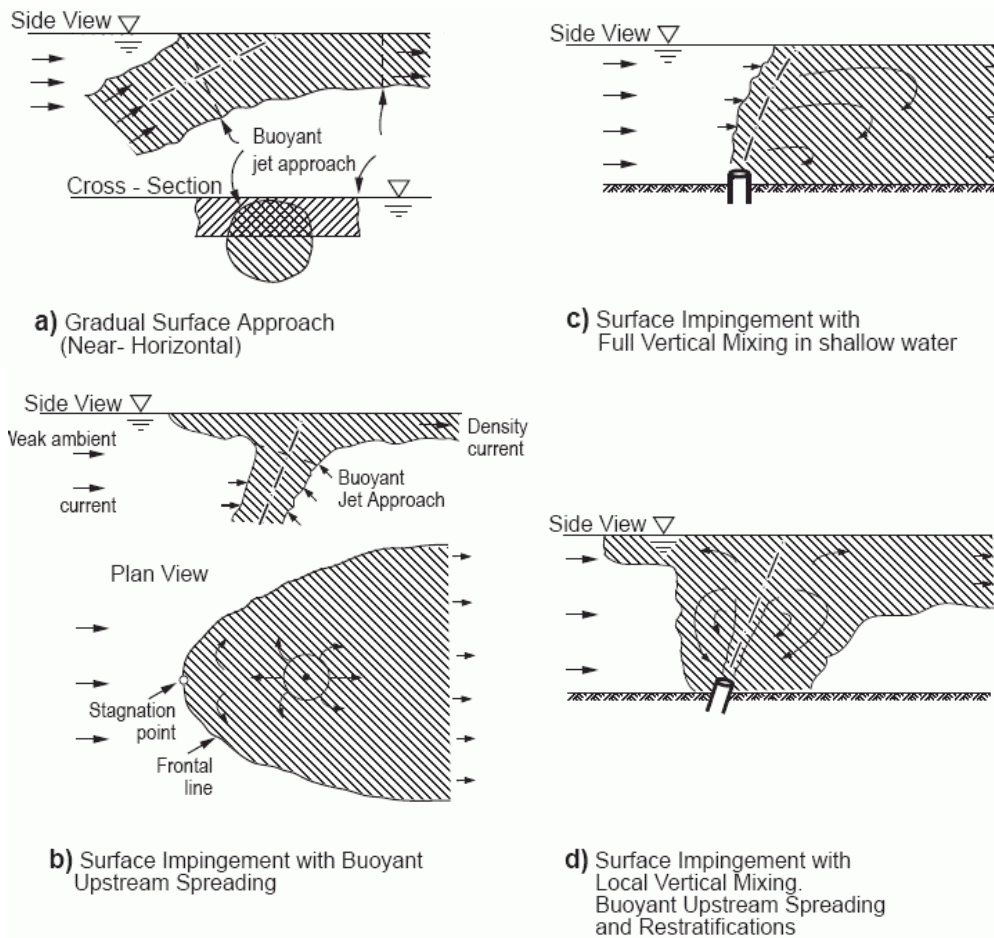


Fig. 66: Examples of boundary interactions for submerged jets in finite depth (reproduced from Jirka et al., 1996)

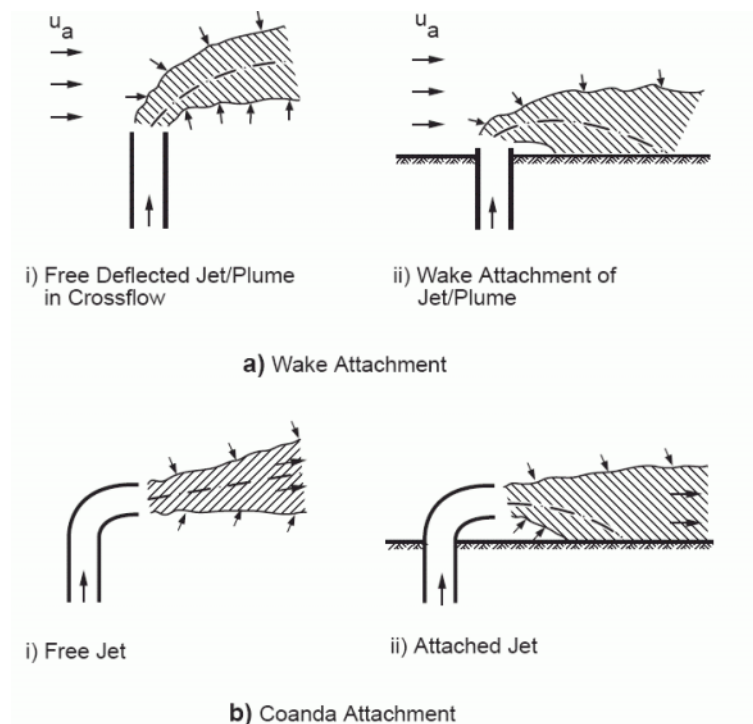


Fig. 67: Examples of *a)* wake attachment and *b)* Coanda attachment conditions for jets discharging near boundaries (reproduced from Jirka et al., 1996)

5.2.3 Buoyant spreading processes

Buoyant spreading processes are related to the plume collapse after boundary or pycnocline interaction. These motions are no longer jet-like and concentration distributions change according to transport motions and spreading motions. Transport motions carry the substances away from the source with ambient velocities. Spreading motions spread the wastefield in the horizontal (Fig. 68). It is there distinguished between the far-field spreading motions by turbulent spreading and the intermediate spreading by density differences. The former is related to mixing motions, whereas the latter are density current like motions, with rather small mixing due to entrainment at the frontal heads of the current. Thus, buoyant spreading collapses the vertical, initially thick wastefield into a thin and wide horizontal layer. The weaker the ambient currents and the stronger the stratification the faster buoyant spreading motions are induced. This holds especially for steady quiescent ambient (i.e. lakes or reservoirs), where density differences of the discharge and the ambient cause density current spreading over large distances at the terminal layer (either surfacing or trapped plumes). Also for weak and steady flow fields (i.e. rivers) situations occur where spreading velocities are high, even causing upstream spreading plumes (Fig. 69). However, reported waste discharge studies in coastal waters generally neglect buoyant spreading processes.

Consequences of large buoyant spreading processes are modified flow fields superimposed on far-field transport processes thus influencing concentration distributions. In addition, near-field dilutions are relatively small during periods with weak ambient velocities. Both in combination cause higher risk for public or environmental impacts. Therefore, the stagnant ambient water case has traditionally been considered as the worst case for discharge assessments, however, only related to pure near-field considerations, i.e. without influence of spreading motions. Furthermore, most recently used approaches using additional far-field dispersion models either do not include any buoyant spreading process, or do have considerable deficiencies in calculating these thin near-field-diluted waste layers, spreading at either the surface or the pycnocline in unsteady environments (see chapters 5.3 and 5.4 for details).

Laboratory studies and field studies in quiescent ambient confirm the importance of such processes (e.g. Koh, 1983; Akar and Jirka, 1994, 1995), provided that the period considered is long enough (i.e. steady) allowing these motions to develop. Akar and Jirka (1995) described criteria for the prediction of the occurrence of buoyant spreading motions, based on dimensionless numbers, parameterized out of ratios of the hydrodynamic length scales (chapter 5.1.2.2). For a stable discharge in unstratified water the criteria for a weak current regime, thus allowing buoyant spreading motions to develop on considerable scales is given by:

$$\frac{L_b}{H} > 0.65 \quad (5.61)$$

where $L_b = J_o/u_a^3$ describes the plume/cross-flow length scale for a single jet. For a multiport diffuser the criterias are scaled with the ratio of two length scales for a stable discharge in unstratified water:

$$\frac{\ell_M}{\ell_m} < 1, \quad (5.62)$$

or for a stable discharge in stratified waters:

$$\frac{\ell_b'}{\ell_a} > 1, \quad (5.63)$$

which both are actually describing the same parameter ratio, denoting whether ambient velocity or buoyancy dominates:

$$\frac{\ell_M}{\ell_m} = \frac{u_a^2}{j_o^{2/3}} = \left(\frac{\ell_b}{\ell_a}\right)^{-1/2} \quad (5.64)$$

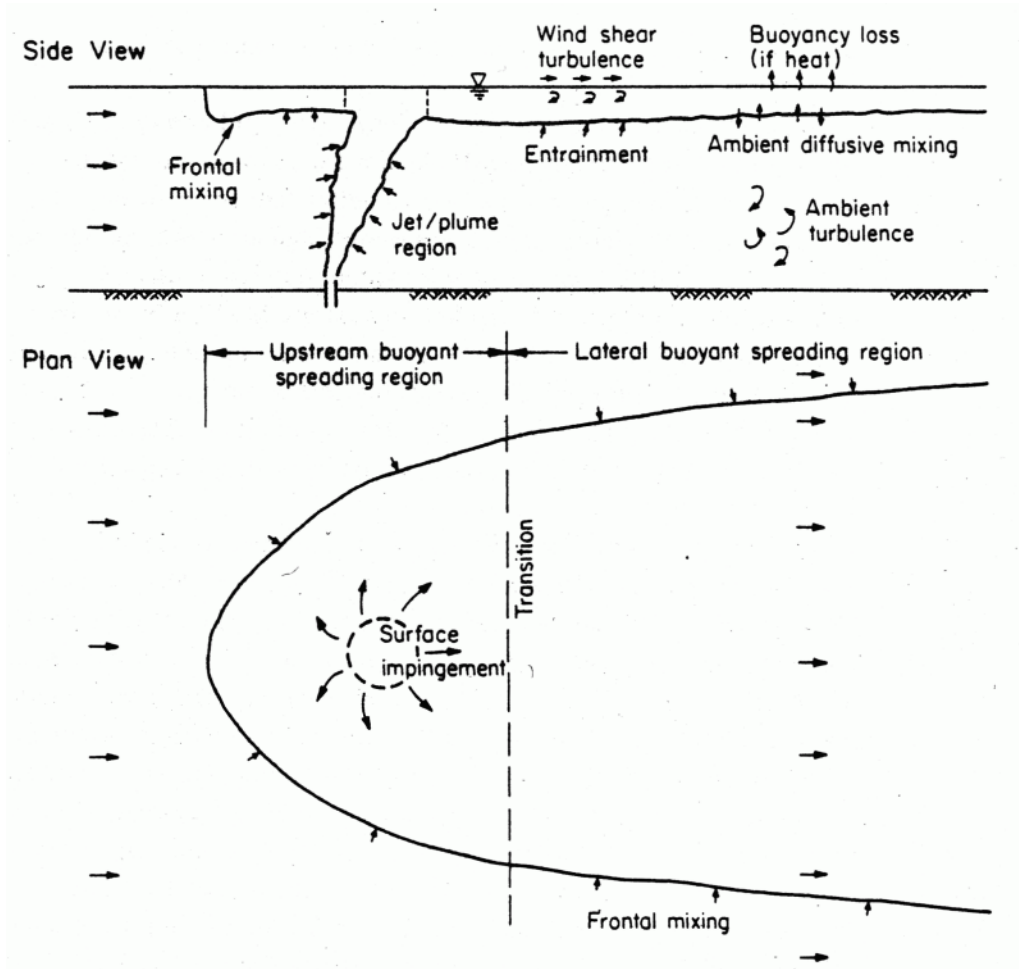


Fig. 68: Buoyant spreading processes after near-field region (upstream and lateral spreading), superimposed on the transport by ambient currents (reproduced from Jirka and Akar, 1991)

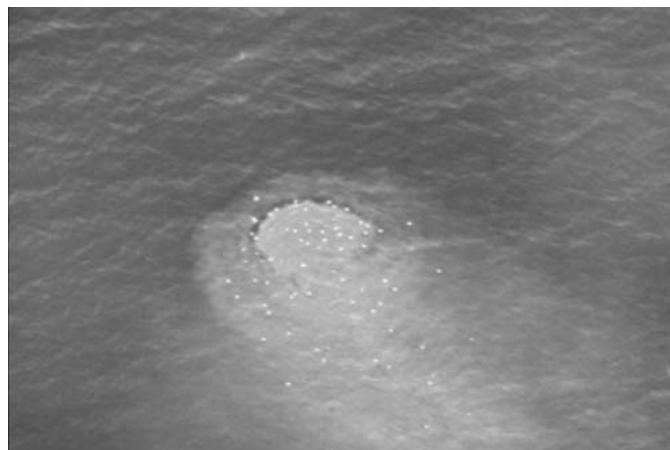


Fig. 69: Buoyant surfacing plume. Boundary (surface) interaction and density difference cause slight upstream spreading of the plume against the ambient current (Source: I. Wood)

These criteria are also implemented in the CORMIX classification scheme regarding the modeling of buoyant spreading motions for waste discharges (see Fig. 72 and Fig. 73, pp. 110, p. 110 for details). However, as distinct from to near-field processes, buoyant spreading motions may extend over time-scales, which are considerably larger than those of the ambient motions and unsteady considerations, become important. Whether or not these processes dominate in unsteady coastal environments at all, depends on the degree of temporal variability. Field studies from Carvalho et al. (2002) for the Ipanema outfall in Rio de Janeiro provided good information on the immediate near-field and also the transition to the far-field, showing that buoyant spreading of the internally trapped or surfaced plume actually occurs in nature (see Jirka and Doneker, 2003). However, Carvalho et al. (2002) concluded that, although scientifically important, buoyant spreading processes do not have major influences on the overall plume dispersion characteristics due to the truly unsteady flow field. This might be true for the observed overall discharge performance regarding weekly or monthly averages, but not for specific ambient conditions for example on a daily basis. Therefore, the present study proposes a flow classification based on a characteristic length-scales to determine when buoyant spreading in unsteady environments dominate plume dispersion.

5.2.3.1 Flow classification regarding buoyant spreading in unsteady ambient

Time scale measures and unsteady length scales, have been proposed by Nash and Jirka (1996), with focus on the parameterization of unsteady plume bending in reversing tidal flows. These processes are similar to the jet in crossflow cases and therefore dominated by the initial momentum flux and the ambient velocity. In addition to the steady diffuser fluxes, they use a value for the time rate of reversal of ambient velocity,

$$\left| \frac{du_a}{dt} \right|. \quad (5.65)$$

Dimensional analysis then leads to the unsteady jet / crossflow length and time scales (modified from Nash and Jirka (1996) for multiport diffusers):

$$\ell_{mu} = \left(\frac{m_o}{|du_a/dt|} \right)^{1/2}, \quad (5.66)$$

a measure of the distance of the forward propagation into the ambient flow of a discharge during the reversal episode, and

$$t_{mu} = \left(\frac{m_o}{|du_a/dt|^3} \right)^{1/4}, \quad (5.67)$$

a measure of the duration over which an effluent may be considered as discharging into stagnant water while the velocity field is reversing.

Nash and Jirka (1996) furthermore showed that for most of the time ambient acceleration is negligible compared to the instantaneous velocity. Only as slack tide is approached the reversal length scale becomes dominant. However, in case of buoyant spreading in unsteady environments it is not the jet to crossflow behavior, but the buoyancy to crossflow, which parameterizes a buoyant spreading process in an ambient flow. Thus, in analogy to Nash and Jirka (1996) it is proposed an unsteady plume /crossflow length and time scale:

$$\ell_{bu} = \frac{j_o^{2/3}}{|du_a/dt|}, \quad (5.68)$$

a measure of the distance of the forward propagation into the ambient flow of a buoyant spreading motion, and

$$t_{bu} = \frac{j_o^{1/3}}{|du_a/dt|}, \quad (5.69)$$

a measure of the duration over which buoyant spreading motions may develop. It is furthermore proposed to use the dimensionless parameter

$$\frac{\ell_{bu}}{L_D}, \quad (5.70)$$

to distinguish whether the length scales of buoyant spreading motions are considerably large or not. Furthermore the dimensionless parameter

$$\frac{t_{bu}}{\Delta t}, \quad (5.71)$$

might be used to distinguish, whether buoyant spreading motions occur over time scales, which are significant compared to the considered time scales Δt . These numbers allow classifying the duration and spatial extents of spreading motions for weak ambient currents. An application of these scales and comparison with field data is discussed in chapter 5.4.2.1.

5.2.3.2 Buoyant spreading models

Estimates for modeling buoyant spreading processes, i.e. the buoyant spreading velocities, might be derived from mass conservation principles, assuming that the entrainment flow needed by the buoyant plume is supplied by an undercurrent distributed uniformly with the vertical and neglecting interfacial friction. Koh (1983) developed a model for line plumes:

$$u_s = \beta^{3/2}(2g'h)^{1/2} \quad (5.72)$$

where u_s denotes the buoyant spreading velocity, $\beta = 0.83$ an experimental coefficient and h = layer thickness. Koh (1983) furthermore rewrote that equation as a function of the initial plume volume flux and initial dilution S :

$$u_s = Sq_o/(2h) \quad (5.73)$$

For the undercurrent velocity it is

$$u_u = (S - 1)q_o/(2(z_{top} - h)) \quad (5.74)$$

where z_{top} = plume top elevation above bed.

For a line diffuser normal to a current, the initial width of the wastewater field can be taken to be equal to the diffuser length; the depth of the field in moving stratified water can be estimated on the basis of continuity considerations and accounting for partial blocking above the base of the field (Brooks, 1972):

$$h = z_{top} \left(\frac{Q_o S / (u_a L_D z_{top})}{1 + Q_o S / (u_a L_D z_{top})} \right) \quad (5.75)$$

Equation (5.76) is expected to hold for $SQ_o/(u_a L_D z_{top}) \leq 2$. These dimensions are needed as initial conditions for transport calculations in the far field. Typical minimal dilutions for weak ambient currents are approximately 100. Assuming an initial volume flux of $q_o = 0.02 \text{ m}^3/\text{s}$ and a water depth of $H = 30 \text{ m}$ the spreading velocity is of the order of 0.1 m/s . As a consequence the spreading plume could reach the beaches if these conditions prevail for at least 8 h and an outfall length of 3000 m.

Akar and Jirka (1995) described a comprehensive surface spreading model. It describes the downstream evolution of a buoyant surface plume in an unstratified ambient flow. The model includes interfacial mixing, additional wind induced mixing and entrainment either due to interfacial shear instabilities or the plume fronts (Fig. 70). Furthermore the model includes a simple calculation regarding passive far-field mixing. The model is implemented into the CORMIX system.

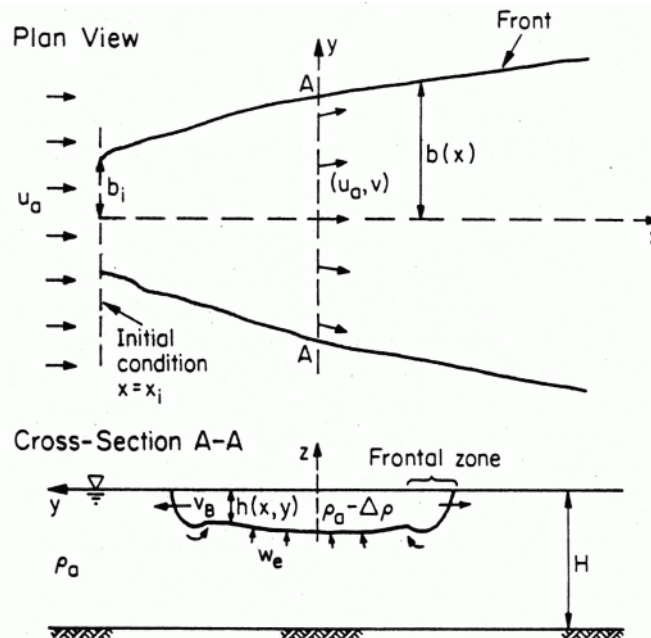


Fig. 70: Definition diagram for surface spreading model for an unstratified ambient water body with uniform velocity (reproduced from Akar and Jirka, 1995)

5.2.4 Intermediate field models

Yet, there are a number of other mixing processes that occur in the intermediate-field of the discharge depending on a given situation, such as internal hydraulic jumps and stratified exchange flow. The CORMIX model is, in fact, a collection of zone models for all these sub-processes. These models are invoked through a length-scale based classification scheme (Jirka and Akar, 1991; Jirka and Doneker, 1991) that first predicts the discharge flow behavior (so-called flow classes) and then consecutively links (couples) the appropriate zone models (so-called modules) to provide a near-field prediction, briefly illustrated in Fig. 71 to Fig. 73. Though CORMIX lacks a limitation of buoyant spreading processes in unsteady environments it includes the most comprehensive intermediate-field analysis for waste-discharges.

- Coupled discharge and transport modeling (CorLink) -

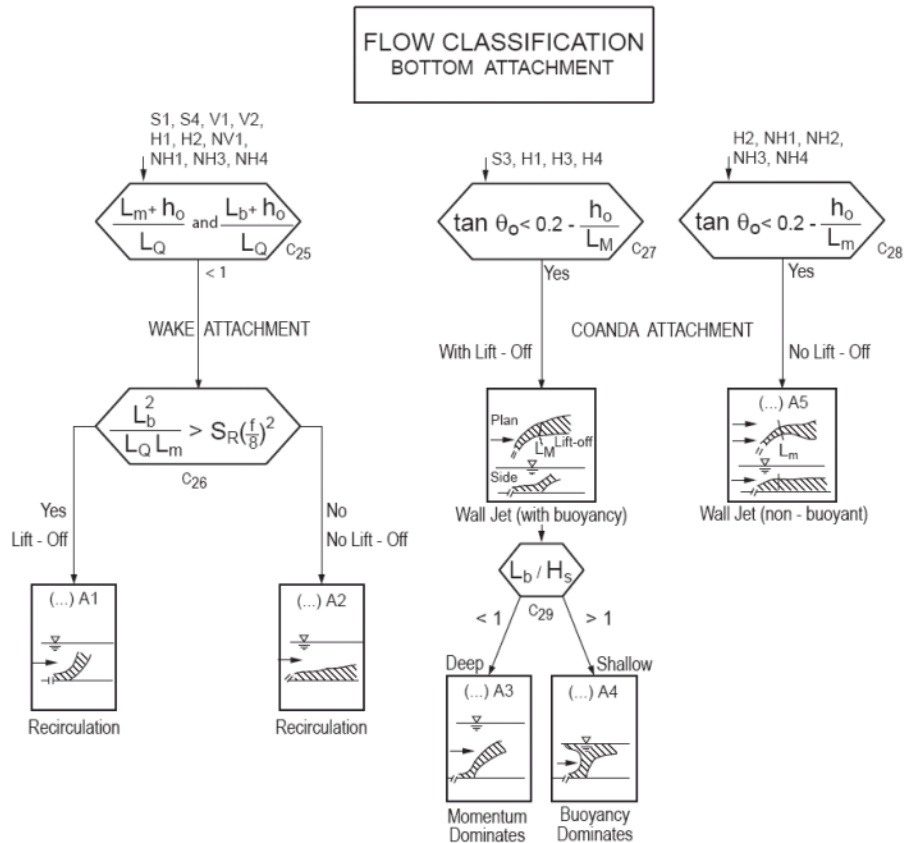


Fig. 71: CORMIX flow classification tree for bottom attachment (reproduced from Jirka et al., 1996)

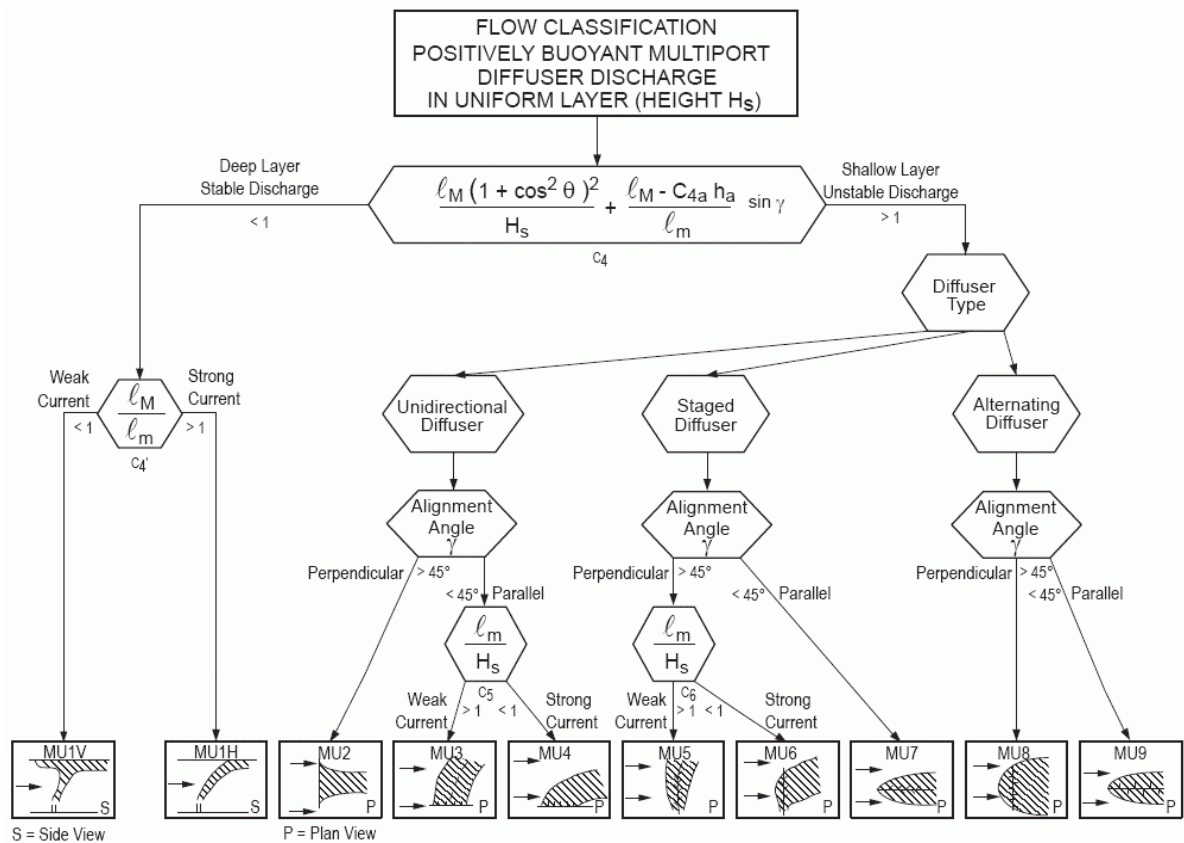


Fig. 72: CORMIX flow classification tree for a buoyant multiport discharge into uniform ambient water (reproduced from Jirka et al., 1996)

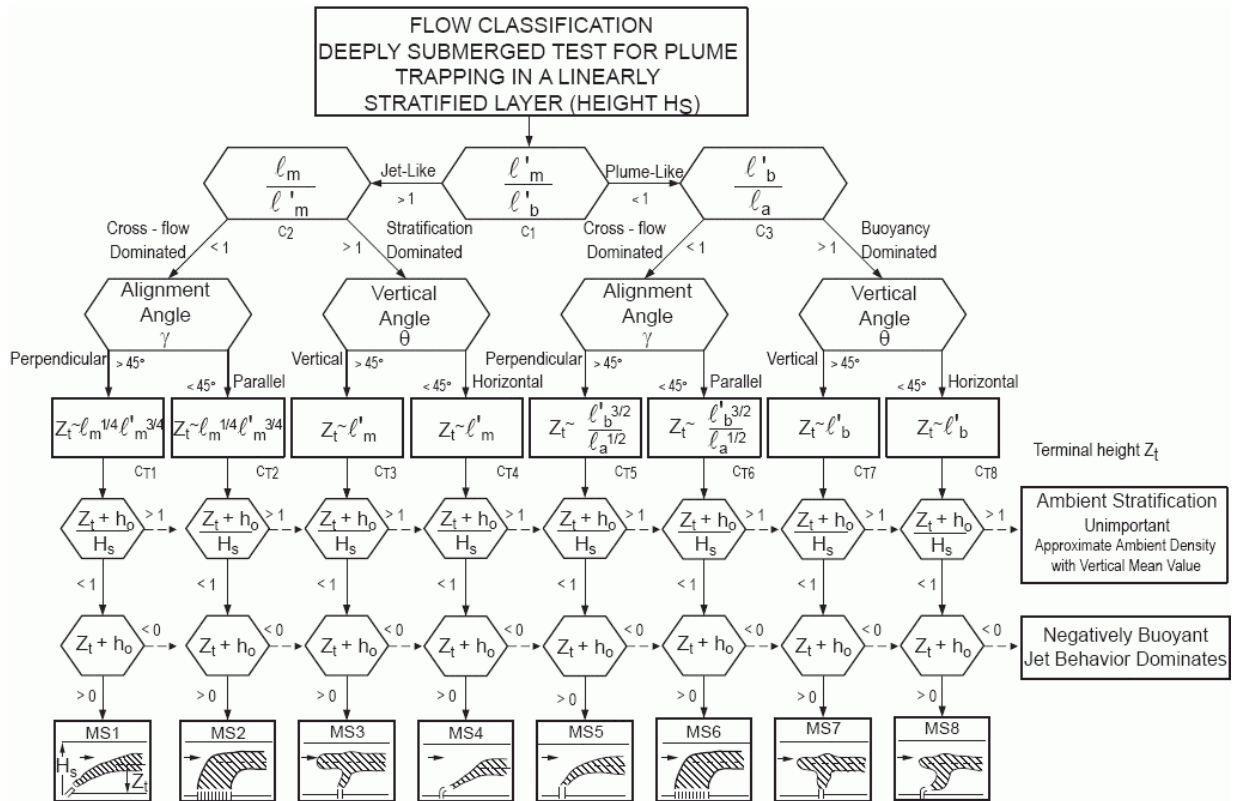


Fig. 73: Flow classification tree within CORMIX, for a buoyant multiport discharge in stratified ambient waters (reproduced from Jirka et al., 1996).

5.3 Far-field processes and modeling applications

Distinct from near-field motions, far-field processes do not focus on the jet, plume, or waste-field driven motions, but on the natural water body motions. Whereas background turbulence and spatial velocity field characteristics can be fully neglected in near-field approaches, they play a considerable role in the far-field region. Therefore, far-field processes are mainly related to the description of natural coastal flows. Once these processes are known, wastefield characteristics as a result from the intermediate region, are coupled with these flows either at the surface level or trapped within density stratification, and transported and dispersed by ambient currents and ambient turbulence.

5.3.1 Passive ambient mixing - empirical dilution equations

The existing turbulence in the ambient environment is the dominating mixing mechanism at sufficiently large distances from the discharge point. In general, the passively diffusing flow grows in width and in thickness until it interacts with the channel bottom and/or banks as illustrated in Fig. 74.

The strength of the ambient diffusion mechanism depends on a number of factors relating mainly to the geometry of the ambient shear flow and the amount of ambient stratification. In the context of classical diffusion theory (Fischer et al., 1979), gradient diffusion processes in the bounded flows of rivers or narrow estuaries can be described by constant diffusivities in the vertical and horizontal direction that depend on turbulent intensity and on channel depth or width as the length scales. In contrast, wide "unbounded" channels or open coastal areas are characterized by plume size dependent diffusivities leading to accelerating plume growth

described, for example, by the "4/3 law" of diffusion. Under high dilution conditions in moving water, the wastewater field is essentially advected passively in a tidal current. Vertical mixing is damped by buoyancy, so that the subsequent dilution is mainly due to horizontal mixing by the turbulent eddies, allowing vertical and longitudinal dispersion to be neglected.

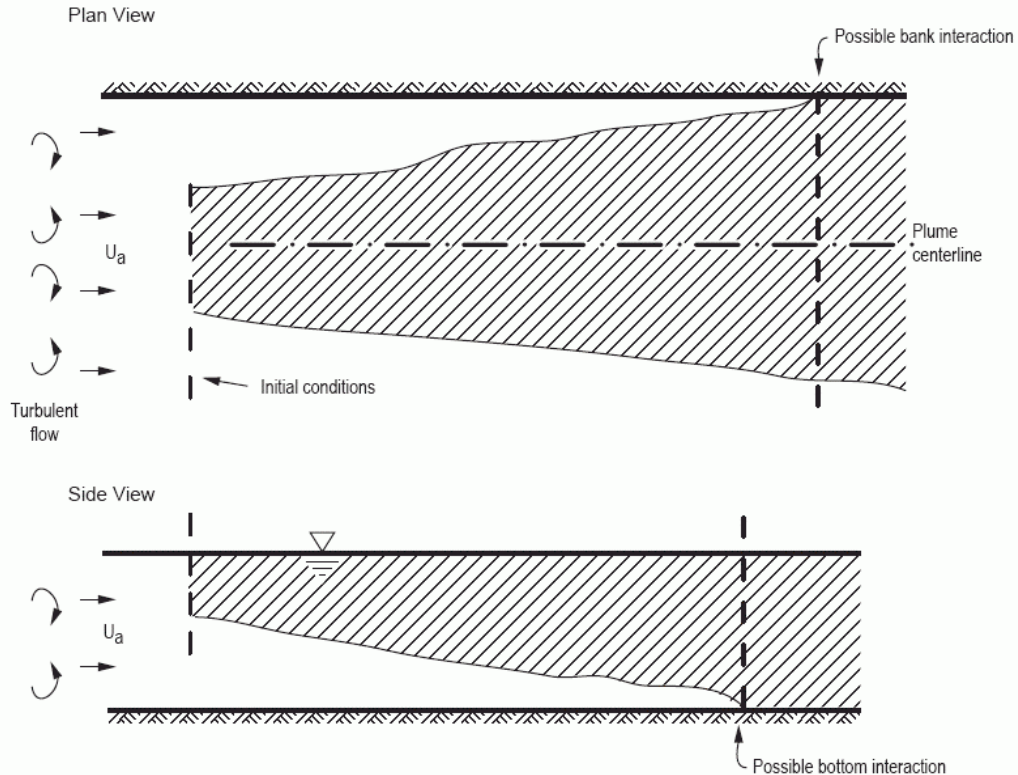


Fig. 74: Passive ambient diffusion process with advection in the far-field (reproduced from Jirka et al., 1996)

Brooks (1960) gives a widely used method of estimating the subsequent dilution of a wastewater field due to lateral mixing by oceanic turbulence. However, rigorous assumptions are necessary, i.e. a steady, two-dimensional, uniform flow condition without external forcing. A line source is assumed with initial conditions determined by the initial near-field mixing phase as discussed in chapter 5.1; the horizontal transport of a pollutant layer of constant thickness in a steady uniform current normal to the source is then formulated according to the intermediate-field as described in chapter 5.2.3.2. By assuming a 4/3 power dependence of the eddy diffusivity on the local plume width and a first order decay with rate constant k , the centerline concentration in the plume is given by:

$$\frac{c_{max}}{c_i} = \left(\operatorname{erf} \left(\frac{3/2}{\left(\left(1 + \frac{8E_i t}{\ell_i^2} \right)^3 - 1 \right)^{1/2}} \right) \right)^{1/2} e^{-kt} \quad (5.76)$$

where t = travel time = x/u_a , E_i = diffusivity corresponding to the initial width of the plume $\ell_i = L_D$, and c_i = initial concentration at the end of the near-field.

Subject to the global flushing constraints, equation (5.76) is useful in giving a conservative estimate for the order of magnitude analysis of the subsequent dilution and elucidating the

relative importance of horizontal diffusion and decay processes. It is, however, limited in following respects, illustrated in Fig. 75: a) coastal currents are unsteady, b) near-shore currents are horizontally non-uniform (e.g. vortex shedding at headlands), and c) coastal currents are vertically non-uniform (wind-generated onshore surface current is usually accompanied by a compensatory offshore bottom current). Munro & Mollowney (1974) have shown that in shallow coastal waters vertical mixing in such a counter current system can lead to substantial additional reductions in concentration. This result is supported by detailed observations of bacterial distributions at several sea outfalls (Gameson, 1982; Munro, 1984).

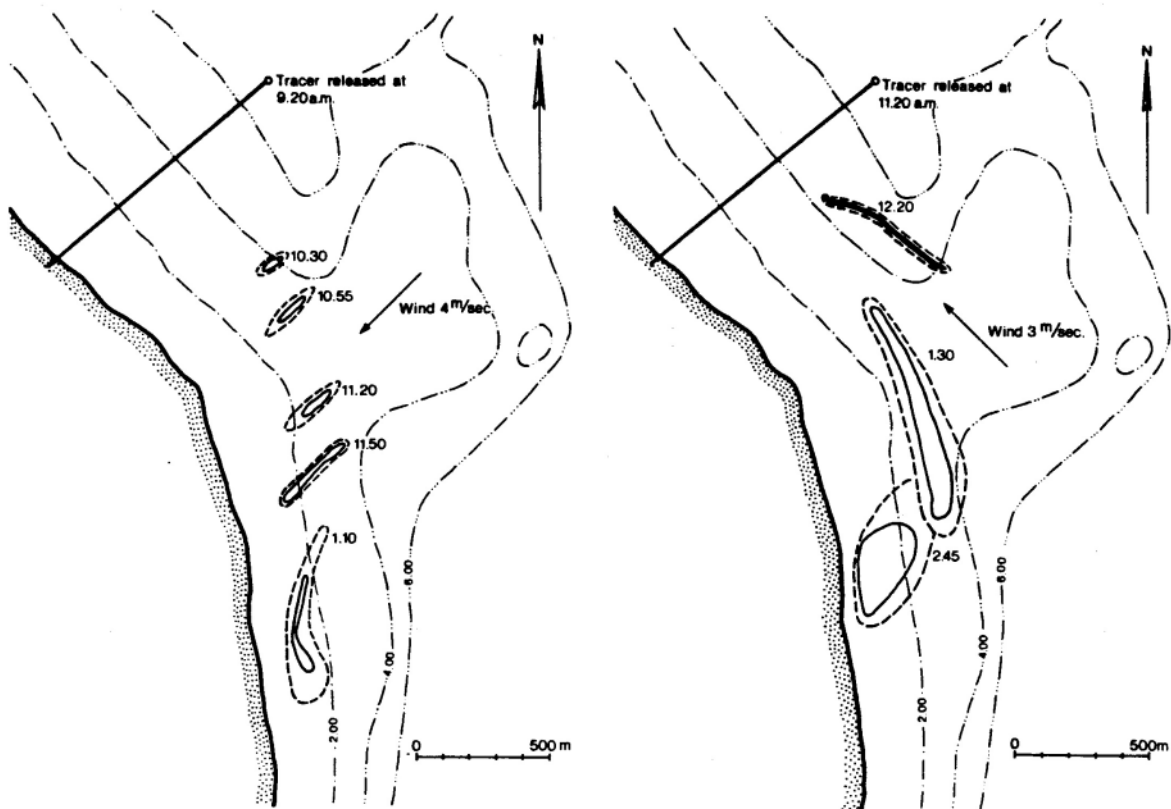


Fig. 75: Example showing far-field waste plume transport and dispersion. The transport is governed by the tidal current and mixing is governed by the wind shear stress (courtesy of Torben Larsen, Denmark)

Thus, the required detail of a far field prediction can vary considerably from case to case. It depends on i) the complexity of the coastal ocean environment, ii) the availability of data, and finally, iii) the severity of the pollution problem:

Regarding *environmental complexity*, for an open coastal environment with a prevailing unidirectional current structure a simple plume model may suffice if a far field calculation is needed at all. As such, the above equation has also been incorporated as an extension of near-field models (e.g. CORMIX). Effects of unsteady motions, if spatially uniform, can be considered through “puff” models, which travel and disperse the plume in 2D according to measured velocity information; however, those are not reliable near the shore. A puff model is included in the Visual Plumes modeling system (called FRFIELD). For estuaries or semi-enclosed bays, a flushing analysis may be required to ascertain the net flow-through and potential long-term accumulation of pollutants. Finally, in coastal environments or tidal networks of complex topography and current structure, numerical transport models have to be employed in order to predict the far-field pollutant distribution under more general conditions

regarding the coastal circulation, mass transport, and transformation (water quality parameters). The velocity field in these transport models may have to be calculated from a separate circulation model or be obtained from detailed field measurements.

Regarding *available data*, good information on current velocities is essential for far-field transport. Estimates show that for long diffusers (e.g. 500 m) it is more important to know where the wastefield goes rather than whether the far-field dilution is of the order of 3 or 5 (Roberts, 1979, 1980). For short diffusers instead far-field dilution increases to considerable values.

Regarding the *pollution problem*, near-field models suffice, if only acute impacts on the outfall zone are of interest. A simple reversal motion with built-up effects can be predicted if currents are clearly oscillating with the tidal cycle. As such, a built-up model (Nash and Jirka, 1996) has also been incorporated as an extension of the near-field model CORMIX. However, near-shore, water-quality (i.e. bacteria) impacts on the bathing zone are related to large and unsteady plume travel times of the order of several hours, defining the necessity of an unsteady tidal flow model. Moreover, because “old” diluted sewage can return with the tidal current the scenario for a computation should be around 24 hours. Finally water quality parameters demand extensive information on additional parameters, like salinity and temperature, and plume depth and geometry (to define light attenuation), to name only a few (Bleninger and Jirka, 2004).

Therefore, large outfall projects for coastal cities should not only include the mentioned “order of magnitude analysis”, but also a full far-field flow analysis. Generally, numerical models in combination with field-measurements provide such information. This far-field analysis may also serve to deduce the relevant parameter for near- and intermediate field analysis, especially if predictions beyond the measured parameters are to be considered. At first sight, this recommendation appears to be rather costly, though it is relatively cheap compared with the considerably large investments for coastal outfalls and even cheaper compared to the relatively strong socio-economic and environmental impacts, for inappropriate solutions.

A full far-field analysis includes a general flow model coupled with a transport model. Both are described in detail in the following chapters.

5.3.2 Governing equations for 3-D shallow water flows

Implementing the simplifications from chapter 3 regarding the far-field region results in the U-RANS (unsteady Reynolds averaged Navier-Stokes) equations for 3 D shallow flows, e.g. after Rodi (1993):

Continuity equation

$$\frac{\partial \bar{u}_i}{\partial x_i} = 0 \quad (5.77)$$

Momentum equation

$$\frac{\partial \bar{u}_i}{\partial t} + \bar{u}_j \frac{\partial \bar{u}_i}{\partial x_j} + 2\Omega_i \times \bar{u}_i = -\frac{1}{\rho} \frac{\partial \bar{p}}{\partial x_i} - \bar{g}_z + \nu \frac{\partial^2 \bar{u}_i}{\partial x_j^2} + \frac{\partial \overline{u_i' u_j'}}{\partial x_j} + \frac{F_{i,e}}{\rho} \quad (5.78)$$

where $\bar{\rho}$ = time averaged density and \bar{p} = time averaged pressure. The term $\frac{\partial \overline{u_i' u_j'}}{\partial x_j}$ is defined as additional stress term called Reynolds stress, which represents the turbulent variations. A turbulence closure is necessary, which is described in the following chapter.

Transport equation

$$\frac{\partial \bar{c}}{\partial t} + \bar{u}_i \frac{\partial \bar{c}}{\partial x_i} + \frac{\partial}{\partial x_i} (\overline{u_i' c'}) = D_m \frac{\partial^2 \bar{c}}{\partial x_i^2} + k \bar{c} \quad (5.79)$$

where \bar{c} = mean substance concentration and c' = concentration variations. A turbulence closure is necessary to describe the term $\frac{\partial}{\partial x_i} (\overline{u_i' c'})$, discussed in the following chapter.

5.3.2.1 Turbulence closure

The term $\frac{\partial \overline{u_i' u_j'}}{\partial x_j}$ in the momentum equation (5.78) and the term $\frac{\partial}{\partial x_i} (\overline{u_i' c'})$ in the transport equation (5.79) require further approximations, a turbulence closure as described in chapter 3.3.2. For the far-field region, a classical turbulence closure based on eddy-viscosity principles is applicable. These define a proportionality factor ν_t , the eddy-viscosity, in analogy to the molecular viscosity. The eddy-viscosity links Reynolds-stresses to the gradients of the mean flow (DVWK, 1999):

$$-\overline{u_i' u_j'} = \nu_t \left(\frac{\partial \bar{u}_i}{\partial x_j} + \frac{\partial \bar{u}_j}{\partial x_i} \right) - \frac{2}{3} k \delta_{ij} \quad (5.80)$$

where δ_{ij} , the Kronecker-Delta, guarantees that the sum of normal stresses is consistent to the definition of the turbulent kinetic energy:

$$k = \frac{1}{2} (\overline{u_i' u_j'})$$

The turbulent diffusion term in the transport equation can be written in analogy to the Reynolds-stress term as:

$$-\overline{u_i' c'} = D_t \frac{\partial \bar{c}}{\partial x_j} \quad (5.81)$$

where D_t = turbulent diffusion coefficient as analogous to the eddy-viscosity ν_t . If ν_t has been calculated by the hydrodynamic flow equations it can directly be used for the calculation of D_t using the turbulent Schmidt number $Sc_t = 1.0 - 1.2$ (DVWK, 1999):

$$D_t = \frac{\nu_t}{Sc_t} \quad (5.82)$$

Otherwise, D_t has to be defined from experimental values.

Turbulent diffusion is of orders of magnitudes larger than molecular diffusion. Therefore, the molecular diffusion term can be neglected and the advection-diffusion equation written as:

$$\frac{\partial \bar{c}}{\partial t} + \bar{u}_i \frac{\partial \bar{c}}{\partial x_i} = \frac{\partial}{\partial x_i} \left(D_t \frac{\partial \bar{c}}{\partial x_i} \right) + k \bar{c} \quad (5.83)$$

Unfortunately, v_t varies with the flow field. Turbulence models therefore try to describe these changes, often in combination with model calibration using experimental data. If sufficient experimental or field data is available, simple approaches like constant eddy viscosities or algebraic or mixing length models (Nezu and Nakagawa, 1993 or Rodi, 1993) might be used with careful calibration. However, these approaches do not include the transport of turbulent structures with the mean flow, which is an important issue for modeling natural flows and transport processes. Furthermore, model calibration is often not possible due to missing data. Thus, models including turbulent transport have to be used. Most experience exists for the k - ε model (Rodi, 1993), which is a standard model for free flow turbulence, therefore i.e. important for far-field processes. The k - ε model tries to describe the distribution of v_t in the flow field according to a characteristic velocity and length scale for turbulent flows, where the turbulent kinetic energy k is used as velocity scale and the dissipation ε as length scale (large eddies define the dissipation rate). Still, model assumption and calibration is necessary to close the equations for k and ε , but those can often be related to general values from experimental studies. The classical equations are (Rodi, 1993):

$$v_t = c_\mu c_D \frac{k^2}{\varepsilon} \quad (5.84)$$

$$\frac{Dk}{Dt} = \frac{\partial}{\partial x_j} \left(\left(v + \frac{v_t}{\sigma_k} \right) \frac{\partial k}{\partial x_j} \right) + P_k - \varepsilon \quad (5.85)$$

$$\frac{D\varepsilon}{Dt} = \frac{\partial}{\partial x_j} \left(\left(v + \frac{v_t}{\sigma_\varepsilon} \right) \frac{\partial \varepsilon}{\partial x_j} \right) + c_{1\varepsilon} \frac{\varepsilon}{k} P_k - c_{2\varepsilon} \frac{\varepsilon^2}{k} \quad (5.86)$$

$$P_k = - \overline{u_i' u_j'} \frac{\partial \overline{u_i}}{\partial x_j} = v_t \left(\frac{\partial \overline{u_i'}}{\partial x_j} + \frac{\partial \overline{u_j'}}{\partial x_i} \right) \frac{\partial \overline{u_i}}{\partial x_j} \quad (5.87)$$

where the source term P_k describes the production of turbulent energy out of mean flow properties. The empirical constants have been defined experimentally (Launder and Spaulding, 1974 and Nezu and Nakagawa, 1993) for a Karman constant of $\kappa = 0.41$ to $c_\mu = 0.09$, $\sigma_k = 1.2$, $\sigma_\varepsilon = 1.2$, $c_{1\varepsilon} = 1.44$, $c_{2\varepsilon} = 1.92$. Several extensions of the classical k - ε model exist depending on the application to be modeled.

However, limitations of the k - ε model are related to flows with adverse pressure gradients or strong buoyant processes, which generally occur only in near-field regions (Rodi, 2004). Therefore, besides the shallow water approximation (hydrostatic assumption) this limitation of far-field models regarding near-field processes probably has the strongest implications. There have been attempts to use other turbulence models (e.g. the k - ω model which performs good near walls or with adverse pressure gradients, but is not appropriate for free flow turbulence (Rodi, 2004)) or tuned versions of existing models to extend far-field model capabilities, but this requires good calibration data, which generally is not available.

5.3.3 Numerical methods - CFD

The far-field equations as listed above cannot be solved analytically. Numerical solution methods divide the problem scales (temporal and spatial) into discrete elements, thus reducing the differential equations to algebraic equations, which can be solved. There are different discretization methods possible for each differential, allowing for different kinds of numerical schemes. In their continuous forms, all these systems are equivalent. Unfortunately, discretization for a numerical model creates truncation errors whose detailed form and behavior differ from one coordinate system to another. Hence, each of these systems may be better suited for certain classes of problems than for others.

5.3.3.1 Spatial discretization methods

Finite Elements method is based on a group of elements comprised of two or more grid points (Fig. 76). Basis functions are chosen to describe the variation of an unknown over the element and coefficients of the basis functions are found by substituting the basis functions as solutions into the governing equations. Unstructured finite elements give better simulation of complex geometries, e.g. usage of different numbers of elements vertically. However mass conservation may be limited, because these equations are not solved themselves, but rather a weighted residual version. This may not be an issue in ocean circulation applications, such as water temperature predictions, but could be important in the simulation of constituents, such as coliform organisms. In addition, computational time for finite element models may be longer, due to high-order interpolation schemes.

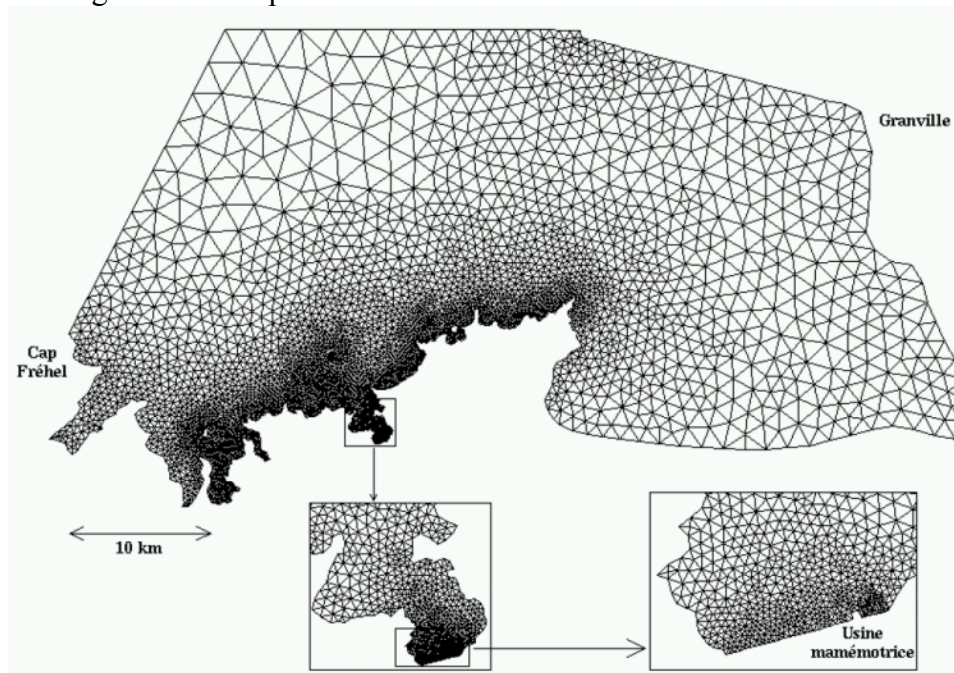


Fig. 76: Unstructured finite element mesh for the Telemac model (www.telemacsystem.com)

Finite Differences, where the differential equations are discretized over the numerical grid, built up from a series of nodes, and derivatives become difference equations that are functions of the values around surrounding cells. This method is the easiest to implement and so far the most widely used method. The restriction of structured finite difference schemes regarding complex geometries can be overcome in coastal engineering by applying curvilinear grids (Fig. 77). However, coastal structures still cannot be resolved sufficiently and unstructured

mesh models should be preferred in that case. A finite volume approach would therefore be more appropriate.

Finite Volumes are a generalization of finite-differences and built up from a group of cells. Fluxes through cells are tracked and the differential equations are integrated over the cell volume. Cells can be of different shapes and unstructured orientation and therefore apply to complex geometries, similar to finite element methods. Finite volume methods generally apply especially for non-hydrostatic modeling.

Especially finite difference methods may use other than the geopotential or z-coordinate formulations for the vertical coordinate. An important alternative for coastal flows are terrain-following (σ -coordinate) systems (Fig. 77). These allow for high vertical resolution in coastal regions, which are most important for waste discharge analysis.

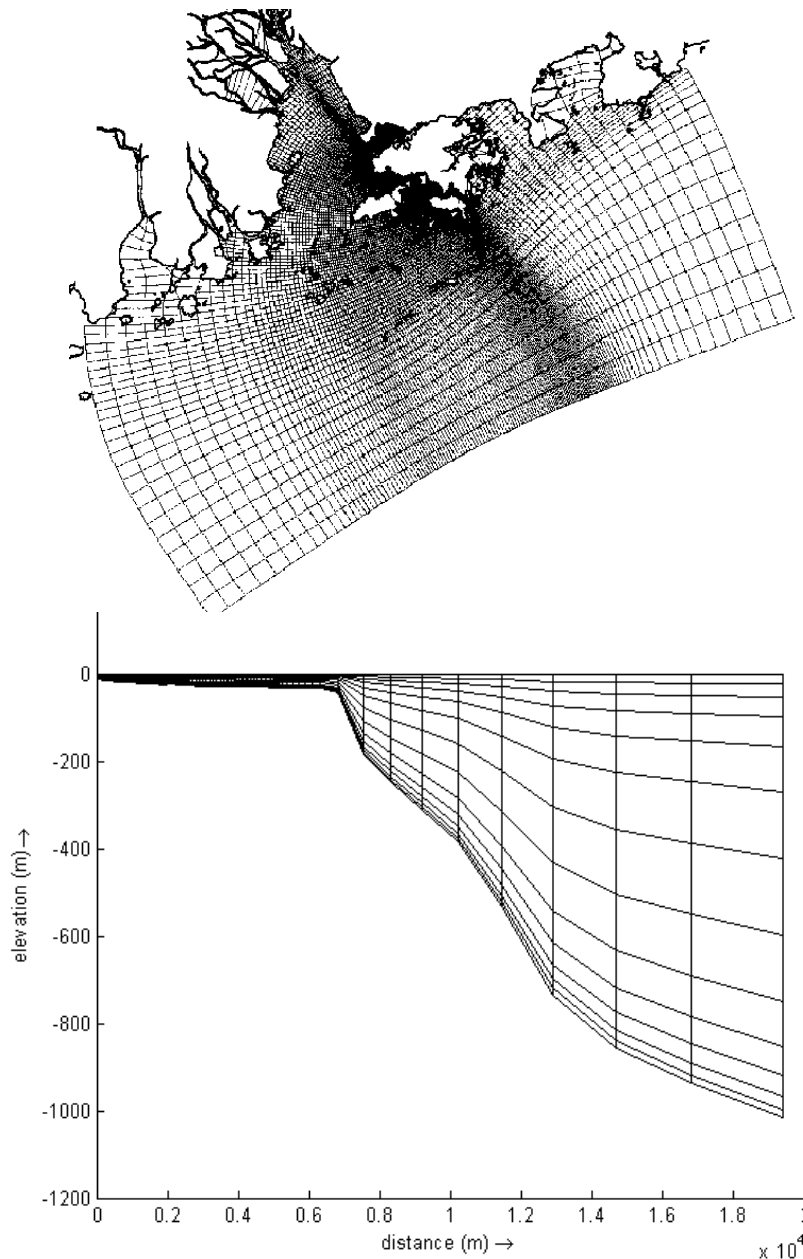


Fig. 77: Structured finite difference mesh for the Delft3D model, *top*: horizontal curvilinear, *down*: vertical σ -coordinate discretization (Delft Hydraulics, 2001)

σ -coordinate equations are based on the transformation (Blumberg and Mellor (1980, 1987):

$$x^* = x, y^* = y, \sigma = \frac{z - \eta}{H + \eta}, t^* = t \quad (5.88)$$

where x, y, z are the conventional Cartesian coordinates, $H(x, y)$ the bottom topography elevation and $\eta(x, y, t)$ the surface elevation.

The main advantage of σ -coordinate systems is that, when cast in a finite difference form, a smooth representation of the bottom topography is obtained (Mellor et al., 2002). On the other hand, it will not always have enough resolution around the pycnocline, especially for steep bathymetric gradients (Stelling, 2001). Mellor et al. (2002) compared z -level grids with σ -coordinates in the vertical and concluded, "the σ grids can tolerate much smaller levels of horizontal viscosity and diffusivity. In shallow water, errors arise in the z -level grid which, depending on viscosity (which itself may be considered a source of error), are of a different nature and obviously much larger than errors due to the sigma pressure gradient error. In the final analysis, the straight σ -coordinate grid may be a good choice for many ocean applications, including basin-scale climate calculations. Adequate resolution of the surface layers are a significant advantage of the σ -coordinate grid. However, if the vertical grid spacing is, say, logarithmically reduced near the surface to adequately resolve the surface layer in the deepest portions of the model domain, then the only penalty of the σ -grid is that, in the shallower portions, the surface layers are over resolved.

5.3.3.2 Temporal discretization methods

Explicit schemes, are easiest to solve because the unknowns are written as functions of known quantities (e.g., concentration at the new time is dependent on concentrations at the previous time step and at upstream (known) locations. However, stability problems arise once the pathway of a fluid particle over one time step Δt is larger than the grid resolution Δx defined as the Courant criterion:

$$Cr = \frac{u\Delta t}{\Delta x} \leq 1 \quad (5.89)$$

This rather strong restriction has the consequence that either high resolutions are needed or models have to be tuned to overcome stability problems.

Implicit schemes are computationally more demanding, because equations for the unknowns are functions of other unknown quantities (e.g. concentration at the new time may depend on other concentrations at the new time or on downstream locations not yet computed). These equations must be solved using matrix algebra. Implicit schemes are generally considered more accurate and do not demand a time step limitation.

In practice numerous computational fluid mechanics (CFD) codes exist, which mainly differ in the applied numerical schemes and therefore are limited to the related application. Although all CFD codes are based on general fluid mechanical principles, they are generally not applicable for all problems. The correct model choice or correct choice of the numerical scheme in a modeling system is a major task for CFD applications. Model results and unfortunately computational efforts generally vary considerably if different schemes are used.

5.3.4 Far-field flow models - coastal circulation

The quality of a discharge assessment strongly depends on a good knowledge of the receiving waters. In contrast to the near-field assessment, a far-field analysis needs much more detail on ambient currents and turbulence than the time and depth averaged values used for the near-field. This holds especially for the description of stratified coastal waters.

Deep-sea oceanography and coastal oceanography hereby offer process descriptions and modeling tools that help to understand main features of the current scheme in an ocean region (Davies et al. 1997a, b). However most of these models are set up for large domains (order of hundreds of kilometers), where near coastal features are not as important, thus not resolved in detail. However, discharge modeling especially needs to know about near coastal flow features for domains of the order of tens of kilometers, with high resolution in the outfall region. Furthermore most oceanographic models are depth averaged (Davies et al., 1997a), which is sufficient for large-scale flows, but not for discharge assessments.

Wind-shear effects on stratified waters, non-uniform velocity profiles, and baroclinic processes require a three dimensional flow representation (Signell et al., 2000). This is even more relevant considering the limitations of field measurements especially regarding the surface layer. Fully three dimensional models, without the hydrostatic assumption are still under development (DVWK, 1999), with one exception (the MIKE3 modeling system from the Danish Hydraulics Institute). On the other hand, there are fully 3D models available, which are generally used in mechanical engineering, but not for coastal currents (Fluent, CFX, etc.). Their deficiencies are related to the free surface, the complexity for grid generation and the appropriate calculation of the dispersion coefficient, which is often directly related to the turbulence model used (Law et al., 2002). Generally, they can only be used for limited regions and several restricting limitations (rectangular geometries, rigid lid surface). However, unless strong vertical motions occur (due to strong bed slopes or breaking of internal or surface waves) a 3D hydrostatic model captures all important processes.

There are more than 20 circulation models in use today. Most are used for oceanographic studies (ocean models), whereas only a few are applied for more resolved coastal circulation studies (coastal models) (Tetrattech, 2000). With a few exceptions, these are all finite difference models. Most cited models are Mike 3 (from DHI - Danish Hydraulics Institute), POM (Princeton Ocean Model - Princeton University), ECOM-si (modified version of POM used at Hydroqual), Delft3D (from Delft Hydraulics), Telemac 3D (from EDF, Electricité de France, and Wallingford), SisBAHIA (University of Rio de Janeiro, COPPE, 2000).

Coastal circulation problems generally demand time-varying velocity information all over the problem domain. The Eulerian flow description is used. The heat (temperature) and salinity conservation equations have to be solved in parallel with the equations of motion since these parameters are linked to the water density by an equation of state.

A drawback of Eulerian models is the requirement of a substantial amount of input data, in terms of detailed topographical information, and temporal and spatial varying ambient data at the open boundary conditions (such as current speeds, temperature and salinity distributions). This data is generally not available and has to be provided from either a larger scale model, where the problem domain is nested in or by field measurements. Optimal would be a combination.

Nonetheless, these models promise to solve the majority of problems related to waste discharges, a few problems are still not solved in that regard. There is for example the problem

of Huntington Beach (California, USGS, 2004) where complex modeling efforts in combination with extensive field-studies have been undertaken to verify hypotheses regarding the bacterial pollution at Huntington Beach. Whether internal waves together with wind induced flow transport may cause bacteria pollution or these are caused by other sources could not finally be solved in that case. Results at least indicate that outfall contributions are not the most significant. The main open question in pollutant transport modeling is whether trapped waste plumes may reach the beaches at certain conditions due to upwelling, internal waves, or other processes.

5.3.4.1 Hydrodynamic model Delft3D-FLOW

For this study the model suite Delft3D from Delft Hydraulics (2003) was chosen for the following reasons regarding the hydrodynamic and software capabilities (model assumptions are all based on those mentioned in chapter 5.3.2 regarding the far-field region if not explicitly stated in the following):

The Delft3D package is composed of several modules, grouped around a mutual interface, while being capable to interact with one another. Delft3D-FLOW is the model providing the hydrodynamics. That includes tidal forcing, Coriolis force, density driven flows (pressure gradient terms in the momentum equations), an advection-diffusion solver to compute density gradients with an optional facility to treat very sharp gradients in the vertical, coupled source and sink term formulations and space and time varying wind fields and atmospheric pressure. Typical intermediate-field processes like buoyant spreading and the damping of vertical exchange due to stratified conditions may be directly modeled and represented in the flow field if sufficiently resolved. Further coupling to transport modeling allows for considerations of mixing, diffusion and decay processes in direct relation to far-field processes.

Delft3D-FLOW solves the unsteady non-linear shallow water equations in three dimensions (hydrostatic assumption). The equations are formulated in orthogonal curvilinear coordinates or in spherical co-ordinates on the globe. In the vertical either a geopotential z -coordinate or a terrain-following, σ -coordinate system can be used. For the latter a built-in anti-creep correction is implemented to suppress artificial vertical diffusion and artificial flow due to σ -grids. The horizontal advection terms are discretized by the Cyclic Method (Stelling and Leendertse, 1991), an extension of the alternate direction implicit (ADI) method based on the dissipative reduced phase error scheme (Stelling, 1984). It is a splitting of a third order upwind finite difference scheme for the first derivative into two second order consistent discretization: a central discretization and an upwind discretization, which are successively used in both stages of the ADI-scheme. For the space discretization of the vertical advection term, a second order central difference is used.

Delft3D-FLOW includes advanced turbulence models (algebraic, k - L or k - ϵ) to account for the vertical turbulent viscosity and diffusivity based on the eddy viscosity concept. The eddy viscosity is anisotropic. The aspect ratio for shallow water flow hereby allows assuming that the production of turbulence is dominated by the vertical and not the horizontal gradients of the horizontal flow and that the horizontal eddy viscosity is much larger than the vertical eddy viscosity. For this project, the k - ϵ turbulence model was chosen for the vertical turbulent viscosity and diffusivity. The standard approach (see chapter 5.3.2.1) has been modified regarding the following processes (Rodi, 1984; Uittenbogaard et al., 1992):

- Turbulent motions are damped in stable stratifications. This process is generally described by a damping function, which depends on the gradient Richardson number (Si-

monin et al., 1989), and determined by fitting mathematical functions, which fulfill the limiting conditions to laboratory data sets. In Delft3D-FLOW, the algebraic eddy viscosity model (AEM) is extended to stratified flows by the formulation of Busch (1972).

- The turbulence model does not account for the vertical mixing induced by shearing and breaking of short and random internal gravity waves, because the turbulent eddy diffusivity at the interface reduces to zero. This process would require an additional transport equation for Internal Wave Energy (IWE-model, Uittenbogaard and Baron, 1989). However, only the simplest approximation of that effect using a constant vertical ambient mixing coefficient of momentum and/or heat and matter has been implemented for the present purpose, to consider such forms of unresolved mixing. Delft Hydraulics (2003) therefore recommended an ambient eddy viscosity in the order of 10^{-4} m²/s for the vertical exchange of momentum, based on experience with highly stratified flows and field experiments.
- The numerical scheme for the vertical advection of heat and salt (central differences) may introduce small vertical oscillations. This computational noise may enhance the turbulent mixing. Delft3D-FLOW has a vertical filtering technique to remove this noise and to reduce the undesirable mixing.
- The logarithmic wall law is used for the turbulent kinetic energy and energy dissipation at the free surface and bottom.

5.3.5 Far-field transport models - transport and mixing

The introduction of solute substances into a hydrodynamic model can either be performed using source terms, which add mass- and momentum fluxes to a grid cell, or through transport boundary conditions, which add mass and momentum fluxes to the specified boundary. The definition of the location of sources in the model domain and the related mass- and momentum fluxes is a challenging and difficult task regarding the complexity of waste plumes from off-shore, submerged wastewater discharges using multipoint diffusers. This in fact is defined as the coupling problem, and a solution is proposed in chapter 5.4.3. However, assuming that information on source location and fluxes is available; two approaches exist for transporting and mixing the substances within the far-field domain, the Eulerian, and the Lagrangian approach.

5.3.5.1 Eulerian transport modeling

Discharges, which affect the hydrodynamic conditions in the far-field region (e.g. large momentum fluxes from thermal discharges or strong and large buoyancy fluxes from river discharges), have to be solved within the Eulerian hydrodynamic model. Substance transport is performed by the advection-diffusion equation, which in that case is coupled to the momentum equation via the equation of state.

For discharges which do not affect the hydrodynamic conditions in the far-field region (regardless of the near-field region, e.g. wastewater discharges) the Eulerian approach solves the advection-diffusion equation subsequently on the same mesh which has been used for the flow or a new, generally smaller mesh using interpolations of the previously obtained hydrodynamic quantities. An advantage of that approach is the possibility to calculate long time periods and interacting hydrodynamics for the whole domain. A disadvantage of Eulerian transport models is additional numerical diffusion due to the relatively coarse grids used for coastal hydrodynamic simulations. Nonetheless, in reality the contaminant concentration in the far-field is often much more dependent on advection by the mean flow than dispersion, as the latter occurs at a lower rate.

5.3.5.2 Lagrangian transport modeling

The Lagrangian approach instead only tracks unknown quantities independently along lines of known values (i.e. velocity field). This approach does not consider active effects of the discharge on the far-field region. These models are also called particle tracking or random walk models, if particles are the observed quantities, which are released at a certain location at different times. If each particle carries an assigned amount of mass, the density distribution of particles can be related to the concentration distribution. Particles follow the prevalent velocity field (advection) and turbulent diffusion is represented by random particle jumps (of length equal to the estimated turbulent length scale). Velocity and turbulence information are taken from the flow model. The transport and diffusion calculation to be considered then results in tracking the location of a quantity using the information of the velocity field:

$$x_i(t+\Delta t) = x_i(t) + u_i(t)\Delta t + [f_i(2\varepsilon_i\Delta t)]^{0.5} \quad (5.90)$$

where $x_i(t+\Delta t)$ = location of a particle at time $t + \Delta t$ after release; u_i = velocity components; ε_i = turbulent diffusion coefficients; f_i = normally distributed random variable that takes the value +1 or -1.

Typically, the last term in (5.90) is negligible if x is in the direction of the predominant current. However, if v or w is small, then the turbulent correction term should not be ignored. Particularly w may denote a small settling velocity or buoyant velocity (for emulsion droplets) and the diffusion term becomes extremely important.

Lagrangian algorithms are often included in either near-field mixing models to track near-field results for measured currents (e.g. Visual Plumes FRFIELD), or within far-field mixing models to track the plume according to the fully predicted velocity field (all of the above-mentioned models contain a particle tracking module).

Advantages relative to Eulerian models are: Numerical diffusion can be eliminated by replacing a concentration model with a Lagrangian particle-tracking model, which is grid size independent. There is no theoretical limitation on the time step size regarding numerical stability, but accuracy determines limits for Lagrangian models. Due to the independent movement of involved particles, the programming structure is preferable for non-homogeneous flow and parallel computing.

Disadvantages relative to Eulerian models are: Within Lagrangian transport models there is no backwards interaction possible with the flow. Thus, transport is limited to quantities, which do not interact with the flow, like solute substance mass. The transport of other quantities (like salinity or heat) can only be accomplished if independently to the flow. Another drawback of particle models is their limitation on short to medium scale time periods due to the statistical analysis for obtaining the particle distributions. Large-scale water quality is limited in that regard.

Within both approaches, reaction or decay processes can be simulated in addition.

5.3.5.3 Transport modeling within Delft3D

The hydrodynamic module Delft3D-FLOW automatically solves the Eulerian formulation of the advection-diffusion equation for salinity and temperature if baroclinic flows are to be considered. The equation is solved in parallel and coupled with the momentum equation via the equation of state. In addition, it may be solved for a solute, conservative substance.

However, advection-diffusion scales are different from those for the hydrodynamics, therefore often additional separate transport models exist, as for the case of Delft3D. The Delft3D model suit allows for both the direct coupling of the flow field with either an Eulerian water quality model or a mid-field particle-tracking model. The hydrodynamic conditions (velocities, water elevations, density, salinity, vertical eddy viscosity, and diffusivity) resulting from the flow field module Delft3D-FLOW are therefore used as input to the other modules of Delft3D, which are: Delft3D-WAQ: Eulerian far-field water quality module or Delft3D-PART: Lagrangian mid-field particle tracking module.

In addition to the Delft3D-FLOW module, the Delft3D-WAQ module allows concentrating the calculation of mixing and transport processes on temporal and spatial scales, which can be considerably different from the hydrodynamic scales (Fig. 78). The advection diffusion equation is solved for the substances of interest only on that spatially limited grid within the time-scales of interest using the hydrodynamic conditions from the results of Delft3D-FLOW. An advantage compared to Delft3D-FLOW only are better temporal resolutions regarding dispersion processes and less numerical diffusion. Moreover, Delft3D-WAQ includes numerous formulations for substance decay and transformation, which will be discussed in the following chapter.

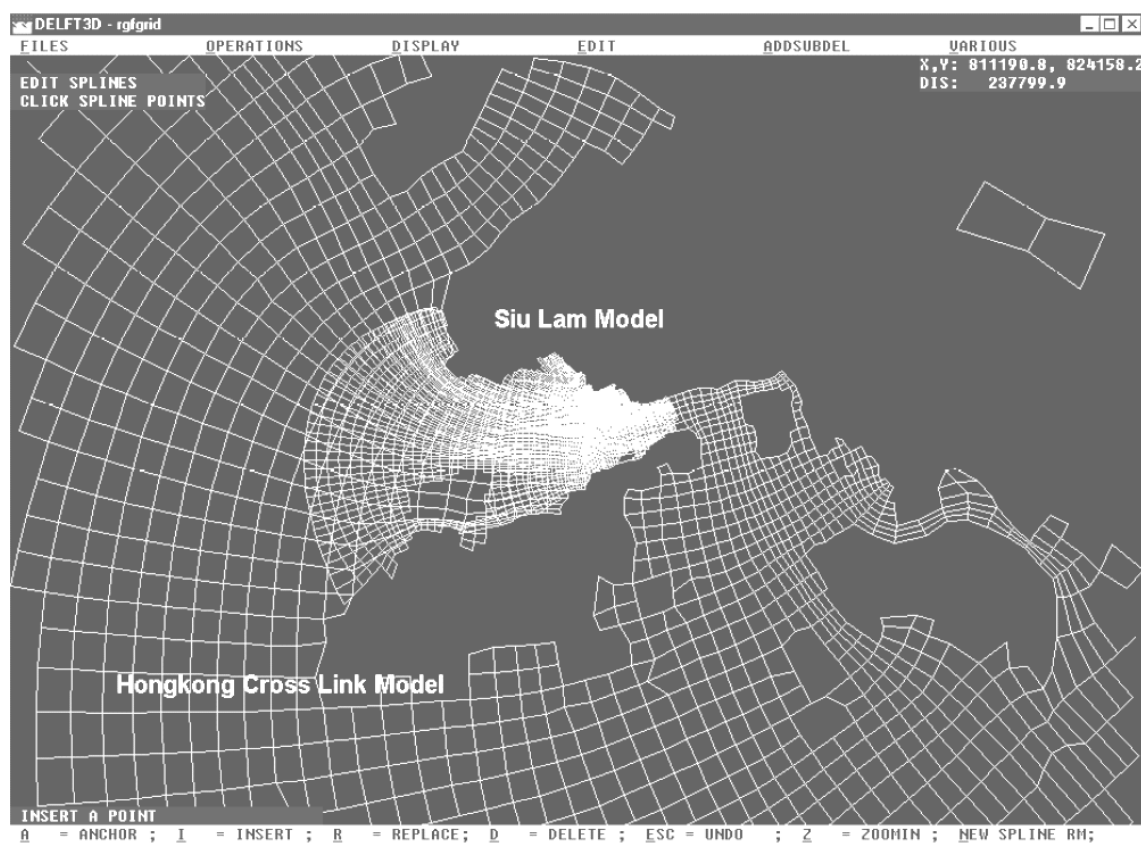


Fig. 78: Nesting of a small-scale water quality model (Siu Lam Model) and a large-scale hydrodynamic model for Hong Kong waters using the Delft3D modeling system (Delft Hydraulics, 2005)

The Lagrangian transport model Delft3D-PART is independent of a grid, thus allowing water quality processes to be described in a detailed spatial pattern, resolving sub-grid concentration distributions. Delft3D-PART is best suited for studies over the mid-field range (200m-15 km) of instantaneous or continuous releases. It calculates advection and diffusion processes using

the Lagrangian approach and the hydrodynamic quantities resulting from Delft3D-FLOW. In addition, reaction or decay processes can be simulated using different particle attributes (density, surface area, and ages). Various realistic features (e.g. the return of previously diluted sewage over the outfall and different source conditions) and especially substance accumulation can be readily simulated by superposition methods.

5.3.6 Water quality modeling - decay and transformation processes

Beside the advection and dispersion, substances might undergo further transformation and decay processes (see chapter 2.1.3). Focus of this study are bacteria concentrations because of its impacts on public health (Roberts, 2004). The chosen indicator bacteria are total coliforms. As soon as these organisms enter the surface waters, they start to die since the conditions are essentially hostile to them. The mortality rate is enhanced by solar radiation, particularly short wavelength, ultraviolet radiation. The decay rate for bacteria is a function of temperature, salinity (or chloride concentration), and UV radiation intensity.

Most bacteria decay models assume a first order decay:

$$\frac{dC}{dt} = -kC \quad (5.91)$$

where C denotes the bacteria concentration, t the time, and k a decay coefficient.

This results in so-called Chick-Watson model

$$\frac{C_t}{C_o} = e^{-kt} \quad (5.92)$$

where C_t = concentration of bacteria at time t , C_o = concentration at time 0

The first order decay is justified by experimental studies, where logarithmic plots follow straight lines. However, there are other experiments showing considerable variations from this straight line.

Environmental hydraulic studies often express the decay rate in terms of a so-called T_{90} value, the time taken for 90% of the bacteria to die-off

$$k = \frac{-\ln(0.1)}{T_{90}} \quad (5.93)$$

Numerous empirical equations exist for the prediction of bacteria decay rates (Guillaud et al., 1997; Bellair et al., 1977; Solic and Krstulovic, 1992; Canteras et al., 1995). Unfortunately there are partly order of magnitudes of differences between some formulations. Values for T_{90} vary between 2 to 15 hours during sunlight and 20 to 100 hours during night. Experimental data, without proposing a specific model can be found in Noble et al. (2004). Probably the most used model for bacteria inactivation in coastal waters is based on the Mancini (1978) formulation, which is also used in the water quality model from Delft3D. Carvalho (2003) presented a modification of the original equation, which also takes in account that plumes might be trapped, thus having different uv radiation. He also showed that bacterial models need accurate position and geometry of waste plumes to be able to predict bacteria decay accurately.

5.4 Model coupling - approaches and algorithms

Table 18 summarizes the previous descriptions regarding the hydrodynamic regions, by comparing characteristic flow quantities. As an example, a typical discharge situation for a large coastal city is described (modified from Jirka, 1982). The example compares two kinds of multiport diffuser discharges with two kinds of ambient flow conditions. The discharges differ only by their flowrate and density representing either a wastewater effluent or a thermal effluent (cooling water). Discharge characteristics are assumed for a population of 1 million people and a diffuser with length $L_D = 400$ m. The ambient conditions just differ in velocity, where the values in brackets indicate higher velocities. Velocity distributions are all assumed uniform, allowing estimating the fluxes using the average velocity. The ambient volume flux estimates result from $Q_{o,a} \approx u_a L_D H$, with an assumed water depth $H = 20$ m.

Variable	medium discharge (I) (e.g. wastewater)	large discharge (II) (e.g. cooling water)	shallow flow (III) (large velocities in brackets)	ratios (I/II ; II/III)
initial velocity U_o, u_a [m/s]	5	5	0.1 (0.5)	50 ; 50 (10 ; 10)
initial total volume flux $Q_o, Q_{o,a}$ [m ³ /s]	8	80	800 (4000)	0.01 ; 0.1 (0.002 ; 0.02)
initial volume flux $q_o = Q_o/L_D$ [m ² /s]	0.02	0.2	2 (10)	0.01 ; 0.1 (0.002 ; 0.02)
init. momentum flux $m_o = U_o q_o$ [m ³ /s ²]	0.1	1	0.2 (5)	0.5 ; 5 (0.02 ; 0.2)
density difference $\Delta\rho/\rho$ [kg/m ³]	0.025 (freshwater)	0.0025 (heated salt-water)	-	-
initial buoyancy flux $j_o = q_o g_o'$ [m ³ /s ²]	0.005 (vertical)	0.005 (vertical)	0 (stable, barotropic)	>> 1
NF dilution S	> 100	> 10	-	-
distributed FF mo- mentum flux $m_{ff} =$ $m_o/H ; m_{o,a}/1$ [m ² /s]	0.005	0.05	0.2 (5)	0.025 ; 0.25 0.001 ; 0.01
order of momentum induced FF velocities $u_{ff,m} = m_o/(S q_o)$ [m/s]	0.05	0.5	0.1 0.5	0.5 ; 5 0.1 ; 1
order of buoyancy induced FF velocities $u_{ff,b} = S q_o/(2(0.3H))$ [m/s]	0.17	0.17	0.1 0.5	1.7 ; 1.7 0.34 ; 0.34

Table 18: Comparison of typical flow quantities at different hydrodynamic regions. Discharge characteristics are assumed for a population of 1 million people and a diffuser with length $L_D = 400$ m discharging at a depth of $H = 20$ m (modified from Jirka (1982)). Considered discharge cases only differ in the total flow and density (e.g. wastewater and thermal). Ambient conditions differ only in velocity, where only the horizontal components of small and medium (in brackets) flows are considered (note that discharge velocities and momentum may act in orientations different to the horizontal).

Several comments regarding the initial quantities (upper half of Table 18) are in order: 1) the strong discharge induced velocity discontinuity indicates the necessity of a highly resolved near-field mixing model, capable to capture these strong shear flow processes. In addition, note that the considered ambient velocities are horizontal velocities, whereas the discharge velocities may act in arbitrary orientations. Thus, diffuser configurations need to be included in near-field models. 2) The discharge volume fluxes per unit length are small compared to the volume flux of the ambient flow passing over the diffuser. Note that cooling water discharges are generally an order of magnitude larger than wastewater discharges (Jirka, 1982).

3) Comparison of initial momentum fluxes per unit length, show a clear dominance of discharge induced momentum for large discharges into weak ambient. However, for stronger ambient flows discharge momentum fluxes are negligible for small discharges. 4) The density difference between the effluent and an average ambient density is generally an order of magnitude smaller for cooling water discharges. 5) Buoyancy acts in the vertical, where the ambient is assumed stable (either uniform or stratified). Both effluents are introduced through a submerged diffuser, causing strong buoyancy induced motions until reaching equilibrium stable conditions.

The comparison of initial quantities is useful for near-field analysis. It is concluded that near-field modeling for *wastewater* outfalls requires a high resolved near-field model with the buoyancy flux as dominant parameter, complemented by interactions of source induced and ambient momentum fluxes.

Comments regarding estimated source flux characteristics beyond the near-field by assuming typical minimal dilutions (lower half of Table 18) are in order: 6) Wastewater outfalls are generally designed and sited to achieve initial dilutions S above 100 to comply with regulatory demands. Thermal discharges often only need to be designed to achieve dilutions above 10. 7) Assuming that the initial momentum flux disperses all over the water depth and acts in the horizontal might allow estimating its importance compared to the ambient momentum. It follows that contributions from large discharges are still considerable when discharging into weak ambient flows. However, momentum fluxes from wastewater discharges have negligible effects on any ambient flow. 8) Another way to compare flow quantities in the far-field are comparisons of induced velocities. The order of the horizontal component of the momentum induced velocity can be estimated by dividing the total discharge related far-field momentum flux (= initial flux m_o) by the total discharge related far-field volume flux ($q_{ff} = Sq_o$). Comparison shows that weak ambient flows are experiencing considerable changes on the velocity field due to the discharge even beyond the near-field region. However, stronger ambient flows are only affected by large discharges. 9) The buoyancy-induced velocities can be estimated by equation (5.73) assuming that buoyant spreading occurs only in the upper third of the water body. Comparison shows that buoyant spreading motions may dominate over far-field motions for weak ambient flows. Moreover, for larger ambient flows, contributions from buoyant spreading are still large.

Consequently conclusions for the intermediate-field / far-field analysis are: Far-field modeling for wastewater outfalls requires a sufficiently resolved model to represent primarily the ambient velocity distribution without any near-field interaction. However, weak ambient flows either require higher resolution models to include effects of buoyant plume spreading, or require a separate intermediate-field model.

Consequently, Table 19 summarizes applications and modeling techniques capable to model the different flows. No specific intermediate-field model has been found, though either near-field or far-field models include intermediate field processes partly, shown by the adjustment to the middle column in Table 19. It is shown, that for the general case of waste discharges, i.e. for large coastal wastewater outfalls, no unique model applies, whereas for restricted cases, modeling efforts might be reduced to one model only. For that reason a zonal modeling approach is necessary (Fig. 79). This approach considers the application of zone models in regions with distinct hydrodynamic properties. It is then possible to simplify the governing equations by dropping unimportant terms. As an example, in the near-field region it is often possible to distinguish specific buoyant jet zones for which integral models apply. These only calculate near-field substance concentrations without explicitly calculating the complex flow

field (NF in Fig. 79). On the other hand, in the far-field region, it is often possible to neglect vertical accelerations and employ the hydrostatic assumption and calculate the far-field flow field omitting the near-field processes (FF in Fig. 79). Thus, zone models have a considerable advantage in the mathematical treatment and improved accuracy and detail in the solution. In addition, different model types can be used in the zonal approach.

Near-field type models	Intermediate-field type related components	Far-field type models
<p>A) General cases:</p> <ul style="list-style-type: none"> - high/low momentum fluxes - high/low buoyancy fluxes - high/low ambient velocities - arbitrary ambient stratification - arbitrary alignment - deep/shallow conditions - boundary interactions - buoyant spreading <p>Specialized mixing models: → CORMIX</p> <p>B) Restricted cases:</p> <ul style="list-style-type: none"> - weak momentum fluxes - high/low buoyancy fluxes - arbitrary ambient stratification - arbitrary alignment - deep conditions - no boundary interactions - no buoyant spreading <p>Jet models: → CORJET, NRFIELD, JETLAG</p> <p>C) Special near-field cases:</p> <ul style="list-style-type: none"> - selected conditions only - negligible or weak buoyancy effects <p>CFD models: → CFX, Fluent</p> <ul style="list-style-type: none"> - hydrostatic conditions - large scale interests <p>Coastal models / ocean models: → Delft3D, Mike3, POM/ECOM, Telemac</p>	<p>Intermediate-field type related components</p>	<p>A) General cases:</p> <ul style="list-style-type: none"> - complex coastal topography and bathymetry - complex current structure (tidal, wind-driven) - free surface flow - hydrostatic conditions - arbitrary stable stratification - baroclinic (high resolved) <p>Specialized coastal models: → Delft3D, Mike3, POM/ECOM, Telemac</p> <p>B) Restricted cases:</p> <ul style="list-style-type: none"> - open ocean - simple current patterns - unsteady currents - simple pollutant kinetics - moderate pollutant loads <p>Dispersion models: → FRFIELD</p> <p>C) Special far-field cases:</p> <ul style="list-style-type: none"> - selected conditions only - steady currents or simple reversals <p>Mixing and transport models: → CORMIX, CFX, FLUENT</p>

Table 19: Overview on modeling techniques regarding waste discharge modeling. Middle column adjusted characteristics denote the capability to model intermediate-field processes.

However, Fig. 79 also illustrates deficiencies of zonal models leading to incomplete and abrupt changes in transitional regions. In addition, major problems remain as time, length scales vary considerably, and solutions are restricted to zones. Thus, there might be a lack of criteria on (i) how to establish a meaningful division of the whole region into zones, (ii) how to provide transition conditions between the zones and (iii) how to combine the zonal predictions. This can be referred to as the “coupling problem”.

Coupling models means introducing flow quantities (e.g. momentum or mass) from one model into the other and vice-versa. There are only two possibilities for introducing flow quantities into a model, either over the boundary conditions, or via source terms. The former may only be specified at model boundaries and have direct effect on the whole flow. The latter only modify the existing flow by adding quantities. In addition, sources can be speci-

fied for single grid cells, i.e. at any vertical location of the domain, which is impossible for open boundary conditions. Both concepts are schematized in Fig. 80.

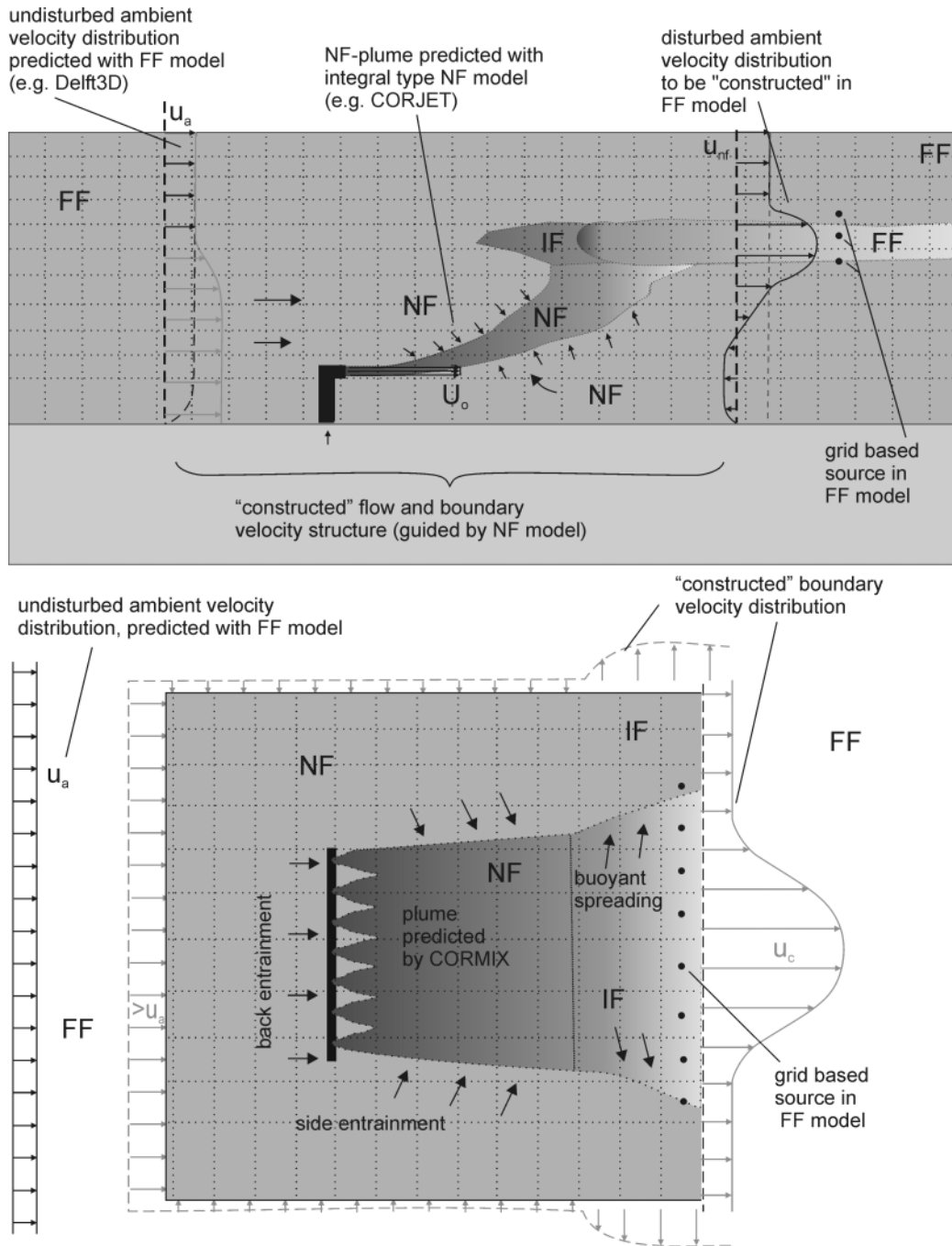


Fig. 79: Schematization of a zonal modeling approach for buoyant waste discharges and the related velocity and substance concentration fields. Hydrodynamic regions are the near-field (NF), the intermediate field (IF) and the far-field (FF).

At first glance, the most straightforward coupling approach would be linking a near-field model (i.e. CorJet) to the far-field model Delft3D. In reality, however, this coupling is quite complicated and no robust standard solutions exist. The reason is the disparate nature of these zone model types:

- 3-D far-field circulation models have an elliptic differential equation structure, i.e. they need distributed boundary conditions at all the domain boundaries (Fig. 80, choice 1).

- Integral type near-field models are parabolic in the governing differential equations. They only need initial boundary conditions (= initial conditions) and then use a forward marching solution technique along a defined trajectory (e.g. buoyant jet motion or density current motion). Thus, the output of such a model does not directly provide all the information that can be used as a boundary condition input for the far-field model.
- Furthermore, the integral type near-field models cannot easily deal with re-entrainment of already mixed water back from the far-field. The only way to do that in these models is by assuming a certain background concentration that is then added to the predicted output.

A nested coupling (Fig. 80, choice 3A) with an integral type zone model requires additional boundaries around the near-field zone. This approach is clearly limited, because near-field models do not provide field information. A boundary condition would need to be “constructed” out of the near-field plume results as schematized in Fig. 79, and a lot of inter- and extrapolation, would be necessary. The superposition approach instead (Fig. 80, choice 3B) does not require the whole field information, but only at characteristic source locations, where near-field flow quantities are introduced as source terms in the far-field model, which is easier to accomplish Fig. 79.

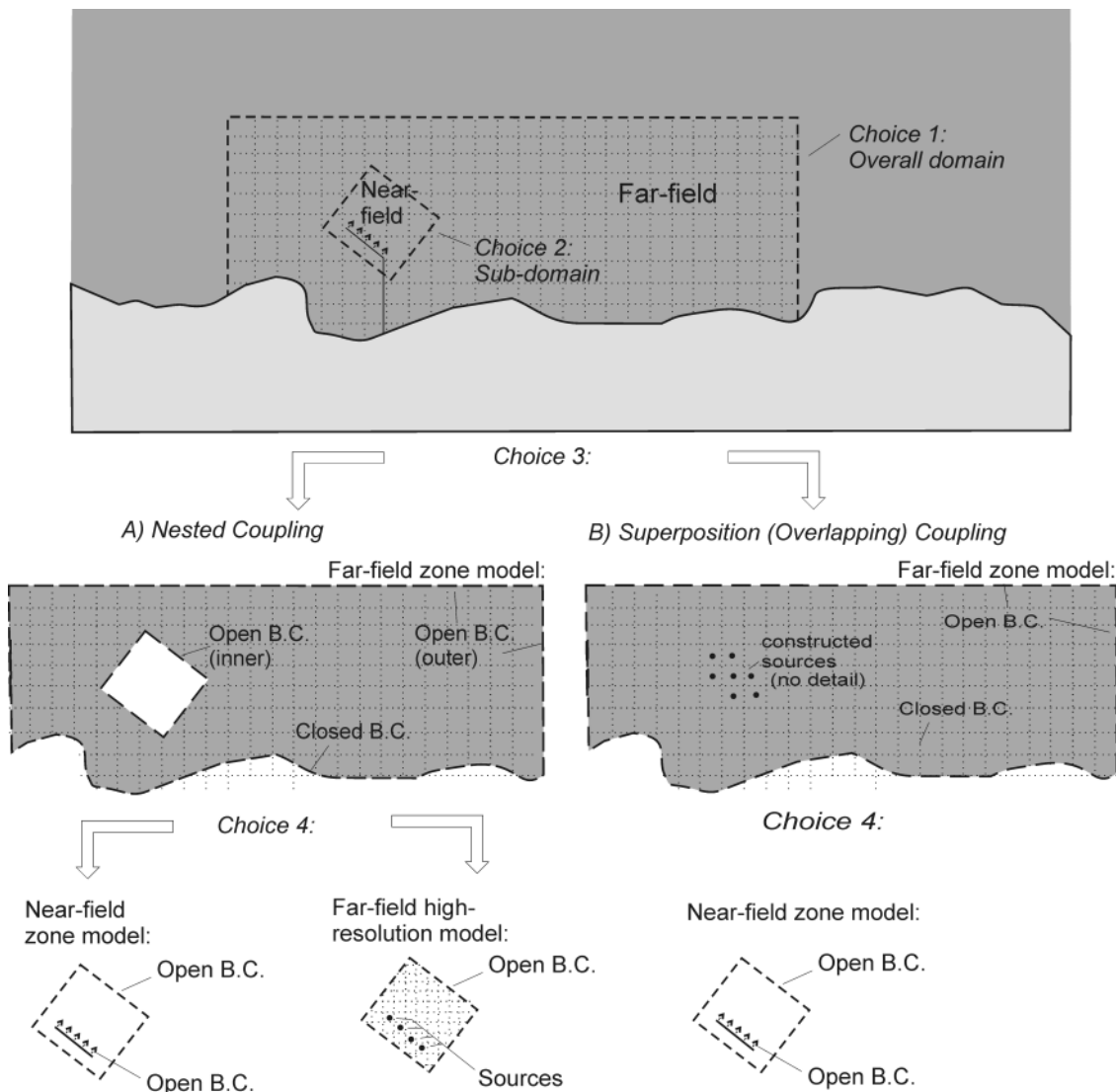


Fig. 80: Schematization of coupling approaches for zone models, either using boundary conditions (B.C.) or source definitions for the near-field representation in the far-field domain.

5.4.1 Review of coupling concepts

All practical model applications for outfall design and siting used the superposition-coupling concept (Fig. 80, choice 3B). Hereby generally, only near-field substance concentrations have been introduced as a source term into the related grid cells of the far-field domain. Roberts (1999) for example used the near-field model NRFIELD coupled to the far-field particle-tracking model FRFIELD for a Hawaii outfall. No circulation model was used in that case but single velocity measurements at the planned outfall position served as velocity information for the particle-tracking algorithm. Zhang and Adams (1999) coupled NRFIELD to the far-field circulation model ECOM-si for the Boston outfall and distributed the near-field concentration over far-field model cells nearest the diffuser. Miller et al. (1996) applied a similar approach for the Sydney outfall. However, all these coupled models neglect any intermediate field process. First, because the applied near-field models do not consider boundary interactions, or buoyant spreading processes, and second because the coupling does not include other flow quantities than the substance concentration. This is especially critical for quiescent ambient conditions, as shown previously.

To overcome these deficiencies Blumberg and Ziegler (1996) proposed including also volume fluxes into the source terms, in addition to the substance mass fluxes. This idea is based on the entrainment approach, which causes the plume volume flux to increase considerably. To guarantee mass balance the entrained fluid needs to be subtracted via sink term formulations. Zhang and Adams (1999) applied that approach for a simple model setup using NRFIELD and ECOM-si, but encountered difficulties due to strong grid dependency and turbulence model formulations. Besides, only a simple approach has been used to define source locations and entrainment flows, because NRFIELD does not provide information on plume trajectories or centerline flux developments. Choi and Lee (2005) recently presented an approach using JetLag for step-wise calculations of the entrained fluid volume during plume rise. The diluted substance mass and fluid volume was then introduced into the upper cells of the far-field domain, while the same amount of fluid is excluded from the domain in the lower cells. This approach is probably the most comprehensive regarding the specific dynamic interactions between the rising plume and the ambient. However, the wastefield collapse and intermediate motions are not fully included. This, because these do not depend on entrainment, but on density currents. The far-field model is generally not capable or not resolved enough to model these thin density currents as consequence of a source term definition. Furthermore, this rather strong, but too coarse far-field forcing is influencing the far field more than would be realistic. A third approach has been mentioned by Kim and Seo (2000) who established a momentum linkage with focus on thermal discharges, by introducing a diffuser line slot as momentum source into the far-field model. Limitations of their approach are especially related to the missing buoyancy representations, thus upstream spreading or buoyant spreading could not be solved sufficiently (also due to the hydrostatic assumption).

A nested coupling approach (Fig. 80, choice 3A) for the present application is not known. Nevertheless, solutions exist for simpler configurations. Dallimore et al. (2001) for example coupled a plunging heavy density current (integral model approach) into a stratified reservoir (2-D circulation model). The ambient hereby affected the plume as a source for entraining mass, momentum, salinity and turbulence and the plume affected the ambient by displacing it and including shear along the interface together with detrainment (sink). However, this approach cannot be generalized, because of a missing unsteady formulation or trapped plume formulation. For that reason, intensive research is actually being undertaken in that direction.

5.4.2 Coupling approach

Existing approaches seem to have problems especially at still water conditions or during slow ambient velocities, which often are considered as the worst-case scenarios. This is explained by the necessary, but too strict division of dilution processes in either near-field mixing processes or far-field transport processes and neglecting intermediate processes. Therefore, an approach will be followed, which is based on elements from Zhang and Adams (1999), Kim et al. (2002) and Choi and Lee (2005), but including special extensions for the intermediate field. Computational efforts are reduced by a previous far-field flow classification in analogy to the CORMIX flow classification (5.2.4). The classification allows distinguishing whether an intermediate field model is needed and which flow quantity is needed.

5.4.2.1 Dynamic aspects - flow classification

Given the different scales of interaction regarding different source strengths (Table 18), there appear two ways to coupling:

i. Passive coupling

Passive coupling assumes that the source-induced flow, though considerably important for near-field mixing, does not change the flow characteristics of the far-field, beyond the near-field or intermediate-field region. Thus, only a linkage between passive flow quantities (i.e. substance concentrations) has to be accomplished between the models. Simple substance-mass conservation principles could therefore be used. Passive coupling requires dynamic criteria, to distinguish when and where source induced motions are negligible. Following the scaling for typical wastewater discharges given in Table 18 this transition occurs right after the near-field for average and large velocities and after the intermediate-field for stagnant or slow flowing ambient.

ii. Active coupling

Once considerable large effluent flows have to be considered (i.e. for thermal discharges) the ambient flow will be strongly disturbed and modified by the discharge induced flows, causing changes in the flow and concentration fields even beyond the near-field and intermediate-field regions. For these cases source induced motions can never and at no region be neglected in the far-field flow model. A coupling of all flow quantities has to be accomplished. Momentum conservation principles have to be considered in addition to fluid and substance mass conservation for that linkage. Stagnant ambient are even more critical in that case.

The present approach will focus on wastewater discharges and therefore only follow a passive coupling. Criteria to distinguish whether a passive coupling is applicable are either the stability criterion (equation (5.60)) or a distributed momentum criterion. Active coupling is therefore necessary if at least one of the following conditions apply:

- i) the near-field is considered unstable (equation (5.60))
- ii) $\ell_m/H > r_{crit}$ (5.94)

The term ℓ_m/H hereby results from the ratio of the discharge momentum distributed over the depth m_o/H and the ambient momentum per unit depth u_a^2 . The critical value has been defined to $r_{crit} = 1$, however this needs to be validated with experiments.

For cases where passive coupling applies it is then distinguished furthermore, if buoyant spreading processes are considerable large or not. The CORMIX classification criteria (equa-

tion (5.62)) are therefore used. Two flow classes result for the intermediate field: a buoyant spreading flow class and a passive diffusion flow class.

Based on that classification coupling locations and times can be specified according to the following definitions.

5.4.2.2 Temporal aspects

The present approach needs to couple a steady state model (CORMIX) to an unsteady state model (Delft3D). It is therefore necessary to include time-averaging of far-field results before a coupling step. The period of time averaging (the coupling time-step) hereby influences coupling accuracy. For example, very short periods ($\Delta t =$ order of minutes) might result in abrupt changes of the near-field results, where locations of source definitions in the far-field domain change in an unrealistic manner, as illustrated in Fig. 81. Too long periods however, cause too much information loss due to a long time-averaging. Unsteady accumulation of waste substances is hereby underrepresented. Reasonable estimates for coupling time-steps are defined in eq. (5.95) based on near-field time scales as described in Table 26 (p. 184).

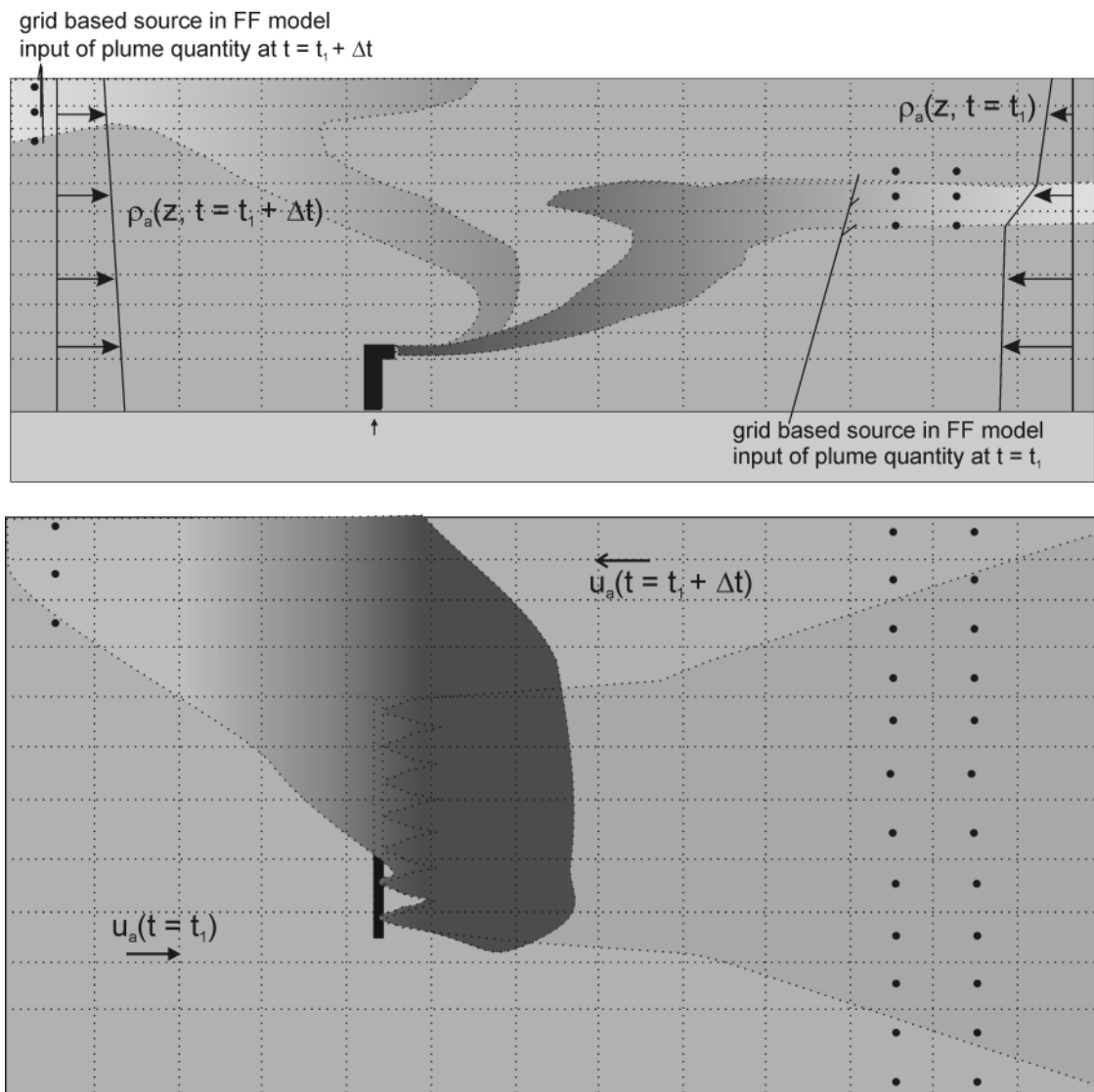


Fig. 81: Definition of source term locations for two different time steps, where ambient conditions changed considerably.

$$\Delta t_c = (1 \text{ to } 3) \max(t_M, t_m) \quad (5.95)$$

The leading factor (1 to 3) expresses some uncertainty depending on local conditions and diffuser design and alignment. This results in coupling time-steps of approximately one hour for typical wastewater diffusers, which has been successfully applied also in previous modeling approaches for typical near-field processes. However, time-scales related to intermediate-field processes are considerably larger. Modifications regarding the coupling position are applied to account for that discrepancy (described in the next chapter). Further limitation for the coupling time-step is either the temporal resolution of the measurements or the time-step chosen for the far-field model.

Regarding model execution, two approaches are possible:

A static (offline) linkage generates the output for one model for the entire time of interest. This output is then specified as boundary or source condition for the other model in a subsequent simulation. This is simple from the viewpoint of computation and data management, but obviously, there is a limited feedback between the two separate simulations. For example, the far-field model is run without any discharge information and saves all results in a database. Afterwards the near-field model is run choosing the appropriate data from the database. The amount of programming necessary is much less than for online coupling due to the clear separation of computations.

A dynamic (online or realtime) coupling the models exchange data after every time-step, thus, the zone models run in parallel. Obviously, the two models must have a great degree of compatibility for this linkage to work efficiently. On the other hand, a much higher degree of accuracy can be attained in this fashion. For example the far-field model is applied for time step 1 and results are handed over to the near-field model, which itself provides input for the next time-step for the far-field model. That kind of linkage generally requires a substantial amount of code modifications in both models. However, dynamic coupling is only necessary if flow quantities from either region are dynamically important. This is only the case for active coupling, but not for passive coupling approaches.

A static coupling approach was chosen for two reasons: i) Wastewater discharges do not demand for a dynamic coupling approach, if intermediate-field processes are modeled appropriately, and ii) Regulators, consultants and water companies generally use different models. Changes in such codes (regardless if commercial or open-source) are generally costly and time-consuming, whereas the application of an onset coupling approach between existing models provides a cheaper and easier solution.

5.4.2.3 Spatial aspects

Problem length scales generally vary considerably from time-step to time-step. Therefore, a criteria is needed to define the proper coupling locations. Fig. 81 schematizes the definition of source locations for two different time steps and illustrates the complexity of the problem.

The coupling locations depend on four criteria:

- i) the flow class
- ii) the coupling time step
- iii) the persistence of a flow class
- iv) either the results from the near-field model or the intermediate-field model

The flow class is defined by the previously described flow classification (flow with or without buoyant spreading). For flows, where buoyant spreading is not important, the coupling location can be defined at the end of the near-field. This location is given by the near-field model. However, theoretically cases exist, where these locations are far away from the source and a limiter is needed to account for unsteady effects. Thus in a second step the plume travel time until the end of the near-field, also given within a CORMIX calculation, is compared with the coupling time step to verify if the assumption of stepwise steady state near-field calculations holds for the considered condition. The persistence of a flow class is not important for cases without buoyant spreading. In a final step, the flow quantities (i.e. substance concentrations) from the near-field model are distributed over the related far-field grid cells, according to the calculated near-field plume geometries and distributions. However, a minimum far-field grid resolution is required in the coupling region to distribute near-field results onto the far-field grid. Therefore, the length scales ℓ_m and ℓ_M provide reasonable estimates (Akar and Jirka, 1991; Jirka and Akar, 1991). Obviously, in a tidal environment with variable u_a , ℓ_m can be highly variable. Typically, low velocity values, such as occurring near slack tide should be used for evaluation, resulting in sub-domain sizes of

$$Size_{NF} = (1 \text{ to } 3) \min(\ell_M, \ell_m, L_D) \quad (5.96)$$

measured in each direction from the centerpoint of the diffuser line (length L_D). The leading factor (1 to 3) expresses some uncertainty depending on local conditions and diffuser design and alignment. To resolve the plume at least 6-8 cells are required. This results in grid resolutions of the order of 50 m for a diffuser with $L_D = 400$ m.

For flow classes where buoyant spreading is important the coupling location is defined beyond the near-field region, at a distance proportional to ℓ_{bu}/L_D (equation (5.70)). However, travel times of plumes until reaching these locations can be considerably larger than typical time-steps specified. Therefore, the unsteady time scale $t_{bu}/\Delta t$ (equation (5.71)) is used as a measure for the flow class persistence. The longer the flow class for buoyant spreading motions prevails, the larger the coupling location can be located away from the source. For highly unsteady flows, however t_{bu} will be small and coupling locations near the near-field coupling locations.

Both measures have to be compared with measurements, to verify, if such parameterization is correct for that process. A case study in chapter 7 will discuss this issue in detail.

5.4.3 Coupling algorithm and program modules

The coupling algorithm is described for the programs CORMIX and Deflt3D. However, it can be used for other programs with similar capabilities, with generally slight modifications only. No modification of the programs is necessary. The algorithm uses the existing in- and output features, generally based on ASCII files.

The coupling classification, data averaging, interpolation and transformation, as well as the modifications regarding specific formats are coded within the commercial software MatLab[®] Release 14 from the company Mathworks[®]. The MatLab m-files are also ASCII files and may easily be recoded for other languages, if MatLab is not available. The m-files are open source. Once passing the beta-testing period the coupling-codes will be embedded into CORMIX.

The coupling modules are in order:

- CorField classifies time-series data from field measurements and converts those into CORMIX input files or Delft3D boundary condition files.
- CorLink classifies CORMIX output files and converts those into Delft3D source-files
- CorTime runs a time-series simulation with CORMIX. This new development for CORMIX has already been implemented and allows reading and run time-series files and summarizes the output.
- CorZone analyses results statistically to be included in regulatory permit procedures.

The coupling algorithm is generally run in the following sequence:

1. CorField: analysis and preparation of field measurements
2. CorTime: baseline near-field / intermediate-field modeling based on measured data
3. Delft3D-FLOW: ambient baseline hydrodynamic modeling using measured data as boundary conditions and to validate coastal hydrodynamics.
4. CorLink: Source representation in far-field model
5. Delft3D-WAQ: Coupled water quality modeling. Running Delft3D-WAQ including source terms generated by CorTime.
6. CorZone: summarize overall results within a statistical analysis based on regulatory parameters (described in chapter 6)

Details of each module are described as follows.

5.4.3.1 Analysis and classification of field measurements - CorField

Field data is essential for discharge modeling. Necessary datasets are bathymetrical information, current profiles, density profiles, wind velocities, water levels, drogue studies, or dye studies. The bathymetry data is the only steady information (assuming no significant morphological changes). All others are generally given as time-series at different locations (horizontally or vertically). CorField input data are ASCII files defining the horizontal and vertical position and time, magnitude, and direction. CorField classification is based on spatial and temporal classification routines summarized in coupling step 1 (Table 20).

Step 1: Classification of measured ambient conditions - CorField
<ul style="list-style-type: none"> - Classify measurements of density profiles according to CORMIX profile classes. - Classify velocity profiles in uniform / non-uniform, unidirectional / non-unidirectional - Statistical analysis of wind data and water level data - Compute classified time-series files according to CorTime input format for datasets measured near outfall location (and eventually also at alternative outfall locations) - Compute classified time-series files according to Delft3D boundary condition format for datasets nearest to open boundaries

Table 20: Coupling step 1: Classification of measured ambient conditions - CorField

Density profiles

CORMIX requires a schematization of the vertical density distribution. Measured profiles are hereby approximated by one of three schematic stratification profile types illustrated in Fig. 82. These are: Type A, linear density profile; Type B, two-layer system with constant densities and density jump; Type C, constant density surface layer with linear density profile in bottom layer separated by a density jump. An example for the approximation step is shown in Fig. 83. An advantage of that classification is the independency of the total water depth, thus predictions can be made for different total depths, and another advantage are reduced datasets. Difficulties during that classification step can be re-evaluated for these special cases using the CORMIX module CORJET, which applies for arbitrary (but stable) density and velocity profiles. A coarse schematization routine is included in CorField resulting in the characteristic parameters describing either of these profiles. These are surface and bottom density for type A, additionally the height h_{int} for type B, and additionally the density difference $\Delta\rho_a$ at the jump for type C.

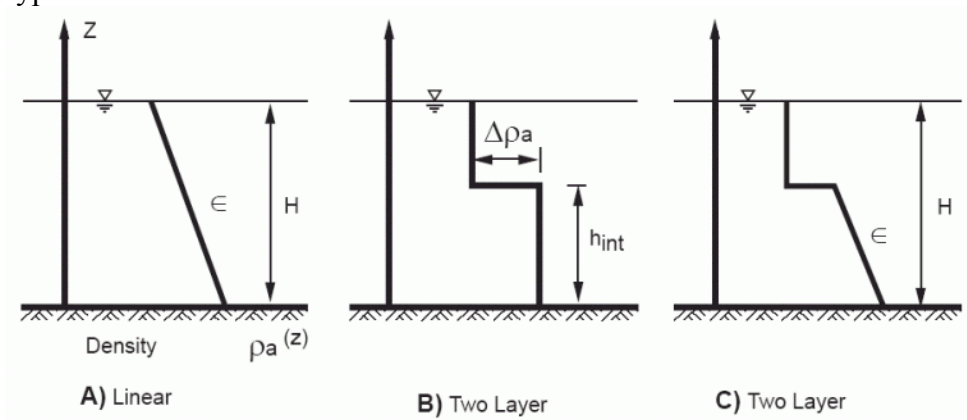


Fig. 82: CORMIX schematization for vertical density profiles. CORMIX distinguishes between a uniform density distribution, a linear distribution (A), a two layer density distribution with constant densities (B), and a two layer system with constant surface density and linear bottom layer density separated with a jump (C) (reproduced from Jirka et al., 1996)

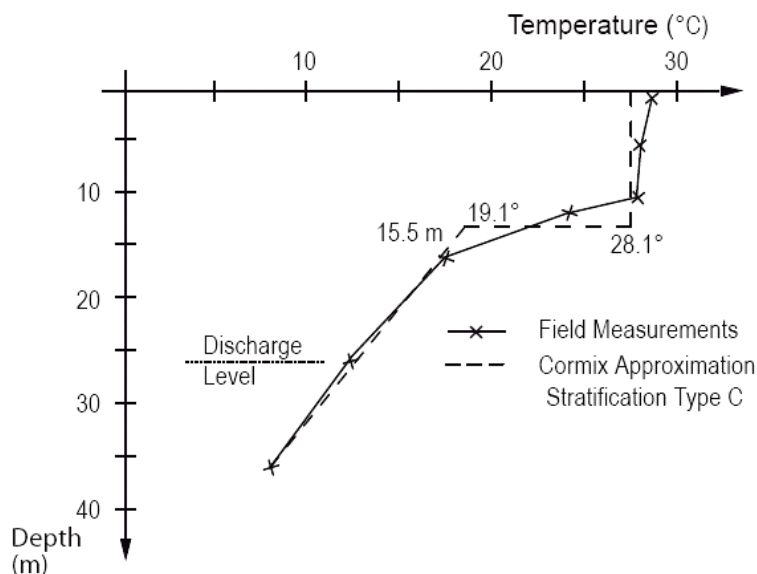


Fig. 83: Example for a CORMIX schematization applied on a measured vertical density profile (reproduced from Jirka et al., 1996)

Velocity profiles

CORMIX requires that the actual cross-section of the water body be described as a rectangular straight uniform channel that may be bounded laterally or unbounded (e.g. the nearest shoreline and an unbounded open sea, Fig. 84). CORMIX only requires the input of a depth averaged velocity u_a (however, universal velocity profiles are used within the CORMIX modules) and its orientation in relation to the diffuser orientation (angle γ).

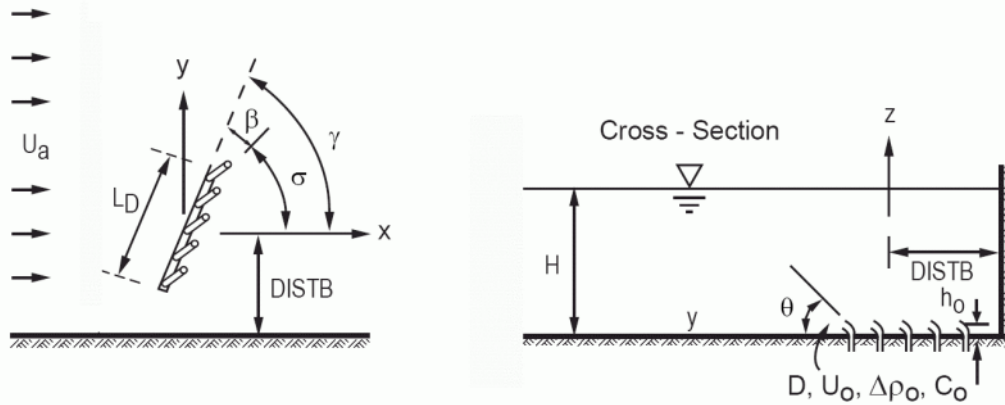


Fig. 84: CORMIX schematization for ambient velocity and diffuser orientation. CORMIX only requires the input of a vertically and horizontally uniform, depth averaged ambient velocity, and its direction related to the diffuser orientation (reproduced from Jirka et al., 1996)

CorField includes a routine to calculate CORMIX ambient velocities u_a and related angles γ . This routine furthermore reports whenever measured velocity profiles differ considerably from this rather strong approximation of ambient conditions. If such, sensitivity studies with the CORMIX post-processor CorJet allow distinguishing whether strongly non-uniform profiles cause considerable changes for the near-field mixing or not. However, comparisons of CorJet calculations for strongly non-uniform velocity profiles and depth-averaged calculations showed only little influence on mixing characteristics. Major influence is only related to the location of the plume trajectory. Regarding near-field lengths scales of the order of meters, however this does not have considerable effects on the overall analysis. For the far-field model, instead a proper representation of the velocity field is essential.

The spatial evolution of the velocity profiles can be analyzed if more than one location has been measured, by subsequent CorField classifications and comparison. CorField therefore includes statistical measures to calculate mean, deviation from mean, standard deviation, and histograms. The temporal evolution of each profile is included by computing statistical parameters of each time-series.

Wind velocities and water levels

Time-series of wind velocities and water levels are also analyzed within CorField, especially for statistical analysis. For example, it is interesting to define the duration of periods with strong onshore wind, which might cause the plume to reach the shore faster than without wind effects. A good knowledge of water level variations, i.e. tidal variations, is important as boundary condition for the far-field model.

Computation of coupling files

The classified and schematized datasets are automatically reformatted within CorField according to either a CorTime input format or a Delft3D boundary condition format. Both can readily be imported in these programs.

5.4.3.2 CORMIX time-series - CorTime

A first engineering design analysis is possible by applying CORMIX for the periods, where measured data is available and running CorTime to calculate plume properties for every given time-step. This near-field baseline modeling is summarized in step 2 (Table 21):

Step 2: Near-field baseline modeling - CorTime
<ul style="list-style-type: none">- Apply CorTime using the following input conditions: general outfall design parameters as discharge conditions and time-series computed in step 1 as ambient conditions- Analysis of CorTime results allows evaluating the mixing performance of the applied engineering diffuser design. Re-running CorTime with either modified design or at alternative locations allows to optimized design and siting regarding the near-field mixing performance.

Table 21: Coupling step 2: Near-field baseline modeling - CorTime

Discharge representation

CORMIX requires detailed input regarding the discharge configuration. For the multiport diffuser installations, it is hereby distinguished between three major diffuser types (Jirka, 1982; Jirka and Akar, 1991) as shown in Fig. 85. There is: the unidirectional diffuser (Fig. 85a), where all ports point in a mostly horizontal direction, more or less perpendicular to the diffuser line, thus $\beta = 90^\circ$, $\theta_o = 0^\circ$, the staged diffuser (Fig. 85b), where all ports point in a mostly horizontal direction, more or less parallel along the diffuser line, thus $\beta = 0^\circ$, $\theta_o = 0^\circ$, and the alternating diffuser (Fig. 85c), where all ports are arranged in an alternating or rosette-like direction relative to the diffuser line, thus $\beta = \pm 90^\circ$, $\theta_o = \text{undefined}$, including simply vertically upward. The overall diffuser configuration is complemented by definitions regarding port and riser configurations, giving diameters and number and orientation of openings.

All information regarding ambient conditions or related to ambient velocity orientations are given by the CorField computed input file, thus no further input is necessary for these parameters.

CorTime output and mixing performance evaluation

CORMIX output is manifold. CorTime automatically creates a CORMIX input file for every single time-step, runs the model, and saves the output reports. These reports contain information regarding plume trajectories and dilutions, as well as detailed information on boundary interactions, flow classes, and even design recommendations (Jirka et al., 1996). It is furthermore possible to visualize the result for every time step as shown in Fig. 86 - Fig. 88. Comparison of model runs for different designs and siting locations allows comparing the mixing performance of each alternative. CorTime may therefore be specified to produce additional output at a fixed distance downstream the diffuser. Comparing dilutions, plume geometries, and plume locations between the different alternatives opens a large field for optimization of either diffuser configurations or siting.

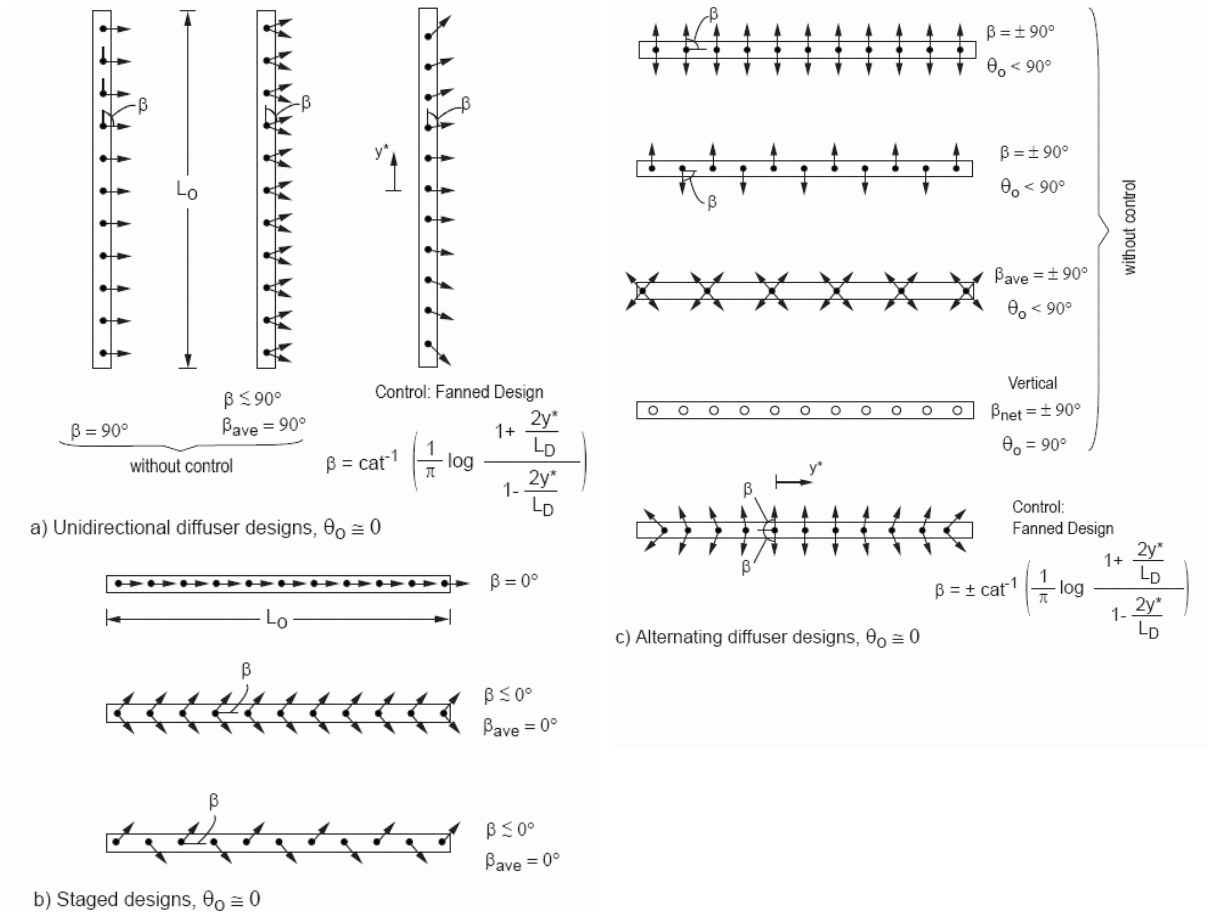


Fig. 85: CORMIX schematization of diffuser configurations (reproduced from Jirka et al., 1996)

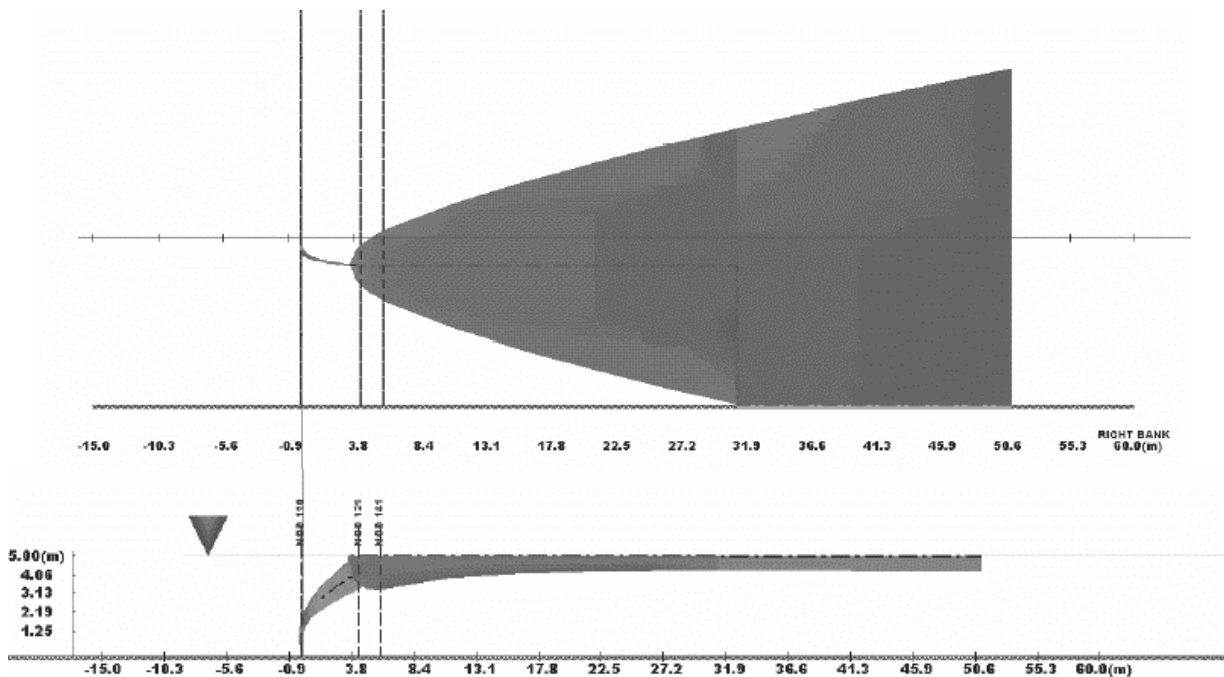


Fig. 86: Example for a 2D CORMIX visualization of a surfacing waste plume discharged from a single port (www.mixzon.com) and contacting the shore after a short distance.

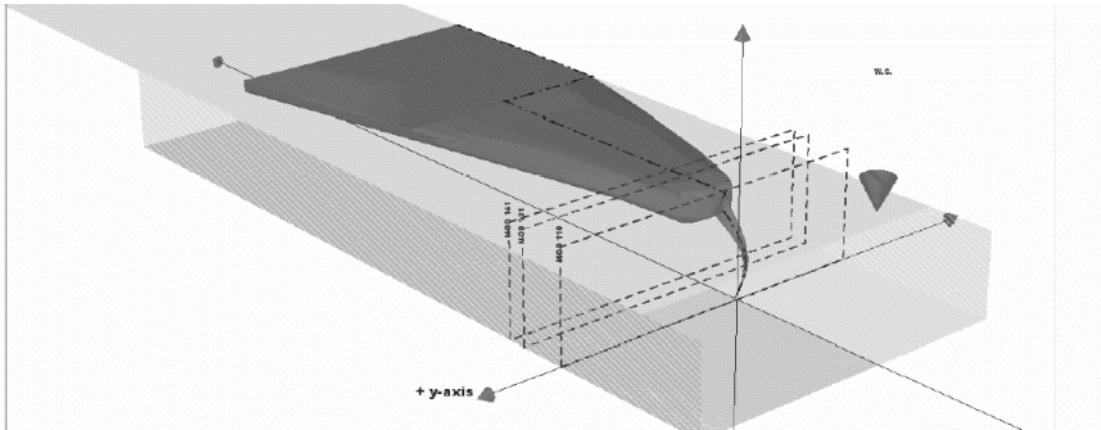


Fig. 87: Example for a 3D CORMIX visualization of a surfacing waste plume discharged from a single port (www.mixzon.com) and contacting the shore after a short distance. The changing flow characteristics after surface interaction can clearly be seen. Blue dashed lines indicate where CORMIX switches to another module to compute the related flow class.

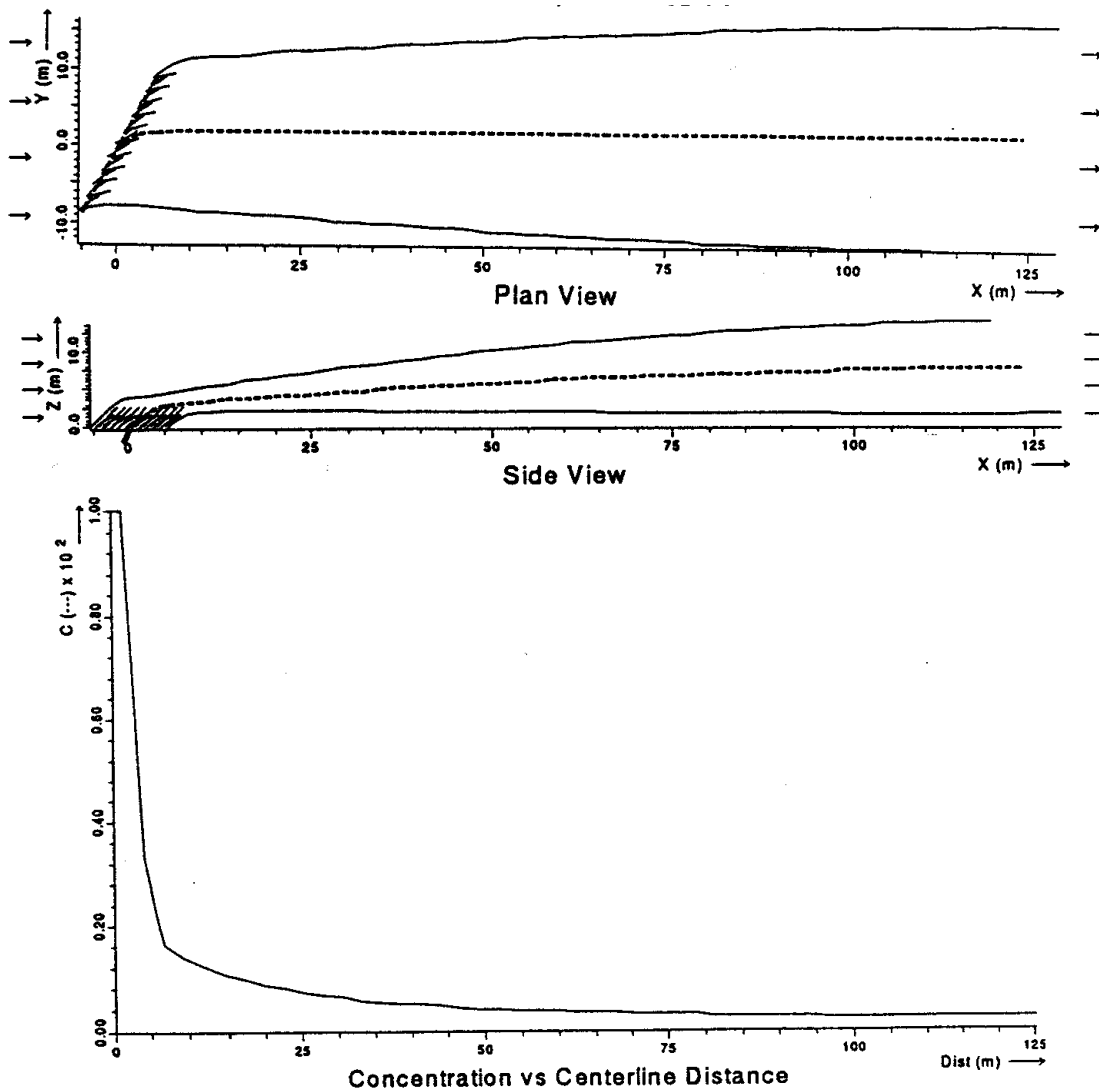


Fig. 88: Example of a CorJet prediction of a diffuser discharge into a stratified flowing environment with an oblique alignment angle ($\gamma = 45^\circ$) seen in the plan view, leading to an internally trapped plume, seen in the side view, resulting in a concentration profile along the plume centerline of an effluent concentration of 100%.

5.4.3.3 Ambient hydrodynamics baseline modeling with Delft3D flow

The base for any coastal water quality analysis is a good knowledge of the coastal hydrodynamics. Field measurements offer important high-resolution information at specific locations; however, spatial measurements are limited to very short time periods. Hydrodynamic modeling offers high-resolution information all over the considered project domain for large time-periods, thus offers a perfect complement for field measurements. Though simple interpolation techniques are helpful tools in the open ocean, complex 3D far-field models are needed for near-coast analysis. Delft3D requires geometrical information for the grid generation and boundary conditions to be specified at open boundaries. Required scales are summarized in step 3 (Table 22):

Step 3: Ambient hydrodynamics baseline modeling with Delft3D flow
<ul style="list-style-type: none"> - Generate far-field grid for project region with special focus on a proper resolution at the planned discharge region(s): a good estimate for a minimum grid size is $L_D/6$ within a region of minimal size = (1 to 3) min (ℓ_M, ℓ_m, L_D). The vertical resolution should consider at least 10 layers, with higher resolutions at the surface, around the pycnocline and the bed. - Define boundary conditions from measured data or large-scale model or both. - Simulate a sufficiently long and characteristic time period (e.g. typical time frame of 10 days up to one month, each for typical seasonal conditions) - Compare simulation results with available field data (e.g. current meter, or temperature time series, drogoue studies). This constitutes, in essence, a validation of the far-field zone modeling.

Table 22: Coupling step 3: Ambient hydrodynamics baseline modeling with Delft3D flow

5.4.3.4 Source representation in far-field model - CorLink

CorLink uses CorTime output in combination with CorField and Delft3D-FLOW results to distinguish between the necessary coupling approaches and to define the appropriate coupling locations. Further linkage with Delft3D is performed via source term definitions, summarized in step 4 (Table 23):

Step 4: Source representation in far-field model - CorLink
<ul style="list-style-type: none"> - Analyze and classify CorTime output in combination with CorField and Delft3D-FLOW results regarding the coupling properties. Passive coupling appropriate for $\ell_m/H < 1$; buoyant spreading important for $\ell_M/\ell_m < 1$, cut-off from buoyant spreading intermediate model result, when either $t_{bu}/\Delta t$ or $\ell_{bu}/L_D \gg 1$.) - Distribute plume properties for every time-step on the related far-field grid cells according the appropriate coupling location and plume characteristics. - Compute time-series source files according to Delft3D input format

Table 23: Coupling step 4: Source representation in far-field model - CorLink

CorTime output generally consists of locations of the plume centerline trajectory and associated dilutions values. The horizontal and vertical concentration distribution at one specific plume cross-section depends on the dominant processes. CORMIX includes four different concentration distributions, illustrated in Fig. 89. A distribution of these continuous distributions on a discrete grid however requires some simplifications. Generally it is not necessary

to represent concentration gradients inside the plume and the calculated centerline concentration be evenly distributed over the considered plume cross-section, as schematized in Fig. 90.

With the near-field computed plume dilutions $D = f(t)$ the far-field volume flux is:

$$Q_{FF} = Q_o D = f(t) \quad (5.97)$$

and the concentration

$$C_{FF} = C_o / D \quad (5.98)$$

The resulting mass flux is

$$Q_{cFF} = Q_{FF} C_{FF} \quad (5.99)$$

Having n grid cells for coupling locations each source term has a mass flux of Q_{cFF}/n .

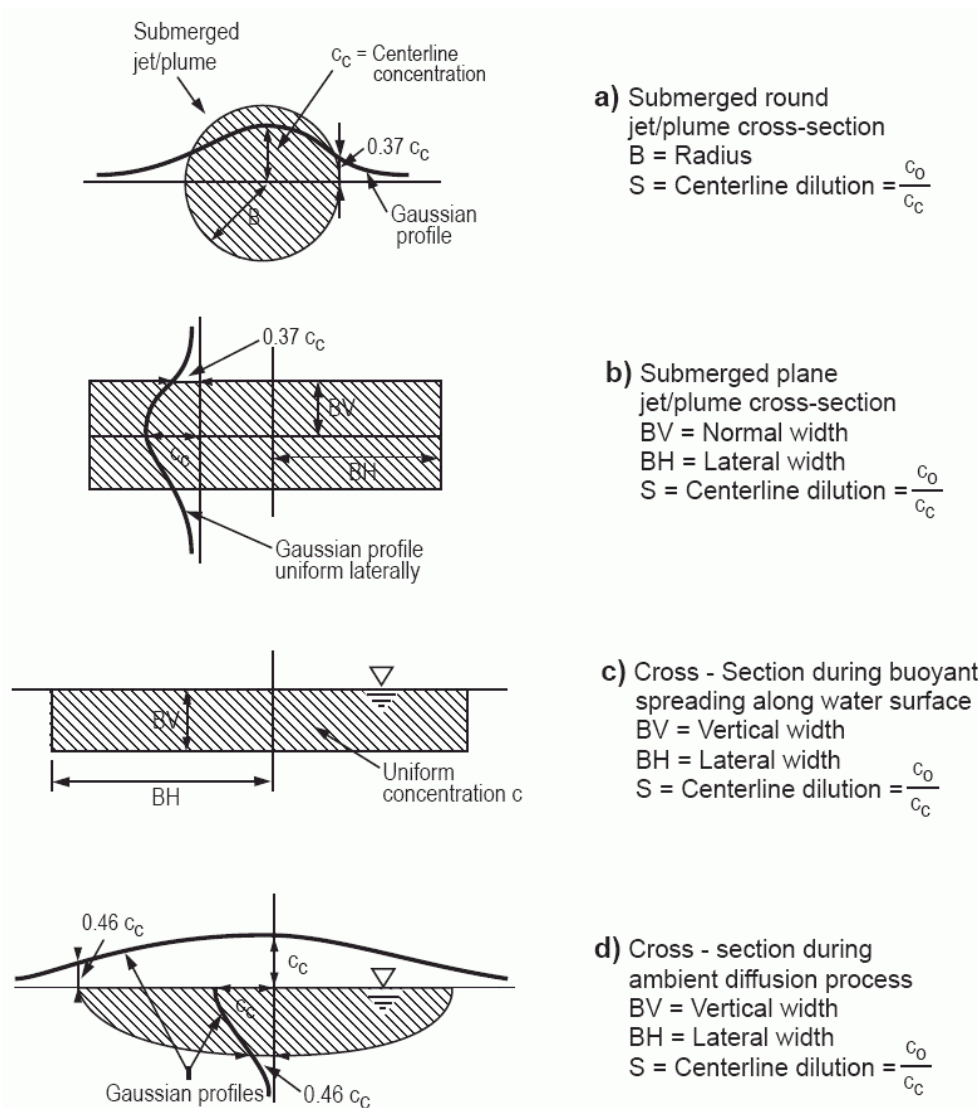


Fig. 89: CORMIX schematization for the horizontal and vertical concentration distributions at one specific plume cross-section, depending on the dominant processes (reproduced from Jirka et al., 1996)

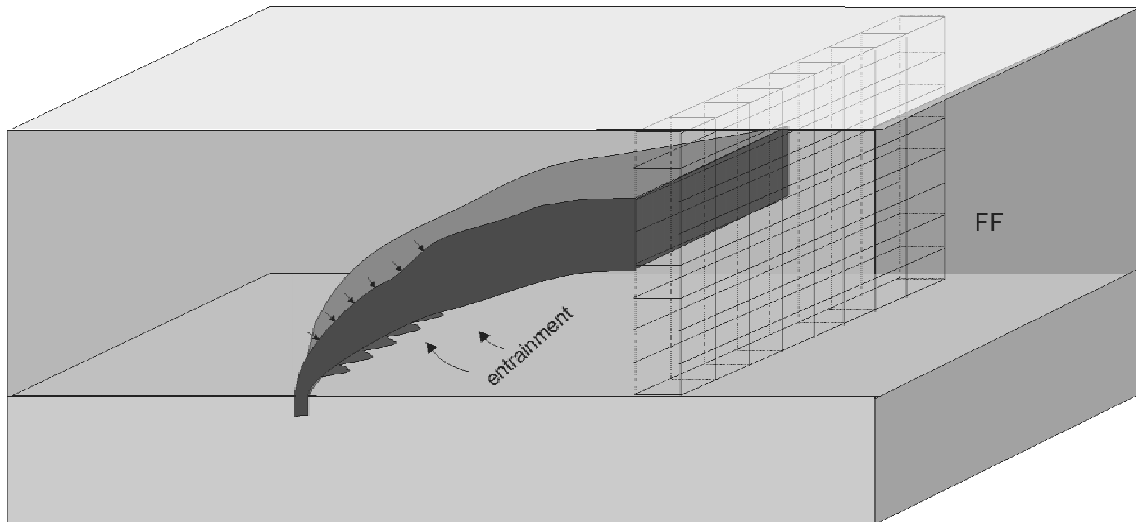


Fig. 90: Example of a CORMIX prediction of a diffuser discharge into a stratified flowing environment, leading to an internally trapped plume, seen in the side view. Superposed are far-field grid characteristics, where source characteristics may enter the far-field model.

5.4.3.5 Coupled far-field transport modeling with Delft3D WAQ

The source definitions from step 4 are then advected and dispersed according to the hydrodynamic velocity field and turbulence quantities using the water quality module Delft3D-WAQ. It includes substance transformation and decay as summarized in step 5 (Table 24):

Step 5: Far field transport modeling with Delft3D Part / WAQ (mixing, transport, decay)
<ul style="list-style-type: none"> - Include source files from step 4 into far-field model from step 3 - Simulate far-field waste transport and mixing for measured periods - Consider transformation and decay processes for the introduced substances. - Evaluate far-field mixing performance and repeat modeling for other alternatives. This includes other sites (e.g. longer and deeper outfalls) or treatment options.

Table 24: Coupling step 5: Far field modeling with Delft3D Part/WAQ (mixing, transport, decay)

Generally, field data is limited to specific climatic conditions and does not necessarily include all-important combinations regarding worst-case scenarios. Thus, the calibrated far-field model can be used with extended or modified boundary conditions (e.g. strong onshore winds and stratified conditions) and analyzed for that specific case. The far-field mixing performance may hereby be compared for different alternatives regarding siting alternatives or treatment options. CorField applied on hydrodynamic model results provides the necessary ambient conditions for CorTime applications.

One way to evaluate far-field performance is the comparison of concentrations at specific locations. Another way already includes information regarding the permitting procedure. The latter provides helpful information on compliance with water quality standards and is described in detail in the following chapter.

6 Regulatory discharge and preservation zone - CorZone

The mixing processes due to discharges into water bodies occur according to the previously described physical principles, and lead to a spatial and temporal configuration of the mass plume and the associated concentration distribution. Public health or environmental risks can be associated with these concentration distributions by comparison with concentration limits. Technological measures to reduce these risks by controlling concentration distributions (or water quality problems in general) have been discussed in chapter 2 and described in detail regarding the discharge technologies in chapter 5. However, problems remain unsolved regarding the decision on which risks to avoid or accept (definition of concentration limits) and which technological measures are advisable and appropriate. Technological approaches like the prediction of bacteria concentrations in receiving waters thus have to be embedded into a regulatory framework. Unfortunately existing regulatory control measures do not necessarily correspond to physical facts. Inconsistent, disproportionate, expensive, or even dangerous decisions regarding discharge permits/licenses on one hand, or beach closures on the other hand might be the consequence (Jirka et al., 2004). Water quality related regulations therefore need to harmonize and clarify measures to guarantee water quality objectives.

6.1 Water quality objectives

Water quality objectives are manifold. Historically they have been related to drinking water only, thus a pure user-oriented approach. Meanwhile environmental concerns extended water quality objectives also to surface and groundwater, which are not necessarily used for drinking water supply. Examples are bathing water or shellfish water regulations. But still most of these existing objectives are related to the water usage (i.e. recreation and fishing) and do only apply in designated regions for example defined as recreational or fishing waters. Nowadays it has furthermore been understood and agreed on, that at least basic water quality objectives have to account for all water bodies or even beyond, for the whole water environment including transitional regions thus closing the water cycle. Experience showed that improvements of water quality are generally driven by legislation. The continuous extension of legislative requirements increasingly involves engineers and scientist.

A prominent example for this new paradigm in water quality objectives is the new European Water Framework Directive (WFD, 2000) which has the objective of an integrated catchment-oriented water quality protection for all European waters with the purpose of attaining a good quality status by the year 2015. The water quality evaluation for surface waters should furthermore rely predominantly on biological (such as flora and fauna) and hydromorphological (such as flow and substrate conditions) parameters - however, aided by the traditional physico-chemical quality components (such as temperature, oxygen, or nutrient conditions) and specific pollutants (such as metals or synthetic organic compounds). A good chemical quality status is provided when the environmental quality standards are met for all pollutants.

In addition to the general protection of surface waters, a new regulation regarding especially bathing waters has been decided on recently (EC bathing water directive, 2006). EC member states shall ensure that, by the end of 2015, all European bathing waters are at least in a sufficient status.

Though other countries and regions recently defined similar objectives or are on the way to do so, the following discussion will be oriented on definitions regarding the European directive.

6.2 Regulatory water quality control measures

The WFD defines new strategies against water pollution because of releases from point or diffuse sources. A new aspect is the “combined approach”, i.e. both limitations on pollutant releases at the source due to promulgation of emission limit values as well as the establishment of environmental quality standards. Releases of pollutants – especially from point sources – must meet both requirements. For most European member countries (but also on the international level) this new policy means a considerable deviation from current water quality management practice by which the releases of pollutants have been controlled by either one of these two control mechanisms, but usually not their combination.

Ragas et al. (1997) have reviewed the advantages and disadvantages of different control mechanisms in the permitting processes of releases into surface water, summarized and illustrated in Fig. 91, Fig. 92:

Emission limit values (ELV), also called effluent standards, present a direct and effective method for the limitation of pollutant loadings by restricting the mass flux of specific pollutants. ELVs are preferred from an administrative perspective because they are easy to prescribe and to monitor (end-of-pipe sampling). From an ecological perspective, however, a quality control that is based on ELVs alone appears illogical and limited, since it does not consider directly the quality response of the water body itself and therefore does not hold the individual discharger responsible for the water body. To illustrate that point consider a large point source on a small water body or several sources that may all individually meet the ELVs but would accumulatively cause an excessive pollutant loading.

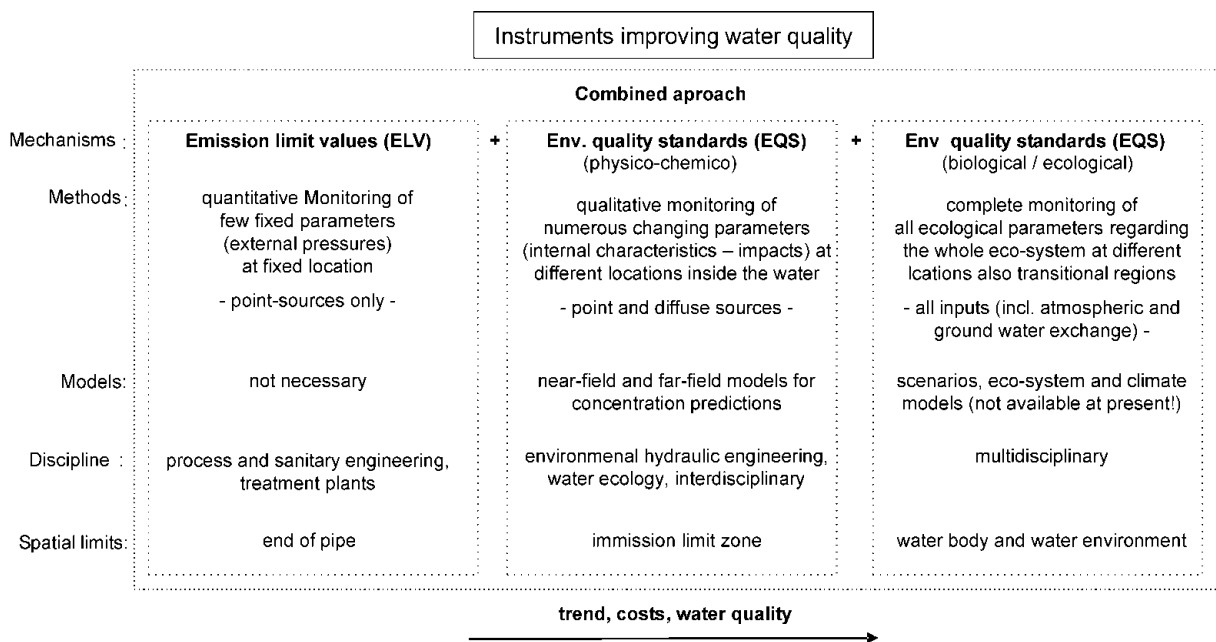


Fig. 91: Overview of instruments improving water quality

Environmental quality standards (EQS), also called ambient standards or immission limit values, set as concentration values for pollutions or pollutant groups, that may not be exceeded in the water body itself (WFD, 2000) They have the advantage that they consider directly the physical, chemical and biological response characteristics due to the discharge and therefore they put a direct responsibility on the discharger. However, a water quality practice that would be based solely on EQSs could lead to a situation in which a discharger would

fully utilize the assimilative capacity of water body up to the concentration values provided by the EQSs. Furthermore, the water quality authorities would be faced with additional burdens because of a more difficult monitoring – where in the water body and how often should be measured? – in the case of existing discharges or due to the increased need for a prediction modeling in case of new discharges. The “combined approach” combines the advantages of both of these quality water control mechanisms while largely avoiding their disadvantages.

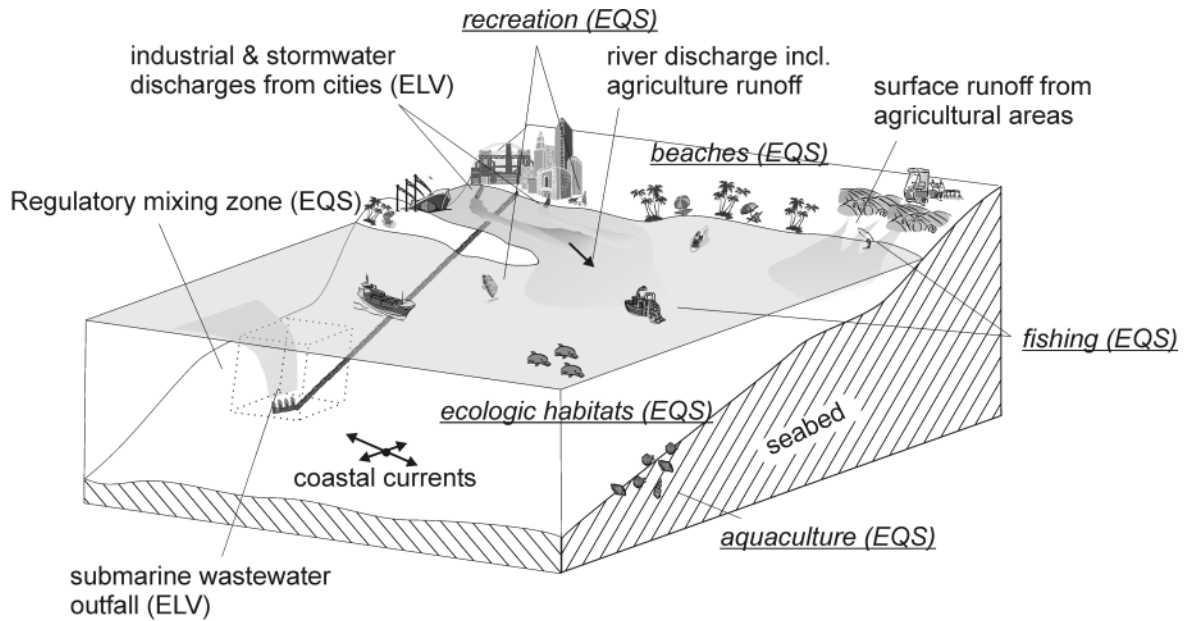


Fig. 92: Pollutant sources and water quality management in coastal waters: Compliance with emission limit values (ELV) for point-source discharges guarantees local protection at the outfall site, whereas compliance with environmental quality standards (EQS) outside a specified regulatory discharge zone (dashed line) guarantees water body usage and preservation (underlined items) partly based on ecological standards (ES).

The relevant values for ELV and EQS for various pollutants and pollutant groups can be found in different directives of the EU (see e.g. Appendix IX of the WFD, or UNEP Guidelines, 1996)) or of the national authorities. By way of example for further analysis, Table 25 contains the values for two chemical pollutants (cadmium and trichlorethane). The ratio ELV/EQS is 10 for trichlorethane and 500 for cadmium. The range of 5 to 1000 is typical for most chemical as well as physical parameters, such as heat (temperature). This ratio describes the impact of the pollutants on the ecosystem, since the ELV is considered to protect against acute (lethal) effects on organisms, while the EQS is supposed to prevent long-time chronic influences. The ratio also expresses the necessary dilution that must be attained through physical mixing or - to some extent - through biological decay and chemical transformation processes.

Pollutant	Emission limit values ELV	Env. quality standards EQS	$\frac{ELV}{EQS}$
Cadmium	0.5 mg/ℓ (83/513/EEC)	1 µg/ℓ (76/464/EEC)	500
Trichlorethane	0.1 mg/ℓ (AbwV, Germany, 2000)	10 µg/ℓ (76/464/EEC)	10

Table 25: Examples for emission limit values (ELV) and environmental quality standards (EQS) for two selected pollutants

There can be other ways of prescribing ELV-values, namely through the specification of a “best available technology (BAT)”. For example, for sea outfalls this may be described as some form of treatment, at least preliminary (e.g. UNEP Guidelines, 1996), or chemically enhanced primary. The requirement may be set by national authorities depending on type of coastal water body and its use (fisheries or recreation) or on sensitive ecological zones. In general, such BAT requirements assure a certain degree of substance removal.

For other parameters, such as indicator bacteria or viruses ELV-values do not even exist, though EQS-values are specified (e.g. for total coliform bacteria given to 500 counts / 100 ml in the EC Bathing Water Directive). Typical total coliform concentrations in raw sewage are 10^6 to 10^8 counts / 100 ml. Concentration reductions are achieved by treating the effluent (e.g. reduction by a factor 100 to 1000 during secondary and by 1000 to 10,000 during tertiary treatment (Larsen, 2000)), and dilution and decay in the natural environment. The latter contribution still needs to be of the order of 2 - 200 assuming an average factor of 1000 for the treatment. This compares with the “traditional” minimum dilution requirements of about 50 to 100 (Lee, 2003) that has been used for many years for outfall design in the coastal waters of several European countries (Larsen, 2000).

Measures, concentration values, and removal degrees are useful to reduce and control water pollution, but the practical implementation does not correspond to physical facts. In particular, one question of central importance to the practice of water authorities has to be concerned: Where in the water body relative to the discharge point do the EQS-values apply?

The “end-of-pipe” specification for the ELV is clear and unequivocal in Art. 2 (40) of the WFD: *“The emission limit values for substances should normally apply at the point where the emissions leave the installation, dilution being disregarded when determining them”*. Surprisingly, and quite illogical from the viewpoint of the physical features of the mixing processes, the WFD does not provide any information on the spatial application of the EQS-values. It also does not oblige the national authorities to establish such specification. Therefore, it must be expected that considerable uncertainties and highly variable interpretations or monitoring methods will occur in the practice of water authorities, both as regards the continuing approval of existing discharges as well as the permitting of new ones. The “combined approach” that appears sensible for an integrated ecological water pollution control is in danger of being by-passed or undermined in its practical implementation.

From discussions with personnel from regional water authorities, two extreme interpretations are known regarding this omission in the WFD (Jirka et al., 2004), as illustrated in Fig. 93:

- i) The EQS-value should be applied “as near as possible” to the discharge point in order to obtain a good chemical status in an area as large as possible. This highly restrictive interpretation negates the fact that the physical mixing process cannot be reduced to extremely small areas (in the limit this approaches an “end-of-pipe” demand EQS synonymous with the ELV-values!), but requires a certain space – in particular for imposed high ELV/EQS ratios. Actual legislation somehow undermines the balanced objectives of the “combined approach” by requiring at least secondary treatment for all coastal discharges, unless environmental impact studies show, that lesser treatment has “no deteriorating effect” on water quality. There is again no statement regarding the definition of deteriorating effects (EQS-values?) or the location where these concentrations apply.
- ii) The EQS-value is supposed to apply “after the completion of initial mixing” (California Ocean Plan, 1988, currently under revision) or “at the beach” or “at the water surface”.

This interpretation negates the unsteady and non-uniform behavior of waste plumes and ambient conditions (Fig. 93) thus the continuously changing region of initial mixing. From the viewpoint of any monitoring program (either with fixed sensors or with prescribed boat traverses), this specification becomes very difficult to verify. In addition, such qualitative statements make them either unenforceable or overly generous. Since the actual physical mixing processes take place gradually leading to a “discharge plume”, considerable areas in the water body would be affected by concentrations above the EQS-values and would have to be considered as “sacrificial regions”, in which a good chemical status would no longer be provided.

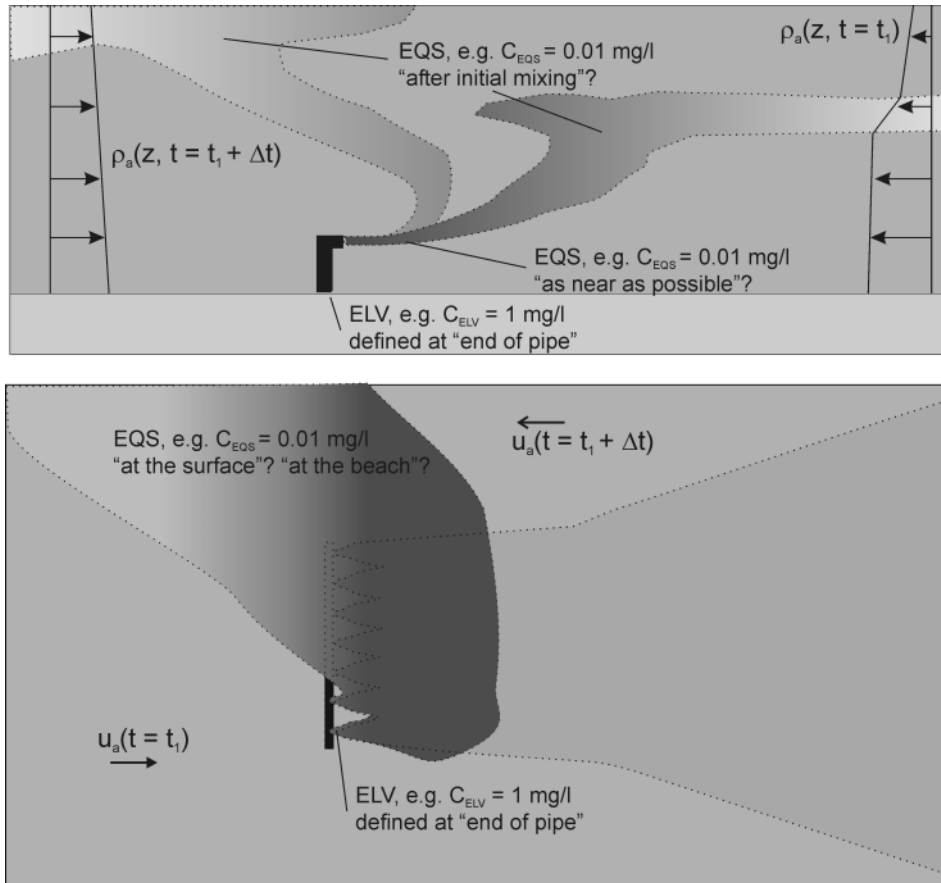


Fig. 93: Illustration of interpretations regarding the location where EQS-values apply

Considering these two extreme interpretations it is obvious that a compromise, in the form of a numeric definition of spatial dimensions appears greatly preferable for permitting and monitoring from both vantage points, that of the discharger and of the authority. This dilemma is not only a European legislation one. Several countries with such new regulations seem to have similar deficiencies in their regulatory formulations (Bleninger et al., 2004), e.g. the Brazilian water quality regulations (CONAMA 20, 2000) or the German water laws (LAWA-Arbeitshilfen, Annex 3, 2002), where guidance documents for the implementation of the WFD suggest: “For the estimation whether a pressure on a water body is significant, the pressure has to be set in relation to the water body (that means, a discharge of equal size is more significant for a small water body than for a large one”. On the other hand countries with a relatively long tradition on immission based water quality regulations already have clear formulations regarding the location where EQS-values apply (e.g. UK: SEPA, 1998, USA: EPA 1994). These regulations serve as base for the development of the following concept.

6.3 Regulatory discharge and preservation zone concept

When performing design work and predictive studies on effluent discharge problems, it is important to distinguish between the physical aspects of hydrodynamic mixing processes that determine the fate and distribution of the effluent from the discharge location, and the administrative formulation of discharge or preservation zone regulations that intend to prevent any harmful impact of the effluent on the aquatic environment and associated uses. These regulatory zones are twofold. Spatial limits exist either for a water body protection, so-called mixing zone regulations or for a water usage preservation (e.g. bathing water regulations).

For example, US regulations define a “Regulatory Mixing Zone (RMZ)”, which is sometimes also referred to as the legal mixing zone. This definition has been established in the scientific literature and even influenced the naming of regulations outside the US. However, substantial misunderstandings have occurred confusing the Regulatory mixing zone with the “near-field mixing zone” or the “initial mixing zone” or the “zone of initial dilution” (Jirka et al., 1996, Bleninger et al., 2004). For that reason and regarding the previously described deficiencies in new regulations, it is proposed to modify the naming to “Regulatory discharge zone” or legal discharge zone. This naming clearly defines a region to be influenced by a discharge without necessarily saying how this influence acts or which processes do occur. In addition, even translations in other languages clearly provide distinguishing between a mixing region and the (Regulatory) discharge region.

On the other hand, numerous regulations exist related to specific water body uses. There is for example the European bathing water directive, or the shellfish directive. To summarize these, the naming of a “Regulatory preservation zone” or legal preservation zone is proposed.

The definition and specification of both is shown in the following sections.

6.3.1 Regulatory discharge zone specification

Jirka et al. (2004) already proposed a future amendment of the EC-WFD and national regulations for its implementation, respectively, containing the following wording: *“The environmental quality standards apply in the case of point sources outside and at the edge of the discharge zone. The discharge zone is a spatially restricted region around the point source whose dimensions should be specified either according to water body type and use or on an ad-hoc basis.”* The discharge zone defined in the above statement is a regulatory formulation with the following general attributes: 1) the term “discharge zone” signifies explicitly that discharges in its related processes require a certain space. 2) The term “spatially restricted” should guarantee that the discharge zone should be minimized by the regulatory authority for attaining the environmental quality goals. 3) While the discharge zone includes a portion of the actual physical mixing processes, these processes will continue beyond the discharge zone where they lead to further concentration drop-offs in the pollutant plume below the EQS-values. 4) The definition is restricted to “point sources” since diffuse sources usually do not contain clearly distinct mixing processes.

In comparison the regulations used by the U.S. Environmental Protection Agency state in its Water Quality Handbook *“... the concept of a mixing zone as a limited area or volume of water where initial dilution of a discharge takes place”* (USEPA, 1994).

The specification of numeric Regulatory discharge zone dimensions however should correspond to hydrodynamic characteristics of outfalls. For coastal discharges with submerged

offshore outfalls, it seems advisable to constrain the Regulatory discharge zone to a limited region around the outfall in which the initial buoyant jet mixing is dominant. In that fashion the EQS-values can be achieved within short distances. Thus, the following specification appears effective: *“The mixing zone is a volume with vertical boundaries in the coastal water body that is limited in its horizontal extent to a distance equal to N multiples of the average water depth H_{ave} at the outfall location and measured in any direction from the outfall structure.”* For a multiport diffuser outfall with many ports arranged along a straight diffuser line it would be a rectangular prismatic volume with attached semicircular cylinders at the diffuser ends located along the diffuser line (Fig. 94). For diffusers with a curved diffuser line or piecewise linear sections the volume would follow the diffuser line. The value N would typically be in the range of at least 1 to about 10 and set by the regulatory authority according to local water use and ecological sensitivity. For highly sensitive waters, the minimum of 1 should be set. Common values for most coastal waters might be $N = 2$ to 3.

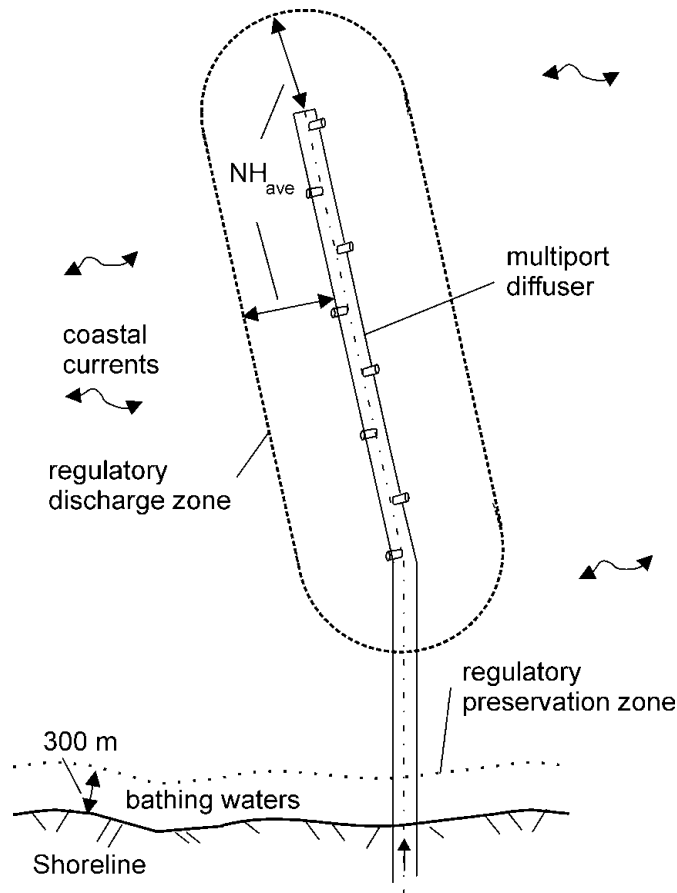


Fig. 94: Definition of a numeric dimension for the regulatory discharge zone in relation to the average water depth H_{ave} and a factor N , and the regulatory preservation zone as a fixed distance from the preserved area (here the beaches).

In addition, Regulatory discharge zone dimensions might be defined in an ad-hoc manner. After prior ecological evaluations or predictions, the discharger can request the authority for a Regulatory discharge zone with a certain dimension with the claim that this would guarantee an integrated water quality protection. Based on its own examinations the authority can agree with that proposal or else demand further restrictions.

6.3.2 Regulatory preservation zone specification

A similar specification is needed for regions of water bodies with special preservation attributes (e.g. bathing waters, natural reserves, protected areas, etc.), where stronger and additional EQS-values apply.

For example UNEP Guidelines (1996) proposed for the Mediterranean sea that the discharge of municipal wastewater into the sea should always take into account the openness of the affected area and the reservation of a 300 m wide band, parallel to the beach line of the coast or the affected area, where no discharges should be made whatsoever the treatment applied to the effluent or the dilution obtained with the outfall.

The proposed wording for a future amendment of regulations is: *“The environmental quality standards for specific water uses and preserved areas apply inside and at the edge of the preservation zone. The preservation zone is a spatially restricted region whose dimensions should be specified according to water body type and use. In the case of point source discharges, no discharge, whatsoever treatment, is allowed inside a preservation zone.”* The preservation zone defined in the above statement is a regulatory formulation with the following general attributes: 1) the term “preservation zone” signifies explicitly that preservation cannot be guaranteed everywhere. 2) The term “spatially restricted” should guarantee that the preservation zone should be optimized by the regulatory authority for attaining the environmental and public health objectives. 3) The additional restriction regarding “point sources” corresponds to the limited scales of mixing process especially in sensitive and physically weak environments.

The specification of numeric Regulatory preservation zone dimensions however should correspond to hydrodynamic characteristics of coastal waters. Thus, the following specification appears effective: *“The preservation zone is a volume with vertical boundaries in the coastal water body that is limited in its horizontal extent to a distance equal to 300 m measured in any direction from the preservation area.”* For a bathing water zone, a 300 m wide band parallel to the beach would result (Fig. 94).

In addition, a black list of improper discharge solutions improves the awareness of discharge technologies. Any discharge should avoid bottom interaction (benthic impacts), or shore hugging, and even small discharges should not be sited in sensitive waters or water bodies with low flushing characteristics (e.g. between groyne).

6.4 Discharge licensing procedure

There are approximately 50,000 discharge permits with 5 years duration in the USA (www.mixzon.com). This is a number of 10,000 permits per year and this is probably similar in other countries. An optimization of the discharge licensing procedure will not only improve the licensing administration, but also water quality.

In addition to the definition of concentration limits (ELVs and EQSs), regulatory discharge, and preservation zone dimensions, it is furthermore important to define relevant time scales. Concentrations in the far-field vary over large distances from near background to near plume maximum centerline concentration. Lee and Neville-Jones (1987) measured dilutions in the near field of effluent plumes from a number of British outfalls and found that with supposedly constant discharge and current speed the standard deviation of the dilution measured at the surface was 40% of the average dilution. High variability is therefore to be expected. A

quantification of environmental impacts and public health risks is still discussed controversial. Three approaches are usually applicable: the worst case, the mean, and the statistical approach. Worst-case scenarios consider a parameter combination leading to a maximum possible concentration at the edge of regulatory zones. Result is a single maximum concentration at the edge of the regulatory zone, which occurrence probability (i.e. the probability of standard violation) is usually unknown. Worst-case predictions are simple but eventually more stringent than necessary. The other extreme would be a long-term average (yearly average). However, there is typically a strong intermittency of standard violations at the edge of the regulatory zones, which cannot be resolved with long term averaging. Unfortunately, standard violations for example for bacteria are most common during the high season, thus causing higher risks, because of high loads and weak ambient conditions. Shorter averaging periods (monthly averages or periods of the order of sampling periods) showed to be more efficient for decreasing public health risks. The probabilistic approach describes time-series or probability distributions. Results are exceedance probability of concentrations at the end of the regulatory zones. The concept of 'visitation frequency' has been suggested and applied to estimate the probability of the wastefield reaching a particular coastal location (Csanady & Churchill, 1987; Roberts, 1999). The exceedance probability is defined as:

$$EP(C_a) = \text{accumulated time for } C > C_a / \text{total time of observed period} \quad (6.1)$$

where C = measured or computed concentration C_a = ambient concentration limit

Once standards, zone dimensions, and times are defined, the previously described coupling approach can be used to design and optimize the discharge installation and the related treatment option. Minimum dilutions necessary to comply with the given standards can be calculated out of the regulatory definitions.

- Regulatory discharge zone (CorZone) -

7 Case study - Cartagena outfall

7.1 Background and problem

The Colombian Caribbean Coast includes complex and dynamic ecosystems whose main biological environments are estuaries, bays, coastal lagoons, coral reefs and mangrove ecosystems. The region is home to many different activities from manufacturing industries, located mainly in Cartagena and Barranquilla, an oil terminal and refinery, international maritime and trade terminals, the Cerrejón mining area, the tourism industry, the agrochemical industry, small-scale and industrial fishing, and agriculture, among others (Roberts and Villegas, 2006). However, environmental degradation and severe public health problems exist due to the lack of planning policy for social welfare, including urbanization issues. Coastal rivers, beaches, bays, and estuaries have been suffering the effects of pollution caused by uncontrolled waste discharges even though the adjacent ocean environment has a high capacity for dilution and dispersion of waste effluents.

Cartagena, is situated at the south coast of the Caribbean Sea (Fig. 95 and Fig. 96). It has a population of about 1 million people, 750,000 of who are classified in the 1, 2, or 3 poverty classes (Hazen and Sawyer, 1998). The cities economy is strongly dependent on tourism industry, which generates an estimated US\$315 million in annual revenue (Libhaber and Roberts, 2002). Aerial views of the city are shown in Fig. 97.

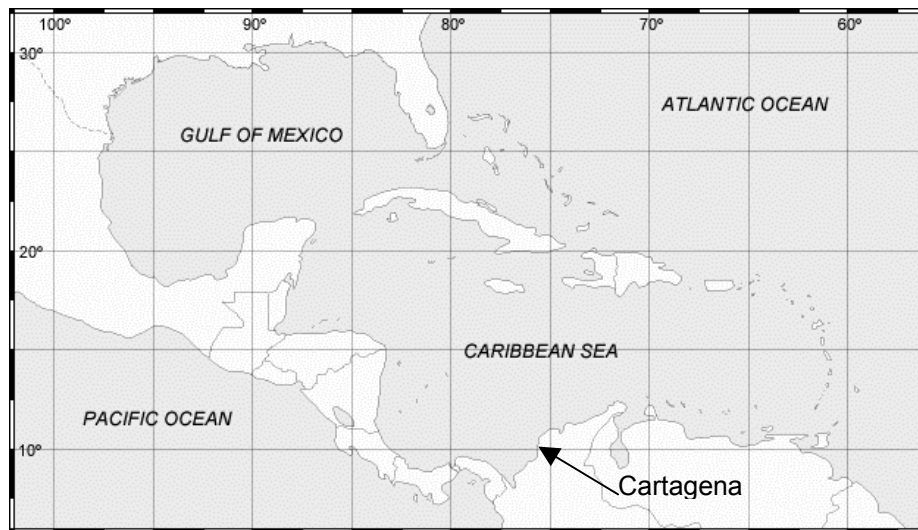


Fig. 95: General map of studied area

The population connected to a sewer system is approximately 60% (Hazen and Sawyer, 1998). The resulting effluent is either preliminary treated or directly discharged into near coast enclosed regions (Fig. 98). Consequences are high bacterial pollution at open sewers and near shore waters, resulting in severe environmental and public health impacts. The water sector reform with private sector participation and World Bank financing resulted in a wastewater master plan (US\$240 million; Libhaber and Roberts, 2002). The project objectives are: Improvements of the sewer system network (almost finished), having a total length of 80 km and 400,000 beneficiaries; upgrading the wastewater treatment to primary treatment; and installation of a long sea-outfall (Fig. 96, ca. 25 million US \$). The outfall has a total

length of about 2.85 km and terminates in 540 m long multiport diffuser that discharges primary treated wastewater at a depth of about 20 m.



Fig. 96: Proposed outfall for Cartagena City, Colombia (Roberts, 2005)



Fig. 97: Aerial views of Cartagena city. Left: prestigious beaches. Right: low-income neighborhoods (courtesy of M. Libhaber, World Bank)

Previous discharge assessments using intensive model applications by Roberts (2003, 2004, 2005) and Roberts and Carvalho (2000) concluded that the planned outfall design complies with the Regulatory discharge zone requirements by achieving high initial (near field) dilutions ranging from 100 to almost 1000 with a median value of about 230 in short distances (approximately of the order of the diffuser length) from the diffuser location. They also concluded that compliance with the rather strict California bathing water standards and WHO standards for bacteria would be met at the shoreline by a wide margin.



Fig. 98: Existing wastewater / drainage situation, where raw sewage flows in open canals or sewers to either the Bahía de Cartagena (40%) or the Ciénaga de Tesca (60%) causing considerable environmental and public health impacts (courtesy of M. Libhaber, World Bank)

However, an inspection panel has reviewed the outfall design project (Inspection Panel, 2005) and raised concerns about the outfall design with respect to three main issues:

1. *The integrity of the database:* Both, the near-field and the far-field model from Roberts (2004) are based on the velocity and density measurements only at the outfall location. Although high-resolution data (in time and space, i.e. the depth) has been measured, it has been suspected by the Inspection Panel (2005) that those velocities and densities especially in the surface layer are not resolved adequately.
2. *The accuracy of the near-field modeling approach:* The Inspection panel (2005) raised concerns with respect to the underestimation of buoyant spreading processes. It was suspected, that during low current periods (thus low dilutions) the plume still surfaces and might extend kilometers due to density spreading processes in the surface layer. Additional onshore wind might then cause increased bacteria concentrations at the shoreline.
3. *The accuracy of the far-field modeling approach:* The Inspection panel (2005) raised concerns with respect to the focus on a single point as base for the transport predictions. Although this approach is considerably conservative due to the over representation of on-shore currents at near-shore locations and other effects (Stolzenbach, 2005), the Inspection panel (2005) suspects that worst case scenarios would cause considerable changes for these predictions.

A first approach to challenge concerns raised from a basic sensitivity analysis on the involved processes (Roberts, 2005 and Annex A, Inspection panel, 2005) did not find full agreement. The inspection panel (2005) therefore asked for a 3-D model study.

7.1.1 Caribbean circulation

The inspection panel (2005) suggested applying a large-scale model (ELCOM) for the southern Caribbean Sea for the above-mentioned considerations. This model application is summarized in Roberts and Villegas (2006), however they conclude, that it is not accurate enough for waste discharge analysis of the Cartagena outfall. Nevertheless, model results serve as important information regarding the boundary conditions for the smaller scale coupled modeling approach presented. Therefore, a very brief summary is given on the large-scale circulation modeling.

ELCOM (Estuary and Lake Computer Model, CWR, 2002) is a three-dimensional numerical modeling tool for lakes and estuaries developed by the Centre for Water Research (CWR) of the University of Western Australia. ELCOM capabilities are based on the hydrostatic assumption, baroclinic forcing, semi-implicit finite differences method developed by Casulli and Cheng (1992), three-dimensional mixing layer approximations derived from a mixing energy budget developed for one-dimensional lake simulation (Imberger and Patterson, 1981), on a structured, rectangular grid. The model domain extended for approximately 1400 x 450 km. Within this domain, a horizontal plaid grid with variable cell sizes was defined, as shown in Fig. 99. The cell sizes range from a minimum of 500 m near the outfall to a maximum of 80 km at the western boundary. There are 17 vertical layers of differing thickness.

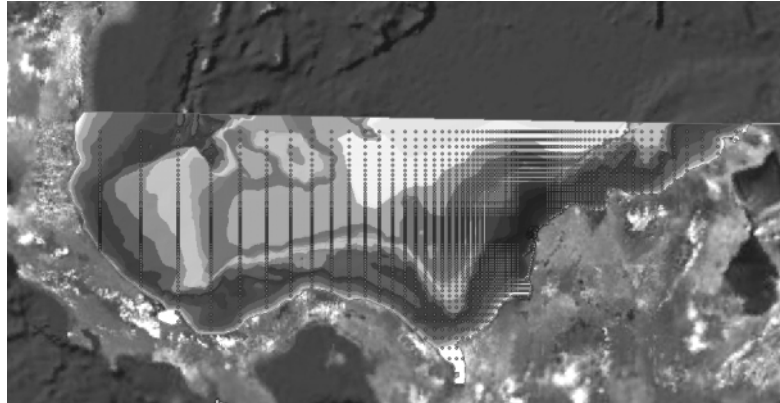


Fig. 99: ELCOM grid nodes in the numerical domain (Roberts and Villegas, 2006)

Major modeled oceanographical circulation features have been compared with literature sources and on-site measurements at the proposed outfall region. Conclusions from Roberts and Villegas (2006) are briefly summarized in the following sections.

7.1.1.1 Panama Colombian Gyre

The Panama Colombian gyre (Fig. 100) is known from previous investigations. This counter current varies significantly with the seasons. The ELCOM model represents the gyre (Fig. 101), however ELCOM predicts a gyre that does not always occur compared with measurements, and the observed current reversals are not predicted.

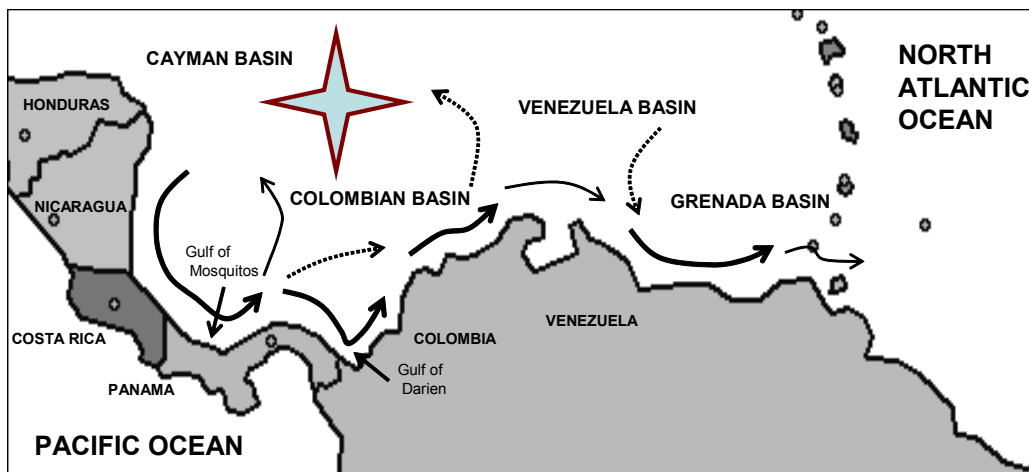


Fig. 100: Schematic representation of the Southern Caribbean Coastal Undercurrent, including the Panama - Colombian gyre (reproduced from Andrade et al., 2003)

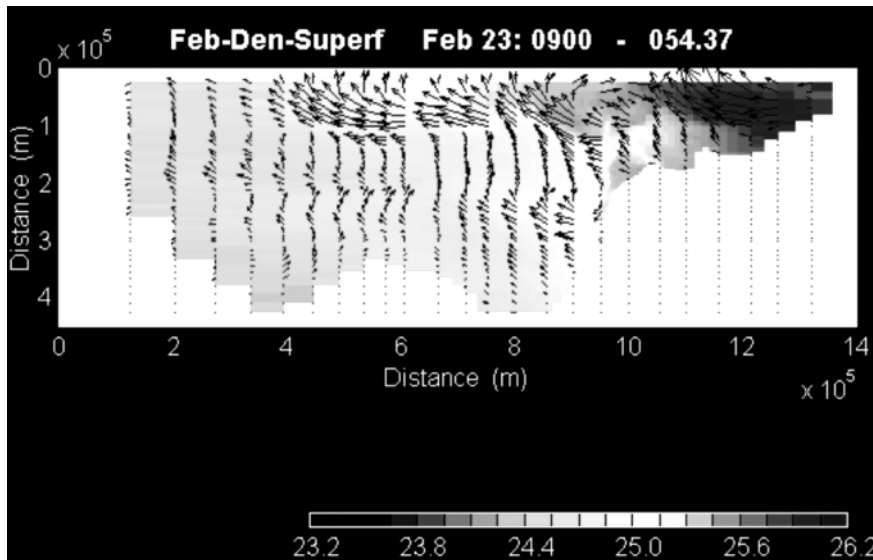


Fig. 101: ELCOM prediction for the Panama-Colombian gyre. Rotating directions are not consistent with measurements or literature for half of the observed scenarios (Roberts and Villegas, 2006)

7.1.1.2 Magdalena river plume

The Magdalena River (average discharge of 7100 m³/s) discharges approximately 100 km north of Cartagena into the Caribbean. Its river plume extends over considerable distances and occasionally reaches Cartagena waters (Fig. 102). Besides, it is known that this river carries high levels of contaminants, however, the manner in which these substances influence the biological and chemical process of the region are unknown. The ELCOM model reasonably reproduced the river plume. Though it does not predict absolute characteristics, related to the previous mentioned problem with gyre and current directions, it is most useful in predicting relative influences of the river plume on the project region. Two calculations have been performed either including, or excluding the river discharge in the model. Roberts and Villegas (2006) show (Fig. 103, Fig. 104) that the effects of the river plume on the project region's density and velocity field is negligible.



Fig. 102: Large scale satellite picture of project region, showing the influence of the Magdalena river plume on the coast around Cartagena (courtesy of M. Libhaber, World Bank)

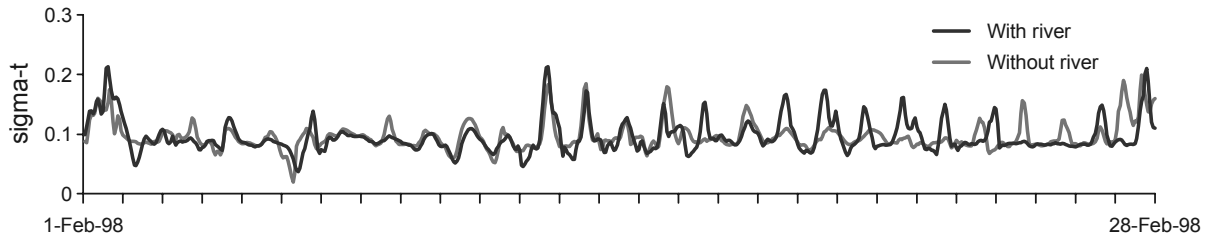


Fig. 103: Comparison of modeled density differences over the vertical at the proposed outfall location for two different boundary conditions related to the inclusion or exclusion of the buoyant river discharge (Roberts and Villegas, 2006)

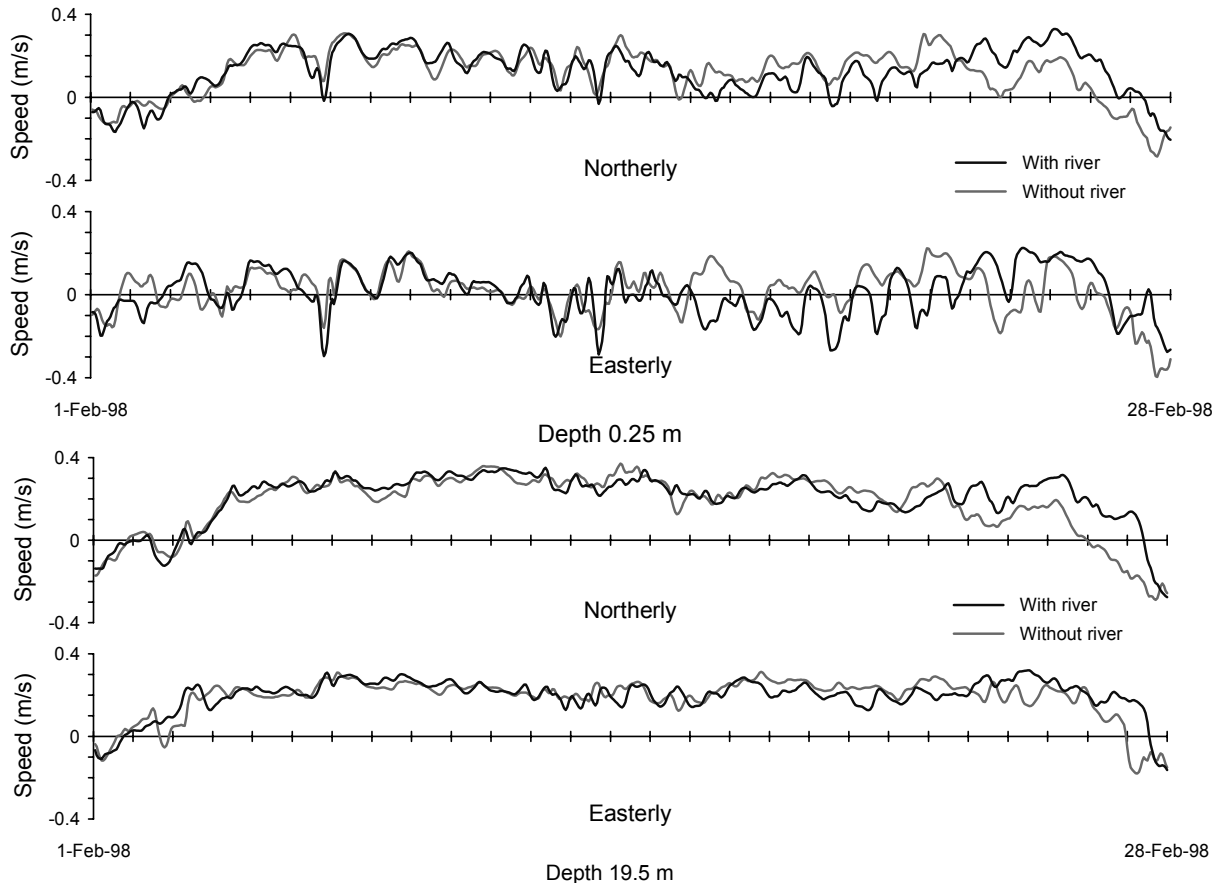


Fig. 104: Comparison of modeled current velocities at two different depths at the proposed outfall location for two different boundary conditions related to the inclusion or exclusion of the buoyant river discharge (Roberts and Villegas, 2006).

7.1.1.3 Flow characteristics in the project region

Field data at the proposed outfall location have been compared with ELCOM model results. Though magnitudes are of the same order, measured currents are much more variable and often in opposite directions (Fig. 105). Furthermore polar scatter plots showed a more dispersed distribution regarding the principal directions (Fig. 106). Thus, Roberts and Villegas (2006) concluded that the discrepancies are too large and would render bacterial predictions at the shoreline unreliable, as local wastefield transport is heavily dependant on advective transport by the currents. The reasons for the discrepancies between the observed and modeled currents are not known. It could be due to the limited boundary conditions that were available to drive the model. It would be desirable to use actual measured winds that vary spatially

over the whole model domain, but these were not available, nor were current measurements at the model boundaries.

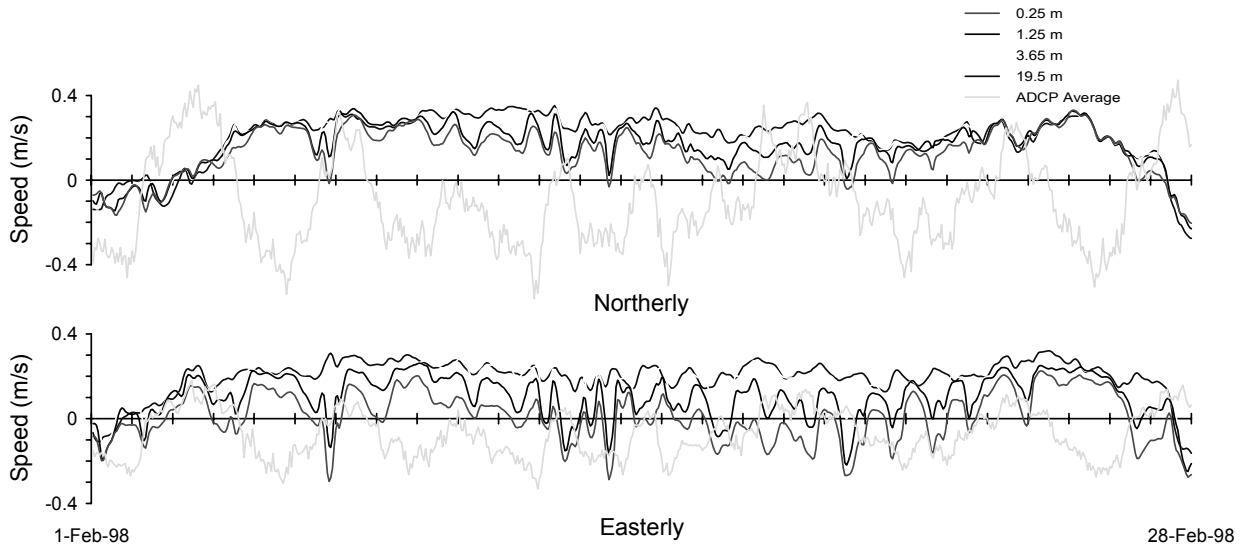


Fig. 105: Magnitudes of modeled velocities compared with measured ADCP data (Roberts and Villegas, 2006)

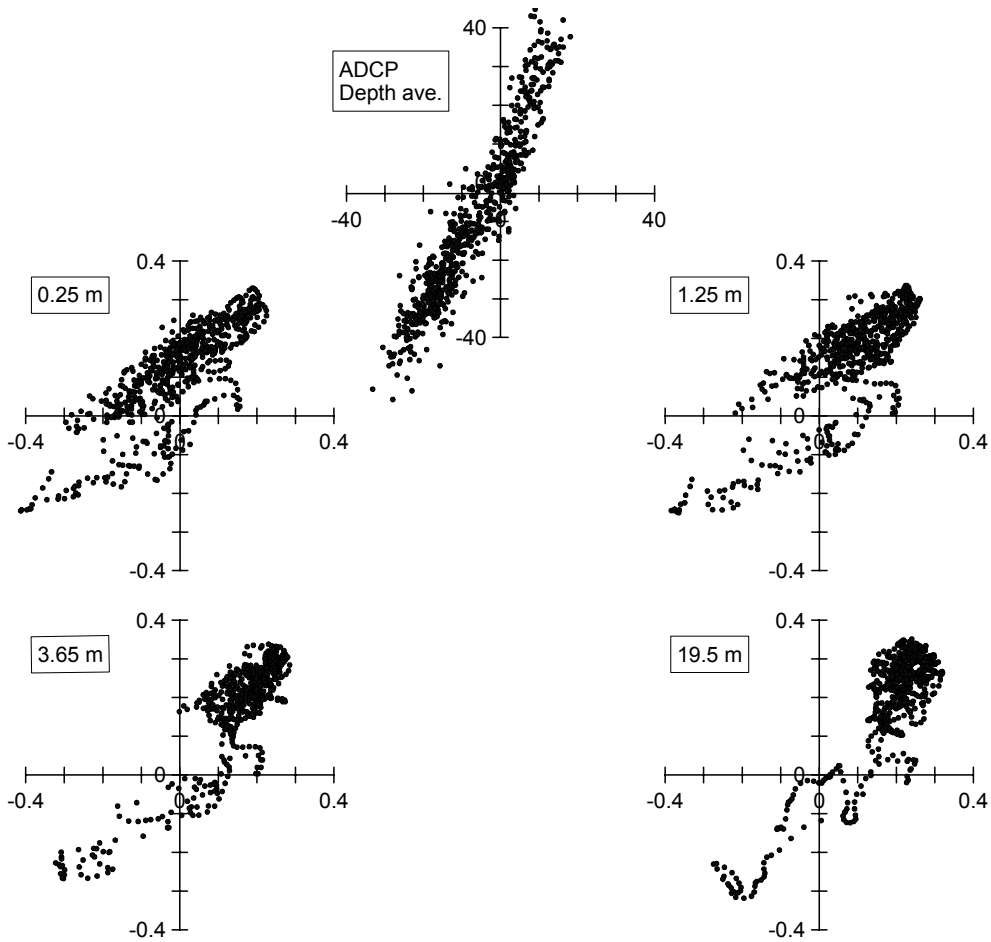


Fig. 106: Polar scatter plots of modeled velocities for different depths and two different months (Roberts and Villegas, 2006).

It was therefore decided to use a local-scale model to predict the fate and transport of the wastefield in the vicinity of the proposed outfall location. The boundary conditions for the local model consisted of the measured currents spatially modified according to the ELCOM predictions. The coupling approach presented will be used for the local-scale model specially representing the processes regarding buoyant spreading motions.

7.2 Data basis - CorField analysis

The entire project data base and especially the extensive measurements of currents, temperature, salinity, waves, and tidal height in the coastal waters at the proposed diffuser site are described in Hazen and Sawyer (1998) and summarized in Roberts (2003, 2004, 2005). Only consolidated datasets prepared for the coupled 3-D modeling will be presented here. Two periods have been modeled, November 1998 and February 1998, considered the worst-case scenarios. However, the results presented in the following only show February 1998, because more datasets have been available for that period, especially regarding the vertical velocity profiles. The only significant differences between both periods are slower depth averaged current velocities for November 1998. Results affected by this difference will be shown in addition to those for February 1998.

7.2.1 Bathymetry and shoreline

Bathymetry and shoreline data was available from different sources, in different resolutions and in different coordinate systems:

- High-resolution digital shoreline and bathymetry information from International Bathymetric Chart of the Caribbean Sea and the Gulf of Mexico (IBCCA, 2003). This data lacks information near the coast (< 5 km distance from coast).
- Digitized nautical chart from the Centro de Investigaciones Oceanograficas e Hidrograficas (CIOH, 2005, Serguei Lonin) for near coast information
- Sonar scans from the outfall location (Hazen & Sawyer, 1998).

The data has been validated, modified, and interpolated to get a final merged dataset of bathymetrical data and shoreline information necessary for the 3D modeling.

7.2.2 Wind

The wind data used in this study are hourly point measurements at the Cartagena airport of the year 1998 and 1999 (Roberts, 2005). Further data for the years 1986 to 1990 (Hazen & Sawyer, 1998, p. 8-3) has only been used for qualitative analysis.

The wind is given as time-series data with magnitude and direction. The magnitude is positive for all values. The direction is measured clockwise to the north. For example, a 45° wind with 5.5 m/s magnitude is blowing from north-east to south west (see Fig. 107). Fig. 108 and Fig. 109 show the output of CorField analysis of the time-series for February 1998.

- Case study -

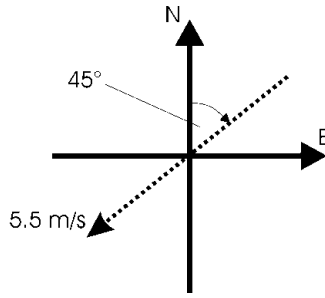


Fig. 107: Wind angle definition diagram. A 45° wind is blowing from northeast to south-west

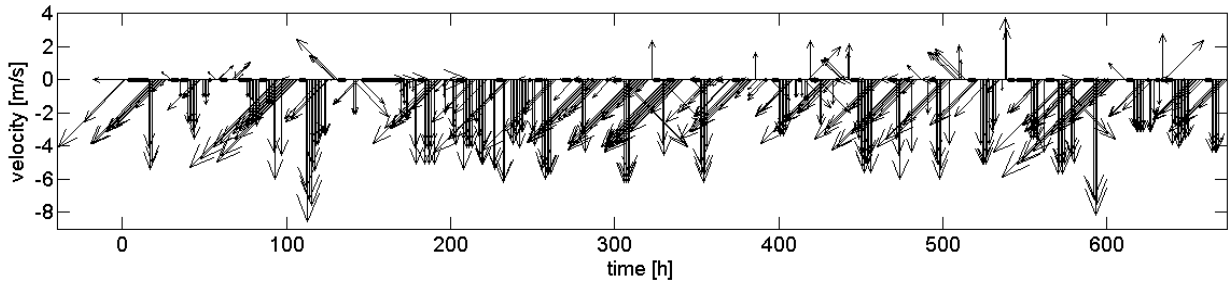


Fig. 108: Time-series feather plot of wind magnitudes and direction measured at the Cartagena airport for February 1998

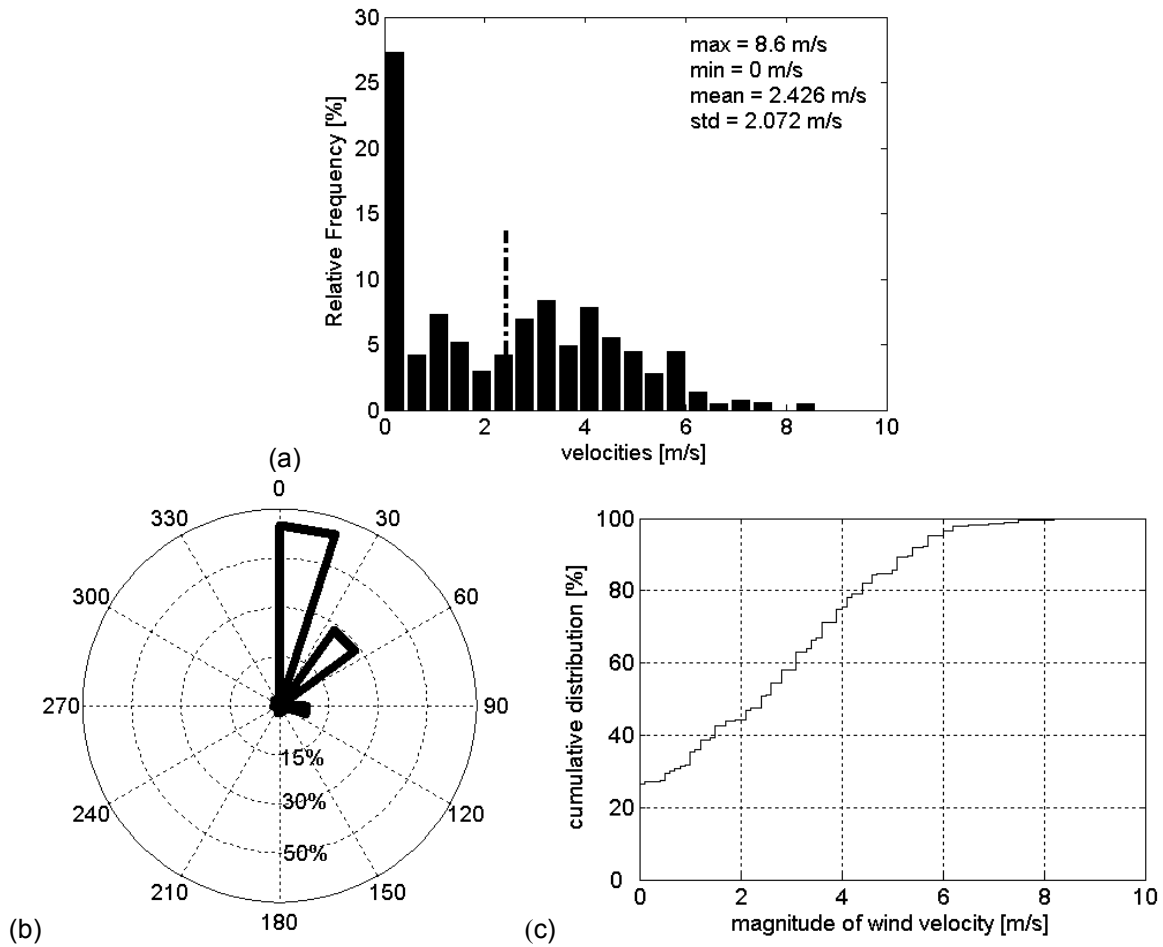


Fig. 109: Histogram of wind velocity magnitudes (a) and direction (b), and a diagram for the cumulative distribution of the velocities (c) for the wind data measured at the Cartagena airport during February 1998

The time-series data printed within CorField as feather plot (Fig. 108) gives a qualitative overview of the wind velocity directions and magnitudes. The histogram for wind velocity magnitudes and direction (Fig. 109a,b) show the occurrence frequencies of typical winds. Winds blow generally from the north or northeastern direction with magnitudes varying from 0 to 6 m/s with an average of approximately 2.4 m/s. The cumulative distribution of wind magnitudes (Fig. 109c) is important to determine the duration of periods with specific wind conditions. For example, for 80 % of the month the wind velocities are lower than 4 m/s. These winds, although relatively near the discharge region, might not fully represent the winds at the outfall location due to geographical features in that region. However, comparison with other wind stations shows similar characteristics. The summarized statistical results for the years 1998 - 2000 (Fig. 110) show that February data is representative compared to the yearly data.

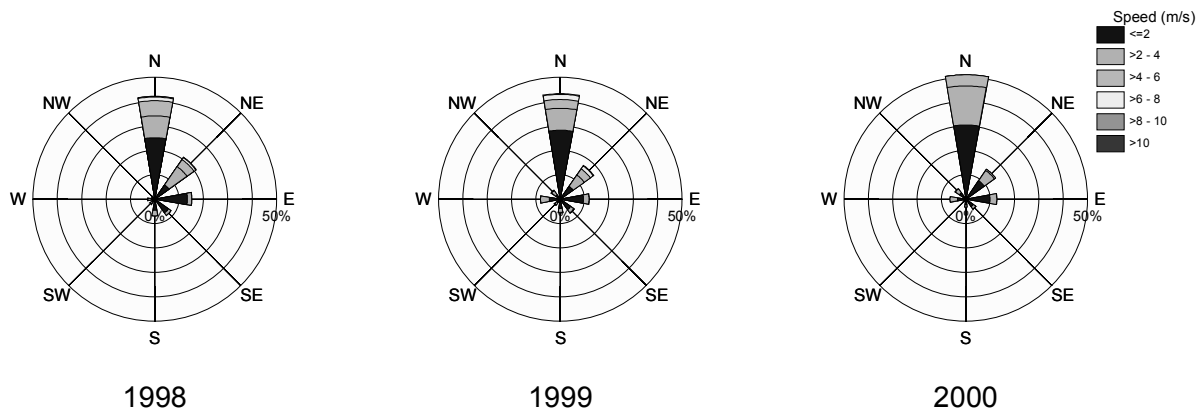


Fig. 110: Statistical analysis of wind directions and velocities for 1998-2000 (reproduced from Roberts, 2005)

7.2.3 Currents

Current velocities were measured with an acoustic Doppler current profiler (ADCP) moored about 2.5 km from Punta Canoas at the planned outfall location from January 1998 until December 1999.

Further data, only used for qualitative analysis in this study:

- Major patterns influenced by River Magdalena (Hazen & Sawyer, 1998, Fig. 8-13)
- 25. June 1997 – 27. February 1998, ADCP depth averaged velocities (Hazen & Sawyer, 1998, Annex 1)

Fig. 111 shows CorField analysis for magnitudes, direction, and histograms of velocities at six different depths. Vertical correlations of velocity directions indicate barotropic conditions. This is confirmed from the density profiles and the large-scale modeling (Roberts and Villegas, 2006). Velocities are reducing from surface to bed, whereas the near surface layers have considerably higher velocities than the other layers. The CorField velocity profile analysis for all profiles of February 1998 is shown in Fig. 112. The standard deviations of velocities over the vertical are at average of the order of 0.3 m/s with generally small deviations regarding the horizontal angle compared to the mean direction. The near-bed points are deviating with largest angles to the mean orientation. However, the deviation from typical logarithmic profiles is not significant, thus CorField classification assumes that depth averaged velocities suffice for the subsequent calculations with CORMIX. The depth-averaged velocities are shown in Fig. 113. A comparison with Fig. 108 shows general correlation with wind velocities. This is confirmed by the large-scale calculations from Roberts and Villegas (2006)

having similar periodicities of winds and currents. There is no clear semi-diurnal periodicity, which would indicate tidal influences. Thus, tides have minor influence on the local circulation.

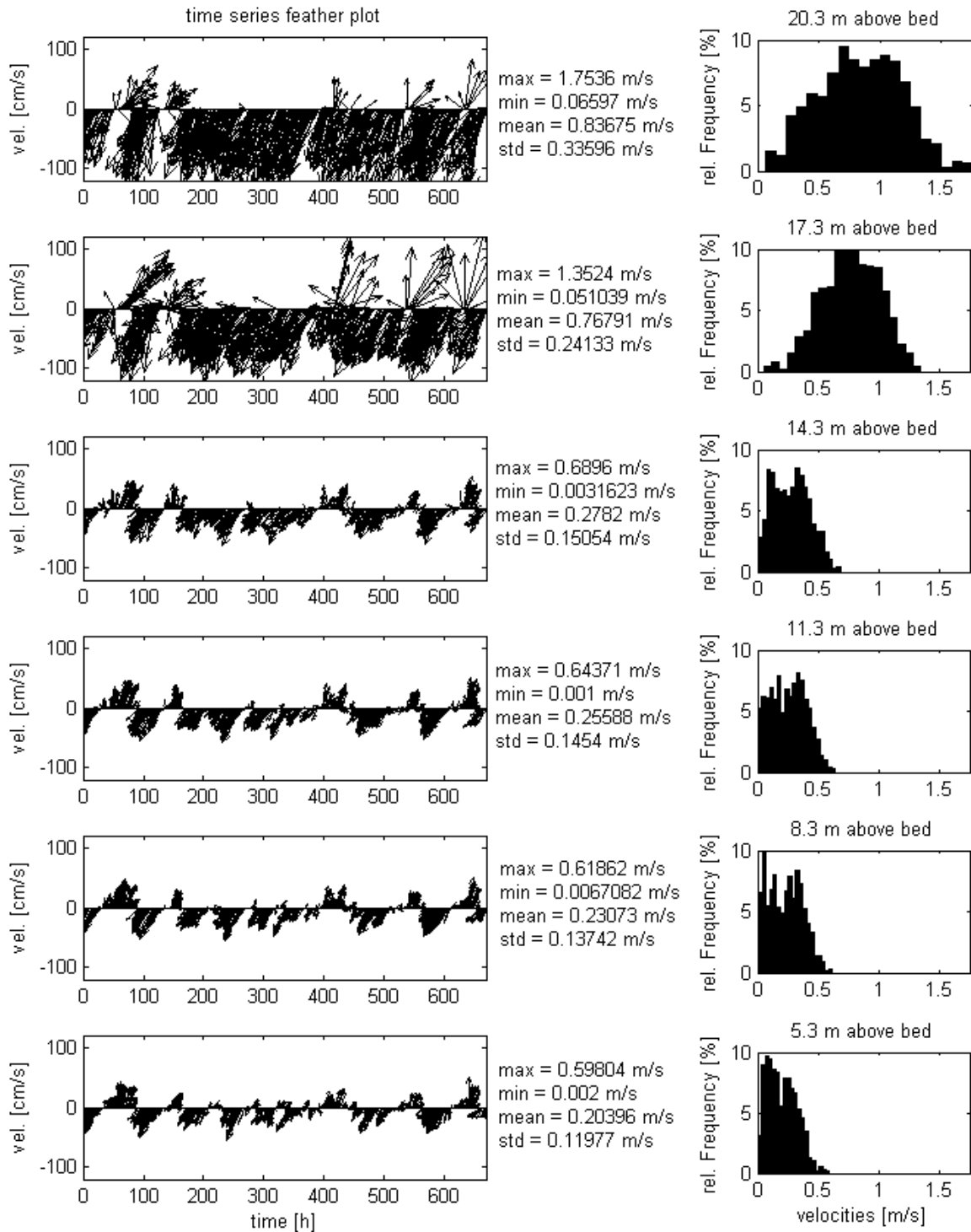


Fig. 111: Feather plots of measured current directions and velocities in different water depths (top is near surface and bottom near bed) for February 1998. Right column shows histograms of velocity magnitude in every layer

Statistical quantities of the depth-averaged currents are summarized in Fig. 114. The relatively strong residual current of 0.3 m/s oriented to the south-west can be related to the large-scale motions (i.e. Panama Colombian Gyre). Roberts (2003) showed for other seasons, that

this residual current changes to the opposite direction in November, shown in Fig. 114(right). The driving forces of these currents are large-scale baroclinic motions in the southern Caribbean Sea with additional wind shear (Roberts and Villegas, 2006).

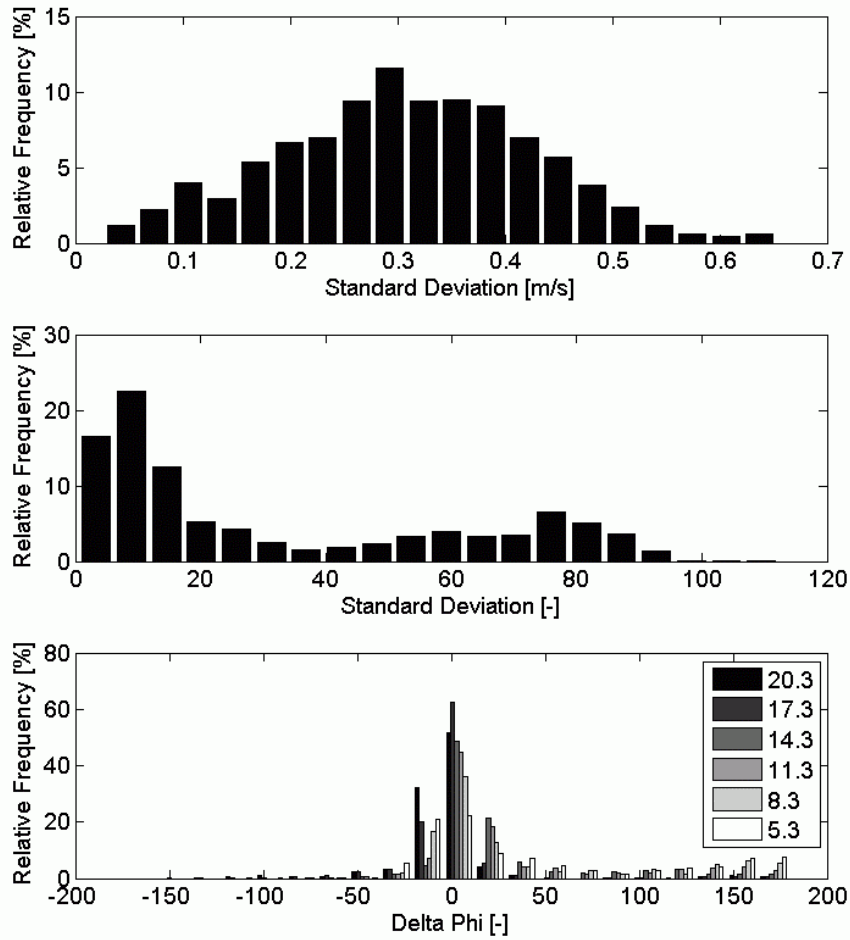


Fig. 112: CorField velocity profile analysis for all profiles of February 1998. Top: histogram of standard deviations of the velocities over the vertical, middle: histogram of standard deviations of the horizontal velocity angles to the depth-averaged mean, bottom: relative frequency of horizontal angles of the velocities compared to the dept-averaged mean, shown for every depth.

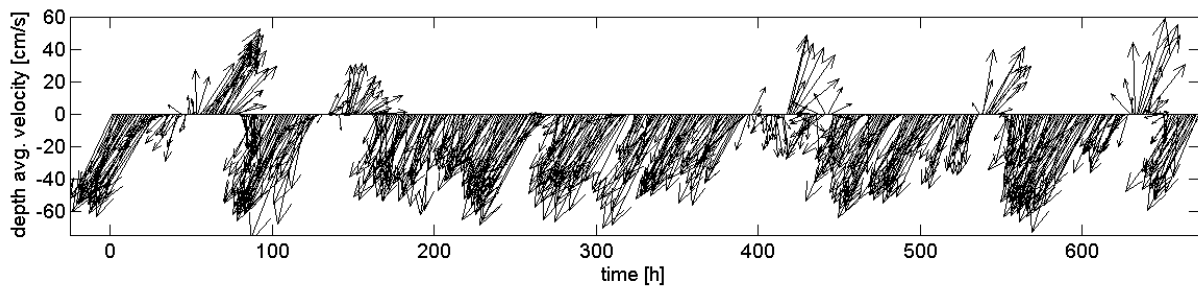


Fig. 113: Feather plot of the depth averaged velocities at Punta Canoas, for February 1998

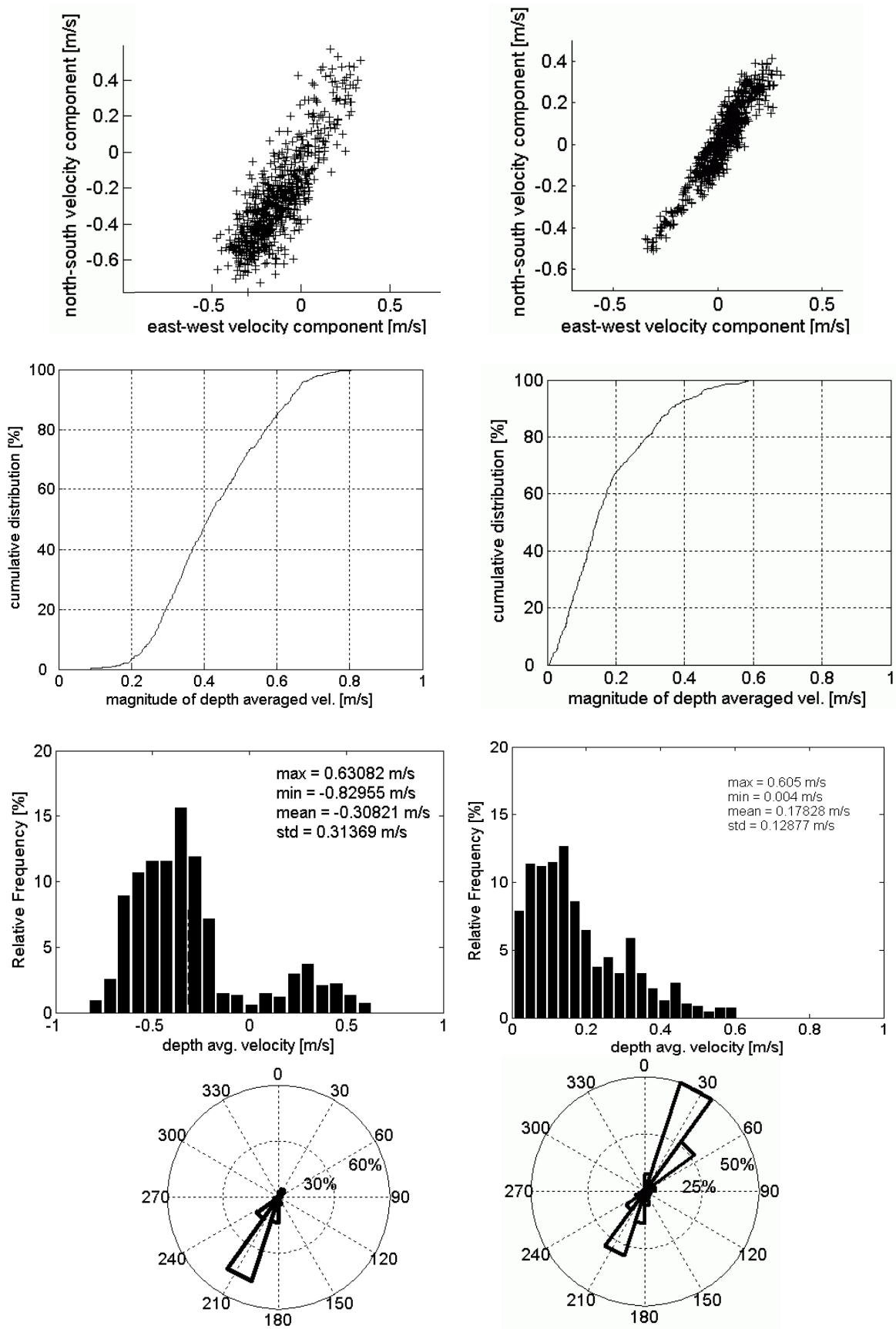


Fig. 114: Scatter plot, cumulative velocity, and histograms for depth averaged velocities and direction, measured from an ADCP moored at Punta Canoas for February 1998 (*left*) and November 1998 (*right*)

7.2.4 Tides

Measurements of water level elevations have been available from three different locations (compare with Fig. 96):

- Tide gauge at Islas del Rosario at depth of 15.3 m, 23.02.1998 - 17.08.1998 (Roberts). Hourly measurements Minimum: -0.59 m, Maximum: 0.51 m
- Tide gauge at Boca Grande at depth of 16 m, 25.09.1997 – 16.08.1998 (Roberts). Hourly measurements, Minimum: -0.37 m, Maximum: 0.52 m
- Tide gauge at Punta Canoas, at depth of 20.6 m, 01.01.1998 – 26.04.99 (Roberts). Hourly measurements, Minimum: -1.7, Maximum: 0.56
- September 1997 – March 1998 (Hazen & Sawyer, 1998, Figs. 8-3pp and 2-12)

Maximum tidal amplitudes are around 0.5 meters. There is almost no phase shift between the different tidal stations. Time-series of the water level variations near the planned outfall at Punta Canoas are shown in (Fig. 115).

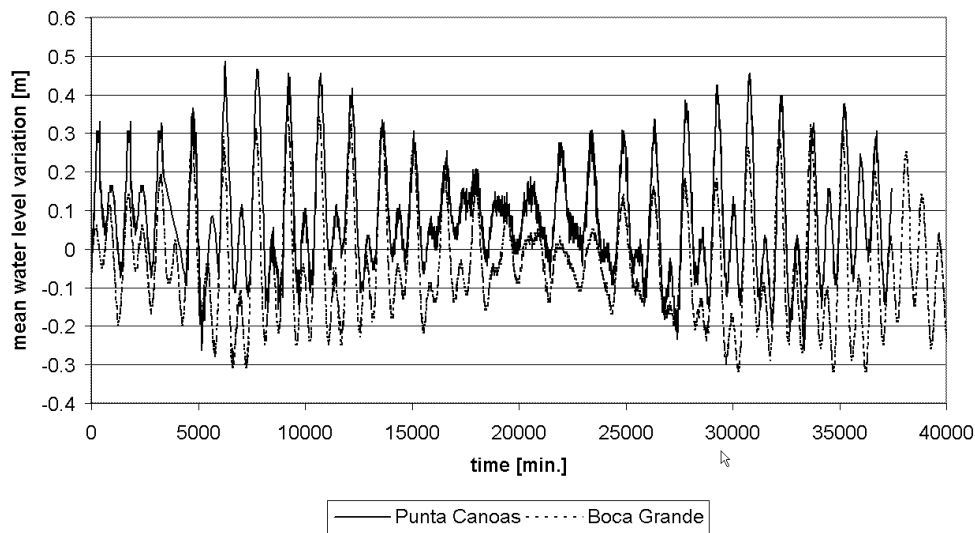


Fig. 115: Tide gauge comparison for February 1998 at Punta Canoas and Boca Grande.

7.2.5 Density (Salinity and Temperature) profiles

Temperature and salinity profiles have been measured all along the coast of Cartagena for short time-periods. Continuous thermistor string measurements (temperature profiles) have been recorded for a long period. The data is summarized in:

- Hazen & Sawyer (1998), Roberts (2003) for periods from 23 January 1998 - 25 June 1998
- Roberts (2006) for the thermistor string data from November 1999 to June 2001

Measurements and model results from Roberts and Villegas (2006, Appendix A) show a negligible salinity variation along the vertical profiles around the outfall location. The continuous thermistor string data (temperature profiles, Fig. 116) indicate only small temperature differences over the water column. This confirms the analysis from Roberts and Carvalho (2000) stating that the water column is frequently homogeneous, i.e. well mixed over depth. There are either uniform density profiles with densities around 1023 kg/m^3 or slightly stratified conditions with a layer of slightly lower salinity and higher temperature above 7-5 m depth, reducing the density at the surface to minimum values of around 1022 kg/m^3 . A typical

measured profile of the latter situation is shown in Fig. 117. Maximum density differences (bed-surface) seem not to exceed 1 kg/m^3 . Salinity and temperature variations at the surface are supposed to result from both the Magdalena River (discharging 100 km north of Cartagena) and solar radiation. This is confirmed by Roberts and Villegas (2006) as discussed in chapter 7.1.1.2.

Thus, the CORMIX type A profile (linear density distribution) applies for almost all time-steps, with only slight differences in surface and bottom density. Both computed out of the data presented in Roberts and Carvalho (2000).

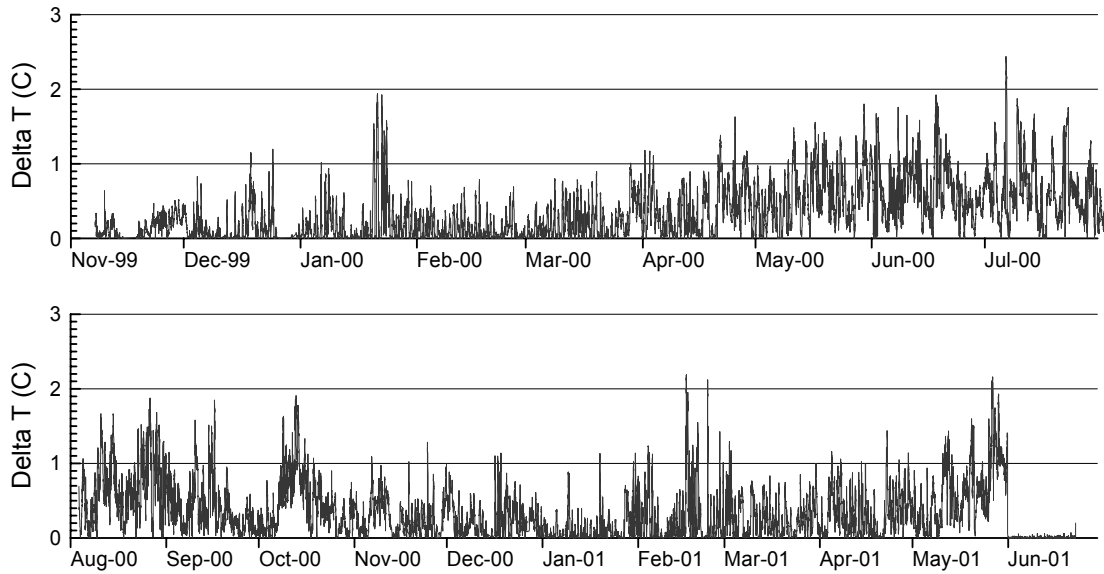


Fig. 116: Temperature data at the planned outfall location showing temperature difference between 5.5 m and 17.4 m probes (Roberts and Villegas, 2006)

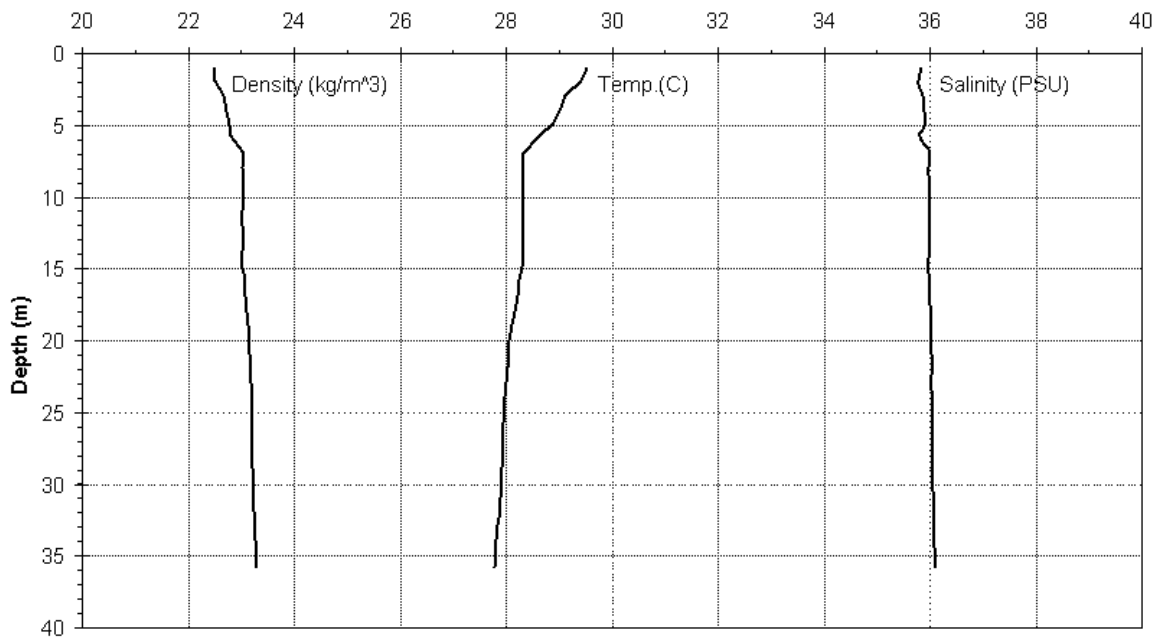


Fig. 117: Typical density profile for maximum stratification. Results from measurements offshore Cartagena (Hazen & Sawyer, 1998)

7.3 Near-field baseline modeling - CorTime

The CorTime coupling module uses the output from the field data converter CorField, such as ambient conditions like the depth average flow velocity and density distributions. However, for scenarios where no measurements are available it would also be possible to take the results from the hydrodynamic model, which then may be processed also using CorField.

Further input is required regarding the effluent characteristics and the outfall geometries. This data is based on the description from Roberts (2003) and Hazen & Sawyer (1998) and summarized as follows:

Effluent characteristics:

- Time variant flow (Fig. 118) with a maximum of $Q_o = 3.9 \text{ m}^3/\text{s}$
- Total coliform concentration of $C_o = 10^7 \text{ MPN}/100 \text{ ml}$ (or $10^{11} \text{ MPN} / \text{m}^3$)
- Effluent density $\rho_e = 998 \text{ kg}/\text{m}^3$

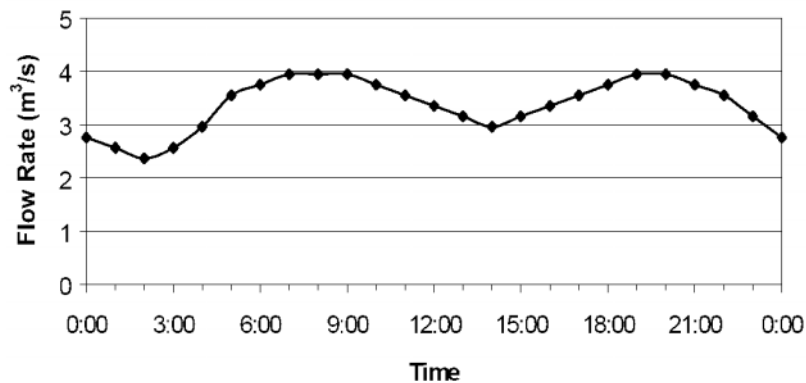


Fig. 118: Assumed flow pattern for the effluent flow rate (Roberts and Carvalho, 2000)

The effluent is discharged approximately 2.85 km offshore at 20 m depth through a diffuser with the following characteristics (Fig. 119):

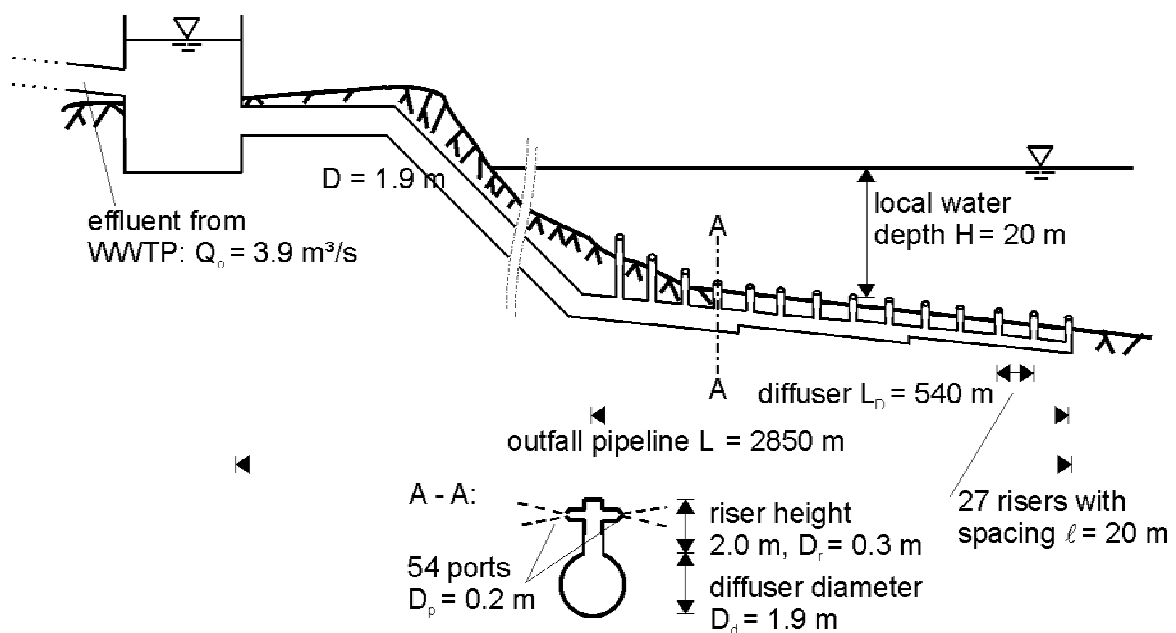


Fig. 119: Proposed design for the Cartagena outfall

CORMIX furthermore requires input on far-field parameters, though these are not going to influence the near-field predictions. Therefore the wind velocity was defined to $u_w = 2$ m/s and for bed friction the mannings friction coefficient to $n = 0.025$. A CORMIX calculation for the example of an average ambient velocity of $u_a = 0.3$ m/s perpendicular to the diffuser and a linear density profile with $\rho_{\text{surf}} = 1023$ kg/m³ and $\rho_{\text{bottom}} = 1023.5$ kg/m³ and a water depth of $H = 20$ m results in the following parameter specifications and plume characteristics:

Equivalent slot width	B_o	= 0.0031 m
Total area of openings	A_o	= 1.7 m ²
Discharge velocity	U_o	= 2.30 m/s
Diffuser alignment angle	γ	= 90°
Vertical discharge angle	θ	= 90°
Horizontal discharge angle	σ	= 0°
Relative orientation angle	β	= 90°
Buoyant acceleration	g_o'	= 0.2441 m/s ²
Stratification	ε	= 0.23E-03
Discharge concentration	C_o	= 100%
Discharge (volume flux)	q_o	= 0.0072 m ² /s
Momentum flux	m_o	= 0.016 m ³ /s ²
Buoyancy flux	j_o	= 0.0017 m ³ /s ³

Length scales:

$\ell_Q = 0.003$ m	$\ell_m = 0.18$ m	$\ell_M = 1.14$ m
$\ell_m' = 4.11$ m	$\ell_b' = 7.81$ m	$\ell_a = 19.38$ m
Slot Froude number	F_o	= 83.02
Port/nozzle Froude number	F_o	= 10.40
Velocity ratio	R	= 7.66

End of near-field:

Pollutant concentration	C_{nf}	= 0.34 %
Dilution	S	= 292.0
Centerline location:	$x = 68.47$ m; $y = 0$ m; $z = 12.83$ m (above the bed)	
Plume dimensions:	half-width = $BH = 273.35$ m (top hat half-width in horizontal plane normal to trajectory)	
	thickness = $BV = 6.94$ m (Gaussian 1/e (37%) half-width in vertical plane normal to trajectory)	
Cumulative travel time:	194.75 s	

Plume conditions in the intermediate field at 1000 m downstream (buoyant spreading motions still continue after that distance):

Pollutant concentration	C_{nf}	= 0.28431 %
Dilution	S	= 351.0
Centerline location:	$x = 1000$ m; $y = 0$ m; $z = 12.83$ m (above the bed)	
Plume dimensions:	half-width = 466.02 m; thickness = 4.91 m	
Cumulative travel time:	3299 s	

This specific plume calculation has been classified as flow class MS5. The flow classification scheme used in CORMIX is shown in Fig. 120. A plume visualization as direct results is shown in Fig. 121. For that specific case, the plume gets trapped at around 13 m above the bed and then spreads horizontally.

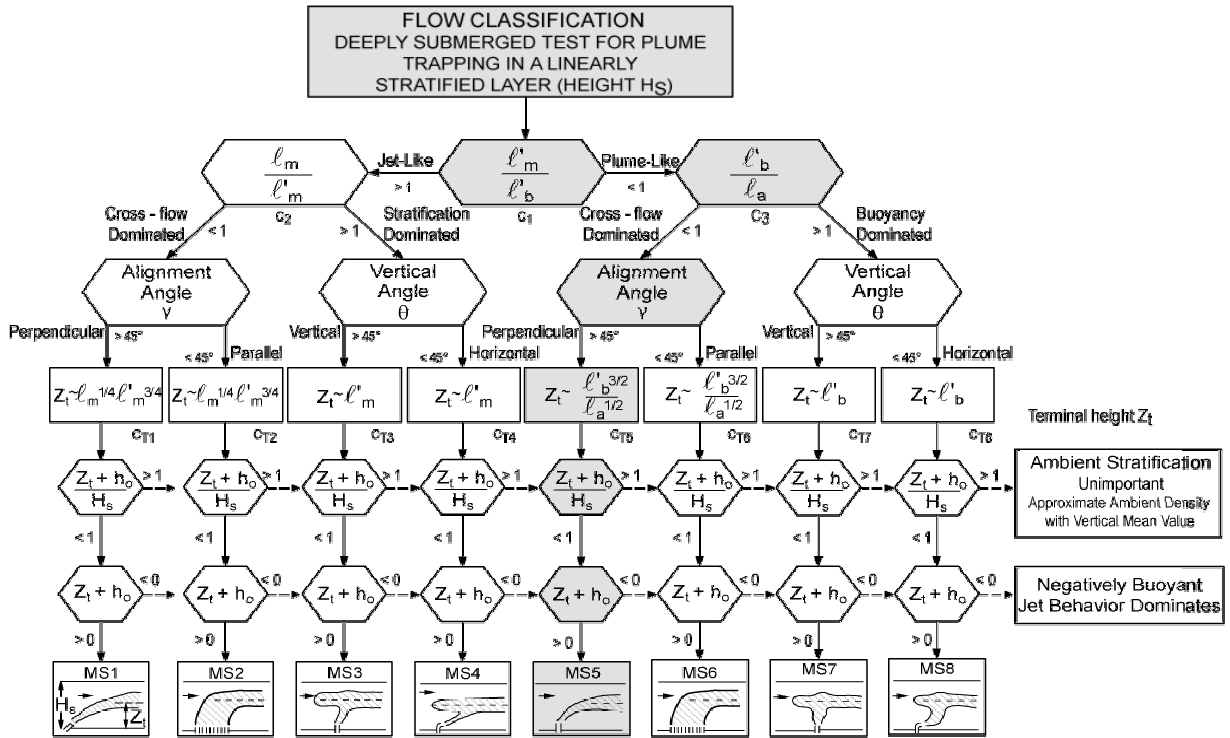


Fig. 120: CORMIX flow classification tree for the basecase example calculation for the Cartagena outfall

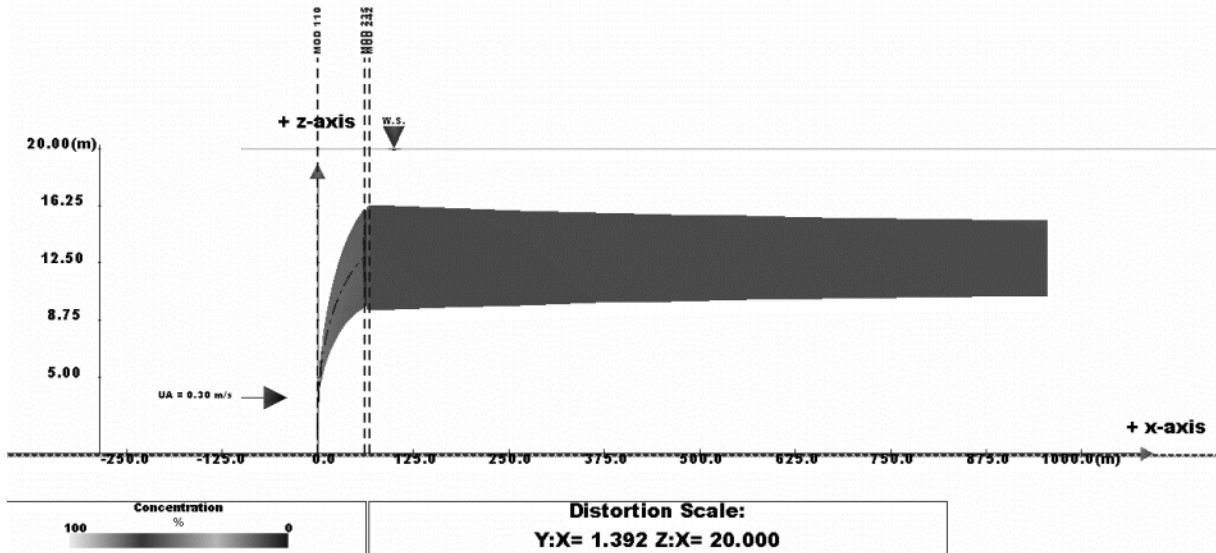


Fig. 121: CORMIX plume visualization (side view) for the example basecase for the Cartagena outfall

A full CorTime application processes all parameters for every time step out of the 672 hourly time-steps for February 1998 data. Results are firstly time-series files for each parameter (Fig. 122), which are then analyzed using histograms (Fig. 123) showing the occurrence frequency of each parameter.

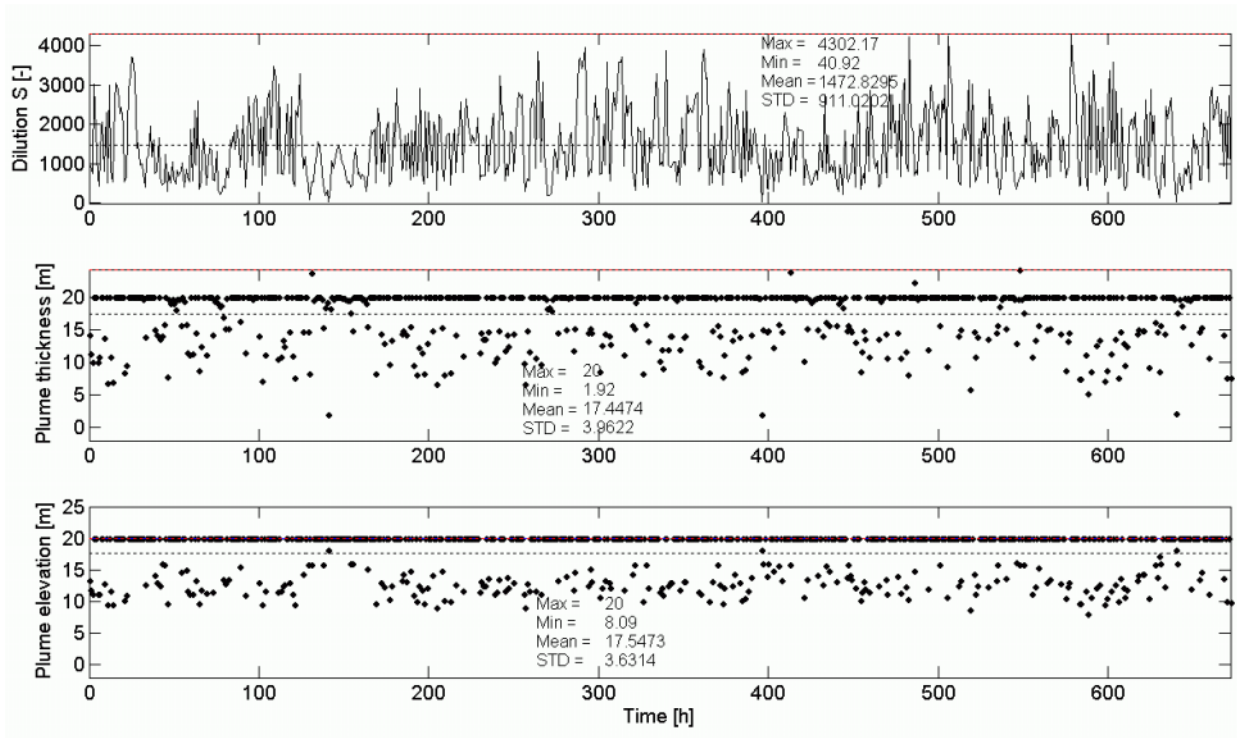


Fig. 122: CorTime output. Time-series of dilution, plume thickness and plume elevation at the end of the near-field / intermediate-field, as predicted by CORMIX for every single time-step out of 672 time-steps for February 1998 data.

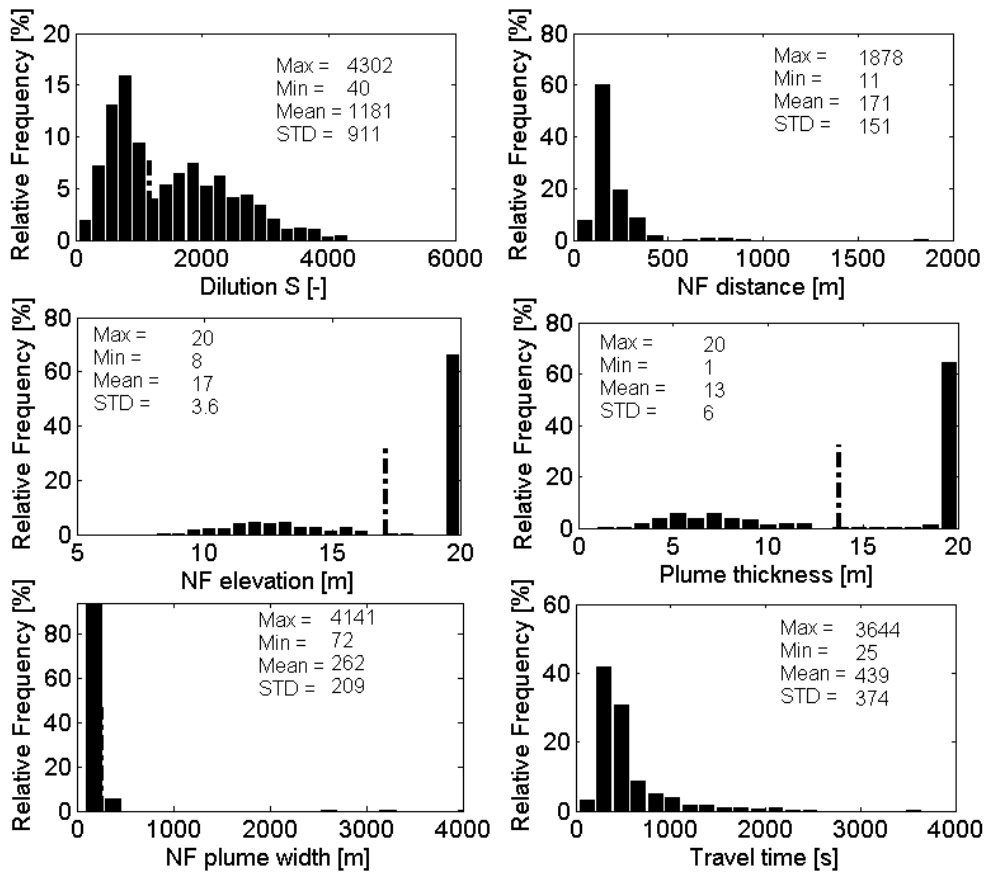


Fig. 123: CorTime histograms for parameters at the end of the near-field / intermediate field: dilution, downstream location, plume elevation, thickness and width and the cumulative travel time.

These results show that the plume is surfacing more than 70 % of the time. This causes high dilutions with an average of about 1000 and dilutions above 100 for about 96 % of the time. The end of the near-field / intermediate-field region is on average 170 m downstream the predominant current and about 98 % of the time encountered before 500 m downstream. The plume width (two times the resulting half width) is for almost all cases of the order of the diffuser length, thus no significant spreading occurred until that position. The average duration to reach the end of the near-field location is about 7 min and for all steps below one hour. These results however are different from those of the near-field modeling studies from Roberts (2001). One explication is the usage of the full velocity profile data considering all 6 pins. Roberts (2001) used 4 instead. However even, CorTime runs using 4 pin data result in considerably higher dilutions (almost double), though the near-field locations and elevations are rather similar. Another explication is the different definition of the near-field region in either model. CORMIX near-field definition partly includes intermediate-field processes (i.e. boundary interaction and buoyant spreading motions), whereas NRField used from Roberts (2001) stops after reaching the terminal level. A comparison of both models would be needed for further evaluation. It is however justified to continue using the CorTime results, because of its extensive validation and if the coupling procedure properly handles the definition of the near-field region.

Further applications of CorTime allows optimizing the mixing performance of the applied engineering diffuser design by re-running CorTime with either modified design or at alternative locations. Furthermore, the results might already be used for evaluating compliance regarding the environmental quality objectives defined for the regulatory discharge zone. For example if defined in a distance of 5 times the average water level elevation of $H = 20$ m, the concentrations in 100 m distance are larger than 100 for 97 % of the time. Alternatively, if defined in larger distances, for example at 500 m downstream relative frequencies and a cumulative distribution of frequencies (Fig. 124) allow estimating the dilutions and concentrations in a larger area, without running a far-field model yet. Fig. 124 demonstrates that dilutions are larger than 400 for more than 95 % of the time.

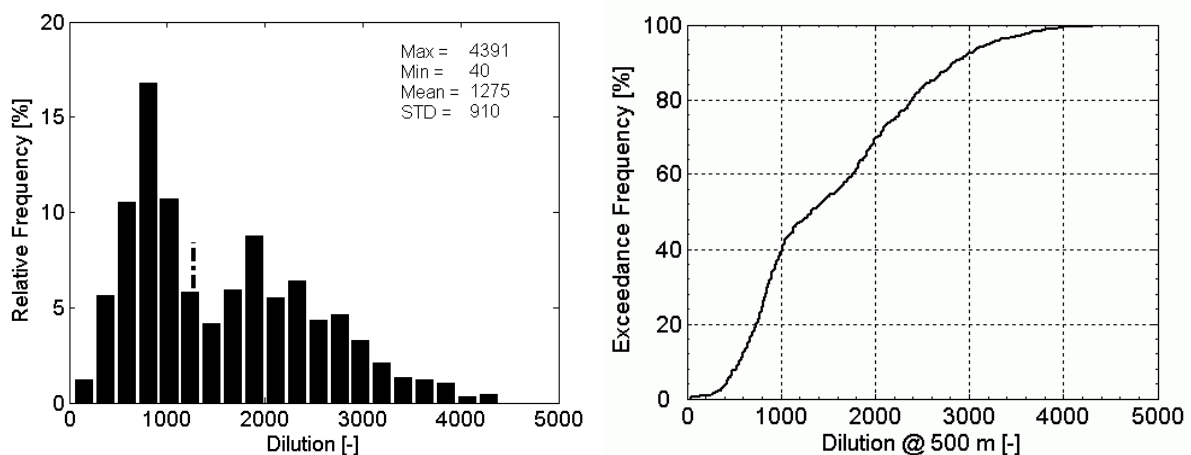


Fig. 124: Statistical analysis of the plume centerline dilution at 500 m downstream the diffuser. *Left:* Histogram of the relative frequency, *right:* cumulative distribution of frequencies.

7.4 Ambient hydrodynamics baseline modeling with Delft3D flow

The base for any coastal water quality analysis is a good knowledge of the coastal hydrodynamics. Field measurements offer important high-resolution information at specific locations; however, spatial measurements are limited to very short time periods. Hydrodynamic model-

ing offers high-resolution information all over the considered project domain for large time-periods, thus perfectly complementing field measurements. Though simple interpolation techniques are helpful tools in the open ocean, complex 3D far-field models are needed for near-coast analysis of stratified non-uniform water bodies.

The Delft3D model package includes all necessary utilities for pre- and post-processing:

- Delft3D-RGFGRID (2004) for generating curvilinear grids
- Delft3D-QUICKIN (2004) for preparing and manipulating grid oriented data, such as bathymetry or initial conditions for water levels, salinity or concentrations of constituents
- Delft3D-GPP (2004) for visualization and animation of simulation results
- Delft3D-QUICKPLOT (2004) a second tool for visualization and animation of simulation results

The solver for the hydrodynamics is Delft3D-FLOW (2003), for the intermediate field particle tracking approach transport Delft3D-PART (2003) and for the full system water quality Delft3D-WAQ (2003).

7.4.1 Computational domain

The domain size was chosen to be approximately 20 km around the proposed outfall location. It is considerably smaller than the large-scale model ELCOM (Fig. 125). However, it is large enough to represent all hydrodynamic features regarding transport and mixing of waste plumes and small enough to assume a negligible influence of spatial climatic variations, like temperature or density fields.

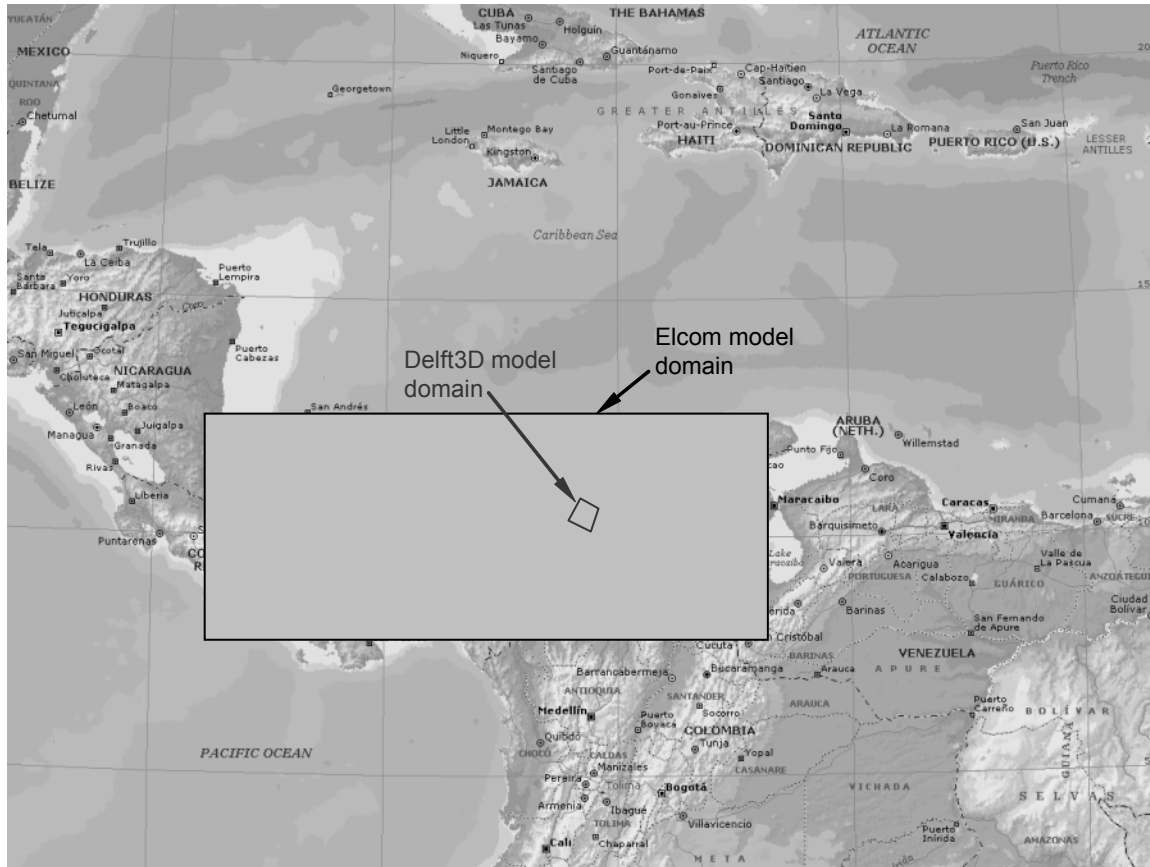


Fig. 125: Model domains for ELCOM and Delft3D (Roberts and Villegas, 2006)

7.4.1.1 Horizontal discretization – structured curvilinear grid along shoreline

The computational grid should have a high resolution at locations of interest and critical hydrodynamics (strong gradients) and lower resolution far away from these points, thus saving computational efforts. A structured curvilinear grid was set up, where grid lines may be curved along land boundaries and channels, so that 'stair case' boundaries (from rectangular grids) are avoided and artificial diffusion is reduced (Delft3D-RGFGRID, 2000).

The minimum grid size for the near-field region has been defined according to chapter 5.4.2.3 to less than $L_D / 6 = 90$ m. The size of the near-field region is estimated with eq. (5.96) to at least $Size_{NF} = (1 \text{ to } 3) \min(\ell_M, \ell_m, L_D) = (1 \text{ to } 3) 540 \text{ m} \approx 1000 \text{ m}$. Grid resolution increases beyond the near-field.

Locations for the open boundaries have been defined by a large-scale flow analysis using the ELCOM model results (Roberts and Villegas, 2006). Observations and analysis of the unsteady flow around the outfall location allowed characterizing areas where only weak spatial gradients and more uniform flows occurred. Together with the bathymetrical data, this information was used to define the location of open boundaries. The domain is bounded by the coastline and three straight open boundaries that encompass an area of about 930 km² (Fig. 126).

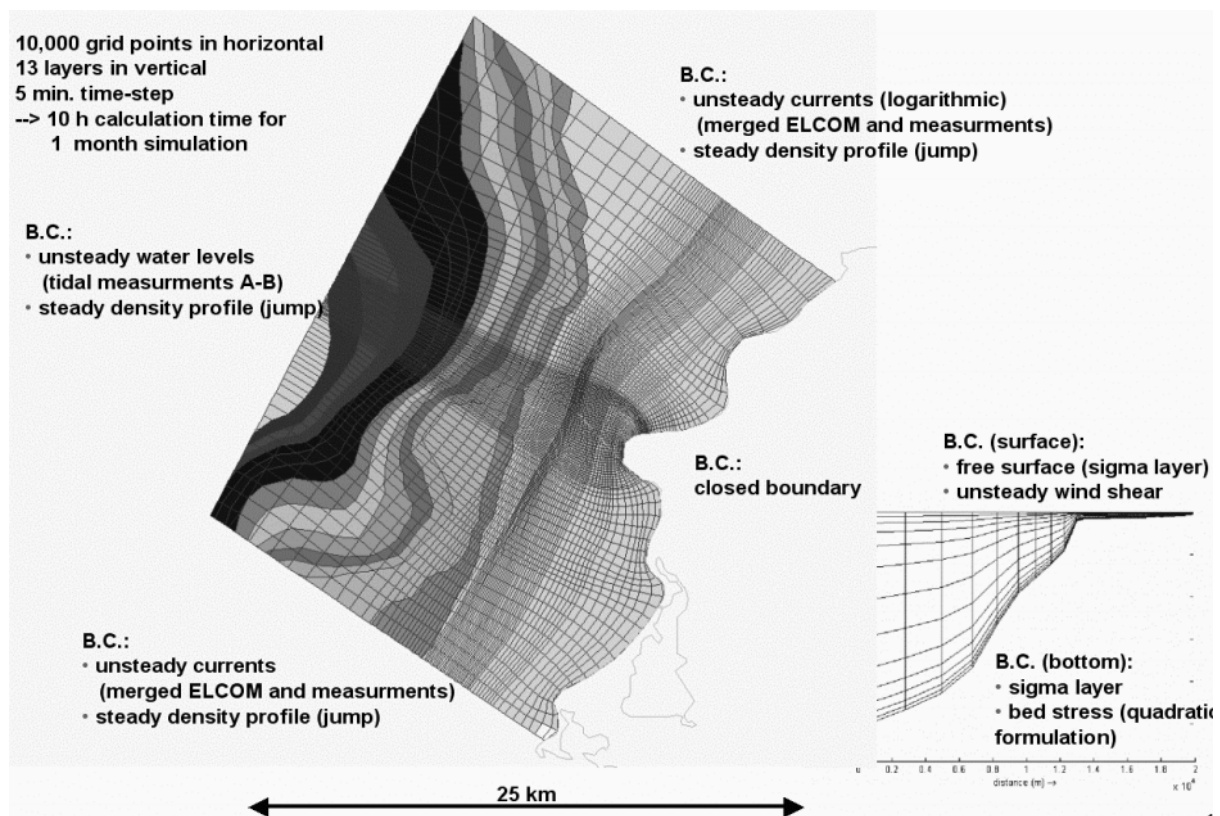


Fig. 126: Delft3D model domain for the Cartagena coastal region. Grayscales indicate different depths. Boundary conditions (B.C.) are described at all open and closed boundaries.

Previous calculations have been performed using a coarser grid. A compromise between grid dependency and computational demands has been found for the present resolution. Influence of grid spacing on the final exceedance diagrams are considered small compared with other modeling uncertainties.

7.4.1.2 Vertical discretization – sigma layers along bathymetry

Available bathymetrical data (see chapter 7.2.1) was interpolated onto the computational grid. The σ -coordinate system was used in the vertical because of its high vertical resolution in coastal regions. To resolve near-bed and near-surface processes, considering the thin fresh-water layer from Magdalena river plume and the waste plume itself while either surfacing or stratifying near the surface, the vertical thickness of the σ -layers was chosen as follows: There were 13 layers going from surface to bottom, and the layer thickness were 2%, 3%, 4.5%, 6.75%, 10%, 15%, 17.5%, 15%, 10%, 6.75%, 4.5%, 3%, 2% of the water depth. Fig. 127 illustrates the applied σ -coordinate system, showing a cross-sectional view through the domain.

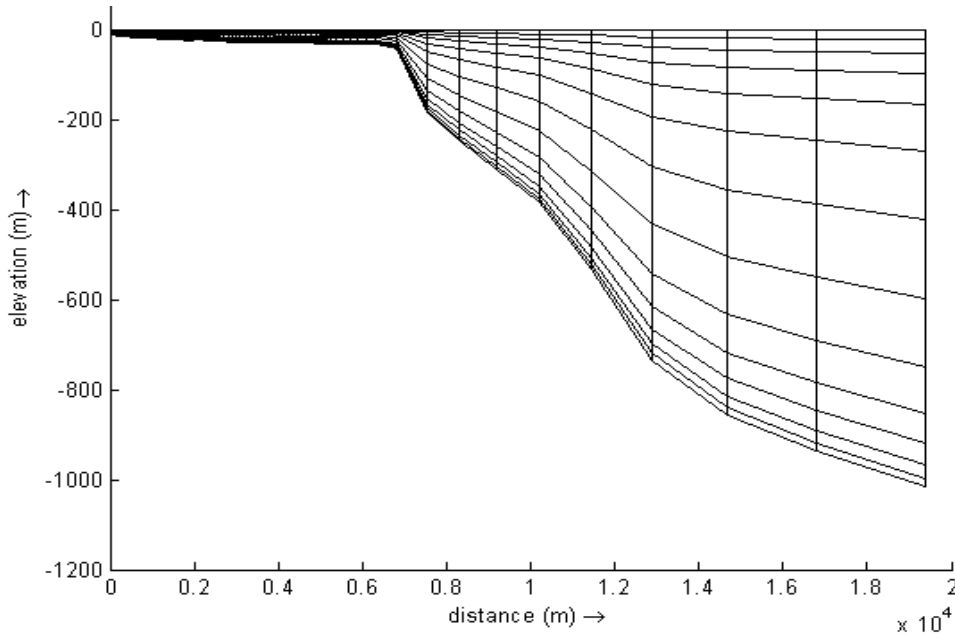


Fig. 127: Vertical cross section through model domain to visualize sigma-layers with high resolution at shallow regions. The diffuser is located at 2.8 km distance from the shore.

7.4.1.3 Temporal discretization

The time step chosen depended upon the grid resolution and was chosen to be 5 min. Calculations have been done for a one-month period resulting in a total of 8064 time-steps for February 1998.

7.4.2 Boundary and initial conditions

The model boundaries and an overview of the boundary conditions are shown in Fig. 126.

7.4.2.1 Closed boundaries - shear stresses

The closed boundaries are defined by the known shoreline and the bathymetry. For shallow flows like the observed coastal waters in the project region, the influence of the shear stresses along the lateral boundaries is neglected and a so-called free slip boundary condition is applied. In the σ -coordinate system, the free surface and the bottom are σ -coordinate surfaces and the vertical velocities are relative to the σ -plane. The impermeability of the surface and the bottom is taken into account. The vertical diffusive flux through the free surface and bed

is set to zero and heat flux through the free surface has been ignored, because no thermal stratification has been observed.

The bed shear stress is related to the current just above the bed. The contribution of the vertical velocity component to the magnitude of the velocity vector is neglected. The first grid point above the bed is assumed to be situated in the logarithmic boundary layer. Bottom friction is accounted for by the Manning equation with $n = 0.025$.

Unsteady wind stress is applied on the free surface and a wind drag coefficient given to $c_{D,w} = 0.0025$.

7.4.2.2 Open boundaries

Open boundaries are necessary to restrict the computational domain. These conditions represent the influence of the outer world, i.e. the area beyond the model area, which is not modeled. The present flow is numerically forced by combinations of time-variant water levels and currents. The hydrodynamic forcing is prescribed using harmonic or astronomical components or as time-series. The transport of salinity, temperature, and/or constituents is prescribed by specifying the inflow concentrations. None of this information was available, thus it is impossible to represent the open boundaries in an accurate way. Therefore, the open boundaries have been chosen far away from the observed project region, that their effects on the problem are negligible. In fact, one of the most difficult aspects of limited-coastal modeling is the adequacy of the open boundary condition information available.

A coarse semi-artificial nesting has been applied between ELCOM, Delft3D, and the measurements. Direction and magnitude for the unsteady logarithmic velocity information has been taken from the measured data and distributed along the boundaries according the modeled linearly interpolated large scale velocity field. At the western boundary only tidal forcing is applied using the water level time-series interpolated between a northern and southern station from Hazen and Sawyer (1998, Annex1).

The transport boundary conditions are uniform at all open boundaries for the unstratified case. For stratified calculations, steady density stratification similar to the measurement and ELCOM predictions has been applied for reasons of simplicity. The stratification showed less density in the first 5 m of the water column, followed by a density jump and further uniform density.

7.4.2.3 Initial conditions

The initial conditions are average water level elevations and zero velocities at all grid points. Forcing this model with the previously mentioned boundary conditions leads to a reasonable solution (without effects of the initial condition) after a few simulation days. The results of the simulation are then used as initial conditions for the next runs.

7.4.3 Hydrodynamic simulation

First runs have often been characterized by unstable solutions leading to unsuccessful calculations and no results. This is caused by inaccurate setups (too coarse temporal or spatial resolutions) or boundary and initial conditions (inaccurate or unstable conditions), as well as the wrong choice of the numerical scheme (e.g. implicit or explicit, 1st order or 2nd order schemes). Once the calculations are stable, results were obtained after a successful run. Cal-

ulation times for a one month simulation, with a time step of 5 min. and approximately 10000 grid points in the horizontal and 13 layers in the vertical takes approximately 5 hours on a 3GHz (1GB RAM) standard single processor PC.

Visualization of large data sets of 3-dimensional, unsteady velocity data is still a challenging task and depends on the interpretation interests. Delft3D postprocessors allow for different spatial data arrangements (profiles, horizontal and vertical cross-sections) and temporal arrangements (time-series or movies). Import options allow for further post-processing with other programs. Following visualizations however have been made by processing the data using either post-processors from Delft3D or the routines from CorField or combinations. An advantage in that regard is the MatLab based post-processor QuickPlot in Delft3D. Basic plots can easily be exported and further processing be done with user-defined variables.

Fig. 128 shows the velocity field of depth averaged velocities in the project region. It clearly points out one of the major advantages of hydrodynamic modeling, giving highly resolved information at all grid points and therefore offering spatial flow analysis, which cannot be done with measured data.

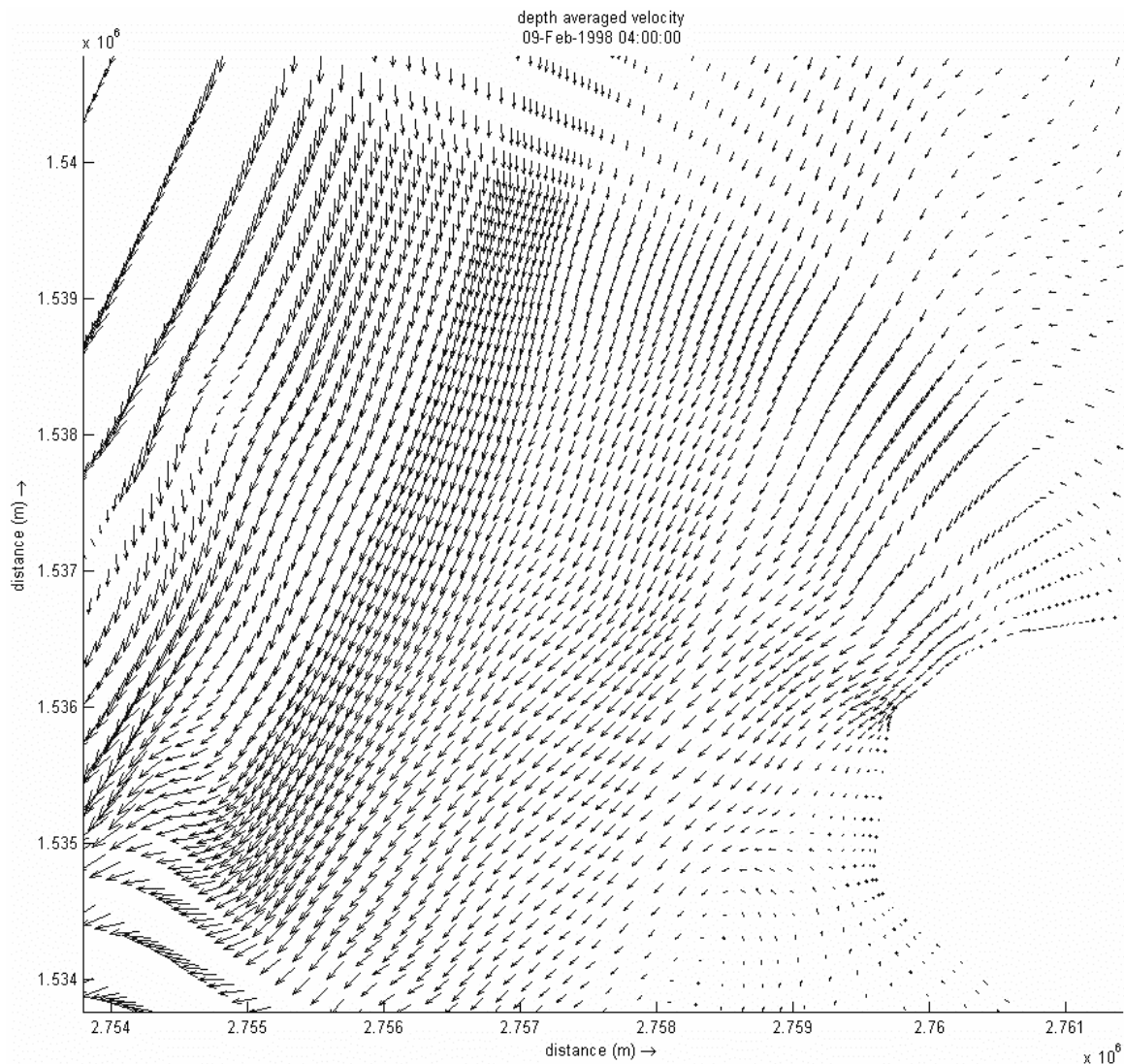


Fig. 128: Depth-averaged velocity field zoomed in to the outfall region at Punta Canoas.

For validation, Fig. 129 compares a computed and measured time-series plot of water levels at Punta Canoas, the planned outfall location, showing good agreement. Comparing the measured velocities at Punta Canoas with the modeled currents indicates whether the model is able to represent major flow characteristics at that point. Fig. 130 and Fig. 131 show time-series plots of depth averaged velocities at the planned outfall location. A relatively good agreement of major flow characteristics can be seen by comparisons of the peak flow events. However, it can also be observed that there are several discrepancies between modeled and measured data. These can be deficiencies of either the model (inaccurate boundaries or resolutions) or the measurements (lack of surface layer velocities and near-bed velocities) or both. Further model calibration and optimization would allow defining the source of inaccuracies in more detail. The comparison of scatter plots, Fig. 132, show that the modeled results seem to be more dispersed in the horizontal than the measured values. This behavior is clearly to the inaccurate boundary conditions or effects of the spatial grid resolution. However, major flow characteristics seem to match reasonably well.

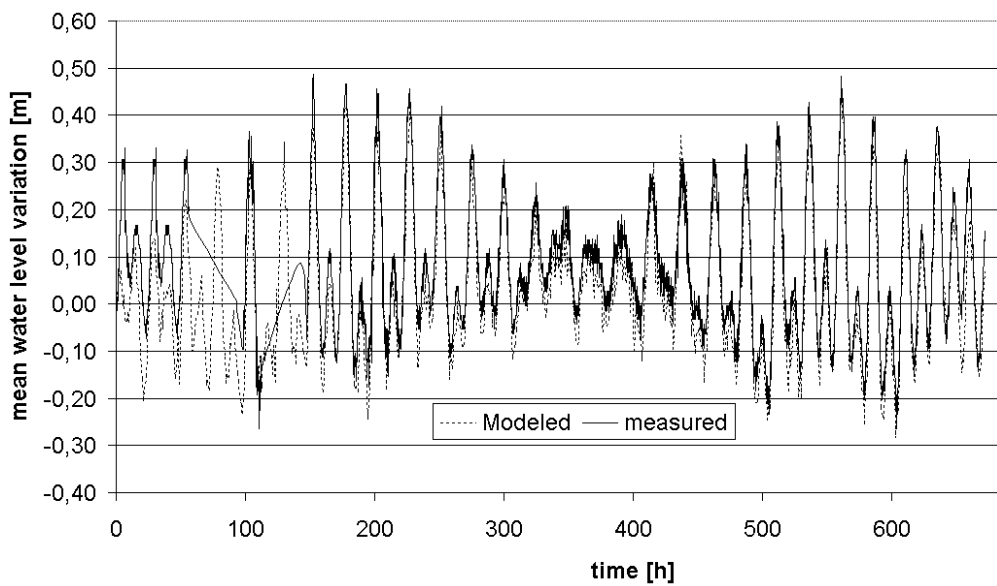


Fig. 129: Time-series of model and measured water levels at Punta Canoas (outfall location) for February 1998

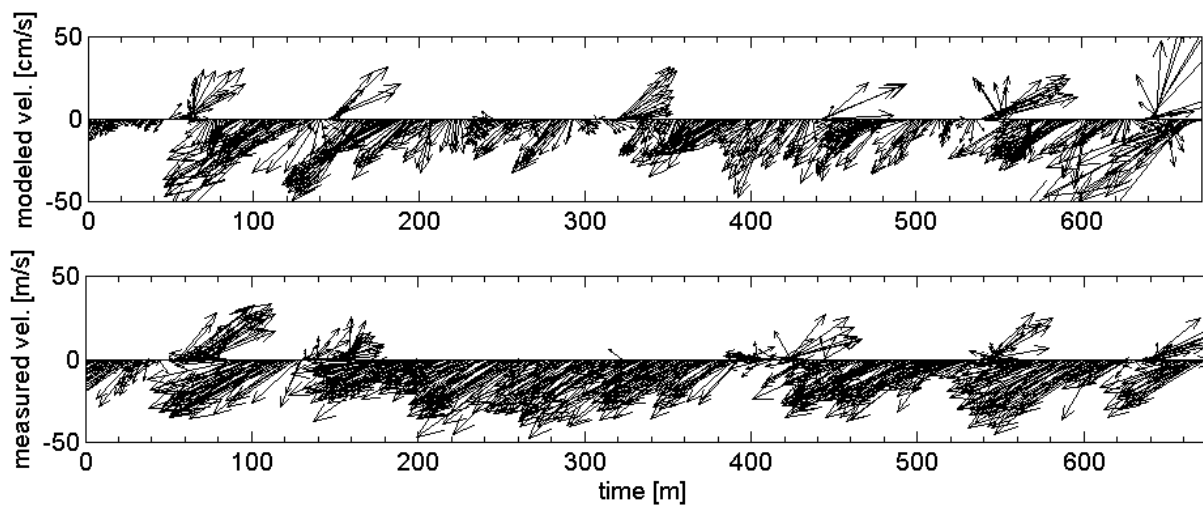


Fig. 130: Time-series feather plot of depth averaged modeled (top) and measured (down) velocities at the planned outfall location for February 1998.

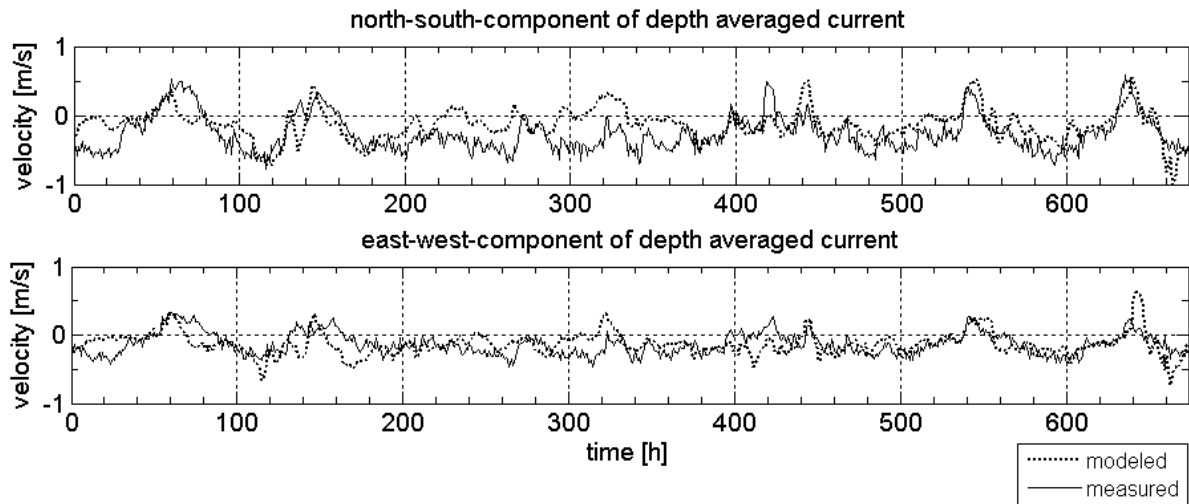


Fig. 131: Time-series of modeled (dashed-line) and measured (continuous-line) depth averaged current components at planned outfall location for February 1998

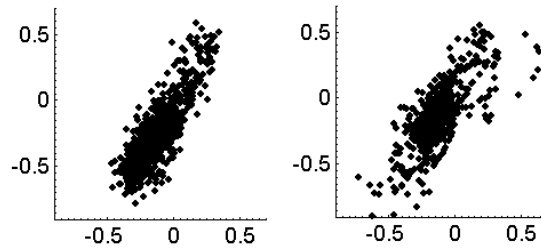


Fig. 132: Scatter plot of measured (*left*) and modeled (*right*) depth averaged currents for February '98.

A second tool for comparing measured and modeled velocities is comparisons of the statistical flow quantities. Fig. 133 shows histograms of frequencies for depth averaged velocity magnitudes and direction. These confirm the previous deficiencies of the model to represent a more constraint distribution of velocities along the major direction.

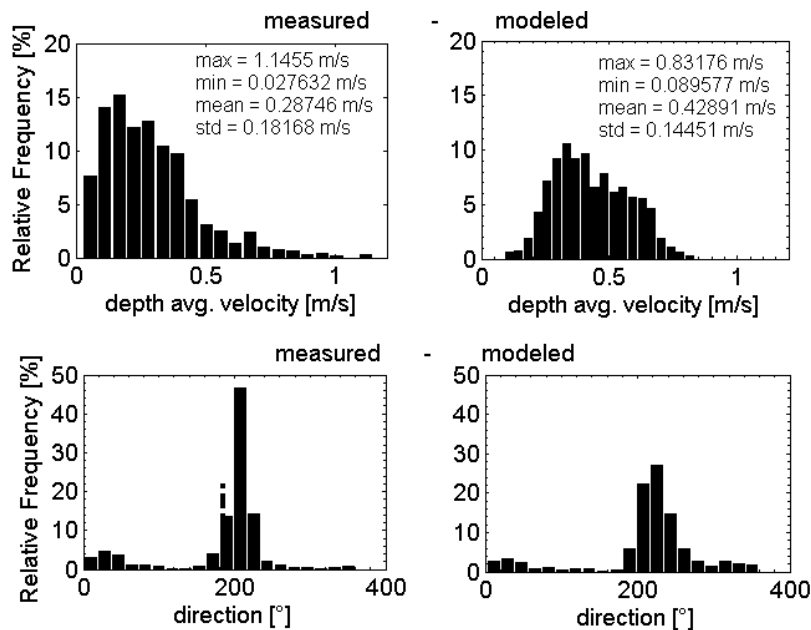


Fig. 133: Statistical comparison of measured (*left*) and modeled (*right*) depth averaged current magnitudes and directions for February 1998.

A third interpretation method is the comparison of the vertical profiles. Fig. 134 shows 3D visualizations of a vertical velocity profile at Punta Canoas for two different time-steps. These visualizations confirm the previous characteristics. At some instances there are quite good agreements between modeled and measured profiles, at other instances there are clear disagreements. Generally, the profiles seem to show that the wind-shear effects, which can be seen in the measured profiles, are underrepresented in the modeled results. Furthermore, the eastern component of velocity seems to be too big, whereas the northern velocities are often too small.

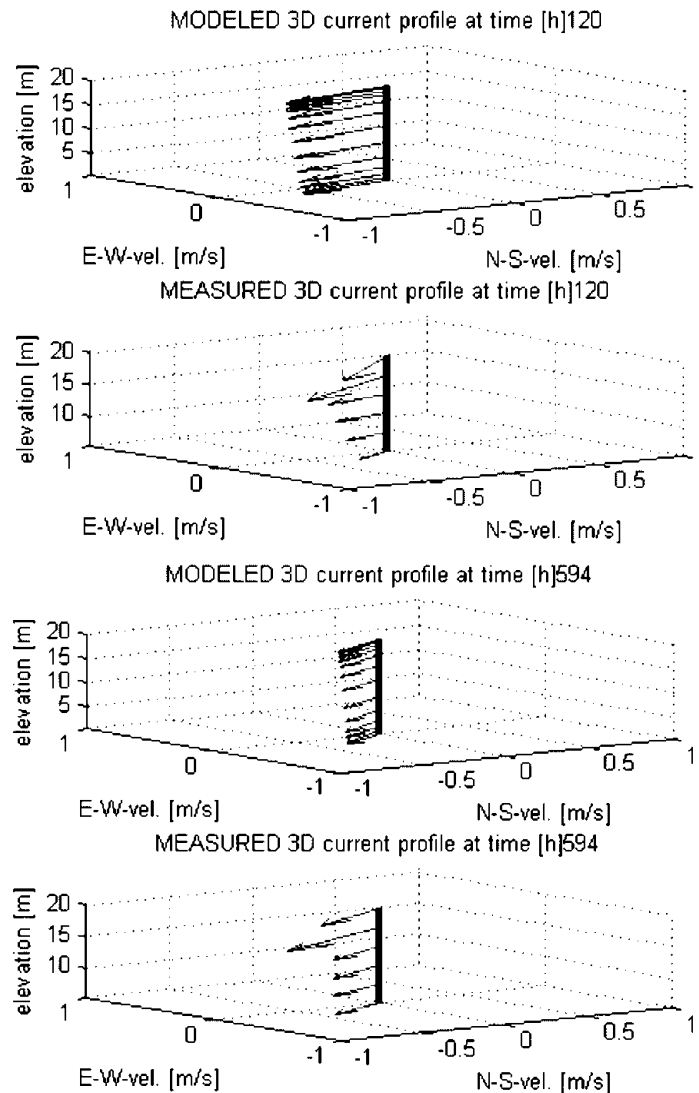


Fig. 134: Comparison of modeled and measured 3-D visualizations of vertical velocity profiles at Punta Canoas for different time steps

It can be concluded for the hydrodynamic modeling that major characteristics are represented in the model, but not all details. More intense optimization and analysis would be necessary for improvements of absolute values. Nevertheless, these results together with the results of the large-scale model and the measurements provide further insight in the flow field around the planned outfall location. Further relative comparisons between the two modeled periods show, that effects regarding the stronger onshore winds during November 1999 do not have considerable consequences on the resulting flow field. In addition, influences of stratification are of minor importance if model results are compared in between each other.

7.5 Source representation in far-field model - CorLink

The coupling module CorLink is used to classify the near-field / intermediate-field results and writing source input files to be included into a Delft3D calculation. The results of the classification can be summarized to:

- The maximum value for ℓ_m/H for all time-steps within February 1998 was 0.8, and the mean value 0.007. Thus, it is justified to follow a passive coupling approach, neglecting momentum fluxes in the coupling procedure. However, for the period of November 1998, 38 time-steps out of 699 exceeded that criterion, especially for almost stagnant ambient velocities.
- There are 6 time-steps, where $\ell_M/\ell_m < 1$. The medium value is about 30. Thus, buoyant spreading processes are only or marginal importance. However, for November 1998, 277 time-steps out of 699 (almost 40 %) are indicating that buoyant spreading processes might be important.
- The unsteady scale analysis for the 6 cases of February 1998, shows, that only one exceeds the ratio of ℓ_{bu}/L_D or $t_{bu}/\Delta t$ respectively. This case has been modified by choosing a shorter distance for the coupling, the other include the full intermediate field results. For November 1998, all time-steps classified as buoyant spreading class exceed the ratios of both ℓ_{bu}/L_D and $t_{bu}/\Delta t$. Thus, model results from CorTime regarding these large spreading motions, have been modified by reducing the coupling distance. The cut-off was proportional to the duration of the period where the plume was classified into the buoyant spreading class.
- Generally, a critical ambient velocity can be defined for average flux values. For $\ell_m/H = 1$ and the average initial momentum flux of $m_o = 0.013 \text{ m}^3/\text{s}^2$ it is $u_{a,crit} = 0.03 \text{ m/s}$. For velocities below that value the near-field momentum flux, might not be neglected during the coupling process.
- Generally, a critical ambient velocity can also be defined for buoyant spreading processes. For $\ell_M/\ell_m = 1$ and the average initial buoyancy flux of $j_o = 0.0015 \text{ m}^3/\text{s}^3$ it is $u_{a,crit} = 0.11 \text{ m/s}$. For velocities below that value buoyant spreading motions are significant.

Ignoring buoyant spreading processes in the near-field - far-field coupling procedure can therefore only be justified if the assumption is valid, that periods with very small velocities do not last for hours. For February 1998, there are only 6 time-steps with duration of maximum one hour. For November 1998, Fig. 135 shows the histogram of durations of the 277 time-steps, where velocities are below 0.1 m/s. The average duration is about 8 h, whereas longer periods occur seldom. The results from the intermediate field calculations can be considerably larger than these periods as summarized in Table 26 for a sensitivity analysis. CorLink classification therefore cuts-off most of the strongly spreaded intermediate-field results, which cannot occur in reality, due to often relatively short durations of such periods.

This sensitivity analysis using CORMIX and including buoyant spreading processes calculated plume properties for a location of 1000 m and 100 m downstream and for stratified and uniform ambient density profiles. The modeling approach from Roberts (2003) using NRFIELD predicts values for the plume width of around 600-700 m at a distance of 100 m downstream. Differences to CORMIX-values are only considerable large for current velocities smaller 0.07 m/s (Table 26, values in brackets are for a distance at 100 m downstream). This sensitivity analysis indicates that different results are to be expected only for periods with velocities smaller than 0.07 m/s and durations longer than 5 hours. Such periods only occur with 7% of November 1998. CorLink classification considers those and modifies the

necessary source files respectively. The modified plume parameters at the end of the intermediate field have been converted into Delft3D source files.

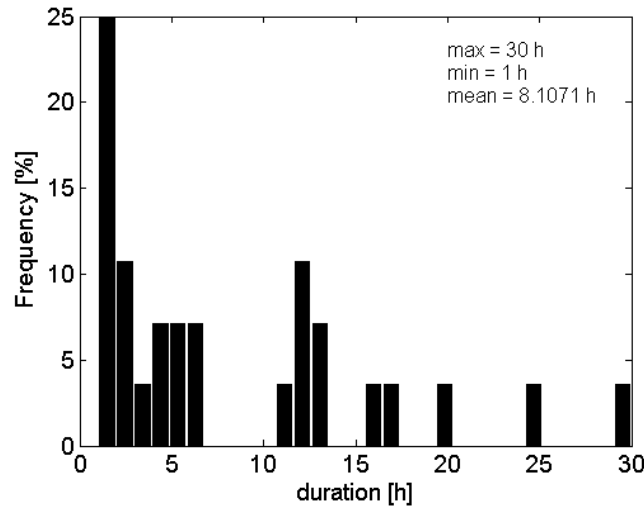


Fig. 135: Histogram of the frequency of duration of periods where ambient velocities are below 0.1 m/s for November 1998.

current velocity u_a [m/s]	stratified density profile				uniform density profile			
	dilution [-]	plume width @1000(@100) [m]	thickness [m]	travel time [h]	dilution [-]	plume width @1000(@100) [m]	thickness [m]	travel time [h]
0.1	158	1600 (700)	4	2.8	418	1700 (700)	9.5	2.7
0.09	140	1660 (700)	3.7	3	396	1940 (700)	9	3
0.08	81	1400 (800)	2.8	3.5	127	2100 (800)	3	3.4
0.07	72	1500 (880)	2.6	4	117	2300 (880)	2.8	3.9
0.06	65	1740 (1000)	2.5	4.6	111	2700 (1000)	2.8	4.6
0.05	60	2000 (1200)	2.4	5.5	80	5200 (1200)	1.2	7.5
0.04	55	2350 (1600)	2.3	7	89	9200 (1600)	1	16
0.03	52	3100 (2400)	2.3	9	44	9400 (2400)	18	72
0.02	52	4800 (4000)	2.2	16	42	14000 (4400)	15	72

Table 26: CORMIX sensitivity analysis for slow current velocities (u_a) and stratified or unstratified conditions. Results are for a plume location at 1000 m downstream. Values in brackets () are plume width results at 100 m downstream.

7.6 Coupled water quality modeling

The source files resulting from CorLink are introduced into Delft3D. These can directly be imported into the water-quality module Delft3D-WAQ that is based on the hydrodynamic results from Delft3D-FLOW. Delft3D-WAQ models bacteria decay using the Mancini (1978) model. Default parameters were used with the first order mortality rate equal to 0.8 1/d, ambient water temperature 15°C, UV irradiation at the upper-boundary segment 160 W/m², and the duration of solar radiation 0.58 d. The integration method chosen was the explicit backward scheme in space and time including diffusion.

Fig. 136 shows total coliform concentration of a certain time-step. The plume is traveling with the predominant velocity field, while unsteady variations cause additional accumulation

or stretching of the plume. Fig. 137 indicates four locations, for which time-series of total coliform concentrations for February are shown in Fig. 138. Highest values occur at the outfall location (the vertical axis at the outfall location is one magnitude larger than at the other positions) and decreasing concentrations away from the diffuser. Near-shore concentrations are very small and show strong intermittency, usually expected for ocean discharges into spatially and temporally varying currents (Roberts, 1999). The intermittency increases and average concentration levels decrease with increasing distance from the source. Because of this intermittency, average levels are much lower than peak values. Concentrations near shore only very occasionally exceed background levels, and when they do, they are of order 1,000 per 100 ml or less.

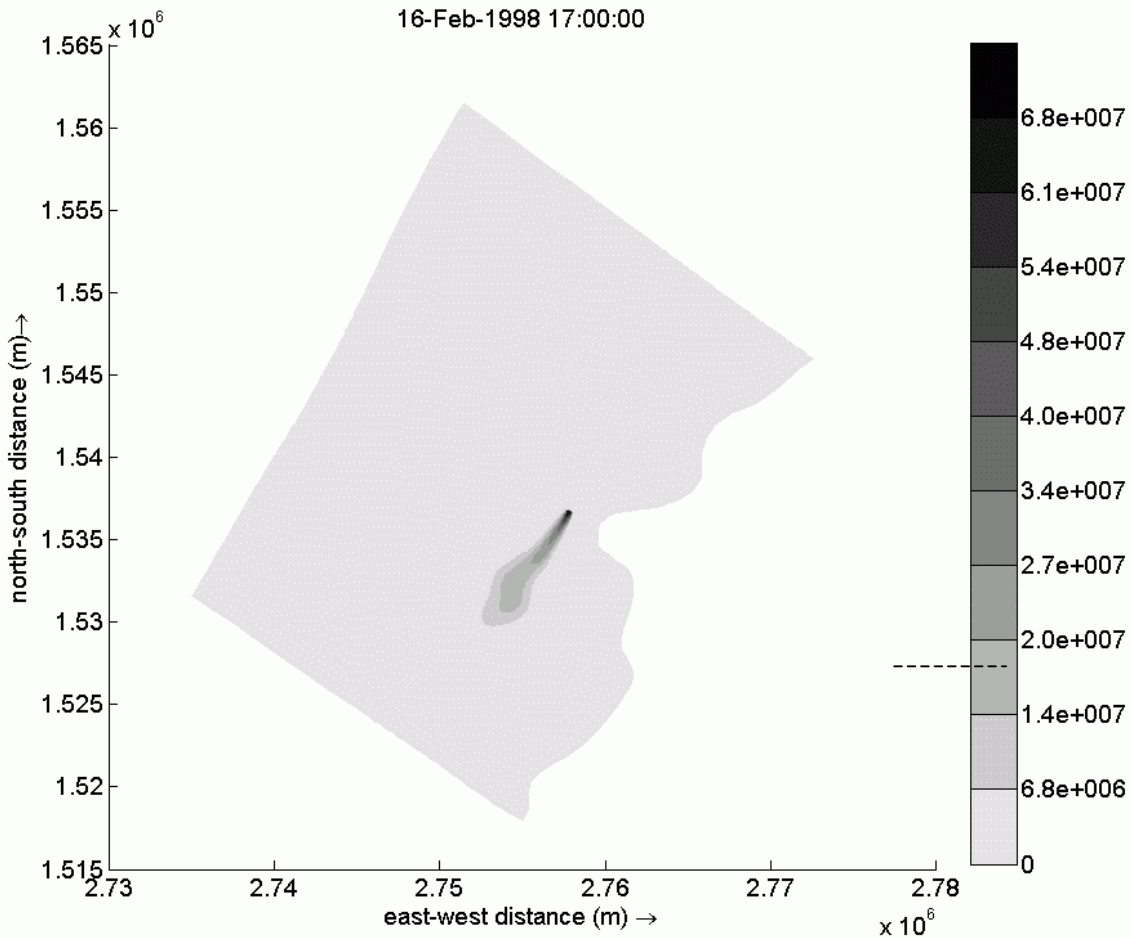


Fig. 136: Modeled depth averaged concentration [MPN/m³] of total coliforms at 21st of February. Effluent concentration is $C_0 = 10^{11}$ MPN/m³. Bathing water standard is $C = 10^7$ MPN/m³ = 10^3 MPN/100 ml (dashed line)

7.7 Regulatory consequences - CorZone

Water quality standards for protection of human health are usually based on indicator organisms that indicate the presence of pathogens. The standards for the Cartagena outfall are discussed in Roberts (2003, 2004, and 2005). The widely adopted California Ocean Plan standards (SWRCB, 2001) have been used here. However, the California standards have recently been revised. The original standards were based on exceedance frequencies, for example, total coliforms should not exceed 1,000 per 100 ml for more than 20% of the time. The new standards (SWRCB, 2005) use geometric means rather than exceedance levels. For example,

the 30-day geometric mean of total coliforms should not exceed 1,000 per 100 ml (10^7 per m^3). The original standards, which have been applied here, are stronger than the new standards and results in the following sections are expressed as the exceedance frequency. These indicate how often during a monthly period this standard is exceeded. The applied standard is a concentration of 10^3 MPN/100 ml (or 10^7 MPN/ m^3) (Roberts, 2004).

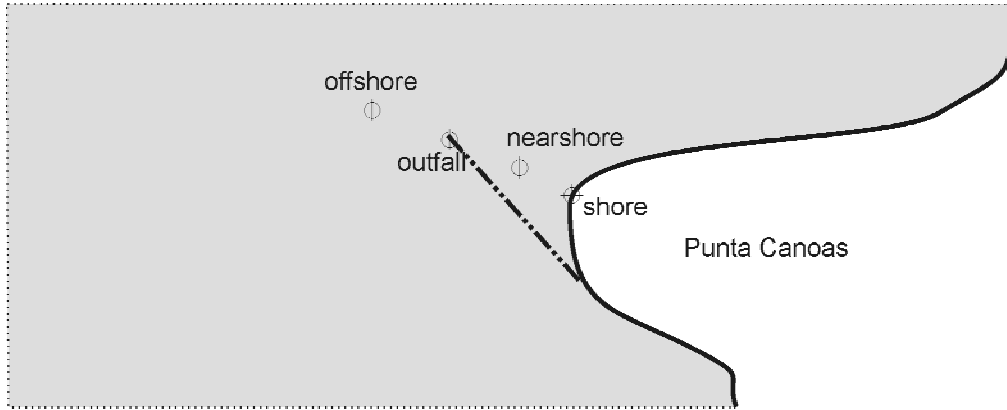


Fig. 137: Positions, where concentration data is saved as time-series, shown in Fig. 138

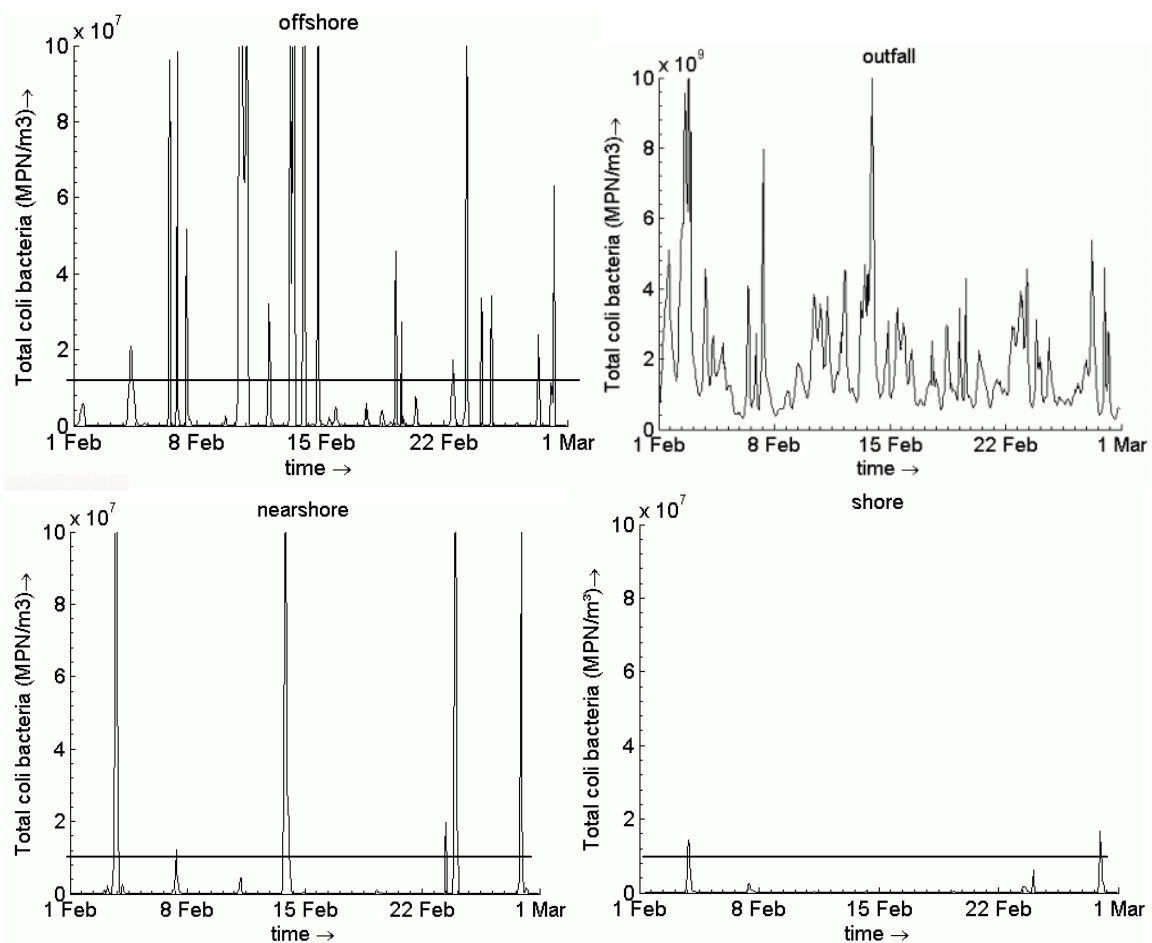


Fig. 138: Time-series of modeled depth averaged concentration [MPN/ m^3] of total coliforms at different locations (Fig. 137). The figure named “outfall” has an axis one magnitude larger than the others. Effluent concentration is $C_0 = 10^{11}$ MPN/ m^3 . Bathing water standard is $C = 10^7$ MPN/ $m^3 = 10^3$ MPN/100 ml (dashed line).

Fig. 139 shows the modeled exceedance frequencies for the month February 1998 and Fig. 140 for November 1999. For February 1998 at approximately four percent of the time, the standard is exceeded at the coast around Punta Canoas. This is in general agreement with the previous calculations made by Roberts (2004), shown in Fig. 141. In Roberts (2005), only yearly-averaged results for 1998 were presented so they cannot be compared directly with the present results for February 1998, although the magnitudes of the shoreline impacts and longitudinal plume extensions are similar. For November 1998, instead a direct comparison is possible. The contours in the present study are more curved around the local topography (Punta Canoas) compared to those in Roberts (2005) that are more linear along the current principal axes. This can be related to the effect of buoyant spreading motions in combination with on-shore winds in the present study. Roberts (2005) assumed the currents spatially homogeneous, which becomes less reliable with increasing distance from the current meter site. Longitudinal plume extension is very similar, though transversal plume extensions are not. Nevertheless, the conclusion is still similar, that the California exceedance standard of 20% is met far from the shore.

Concentrations in lower layers are smaller than in the surface layer. Beyond the 6th σ -layer (at the outfall location in a depth of about 9 m) almost no bacteria is found.

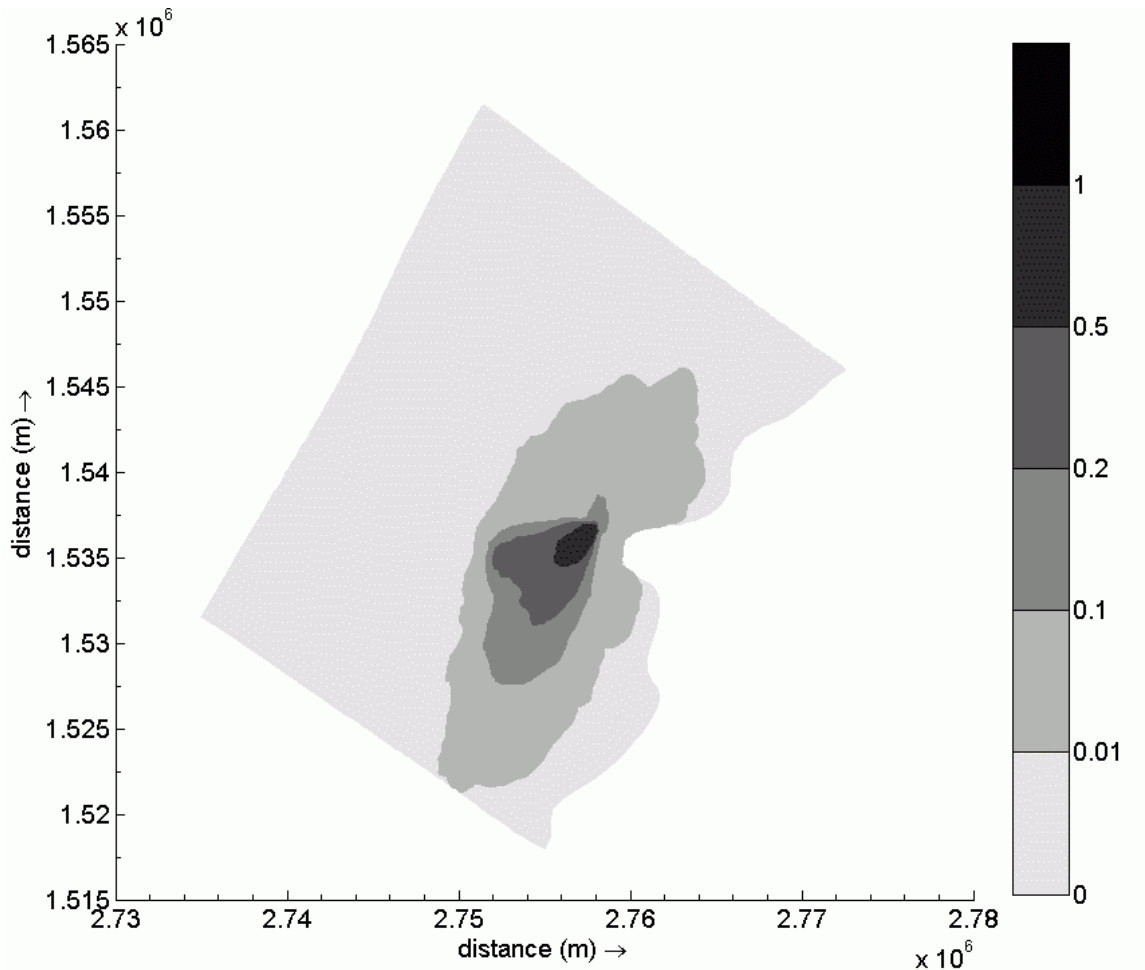


Fig. 139: Exceedance frequency of total coliforms exceeding 1000 MPN/100 ml for the month February 1998. Effluent concentration is $C_0 = 10^{11}$ MPN/m³.

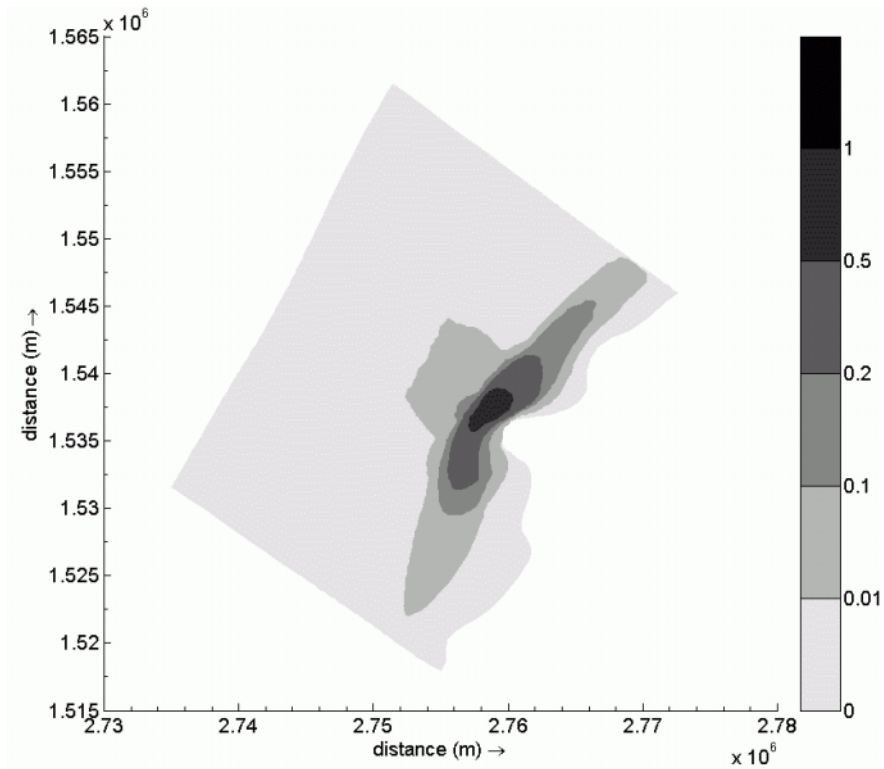


Fig. 140: Exceedance frequency of total coliforms exceeding 1000 MPN/100 ml for the month November 1998

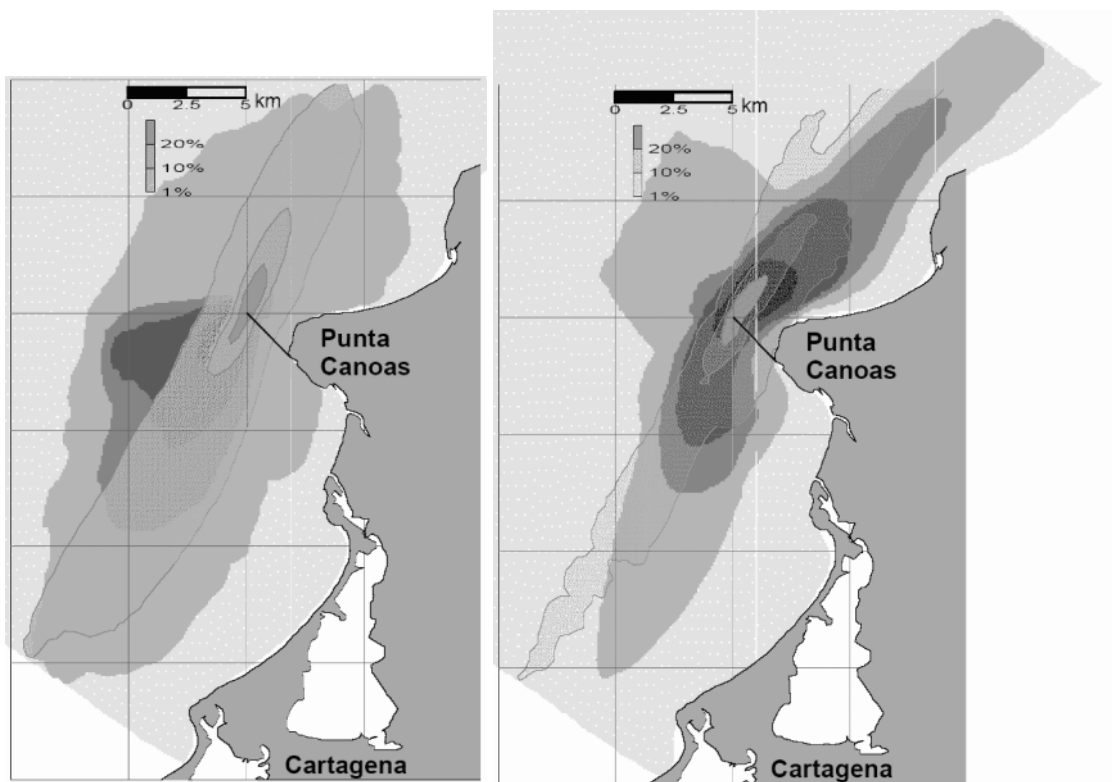


Fig. 141: Frequency that total coliforms exceed 1000 MPN / 100 ml, *left*: for Feb. 1998 (Delft3D) and the whole year 1998 (Roberts, 2005), and *right*: for Nov. 1998. Contours in foreground are modeled with NRFIELD-FRFIELD (exceedance frequencies for 1%, 10% and 20%, reproduced from Roberts, 2005) compared with the final results of the 3-D coupled modeling (*background*, where exceedance frequencies are shown for 1%, 10%, 20% and 50%).

7.8 Discussion and recommendations

A three-dimensional model was applied to the coastal environment around Cartagena, Colombia. The model used was Delft3D, developed by Delft Hydraulics. The model incorporates the ocean bathymetry and predicts ocean currents through the water column that are generated by wind stresses and the appropriate boundary conditions.

Although not sufficient boundary condition data has been available the present model setup allowed representing major characteristics of both, the measured velocity data at the outfall location and the large-scale influences compared with a large-scale model. Statistical characteristics are in reasonable agreement.

The hydrodynamic model was used to predict bacteria concentrations resulting from a planned wastewater discharge of the Cartagena district. The effluent is discharged via a 2.8 km long submerged outfall including a diffuser installation. Model linkage was realized by coupling the hydrodynamic results with the near-field mixing model CORMIX and linking both to a water quality model in Delft3D to predict bacteria concentrations including the modeling of bacterial decay.

Results show that compliance with near-shore water quality standards is guaranteed for 97 % of the time for worst-case scenarios of the months February 1998 and November 1999. This means, that compliance is even higher for all other months. A worst-case consequence would be a half-day beach closure on a monthly basis due to elevated bacteria concentrations. This is more than adequate in comparison with national or international public health standards. Furthermore, it allows for an effective solution of the existing water quality problems due to onshore discharges.

Comparison with results from Roberts (2005) show the advantage of the proposed coupling approach, which releases limitations for weak currents and spatial current variations, often resulting in underestimation of near-shore currents and intermediate-field processes. However, difficulties exist regarding the missing boundary condition information, such as current speed and direction and density over depth, and their variability with time. Coastal waters are usually very much undersampled, especially spatially, and such detail is almost never available. A complementary approach using both data sources is even more important for the modeling of flow conditions, which have not been covered by measurements. The present approach allows extending simulations in that direction. However, the present more rigorous and detailed approach confirms the other results that shoreline bacterial standards will be met by a large margin.

It has been shown, that buoyant spreading and wind-induced velocities enhance the plume transport, especially during periods of weak velocities. However, particularly during the worst-case November 1999, the shoreline bacterial levels were still considerably below the water quality standards. Moreover, instances of low current speeds are infrequent, and, when they occur, of short duration. Thus, concerns from the Inspection panel (Inspection panel, 2005) regarding limitations of the previously applied modeling approach and the present approach have been eliminated.

The results thus confirm that the present outfall design and siting complies with national and international standards. Compliance on one hand with near-field discharge criteria assuring protection of the area around the outfall itself and compliance on the other hand with bacteria standards improving public health.

- Case study -

8 Conclusions

Coastal waters are of enormous natural and economic importance for most countries in the world. However, coastal water quality is threatened in large part by uncontrolled wastewater discharges, causing severe public health impacts and environmental degradation. Unfortunately, the choice for the appropriate technological measure is manifold and the response of the coastal waters difficult to predict. The option for submarine outfalls in the form of submerged multiport diffusers has shown to be a very positive and reliable element in coastal water quality management. Prevailing uncertainties in the design of multiport diffusers and of predictions regarding the environmental impacts have been discussed and reduced. The integral approach taken allows designing the engineering structure optimized by parameters defining its integration into the environment. In addition, formulations for water quality regulations have been improved to correspond to physical processes and allow communicating predictive results to the beneficiary. This thesis covered the following contributions: First a multiport diffuser design program was developed. Secondly, two model systems for discharge analysis, CORMIX for the near-field and intermediate-field and Delft3D for the far-field were coupled, and third a regulatory procedure was proposed to license and monitor outfall installations.

CorHyd, the computer program developed for the hydraulic design of multiport diffusers, bypasses restrictions of previous diffuser programs by considering flexible geometry specifications with high risers and variable area orifices, all with automatic definition of loss coefficients. It calculates the flow distribution along the diffuser and the related pressure losses in the pipe system. Additional design features regarding blocked or closed ports, a sensitivity analysis and performance evaluation for varying parameters guarantees a proper diffuser operation and reduced costs for installation, operation and maintenance. Program capabilities have been demonstrated within two case studies for the Ipanema outfall in Rio de Janeiro, Brazil and the Berazategui outfall in Buenos Aires, Argentina. The applications showed strong sensitivity to the representation and formulation of local losses even for relatively simple riser/port configurations. The proposed optimization methodology converged relatively fast accounting for a homogeneous discharge distribution along the diffuser, minimization of the total head and prevention of sedimentation or ambient water intrusion in the diffuser under varying inflow and ambient conditions.

Submarine outfalls for treated municipal wastewater discharging in coastal waters pose a challenge for pollutant modeling because of large scale disparities. The waste dispersal can be conceptualized to occur in three hydrodynamic regions, according to dominant mixing processes. The near-field region is dominated by the source induced turbulent mixing in form of buoyant jets. The intermediate-field is characterized by small mixing, but strong spreading motions due to boundary interactions and buoyant spreading processes. The far-field region is dominated by the ambient flow, where advection causes the wastefield to be transported and ambient diffusion causes further wastefield spreading. Time scales of far-field processes can be large, thus water quality parameters need to be considered in addition to physical processes. Scale analysis showed, that the only feasible modeling approach is by coupling zonal models applied for each hydrodynamic region. The chosen models are CORMIX for the near-field and intermediate-field and Delft3D for the far-field. Special attention was given to the intermediate-field modeling, which generally has been neglected in previous coupling approaches. The CORMIX flow classification system proved to be an important component for the modeling approach. It allows distinguishing between the hydrodynamic regions in general

and applicable modeling tools for specific flow conditions in particular. The existing set of length scales as base for the flow classification has been extended by additional unsteady length and time scales. These define, whether buoyant spreading results as predicted by the steady intermediate-field model, correlate to the unsteady motions in the receiving waters. The proposed coupling approach is based on three main steps. Firstly, the coupling module CorField classifies and analyses available field-data. Resulting time-series are computed to correspond with CORMIX and Delft3D input file formats. Secondly, the CorTime module is applied to a baseline near-field / intermediate-field modeling. Resulting time-series include dilutions, plume locations and plume geometries until the end of the intermediate-field region for every single time-step. An evaluation of the mixing performance might be used for optimizations regarding the outfall configuration. Thirdly, CorTime results are classified with the new unsteady scales, to define the appropriate coupling position. The CorLink coupling module therefore computes source-files for the Delft3D model according to the chosen far-field grid resolution and intermediate-field plume geometry and concentration. The water quality model within Delft3D is then run with these source files to compute the substance concentrations.

The coupling approach was applied to the planned outfall for the city of Cartagena in Colombia. The study incorporated the ocean bathymetry and predicted ocean currents and density distributions through the water column that are generated by wind stresses and the appropriate boundary conditions. Although insufficient boundary condition data has been available the present model setup allowed representing major characteristics of both the measured velocity data at the outfall location and the large-scale influences compared with a large-scale model. Statistical characteristics are in reasonable agreement. The flow classification system showed that intermediate-field processes are significant especially for the period of November 1998. Model linkage was realized by coupling the hydrodynamic results with the near-field mixing model CORMIX and linking both to a water quality model in Delft3D to predict bacteria concentrations including the modeling of bacterial decay. Results show that compliance with near-shore water quality standards is guaranteed for 97% of the time for worst-case scenarios of the months February 1998 and November 1999. Furthermore the coupled computation gives more realistic results than previous approaches.

Unfortunately, existing regulatory control measures (e.g. those in the EU-WFD) do not necessarily correspond to physical facts involved in coastal wastewater discharges. Most water quality regulations omit the definition of the location, where environmental quality standards apply. Therefore two regulatory amendments have been proposed. First, the *regulatory discharge zone* defines a limited region around the outfall, where general environmental quality standards apply. This definition accounts for the fact, that mixing processes need space and time to reduce effluent concentrations. Second, the *regulatory preservation zone* defines a limited region around preserved areas, like beaches or protected areas, where specific environmental quality standards are defined in addition to the general ones. Both definitions improve the procedure of either licensing or monitoring wastewater outfalls. The application within the case study for the Cartagena outfall shows that results presented in that way considerably improve the understanding of coastal wastewater discharges and their efficiency in improving water quality and public health for the coastal environment.

9 Outlook

The computed pollutant concentrations of this study were based on measured scenarios, calculating the missing velocity data on one hand and predicting the changes due to a planned discharge on the other hand. Due to moderate computation times it might be feasible to extend that hindcasting to a full forecasting system. Therefore the existing model could be used to run scenarios with modified boundary conditions, for example linked to forecasted meteorological data or even climate change models and predict concentration distributions for the near future or long term impacts due to climate change. Similar to a weather forecast and storm warning systems such a system could be used as a forecast or warning system for beach water quality. Such systems are planned (e.g. from NOAA for the Great Lakes, www.glerl.noaa.gov), already in operation (e.g. from DHI at Copenhagen beaches, <http://bathingwater.dhigroup.com>), and will be increasingly developed.

The present study was focused on wastewater discharges into coastal waters using multipoint diffuser installations. Amplifications of the approach presented are specifically interesting for considerations of other effluents and receiving waters. For example dense discharges from desalination plants, or thermal discharges from power plants or accidental spills might be of major interest for further studies. Especially dense discharges pose a challenging problem, because of the irregular bathymetry strongly influencing the resulting density currents. Discharges into rivers or lakes, however, can probably be modeled directly with the present approach, because the current fields are uni-directional and less unsteady.

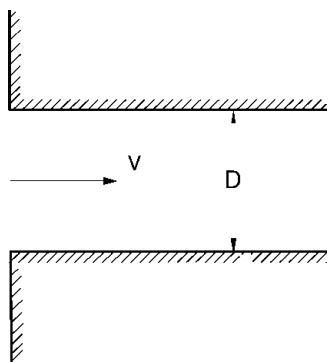
Another amplification should consider the transport of non-dissolved substances, like pollutants attached to particles, which undergo further settling and resuspension. This would extend the predictions regarding environmental impacts to more ecological parameters, including sediment quality or biotic life and habitat conditions. Wave motions then might influence the problem and thus be included in the modeling approach.

However, a major problem is still related to an accurate representation of the coastal current and density fields. Hydrodynamic models still may include a high degree of uncertainty, especially, when only little field data is available. A good measure for evaluating uncertainty for coastal water flows is near-coast oceanographic analysis based on oceanographic principles. An inclusion of such analysis in engineering hydraulics would probably improve the understanding of coastal flows. Another issue is the uncertainties related to real predictions or forecasts, rather than hindcasting. The application of climate models would then be needed to predict winds and temperatures, water levels and densities. However, this is only possible on large scales, but not on scales influenced by a submarine outfall discharge. This problem seems to remain even with the perspective of strongly increasing computer power. Increasing domain sizes and resolutions and higher order numerical methods still demand proper boundary conditions. An improvement of spatial field-measurement techniques, like the Ocean Surface Current Radar (OSCR) will probably contribute more to the solution of that problem than different numerical schemes.

- Conclusions -

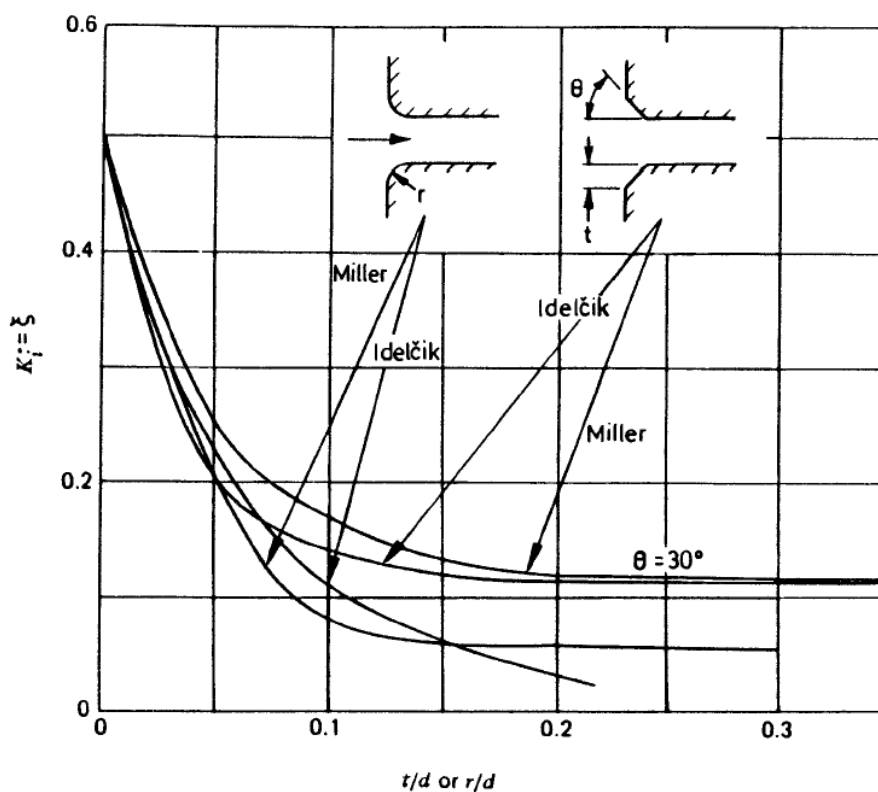
Annex A Loss coefficients in CorHyd

Type	Definition
Inlet (Reference velocity is V)	Sharp edged inlet (Idelchik, 1986) $\zeta = 0.5$



The value $\zeta = 0.5$ is automatically implemented in the code, if a feeder pipe exists. Although most of the constructions do have sharp edged inlets from the headworks into the feeder pipe other configurations may be applied by using the following graphs and changing the code in the mentioned files (zeta_entry = "new value").

Rounded inlets (Idelchik, 1986, Miller, 1978)

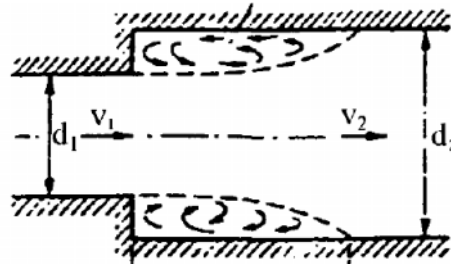


The loss coefficient ζ for rounded (radius r) or edged inlets (angle Θ and edge width t) depends on either the relation of rounding radius r and the pipe diameter d or the edge width t and the pipe diameter d as well as the angle Θ .

Expansion Sudden expansion (Idelchik, 1986)

(Reference velocity is V_1)

$$\zeta_e = \left(1 - \frac{A_1}{A_2}\right)^2 = \left(1 - \left(\frac{d_1}{d_2}\right)^2\right)^2$$



Gradual expansion (Idelchik 1986)

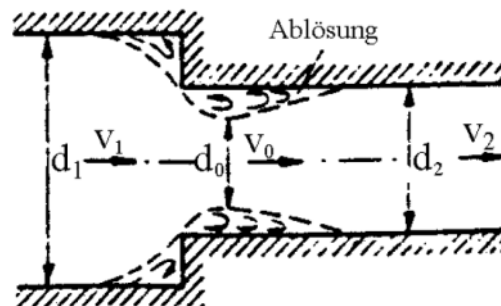
$$\zeta_e = 3.2 \cdot \tan \frac{\beta}{2} \cdot \sqrt[4]{\tan \frac{\beta}{2} \left(1 - \frac{A_1}{A_2}\right)^2}$$

with β in rad

Contraction Sudden contraction (Idelchik, 1986)

(Reference velocity is V_2)

$$\zeta_c = 0.5 \cdot \left(1 - \frac{A_2}{A_1}\right)^{3/4} = 0.5 \cdot \left(1 - \left(\frac{d_2}{d_1}\right)^2\right)^{3/4}$$



Gradual contraction (Idelchik 1986)

$$\zeta_c = \left(-0.0125 \cdot n_0^4 + 0.0224 \cdot n_0^3 - 0.00723 \cdot n_0^2 + 0.0044 \cdot n_0 - 0.00745\right) \cdot (\beta^3 - 2\pi\beta^2 - 10\beta)$$

with $n_0 = \frac{A_0}{A_1} \leq 1.0$ and β in rad

Bending Bend (Kalide 1980)

(reference velocity = velocity after bending)

$$\zeta_0 = \left[0.131 + 0.159 \left(\frac{D}{R}\right)^{3.5}\right] \cdot \frac{\delta}{180^\circ}$$

where D is the pipe diameter and R the radius of the bend. Often applied as $R = 3D$. Delta is the angle of the bend (e.g. 90° for rectangular bends).

Friction due to bend (Idelchik 1986)

$$\zeta_{fr} = \lambda \frac{L}{D} \text{ with } \frac{L}{D} = \pi \frac{\delta}{180^\circ} \frac{R}{D}$$

Division of flow **T-division** (Idelchik 1986)

$$\zeta_t = 1 + 1.5(\alpha A_r/A_p)^2$$

Flow is divided equally at an end of a pipe.

Unequal flow division (Idelchik 1986)

Branch (entering riser): $\zeta_s = \zeta_{c,s} / (V_r/V_d)^2$

Main pipe: $\zeta_{st} = \zeta_{c,st} / (V_r/V_d)^2$

with an angle between riser and diffuser axis assumed to be nearly 90°, and where $\zeta_{c,st}$ from Fig. 142 - Fig. 144 (Idelchik, 1986), $\zeta_{c,s} = A_\zeta \zeta'_{c,s}$, with

determination of A_ζ from Idelchik (1986, Paragraph 15)

$A_r/A_d \leq 0.35$ and $q_r/q_d \leq 0.4$ $A_\zeta = 1.1 - 0.7 q_r/q_d$

$A_r/A_d \leq 0.35$ and $q_r/q_d > 0.4$ $A_\zeta = 0.85$

$A_r/A_d > 0.35$ and $q_r/q_d \leq 0.6$ $A_\zeta = 1 - 0.65 q_r/q_d$

$A_r/A_d > 0.35$ and $q_r/q_d > 0.6$ $A_\zeta = 0.6$

and determination of $\zeta'_{c,s}$

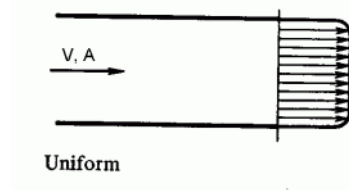
$D_r/D_d \leq 2/3$ $\zeta'_{c,s} = 0.7956(V_r/V_d)^2 + 0.2732(V_r/V_d) + 0.956$

$D_r/D_d = 1$ $\zeta'_{c,s} = 0.3(V_r/V_d)^2 + 1$

$2/3 < D_r/D_d < 1$ $\zeta'_{c,s} = 0.3(V_r/V_d)^2 + 1 + (1 - D_r/D_d)(1 - 2/3)((0.7956(V_r/V_d)^2 + 0.2732(V_r/V_d) + 0.956) - (0.3(V_r/V_d)^2 + 1))$

Orifices **Straight orifice**

$$\zeta = 1$$



In addition, especially for straight orifices covered with perforated plates further losses can be added (e.g. Fig. 145 - Fig. 147)

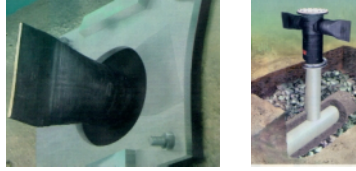
Side branching orifice (Fischer et al. 1979)

For sharp-edged and rounded orifices see eq. (4.25) and (4.26)

Flexible orifices (duckbills)

Lee et.al. (1998) , Red Valve Company, Abromaitis 1995, Elasto-Valve Rubber Products (EVR)

$$\zeta_{duck} = \frac{H \cdot (\rho_e \cdot g)}{\rho_e \cdot \frac{V_{duck}^2}{2}} = \frac{2 \cdot H \cdot g}{V_{duck}^2}$$



Where H denotes the headloss, V_{duck} the discharge velocity which depends on the effective open area A_{duck} which depends on the flow through the valve. All these parameters are dependent also on the used stiffness of the rubber material. The following formulas are taken from Lee et al. (1998) but should be adapted to the used material from the providing company. If other materials are used the following formulations have to be modified in the code.

Tideflex	H [m]	A_{duck} [cm ²]	V_{duck} [m/s]
TF 100	0,0634 * Q	13,075 ln Q - 9,201	1,3485 $Q^{0,5536}$
	0,0606 * Q		0,9090 $Q^{0,6089}$
TF 150	0,0232 * Q	38,828 ln Q - 27,300	0,5277 $Q^{0,5558}$
	0,0235 * Q		0,6084 $Q^{0,5638}$
TF 200	0,0124 * Q	40,466 ln Q - 6,429	0,2917 $Q^{0,5967}$
	0,0129 * Q		0,4692 $Q^{0,5395}$
TF 305	0,0067 * Q	95,950 ln Q - 200,940	0,4529 $Q^{0,4732}$
	0,0052 * Q		0,3091 $Q^{0,5203}$

with Q in [l/s]

Inaccuracies in pipe siting

$\zeta = n \zeta_s$, where n is the number of fittings (ATV-DVWK A110, 2001)

D [mm]	ζ_s
200	0.017
300	0.014
400	0.012
500	0.010
600 - 1000	0.005
> 1000	0

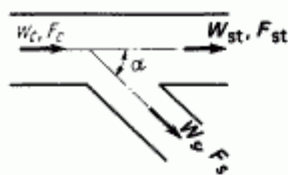
Inaccuracies in pipe fittings

$\zeta = n \zeta_f$, where n is the number of fittings (ATV-DVWK A110, 2001)

D [mm]	ζ_f
200	0.009
300	0.006
400	0.004
500	0.003
600 - 1000	0.0015
> 1000	0.001

Diverging wye of the type $F_s + F_{st} > F_c$; $F_{st} = F_c$;
 $\alpha = 0-90^\circ$. Side branching. [10]

Diagram
 7-15



1. $0 < \alpha < 60^\circ$ and $\alpha = 90^\circ$ at $h_s/h_c \leq 2/3$:

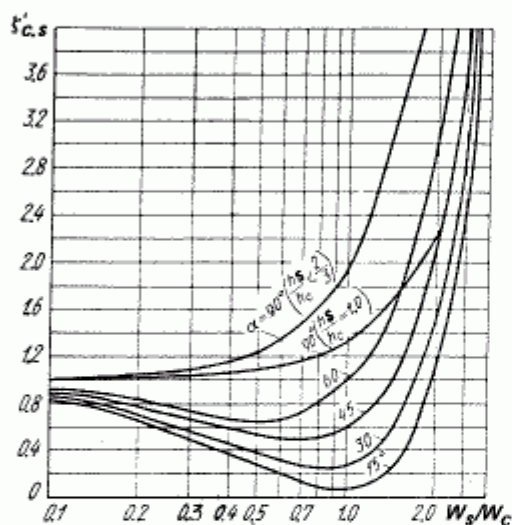
$$\zeta_{c,s} = \frac{\Delta p_s}{\rho w_c^2 / 2} = A' \left[1 + \left(\frac{w_s}{w_c} \right)^2 - 2 \frac{w_s}{w_c} \cos \alpha \right] = A' \zeta'_{c,s}$$

2. $\alpha = 90^\circ$ and $h_s/h_c = 1.0$ (up to $w_s/w_c \approx 2.0$):

$$\zeta_{c,s} = \frac{\Delta p_s}{\rho w_c^2 / 2} = A' \left[1 + 0.3 \left(\frac{w_s}{w_c} \right)^2 \right] = A' \zeta'_{c,s}$$

where for $\zeta'_{c,s}$, see the curves $\zeta'_{c,s} = f(w_s/w_c)$ at different α ; for A , see paragraph 15.

h_s is the height of the cross section of the side branch;
 h_c is the height of the cross section of the common straight channel



$$\zeta_s = \frac{\Delta p_s}{\rho w_s^2 / 2} = \frac{\zeta_{c,s}}{(w_s/w_c)^2}$$

$$\frac{w_s}{w_c} = \frac{Q_s F_c}{Q_c F_s}$$

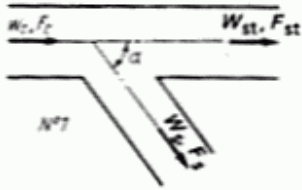
Values of $\zeta'_{c,s}$

$\frac{w_s}{w_c}$	$\alpha, ^\circ$				$\alpha = 90^\circ$	
	15	30	45	60	$h_s/h_c \leq 2/3$	$h_s/h_c = 1.0$
0	1.0	1.0	1.0	1.0	1.0	1.0
0.1	0.82	0.84	0.87	0.91	1.01	1.0
0.2	0.65	0.70	0.75	0.84	1.04	1.01
0.4	0.38	0.46	0.60	0.76	1.16	1.05
0.6	0.20	0.31	0.50	0.65	1.35	1.11
0.8	0.09	0.25	0.51	0.80	1.64	1.19
1.0	0.07	0.27	0.58	1.00	2.00	1.30
1.2	0.12	0.36	0.74	1.23	2.44	1.43
1.4	0.24	0.70	0.98	1.54	2.96	1.59
1.6	0.46	0.80	1.30	1.98	3.54	1.77
2.0	1.10	1.52	2.16	3.00	4.60	2.20
2.6	2.75	3.23	4.10	5.15	7.76	-
3.0	7.20	7.40	7.80	8.10	9.00	-
4.0	14.1	14.2	14.8	15.0	16.0	-
5.0	23.2	23.5	23.8	24.0	25.0	-
6.0	34.2	34.5	35.0	35.0	36.0	-
8.0	62.0	62.7	63.0	63.0	64.0	-
10	98.0	98.3	98.6	99.0	100	-

Fig. 142: Diagram for the coefficients to compute the loss coefficient for a flow division (reproduced from Idelchik, 1986)

Diverging wye of the type $F_s + F_{st} > F_c$ and $F_s + F_{st} = F_c$;
 $\alpha = 0-90^\circ$. Passage [10]

Diagram
 7-17

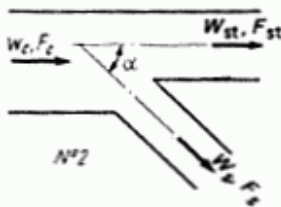


No. 1. $F_s + F_{st} > F_c$ at $w_{st}/w_c \leq 1.0$:

$$\zeta_{c,st} = \frac{\Delta p_{st}}{\rho w_c^2 / 2} \approx 0.4 \left(1 - \frac{w_{st}}{w_c}\right)^2$$

1. Values of $\zeta_{c,st}$

$\frac{w_{st}}{w_c}$	$\alpha = 15-90^\circ$ at $F_{st}/F_c = 0-1.0$
0	0.40
0.1	0.32
0.2	0.26
0.3	0.20
0.4	0.14
0.5	0.10
0.6	0.06
0.8	0.02
1.0	0



No. 2. $F_s + F_{st} = F_c$ at $w_{st}/w_c \geq 1.0$:

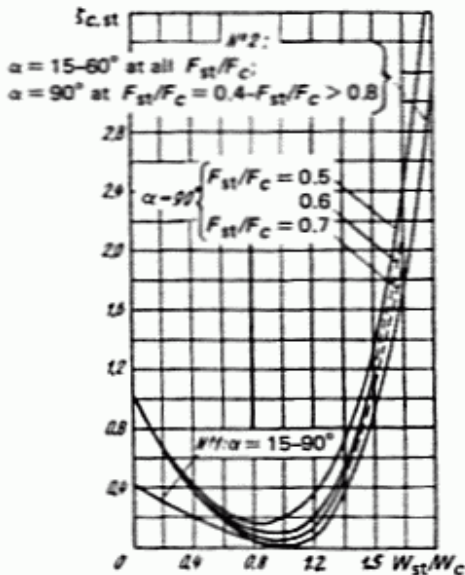
$$\zeta_{c,st} = \frac{\Delta p_{st}}{\rho w_c^2 / 2}$$

see the curves $\zeta_{c,st} = f(w_{st}/w_c)$:

$$\zeta_{st} = \frac{\Delta p_{st}}{\rho w_{st}^2 / 2} = \frac{\zeta_{c,st}}{(w_{st}/w_c)^2}$$

$$\frac{w_{st}}{w_c} = \frac{Q_{st} F_c}{Q_c F_{st}}$$

Values of $\zeta_{c,st}$

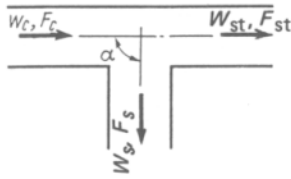


$\frac{w_{st}}{w_c}$	α					
	$15-60^\circ$		90°			
	F_{st}/F_c					
	0-1.0	0-0.4	0.5	0.6	0.7	>0.8
0	1.00	1.00	1.00	1.00	1.00	1.00
0.1	0.81	0.81	0.81	0.81	0.81	0.81
0.2	0.64	0.64	0.64	0.64	0.64	0.64
0.3	0.50	0.50	0.52	0.52	0.50	0.50
0.4	0.36	0.36	0.40	0.38	0.37	0.36
0.5	0.25	0.25	0.30	0.28	0.27	0.25
0.6	0.16	0.16	0.23	0.20	0.18	0.16
0.8	0.04	0.04	0.17	0.10	0.07	0.04
1.0	0.00	0.00	0.20	0.10	0.05	0.00
1.2	0.07	0.07	0.36	0.21	0.14	0.07
1.4	0.39	0.39	0.79	0.59	0.39	-
1.6	0.90	0.90	1.40	1.16	-	-
1.8	1.78	1.78	2.44	-	-	-
2.0	3.20	3.20	4.00	-	-	-

Fig. 143: Diagram for the coefficients to compute the loss coefficient for a flow division (reproduced from Idelchik, 1986)

Threaded wyes of the type $F_s + F_c > F_c; F_{st} = F_c$;
made of malleable iron; $\alpha = 90^\circ$ [2]

Diagram
7-18



Side branch

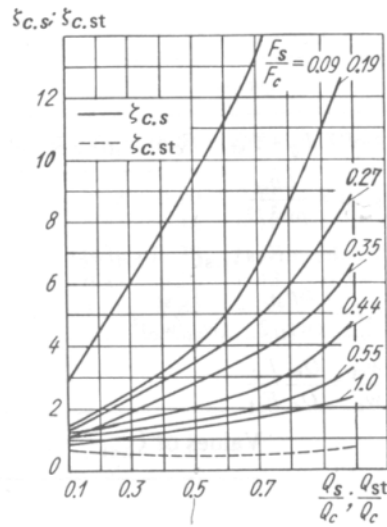
$$\zeta_{c.s} = \frac{\Delta p_s}{\rho W_s^2 / 2}, \text{ see the curves } \zeta_{c.s} = f(Q_s / Q_c) \text{ at different } F_s / F_{st};$$

$$\zeta_s = \frac{\Delta p_s}{\rho W_s^2 / 2} = \frac{\zeta_{c.s}}{(Q_s F_c / Q_c F_s)^2}$$

Straight passage

$$\zeta_{c.st} = \frac{\Delta p_{st}}{\rho W_{st}^2 / 2}, \text{ see the curve } \zeta_{c.st} = f(Q_{st} / Q_c) \text{ at all } F_s / F_c;$$

$$\zeta_{st} = \frac{\Delta p_{st}}{\rho W_{st}^2 / 2} = \frac{\zeta_{c.st}}{(1 - Q_s / Q_c)^2 (F_c / F_{st})^2}$$



Values of $\zeta_{c.s}$ and $\zeta_{c.st}$

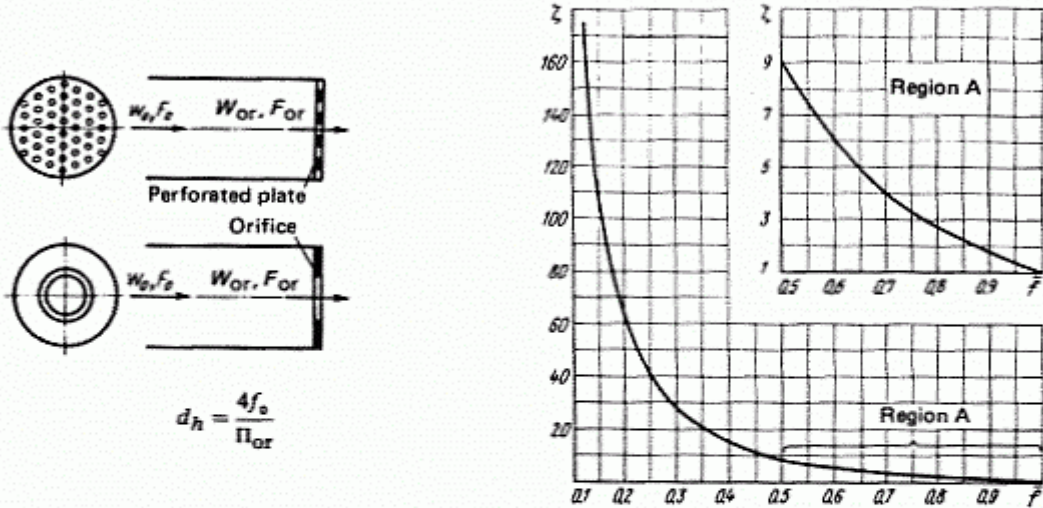
F_s / F_c	Q_s / Q_c (Q_{st} / Q_c)									
	0.1	0.2	0.3	0.4	0.5	0.6	0.7	0.8	0.9	1.0
	Values of $\zeta_{c.s}$									
0.09	2.80	4.50	6.00	7.88	9.40	11.1	13.0	15.8	20.0	24.7
0.19	1.41	2.00	2.50	3.20	3.97	4.95	6.50	8.45	10.8	13.3
0.27	1.37	1.81	2.30	2.83	3.40	4.07	4.80	6.00	7.18	8.90
0.35	1.10	1.54	1.90	2.35	2.73	3.22	3.80	4.32	5.28	6.53
0.44	1.22	1.45	1.67	1.89	2.11	2.38	2.58	3.04	3.84	4.75
0.55	1.09	1.20	1.40	1.59	1.65	1.77	1.94	2.20	2.68	3.30
1.00	0.90	1.00	1.13	1.20	1.40	1.50	1.60	1.80	2.06	2.80
	Values of $\zeta_{c.st}$									
At all F_s / F_c	0.70	0.64	0.60	0.57	0.55	0.51	0.49	0.55	0.62	0.70

Fig. 144: Diagram for the coefficients to compute the loss coefficient for a flow division (reproduced from Idelchik, 1986)

Discharge from a straight tube through an orifice or a perforated plate (grid) with sharp-edged orifices ($l/d_h = 0-0.015$);
 $Re = w_{or} d_h / \nu > 10^5$ [14-16]

Diagram
 11-18

$$\xi = \frac{\Delta p}{\rho w_0^2 / 2} = (1 + 0.707 \sqrt{1 - \bar{f}})^2 \frac{1}{\bar{f}^2}, \text{ see the graph}$$



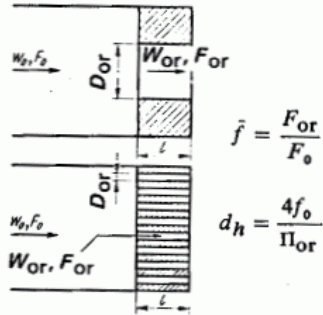
\bar{f}	0.05	0.10	0.15	0.20	0.25	0.30	0.35	0.40	0.45
ξ	1140	280	122	67	41.6	30.0	20.2	15.0	11.5
\bar{f}	0.50	0.55	0.60	0.65	0.70	0.75	0.80	0.85	0.9
ξ	9.00	7.40	6.20	4.80	3.90	3.30	2.70	2.22	1.80

Fig. 145: Additional loss coefficients for orifices (reproduced from Idelchik, 1986)

Discharge from a straight tube through an orifice or a perforated plate (grid) with differently shaped orifice edges; $Re = w_{or} d_h / \nu > 10^4$ [14-16]

11-19

Scheme and graph Resistance coefficient

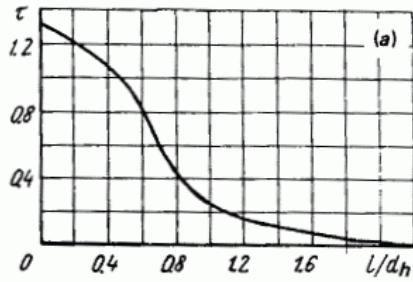
$$\zeta = \frac{\Delta p}{\rho w_o^2 / 2}$$


$$\zeta = \left\{ \left[1 + 0.5(1 - \bar{f}) + \tau \sqrt{1 - \bar{f}} \right] + \lambda \frac{l}{d_h} \right\} \frac{1}{\bar{f}^2}$$

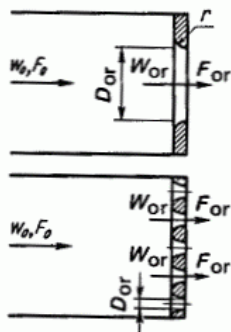
$$= \left(\zeta_o + \lambda \frac{l}{d_h} \right) \frac{1}{\bar{f}^2}$$

where $\zeta_o = 1 + 0.5(1 - \bar{f}) + \tau \sqrt{1 - \bar{f}}$; for λ , see Diagrams 2-1 through 2-6; $\tau = f(l/d_h)$

Thick walled orifices



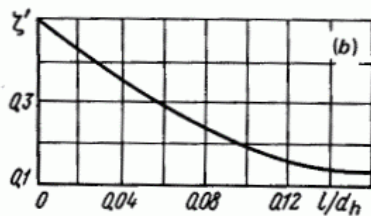
$\frac{l}{d_h}$	0	0.2	0.4	0.6	0.8
τ	1.35	1.22	1.10	0.84	0.42
$\frac{l}{d_h}$	1.0	1.2	1.6	2.0	2.4
τ	0.24	0.16	0.07	0.02	0



$$\zeta = [1 + \sqrt{\zeta'(1 - \bar{f})}]^2 \frac{1}{\bar{f}^2}$$

where $\zeta' = f(l/d_h)$

Orifice edges beveled in the flow direction



$\frac{l}{d_h}$	0.01	0.02	0.03	0.04
ζ'	0.46	0.42	0.38	0.35
$\frac{l}{d_h}$	0.06	0.08	0.12	0.16
ζ'	0.29	0.23	0.16	0.13

552

Fig. 146: Additional loss coefficients for orifices (reproduced from Idelchik, 1986)

(Continued)

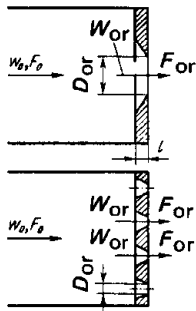
Discharge from a straight tube through an orifice or a perforated plate (grid) with differently shaped orifice edges; $Re = w_{or} d_h / \nu > 10^4$ [14-16]

Diagram
11-19

Resistance coefficient

Scheme and graph

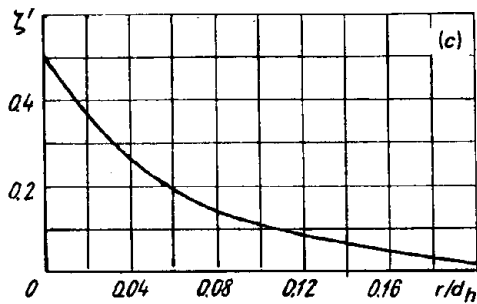
$$\zeta = \frac{\Delta p}{\rho w_0^2 / 2}$$



$$\zeta = [1 + \sqrt{\zeta'(1 - \bar{f})}]^2 \frac{1}{\bar{f}^2}$$

where $\zeta' = f\left(\frac{r}{d_h}\right)$

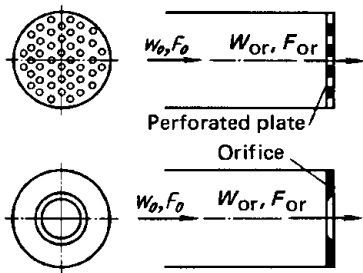
Orifice edges rounded in the flow direction



$\frac{r}{d_h}$	0	0.01	0.02	0.03	0.04	0.05
ζ'	0.50	0.44	0.37	0.31	0.26	0.22
$\frac{r}{d_h}$	0.06	0.08	0.12	0.16	0.20	
ζ'	0.19	0.15	0.09	0.06	0.03	

Discharge from a tube through an orifice or a perforated plate (grid) with differently shaped orifice edges in transition and laminar regions ($Re = w_{or} D_h / \nu < 10^4 - 10^5$, tentatively) [14-16]

Diagram
11-20



1) $25 < Re < 10^4 - 10^5$:

$$\zeta = \frac{\Delta p}{\rho w_0^2 / 2} = \zeta_\phi \frac{1}{\bar{f}^2} + \bar{\epsilon}_0 Re \zeta_{qu}$$

2) $10 < Re < 25$:

$$\zeta = \frac{33}{Re} \frac{1}{\bar{f}^2} + \bar{\epsilon}_0 Re \zeta_{qu}$$

3) $Re < 10$:

$$\zeta = \frac{33}{Re} \frac{1}{\bar{f}^2}$$

$$D_h = \frac{4F_{or}}{\Pi_{or}}$$

$$\bar{f} = \frac{F_{or}}{F_0}$$

where $\bar{\epsilon}_0 Re = f_2(Re)$ and $\zeta_\phi = f_1(Re, F_0/F_1)$, see Diagram 4-19 (it is assumed that $\bar{f} = F_{or}/F_0$ corresponds to F_0/F_1); ζ_{qu} is determined as at $Re > 10^4 - 10^5$ from Diagrams 11-18 and 11-19.

Fig. 147: Additional loss coefficients for orifices (reproduced from Idelchik, 1986)

Annex B Example of CorHyd report

If the report radio button has been activated for the output, an ASCII file is written to the program directory containing the following information:

The header with the date:

```

                Summary of the results
27-Apr-2005
-----
-----

```

Input data:

```

INPUT ambient data
Water level Hd [m] above datum (z = 0 m): Hd =
  4.00
Ambient density rho_0 in [kg/m³]
1000.00
-----

```

```

INPUT effluent data
Density rho_e of effluent in [kg/m³]
999.00
Flowrate of effluent in [m³/s]
 33.62
-----

```

```

INPUT outfall sections
Length, slope, x, y, and z coordinates for different sections
#   Length Slope      x          y          z
-   -         -      -          -          -
1   450.00   0.00  7050.00      0.00   0.00  -2.50
2   500.00   0.00  6550.00      0.00   0.00  -2.50
3   2050.00          0.00  4500.00      0.00   0.00  -2.50
4   4480.00          0.00   20.00      0.00  -2.50
5    21.03   0.31   0.00    0.00   4.00
-----

```

Output data:

```

OUTPUT flowrates and velocities
Riser Discharges (q), Total discharge (Q), Port Velocities (Vp) and diameter (Dp), Jet
Velocities (Vj), Riser Velocities (Vr),
Densimetric Froude number, Diffuser diameter (Dd) & Diffuser Velocities (Vd) upstream
of port #
#   q [m³/s]          Q [m³/s]          Vp[m/s] Dp[m]          Vj[m/s] Vr [m/s] Fr[-]
Vd [m/s] Dd [m]
1   4.633519e-001  4.633519e-001  5.1034  0.170  5.1034  1.6388  124.9  0.3010  1.400
2   4.595955e-001  9.229474e-001  5.0621  0.170  5.0621  1.6255  123.9  0.5996  1.400
3   4.579980e-001  1.380945e+000  5.0445  0.170  5.0445  1.6198  123.5  0.8971  1.400
4   4.558982e-001  1.836844e+000  5.0213  0.170  5.0213  1.6124  122.9  1.1932  1.400
5   4.548185e-001  2.291662e+000  5.0095  0.170  5.0095  1.6086  122.6  1.4887  1.400
6   4.550564e-001  2.746719e+000  5.0121  0.170  5.0121  1.6094  122.7  1.7843  1.400
7   4.569866e-001  3.203705e+000  5.0333  0.170  5.0333  1.6163  123.2  2.0812  1.400
8   4.610083e-001  3.664713e+000  5.0776  0.170  5.0776  1.6305  124.3  2.3806  1.400
...
-----

```

```

OUTPUT riser locations - intersection with pipe centerline

```

```

#   x          y          z
1   7500.000      0.000  -2.500
2   7450.000      0.000  -2.500
3   7400.000      0.000  -2.500
4   7350.000      0.000  -2.500
5   7300.000      0.000  -2.500
6   7250.000      0.000  -2.500
7   7200.000      0.000  -2.500
8   7150.000      0.000  -2.500
9   7100.000      0.000  -2.500
10  7050.000      0.000  -2.500
11  7000.000      0.000  -2.500
....
-----

```

```

OUTPUT losses and total head

```

Name of loss	Loss [m]	% of the relative head
Inlet head loss [m]	0.080	1.3
Feeder head loss [m]	5.141	81.4
Diffuser head loss [m]	0.206	3.3
Av. port/riser headloss [m]	0.069	1.1
(Max. port/riser headloss [m])	0.226	3.6
(Min. port/riser headloss [m])	-0.000	-0.0

- Annex -

Av. jet velocity head [m]	0.196	3.1
(Max. jet velocity head [m])	0.213	3.4
(Min. jet velocity head [m])	0.184	2.9
Density head difference [m fresh water]	0.676	10.7

Sum of averages [m]	6.368	100.8
(Sum of all maximum losses [m])	6.543	103.6
(Sum of all minimum losses [m])	6.287	99.5

Calc. relative total head, above sea level [m]	6.316
Calc. absolute total head [m]	33.316

Losses in port/riser configuration at position i

#	Headloss in port/riser [m]
1	0.879
2	0.905
3	0.926
4	0.962
5	1.008
6	1.067
7	1.143
8	1.236
....	

 OUTPUT design recommendations (Fischer et al, 1979)

(Sum of Area of ports cross-sections downstream) / (Area of diffuser cross sections)

#	(Sum Ap(#)) / Ad(#)
1	0.059
2	0.118
3	0.177
4	0.236
5	0.295
6	0.354
....	

END OF RESULTS

References

- Abessa, D.M.S., Carr, R.S., Rachid, B.R.F., Sousa, E.C.P.M., Hortelani, M.A., and Sarkis, J.E., 2005, "Influence of A Brazilian sewage outfall on the toxicity and contamination of adjacent sediments", *Marine Pollution Bulletin*, 50, 875-885
- Abromaitis, A.T., and Raftis, S.G., 1995, "Development and Evaluation of a Combination Check Valve / Flow Sensitive Variable Orifice Nozzle for use on Effluent Diffuser Lines", *Proceedings of the 68th Annual Conference & Exposition "Water Environment Federation"*, October 21 –25, Miami Beach, USA,
- Adams, E.E., Stolzenbach, K.D., and Harleman, D.R.F., 1975, "Near and far field analysis of buoyant surface discharges into large bodies of water", Techn. Rep. 205, *MIT Parsons Laboratory*
- Akar, P.J., and Jirka, G.H., 1994, "Buoyant Spreading Processes in Pollutant Transport and Mixing. Part I: Lateral Spreading in Strong Ambient Current", *J. Hydraulic Research*, 32, 815-831
- Akar, P.J., and Jirka, G.H., 1991, "CORMIX2: An expert system for hydrodynamic mixing zone analysis of conventional and toxic submerged multiport diffuser discharges", *U.S. Environmental Protection Agency*, Tech. Rep. EPA/600/3-91/073, Env. Res. Lab, Athens, Georgia
- Akar, P.J., and Jirka, G.H., 1995, "Buoyant Spreading Processes in Pollutant Transport and Mixing. Part II: upstream spreading in weak ambient current", *J. Hydraulic Research*, 33(1), 87-100
- Alfredini, P. and Roma, M.C.B., 1999, "As condicionantes referents a Hidraulica Maritima na Disposicao Oceanica de Esgoto na Costa Paulista", Relatorio 2, *Escola Politecnica da Universidade de Sao Paulo*, Departamento de Engenharia Hidraulica e Sanitaria, Brazil
- Arasaki, E., 2004, "Sistemas predominantes de tratamento de esgoto na costa paulista - metodologia para a tomada de decisao", Ph.D. thesis, *Escola Plitechnica da Universidade de Sao Paulo*, Brazil
- ATV-DVWK A110, 2001, "*Hydraulische Dimensionierung und Leistungsnachweis von Abwasserkanälen und -leitungen*", ISBN 3-935669-22-4 (based on DIN EN 1671), www.dwa.de
- ATV-DVWK-A 116, 2005, "*Teil 2: Druckentwässerungssysteme ausserhalb von Gebäuden*", März 2005, ISBN 3-937758-15-1, www.dwa.de
- Avanzini, C., 2003, "Construction techniques, supervision, "As built report", maintenance and monitoring planning as a key to a successful operation of submarine outfalls", *Proceedings Workshop: Submarine Outfalls: Design Considerations and Environmental Performance Monitoring*, Sao Paulo, Brazil
- Bellair, J.T., Parr-Smith, A., Wallis, I.G., 1977, "Significance of diurnal variations in fecal coliform die-off rates in the design of ocean outfalls", *Journal WPCF*, 2022-2030
- Bennett J.V., Holmberg S.D., Rogers M.F., and Solomon S.L., 1987, "Infectious and Parasitic Diseases", In: Amler RW, Dull HB, eds. *Closing the Gap: The Burden of Unnecessary Illness*, New York, *Oxford University Press*, 102-114.
- Berzin, G., 1992, "Monitoring of the Santos Submarine Outfall, Sao Paulo, Brazil, 10 years in operation", *Water Science and Technology* Vol. 25, No. 9, 59-71
- Bitton, G., 1994, "*Wastewater Microbiology*", Wiley-Liss, New York
- Bleninger T. , Avanzini, C.A., and Jirka, G.H., 2004, "Hydraulic and technical evaluation of single diameter diffusers with flow rate control through calibrated, replaceable port exits", *Proc. Int. Conf. Marine Waste Water Discharges and Marine Environment*, Catania, Italy
- Bleninger T., and Jirka G.H., 2004, "Near- and far-field model coupling methodology for wastewater discharges", *Proceedings, 4th International Symposium on Environmental Hydraulics and 14th Congress of Asia and Pacific Division, International Association of Hydraulic Engineering and Research*, Hong Kong, China, 15. - 18.12., Lee J.H.W., Lam K.L., Eds.
- Bleninger T., Hauschild I., Jirka G. H., Leonhard D., and Schlenkhoff, 2004, "Immissionsorientierte Bewertung von Einleitungen in Gewässer: Mischzonen oder Opferstrecken, wo gelten die Gütek-

- riterien?“, *KA - Abwasser, Abfall*, 51.Jahrgang, Nr.3, , bzw. *Wasserwirtschaft*, 94.Jahrgang, Nr.4, April 2004
- Bleninger T., Lang C., and Weitbrecht V., 2004, "Generalentwässerungsplan Stadt Mainz Neubau Auslass Gassnerallee, Hydraulische Berechnungen im Rahmen der Optimierung der Abflussverhältnisse im Auslassbauwerk Gassnerallee", *University Karlsruhe*, Institutsbericht, Instituts für Hydromechanik, Nr. 810,
- Bleninger T., Perez L.M., Milli H., and Jirka G.H., 2005, "Internal hydraulic design of a long diffuser in shallow water: Buenos Aires sewage disposal in Rio de la Plata estuary", *Proc. XXXI International Association of Hydraulic Engineering and Research Congress*, 11.-16.09.2005, Byong-Ho Jun (Ed.), Seoul, South Korea
- Bleninger, T., and Jirka, G.H., 2002, "Outfalls database and information exchange", *Proc. Int. Conf. Marine Waster Water Discharges*, Istanbul, Turkey, 16.-20.Sep
- Bleninger, T., Lipari, G., and Jirka, G.H, 2002, "Design and optimization program for internal diffuser hydraulics", *Proc. Int. Conf. Marine Waster Water Discharges 2002*, Istanbul, Turkey, 16.-20.Sep
- Blumberg, A.F. and Mellor, G.L., 1985, "Modelling vertical and horizontal diffusivities with the sigma coordinate system", *Monthly Weather Review*, Vol. 113, No. 8
- Blumberg, A.F., Ji, Z.G. and Ziegler, C.K., 1996, "Modeling outfall plume behaviour using far field circulation model", *Journal of Hydraulic Engineering*, Vol. 122, No. 11
- Blumberg, A.F., Signell, R.P., and Jendter, H.L., 1993, "Modeling transport processes in the coastal ocean" *Journal of Marine Environmental Engineering*,1, 31-52
- Braga, E.S., Bonetti, C.V.D.H., Burone, L., and Bonetti Filho, J., 2000, "Eutrophication and Bacterial Pollution caused by industrial and domestic Wastes at the Baixada Santista Estuarine System - Brazil", *Marine Pollution Bulletin*, Vol. 40, No. 2, 165-173
- Brooks, N.H. , 1960, "Diffusion of sewage effluent in an ocean current", *Proc. of First International Conference on Waste Disposal in the Marine Environment*, Univ. of California, Pergamon Press, New York
- Brooks, N.H. and Koh, R.C.Y., 1965, "Discharge of sewage effluent from a line source into a stratified ocean", *XI Congress, IAHR*, Paper No. 2.19, Leningrad
- Brooks, N.H., 1972, "Dispersion in hydrologic and coastal environments", *W.M. Keck Laboratory of Hydraulics and Water Resources, California Institute of Technology*, Rep. KH-R-29
- Brooks, N.H., 1980, "Synthesis of stratified flow phenomena for design of ocean outfalls", *Second International Symposium on Stratified Flows*, Trondheim, Norway, 24-27 June, 809-831
- Brooks, N.H., 1988, "Seawater intrusion and purging in tunneled outfall" *Schweizer Ingenieur und Architekt*, 106(6), 156-160 (I think this is a journal, oder?)
- Brooks, N.H.,1984, "Dispersal of wastewater in the ocean - a cascade of processes at increasing scales", *Proc. of the Conf. Water for Resource Development*, Coeur d'Alene, Aug 14-17
- Burrows, R., 2001, "Outfalls I: Pipeline and diffuser manifold design and hydraulic performance", *IAHR Short Course Environmental Fluid Mechanics: Theory, Experiments and applications held at University Dundee*
- Burrows, R., Neves, M.J.V., Larsen, T., Carratelli, E.P., Veltri, P., 1998, "European attitude to the disposal of wastewater in the sea: the case for a (european) network for sea outfall research", *Water Science and Technology*, Vol. 38, No. 10, 317-321
- Busch, N.E., 1972. On the mechanics of atmospheric turbulence. Workshop on micrometeorology, A. Met. Soc., 1-65.
- Canteras, J.C., Juanes, J.A., Perez, L., Koev, K.N., 1995, "Modelling the coliforms inactivation rates in the Cantabrian Sea (Bay of Biscay) from in situ and laboratory determinations of T_{90} ", *Water Science and Technology*, Vol. 32, No. 2, 37-44
- Carvalho, J.L.B., 2003, "Modelagem e análise do lançamento de efluentes através de emissaries sub-marines", Ph.D. thesis, *Federal University of Rio de Janeiro (COPPE-UFRJ)*, Brazil
- Carvalho, J.L.B., Roberts, P.J.W. and Roldao, J., 2002, "Field Observations of Ipanema Beach Outfall", *Journal of Hydraulic Engineering*, Vol. 128, No. 2, 151-160

- CETESB (Companhia de Tecnologia de Saneamento Ambiental), 2005, "Relatoria de qualidade das águas litorâneas no estado de São Paulo, Balneabilidade das praias 2004", CETESB, Brazil
- Chin, D.A. and Roberts, P.J.W., 1985, "Model of dispersion in coastal waters", *J. of Hydraulic Engineering, ASCE*, 111(1), 12-27
- Choi, K.W. and Lee, J.H.W., 2005, "A new approach to effluent plume modelling in the intermediate field", *Proc. 31st IAHR Congress*, Seoul, Korea, September 11-16, 2005, 4303-4311
- Chyan, J. and Hwung H., 1994, "On the interaction of a turbulent jet with waves", *J. Hydr. Research*, 31 (6), pp. 791-810
- Chyan, J., Hwung H. and Chang Y., 1991, "Wave effects on the mean flow characteristics of turbulent round jets", *Environmental Hydraulics*, Lee J. and Cheung Y. (eds.), Balkema, Rotterdam
- CIOH, 2005, Centro de Investigaciones Oceanográficas e Hidrográficas, <http://www.cioh.org.co>
- CONAMA 20, 2000, Article 23, §3, Conselho Nacional do Meio Ambiente, *Ministerio do Meio Ambiente*, Brasilia, Brazil
- Connolly, J.P., Blumberg, A.F., Quadrini, J.D., 1999, "Modeling fate of pathogenic organisms in coastal waters of Oahu, Hawaii", *J. Environmental Engineering*, Vol. 125, No. 5
- COPPE, 2000, "SisBAHIA - Sistema de Base Hidrodinâmica Ambiental, Documentação técnica", COPPE, *Universidade Federal de Rio de Janeiro*
- Courant, R. and Hilbert, D., 1962, "*Methods of mathematical physics*", Interscience, New York
- Crosignani, L., Alsina, J., and Piaggio, R., 2002, "Montevideo Outfall, 14 years of a wastewater discharge in a large and shallow estuary", *Proc. Marine Waste Water Discharges, MWWD 2002*, Istanbul, 16-20 September
- Csanady, G.T. and Churchill, J.H., 1987, "Environmental engineering analysis of potential dumpsites", In T.P.O'Connor (ed.), *Ocean processes in marine pollution*, 2, 21-31
- Csanady, G.T., 1983, "Dispersal by randomly varying currents" *Journal of Fluid Mechanics*, 132, 375-394
- Dallimore, Imberger and Hodges, 2001, "Coupling an underflow model to a 3d hydrodynamic model", *Journal of Hydraulic Engineering*, Centre for Water Research reference ED-1474CD
- Davies, A.M., Jones, J.E., and Xing, J., 1997a, "Review of Recent Developments in tidal hydrodynamic modeling. I: Spectral Models", *J. Hydr. Eng.*, Vol. 123, No. 4, 278-292
- Davies, A.M., Jones, J.E., and Xing, J., 1997b, "Review of Recent Developments in tidal hydrodynamic modeling. II: Turbulence Energy Models", *J. Hydr. Eng.*, Vol. 123, No. 4, 293-302
- Davies, P.A., 2003, "Submarine Outfalls: Design and construction", *Proc. Submarine Outfalls: Design, Compliance and Environmental Monitoring*, 1.-3.12.2003, CETESB, São Paulo, Brazil
- Davis, L.R., 1999, "*Fundamentals of environmental discharge modeling*", CRC Press, Baton Raton, FL.
- Delft Hydraulics, 1995, User Manual v.1.0 "Diffflow - A simulation program for the design of a multi-port diffuser", Author: G.A.L. Delvigne, Delft, Netherlands
- Delft Hydraulics, 2001, "Delft3D user interface, Capabilities and applications", *Delft Hydraulics*, Delft
- Delft Hydraulics, 2005, "Delft3D-NESTWQ - Offline nesting of water quality models", User Manual, Delft Hydraulics, the Netherlands
- Delft3D-FLOW, 2003, "Simulation of multi-dimensional hydrodynamic flows and transport phenomena including sediment - User Manual", *Delft Hydraulics*, Delft, Netherlands, www.wldelft.nl, March, 2003
- Delft3D-GPP, 2004, "Visualisation of Delft3D simulation results and measurement data - User Manual", *Delft Hydraulics*, Delft, Netherlands, www.wldelft.nl, April, 2004
- Delft3D-PART, 2003, "Simulation of mid-field water quality and oil spills, using particle tracking - User Manual", *Delft Hydraulics*, Delft, Netherlands, www.wldelft.nl, March, 2003

- Delft3D-QUICKIN, 2004, "Generation and manipulation of gridrelated parameters such as bathymetry, initial conditions and roughness - User Manual", *Delft Hydraulics*, Delft, Netherlands, www.wldelft.nl, April, 2004
- Delft3D-QUICKPLOT, 2004, "Visualisation and animation program for analysis of simulation results - User Manual", *Delft Hydraulics*, Delft, Netherlands, www.wldelft.nl, August, 2004
- Delft3D-RGFGRID, 2004, "Generation and manipulation of curvilinear grids for FLOW and WAVE - User Manual", *Delft Hydraulics*, Delft, Netherlands, www.wldelft.nl, October, 2004
- Delft3D-WAQ, 2003, "Versatile water quality modelling in 1D, 2D or 3D systems including physical, biochemical and biological processes - User Manual", *Delft Hydraulics*, Delft, Netherlands, www.wldelft.nl, March, 2003
- DHI, *Danish Hydraulic Institute*, 2000, "Mike3 Estuarine and Coastal Hydraulics and Oceanography", Scientific Documentation
- Domenichini, P., Bazurro, N., Avanzini, C., Da Molo, E., Marchese, A., Ottonello, P., and Roccatagliata, E., 2002, "Outfall operation monitoring and environmental control: the experience of LIFE - Aquarius Project", *Proc. Marine Waste Water Discharges, MWWD 2002*, Istanbul, 16-20 September
- Doneker, R.L. and Jirka, G.H., 1990, "CORMIX1: An Expert System for Hydrodynamic Mixing Zone Analysis of Conventional and Toxic Submerged Single Port Discharges", Tech. Rep., *DeFrees Hydraulics Laboratory, School of Civil and Env. Eng., Cornell University* (also published by U.S. Environmental Protection Agency, Tech. Rep. EPA/600/3-90/012, Environmental Research Lab, Athens, Georgia, 1990)
- Doneker, R.L., Jirka, G.H., 1990, "Expert system for hydrodynamic mixing zone analysis of conventional and toxic submerged single port discharges (CORMIX1)", Rep. No. EPA/600/3-90/012, U.S. Environmental Protection Agency, Washington, D.C.
- DVWK (*Deutscher Verband für Wasserwirtschaft und Kulturtechnik*, now DWA), 1999, "Numerische Modelle von Flüssen, Seen und Küstengewässern", Heft 127
- EC Bathing water directive, 2006, "Directive concerning the management of bathing water quality and repealing Directive 76/160/EEC", Directive 2006/7/EC, the *European Parliament and Council*, 15 of February, 2006
- Esrey, SA, Potash, JB, Roberts, L & Shiff, C, 1991, "Effects of Improved water supply and sanitation on ascariasis, diarrhoea, dracunculiasis, hookworm infection, schistosomiasis and trachoma". *Bull WHO*, 69 (5):609-621
- EU-Commission, 2002, Faltblatt der EU-Kommission zur Wasserrahmenrichtlinie: „Wasser ist Leben“, *Europäische Gemeinschaft*
- Faisst, W.R., McDonald, M., Noon, T. and Marsh, G., 1990, "Iona outfall, plume characterization study", *Proc. 1990 Nat. Conf. on Hydraulic Engineering*, H.Chang, ASCE, New York
- Falconer, R.A., Lin, B., 2005, "Water quality management of river and estuarine waters", *Proc. Environmental Hydraulics and Sustainable Water Management*, Lee and Lam (Eds.), Tayler and Francis Group, London
- Ferziger, J.H., Peric, M., 2002, "*Computational Methods for Fluid Dynamics*", Springer Berlin / Heidelberg / New York
- Fischer, H.B., List, E.J., Koh, R.C.Y., Imberger, J. and Brooks, N.H., 1979, "*Mixing in Inland and Coastal Waters*", Academic Press, New York
- Fox, D.C., 1970, "Forced plume in a stratified fluid", *J. Geophys. Res.*, Vol. 75, 33, 6818-35
- French, J., May 1972, "Internal hydraulics of multiport diffusers", *Journal WPCF*, Vol. 44, No. 5, p. 782pp
- Frick, W.E., Roberts, P.J.W., Davis, L.R., Keyes, J., Baumgartner and D.J., and George, K.P., 2001, "Dilution Models for Effluent Discharges, 4th Edition, (Visual Plumes)", *Environmental Research Division, NERL, ORD, U.S. Environmental Protection Agency*, Athens, (http://www.cee.odu.edu/model/visual_plume.php)

- Galindo, U.R., and Simpson, G.L., 2003, "Nuevas tendencias centrales del diseño ambiental robusto de un emisario submarino: experiencia obtenido del programa de sanamiento de Valparaíso", *Proc. XV Congreso de ingeniería sanitaria y ambiental*, AIDIS - Chile, Concepción, October 2003
- Gameson, A.L.H., 1982, "Investigations of sewage discharges to some British coastal waters, Chapter 5, Bacterial distributions", Part 4, Tech. Rep., *Water Research Centre*
- Garber, W.F., 1998, "Wastewater treatment and risk assessment in ocean outfall evaluations", *Water Science and Technology*, Vol. 38, No. 10, 309-316
- Gillaud, J.F., Derrien, A., Gourmelon, M., and Pommepuy, M., 1997, "T90 as a tool for engineers: interests and limits", *Water Science and Technology*, Vol. 35, No. 11-12, 277-281
- Grace, R.A., 1978, "*Marine Outfall Systems, planning, design, and construction*", Department of Civil Engineering, University of Hawaii at Manoa Honolulu, Prentice-Hall, New Jersey ISBN 0-13-556951-6
- Gunnerson, C.G., February 1988, "Wastewater Management for Coastal Cities: The Ocean Disposal Option", *World Bank Technical Paper Number 77*, pdf: http://www-wds.worldbank.org/servlet/WDS_IBank_Servlet?pcont=details&eid=000178830_98101904165665
- Hazen and Sawyer, 1998, "Mediciones Oceanograficas y Hidrodinamicas Diseño Detallado," Memorando Tecnico, report for the World Bank
- Harleman, D.R.F. and Murcott, S., 2001, "CEPT: challenging the status quo. *Water 21*, 57-59
- Henze, M., Harremoes, P., Jansen, J.C., and Arvin, E., 2002, "*Wastewater treatment, Biological and Chemical processes*", Springer, Berlin
- Ho, C.M. and Gutmark, E., 1987, "Vortex induction and mass entrainment in a small aspect ratio elliptic jet", *J. Fluid Mech.*, 179, 383-405.
- Hodgins, D.O., Tinis, S.W., and Taylor, L.A., 1998, "Marine Sewage outfall assessment for the capital regional district, British Columbia, using nested three-dimensional models", *Water Science and Technology*, Vol.38, No. 10, 301-308
- Holley, E.R. and Jirka, G.H., 1986, "Mixing and solute transport in rivers", Field Manual, Waterways Experiment Station, Tech. Report E 86 11, *U.S. Army Corps of Engineers*, Vicksburg, Miss.
- Huang, W. and Spaulding, M., 1996, "Modelling horizontal diffusion with sigma coordinate system", *Journal of Hydraulic Engineering*, Vol. 122, No. 6, 349-352
- Huber, A.B., Tanik, A.B., Gercek, M., 1995, "Case studies on preliminary treatment facilities at marine outfalls", *Water Science and Technology*, Vol. 32, No. 2, 265-271
- HydrosCH2MHill, 2000, "Modelamento da campanha de tracadores", COPPE, *Federal University of Rio de Janeiro*, Consulting - Report HydrosCH2MHill, PENO-565
- IBCCA, 2003, International Bathymetric Chart of the Caribbean Sea and the Gulf of Mexico, <http://www.ngdc.noaa.gov/mgg/ibcca/>
- Idelchik, I.E., 1986, "*Handbook of Hydraulic Resistance*", Springer-Verlag, Berlin
- IETC, 2000, "International Source Book on Environmentally Sound Technologies for Wastewater and Stormwater Management", *United Nations Environment Programme (UNEP), Division of Technology, Industry, and Economics (DTIE)*, International Environmental Technology Centre (IETC) , Osaka, http://www.unep.or.jp/Ietc/Publications/TechPublications/TechPub-15/main_index.asp
- IMPRESS, 2002, „Guidance for the analysis of Pressures and Impacts in accordance with the Water Framework Directive“, <http://www.wasserblick.net>, 21.11.2002
- Inspection Panel, 2005, "Investigation Report Colombia: Cartagena Water Supply, Sewerage and Environmental Management Project (Loan No. 4507-CO)," *The World Bank*, Report No. 32034-CO
- Jirka G. H., Bleninger T., Burrows R., and Larsen T., 2004, "Environmental Quality Standards in the EC-Water Framework Directive: Consequences for Water Pollution Control for Point Sources", *European Water Management Online (EWMO)* www.ewaonline.de, January 26, 2004
- Jirka G.H., 1982, "Multiport Diffusers for Heat Disposal: A Summary," *J. Hydraulics Division, ASCE*, (108), HY12, pp. 1423-68
- Jirka G.H., Bleninger T., 2004, " Design of multiport diffuser outfalls for coastal water quality protection", Proceedings, XXI Congreso Latinoamericano de Hidráulica, *International Association for*

- Hydraulic Research and Engineering (IAHR)*, São Pedro, Brazil, October 18-22, A.M. Genovez, Ed. (english+spanish, <http://www.ifh.uni-karlsruhe.de/people/Bleninger/>)
- Jirka, G.H. & Akar, P.J., 1991a, "Hydrodynamic Classification of Submerged Single-Port Discharges", *J. Hydraulic Engineering*, ASCE, (117), 1095-1111, HY9
- Jirka, G.H. & Doneker, R.L., 1991b, "Hydrodynamic Classification of Submerged Multiport Diffuser Discharges", *J. Hydraulic Engineering*, ASCE, (117), 1113-1128, HY9
- Jirka, G.H. and Harleman, D.R.F., 1973, "The mechanics of submerged multiport diffusers for buoyant discharges in shallow water", R.M. Parsons Lab. Water Res. Hydrodyn., Tech. Rep. 169, *Mass. Inst. Tech., Cambridge, Mass.*
- Jirka, G.H. and Lee, J. H. W., 1994, "Waste disposal in the ocean", in *Water Quality and its Control*, Vol. 5 of Hydraulic Structures Design Manual, M. Hino (Ed.), A.A.Balkema Publishers, Rotterdam
- Jirka, G.H., 1979, Discussion of 'Line plume and ocean outfall dispersion' by P.J.W. Roberts, *J. Hydr. Div.*, ASCE, HY 12
- Jirka, G.H., 1982, "Turbulent Buoyant Jets in Shallow Fluid Layers", in *Turbulent Jets and Plumes*, Rodi, W. (Ed.), Pergamon Press
- Jirka, G.H., 1994, "Shallow Jets", in *Recent Advances in the Fluid Mechanics of Turbulent Jets and Plumes*, P.A. Davies and M.J. Valente Neves (Ed.s), Kluwer Academic Publishers, Dordrecht
- Jirka, G.H., 2001, "Hydromechanik", Lecture notes, *University Karlsruhe*, Institute for Hydromechanics
- Jirka, G.H., 2003, "Mixing processes in wastewater discharges, jets and plumes, effect of currents and stratification", *Workshop at the IAHR Congress*, 24.08.03-29.08.03, Thessaloniki, Greece
- Jirka, G.H., 2004, "Integral Model for Turbulent Buoyant Jets in Unbounded Stratified Flows. Part 1: The Single Round Jet", *Env. Fluid Mech.*, Vol. 4, 1-56
- Jirka, G.H., 2006, "Integral Model for Turbulent Buoyant Jets in Unbounded Stratified Flows, Part 2: Plane Jet Dynamics Resulting from Multiport Diffuser Jets", *Environmental Fluid Mechanics*, Vol. 6, No. 1, 43-100
- Jirka, G.H., Abraham, G., and Harleman, D.R.F., 1976, "An Assessment of Techniques for hydrothermal prediction", *Department of Civil Engineering, MIT for U.S. Nuclear Regulatory Commission*, Cambridge
- Jirka, G.H., and Doneker, R.L., 2003, Discussion of "Field Observation of Ipanema Beach Outfall" by J.L.B. Carvalho, P.J.W. Roberts and J. Roldao, *J. Hydraulic Engineering*, Vol.129, 10, 823-6
- Jirka, G.H., and Harleman, D.R.F., 1979, "Stability and mixing of a vertical plane buoyant jet in confined depth", *Journal of Fluid Mechanics*, 94(2), 275-304
- Jirka, G.H., Doneker, R.L. and Hinton, S.W., 1996, "User's Manual for CORMIX: A Hydrodynamic Mixing Zone Model and Decision Support System for Pollutant Discharges into Surface Waters", Tech. Rep., DeFrees Hydraulics Laboratory, Cornell University (also published by U.S. *Environmental Protection Agency*, Tech. Rep., Environmental Research Lab, Athens, Georgia)
- Jirka, G.H., T. Bleninger, R. Burrows & T. Larsen, 2004, "Management of point source discharges into rivers: where do environmental quality standards in the new EC-water framework directive apply?" *Journal of River Basin Management*, Vol. 2, Issue 1, 2004, www.jrbm.net
- Jirka, G.H., Wilkinson, H.I., and Bell, I.R., "Jet interaction in a still environment", *World Scientific Publ.*, Singapore
- Kalide, W., 1980, "Technische Strömungslehre", Carl Hanser Verlag, München Wien, 5th edition,
- Kim, D.G., and Seo, I.W., 2000, "Modeling the mixing of heated water discharged from a submerged multiport diffuser", *Journal of Hydralic Research*, Vol, 38, No. 4, 259-269
- Kim, Y.D., Seo, I.W., Kang, S.W., and Oh, B.C., 2002, "Jet Integral-Particle Tracking Hybrid Model for Single Buoyant Jets", *J. Hydraulic Engineering*, vol. 128, No. 8, 753-760
- Koh, R.C.Y., 1983, "Wastewater field thickness and initial dilution", *J. of Hydraulic Engr.*, ASCE, 109(HY9), 1232-1240

- Kolmogorov, A.N., 1942, "Equations of turbulent motion in incompressible fluid", *Izv. Akad. Nauk. SSR, Seria fizicheska Vi.*, No.1-2, 56-58 (English translation: 1968 Imperial College, Mech. Eng. Dept. Rept. ON/6)
- Kuang, C.P. and Lee, J.H.W., 2001, "Numerical experiments on the mixing of a duckbill valve jet", *Proc. Third Int. Symp. on Env. Hydraulics, Arizona State University, Tempe, Arizona.*
- Kwon, S.J., and Seo, I.W., 2005, "Experimental Investigation of Wastewater Discharges from a Rosette-type Riser using PIV", *J. Civil Engineering, KSCE*, Seoul, Vol.9, No.5, 355-362
- Lattemann, S., and Höpner, T., 2003, "Seawater desalination - impacts of brine and chemical discharge on the marine environment", Balaban Desalination Publicatinos, L'Aquila, Italy
- Lamparelli, C., 2003, "Commissioning and monitoring challenges regarding ocean outfalls: São Paulo State Experience", *Proc. Submarine Outfalls: Design, Compliance and Environmental Monitoring*, 1.-3.12.2003, CETESB, Sao Paulo, Brazil
- Larsen, T., 2004, "Far-field modeling issues", *Proc. Short course B, Marine Waste Water Discharges, Catania, 2004*
- Larsen, T., 2000, "Necessity of Initial Dilution for Sea Outfall Diffusers in Respect to the European Directive on Municipal Discharges", *Proc. Marine Waste Water Discharges, Genova, November 2000*
- Larsen, T., 2004, "Unsteady pipe and diffuser hydraulics - transient flow", *Proc. Short course B, Marine Waste Water Discharges, Catania, 2004*
- Lauder, B.E., and Spalding, D.B., 1974, "The numerical computation of turbulent flows", *Computer Methods in Applied Mechanics and Engineering*, 3, pp. 269-289
- Law, A.W.K., Lee, C.C., and Qi, Y., 2002, "CFD Modeling of a Multi-Port Diffuser in an Oblique Current", *Proc. Marine Waste Water Discharges, MWWD 2002, Istanbul, 16-20 September*
- LAWA (Länderarbeitsgemeinschaft Wasser), 2003, „Arbeitshilfe zur Umsetzung der EG-Wasserrahmenrichtlinie“ "German Guidance Document for the implementation of the EC Water Framework Directive", <http://www.wasserblick.net>, 30.04.2003
- Lee J.H.W. "Need for sea outfalls, wastewater disposal, environmental regulation", *International Short Course*, August 21-22, 2003, Thessaloniki, Greece
- Lee J.H.W., Karandikar J., and Horton, P.R., 1998, "Hydraulics of DuckBill Elastomer Check Valves", *Journal of Hydraulic Engineering*, April
- Lee J.H.W., Wilkonson D.L., and Wood I.R., 2001, "On the head-discharge relation of a "duckbill" elastomer check valve", *Journal of Hydraulic Research*, Vol. 39, 2001, no. 6
- Lee, J.H.W. and Cheung, V., 1990, "Generalized Lagrangian model for buoyant jets in current", *Journal of Environmental Engineering*, ASCE, 116(6), pp. 1085-1105
- Lee, J.H.W., and Jirka, G., 1981, "Vertical round buoyant jet in shallow water", *Journal of the Hydraulics Division*, ASCE, 107(HY12), 1651-1675
- Lee, J.H.W., and Neville-Jones, P., 1987, "Initial dilution of horizontal jet in crossflow" *Journal of Hydraulic Engineering*, ASCE, 113(5), 615-629
- Lee, J.H.W., Cheung, V., Wang, W., and Cheung, S.K.B., 2002, "Lagrangian modeling and visualization of rosette outfall plumes", *Department of Civil Engineering, Department of Computer Science & Information Systems, The University of Hong Kong, Hong Kong, China* <http://www.aoe-water.hku.hk/visjet/visjet.htm>
- List, E.J., Gartrell, G., and Winant, C.D., 1990, "Diffusion and Dispersion in Coastal Waters", Vol. 116, No. 10
- Ludwig, R.G., "Evaluacion del impacto ambiental ubicacion y desno de emisarios submarinos", *CEPIS (Centro Panamericano de Ingenieria Sanitaria, Lima, PE)*
- Maier, R.M., Pepper, I.L., Gerba, C.P., 2000, "Environmental Microbiology", Academic Press, San Diego
- Mellor, G., Häkkinen, S., Ezer, T. and Patchen, R., 2002, "A Generalization of a Sigma Coordinate Ocean Model and an Intercomparison of Model Vertical Grids", *Ocean Forecasting: Conceptual Basis and Applications*, N. Pinardi, J. Woods (Eds.), Springer, Berlin, 55-72

- Libhaber, M., Roberts, P.J.W., 2002, "Social aspects of wastewater submarine outfalls in developing countries: the case of Cartagena, Colombia", *Proc. Marine Waste Water Discharges*, 16.-20. September, Istanbul
- Mendéz Díaz, M.M. and Jirka, G.H., 1996, "Trajectory of Multiport Diffuser Discharges in Deep Co-Flow", *J. Hydraulic Engineering*, 122, 8, 428-435
- Meybeck M, Chapman D and Helmer R, 1990, "*Global freshwater quality a first assessment*", Oxford, Blackwell
- Miller, B.M., Peirson, W.L., Wang, Y.C., and Cox, R.J., 1996, "An overview of Numerical Modelling of the Sydney Deepwater Outfall Plumes", *Marine Pollution Bulletin*, Vol, 22, No: 7-12, 147-159
- Miller, D.S., 1990, "Internal Flow Systems", BHRA, Cranfield
- Mort, R. B., September 1989, "The Effects of wave action on long sea outfalls", *Ph.D. thesis, University of Liverpool*
- Muellenhoff, W.P., Soldate Jr., A.M., Baumgartner, D.J., Schuldt, M.D., Davis, L.R., and Frick, W.E., 1985, "Initial mixing characteristics of municipal ocean outfall discharges: Volume 1. Procedures and Applications", *EPA/600/3-85/073a*, Athens
- Munro, D. and Mollowney, B.M., 1974, "The effect of a bottom countercurrent and vertical diffusion on coliform concentrations at the shore due mainly to wind-induced onshore currents, *Rapports et Proces-verbaux des Reunions Conseil International pour l'Exploration de la Mer*, 167, 37-40
- Munro, D., 1984, "Sewage dilution between outfall and shore", *Public Health Engineer*, 12(2), 113-114
- Murphy S, 1999, "Emerging Microbes 101: A Basic Course", *Journal of the American Water Works Association*, 91(9):10-11.
- Nash, J.D., 1995, "Buoyant discharges into reversing ambient currents", Master thesis, DeFrees Hydraulics Laboratory, Cornell University, Ithaca NY
- National Research Council, 1993 "*Managing Wastewater in Coastal Urban Areas*", National Academy Press, Washington D.C.
- Neves, M. and Neves, A. 1992, "Descarga de Águas Residuais no Mar. Exutores Submarinos", *Actas do I Encontro da Engenharia Civil Ibero-Americana*, Cáceres, Espanha e Revista nº62 da Ordem dos Engenheiros
- Neves, R., 2003, "Modelling Applied to Waste Disposal systems. Application of MOHID for simulating trophic activity in the Tagus and for assessing the impact of Costa do Estoril submarine outfall", *Proc. Submarine Outfalls: Design, Compliance and Environmental Monitoring*, 1.-3.12.2003, CETESB, Sao Paulo, Brazil
- Neville-Jones, P.J.D., and Chitty, A.D., 1996a, "Sea outfalls - construction, inspection and repair. An engineering guide", *CIRIA*, R159, UK
- Neville-Jones, P.J.D., and Chitty, A.D., 1996b, "Sea outfalls - inspection and diver safety", *CIRIA*, R158, UK
- Nezu, I., Nakagawa, H., 1993, "Turbulence in Open-channel flows", *IAHR, Monograph Series*, A.A. Balkema/Rotterdam/Brookfield
- Noble, R.T., Lee, I.M., Schiff, K.C., 2004, "Inactivation of indicator micro-organisms from various sources of faecal contamination in seawater and freshwater", *J. of applied microbiology*, 96, 464-472
- Paul, J.H., 2001, "*Methods in Microbiology*", Volume 30, Marine Microbiology, Academic Press, San Diego
- Philip, N.A., and Pritchard, T.R., 1996, "Australia's First Deepwater Sewage Outfalls: Design Considerations and Environmental Performance Monitoring", *Marine Pollution Bulletin*, Vol. 33, Nos 7-12, pp 140-146
- Ragas, A.M.J., Hams, J.L.M., and Leuven, R.S.E.W., 1997, "Selecting water quality models for discharge permitting", *European Water Pollution Control*, 7(5), 59-67

- Revilla, J.A., Álvarez, C., García, A., Medina R., and Juanes, J.A., 2002, "Environmental design of submarine outfall according to the European Water Framework Directive", *Proc. 2nd Int. Conf. On Marine Waste Water Discharges*
- Ridge, M.M., 2002, "Three-dimensional simulation of pollutant dispersion in coastal waters", *Ph.D. thesis, Universitat Politècnica de Catalunya*, Barcelona, partly included in Sanchez-Arcilla, A., Rodriguez, A., Mestres, M., 1998, "A three-dimensional simulation of pollutant dispersion for the near- and far-field in coastal waters, *Journal of Marine and Environmental Engineering*, 4, 217-243
- Roberts, P.J.W. and Carvalho, J. L., 2000, "Modeling of ocean outfall for Cartagena, Colombia", 23 June 2000, report for *World Bank*
- Roberts, P.J.W. and Villegas, 2006, "Three-Dimensional Modeling of Bacterial Transport for the Cartagena Ocean Outfall", for Aguas de Cartagena, Atlanta, 2006
- Roberts, P.J.W., 1977, "Dispersion of Buoyant Waste Water Discharged from Outfall Diffusers of Finite Length", W.M. Keck Laboratory of Hydraulics and Water Resources Report No. KH-R-35, *California Institute of Technology*, Pasadena, Calif., 1977, 183pp.
- Roberts, P.J.W., 1979, "Line plume and ocean outfall dispersion", *J. of Hydraulics Div.*, ASCE, 105(HY4), 313-331 (see also discussion by G. H. Jirka, HY12, 1573-1575)
- Roberts, P.J.W., 1980, "Ocean outfall dilution: Effects of Currents" *Journal of the Hydraulics Division, ASCE*, 106(HY5), 313-330
- Roberts, P.J.W., 1986, "Engineering of ocean outfalls", In: *The Role of the Oceans as a Waste Disposal Option*, G. Kullenberg, ed., *NATO ASI Series C*, 172, 73-109
- Roberts, P.J.W., 1990, "Outfall design considerations", in *The Sea: Ocean Engineering Science*, B. Le Mehaute and D.M. Hanes (Ed.s), *Wiley-Interscience*
- Roberts, P.J.W., 1996, "Sea outfalls", in *Environmental Hydraulics*, V.P. Singh and W.H. Hager, (Eds.), *Kluwer Academic*
- Roberts, P.J.W., 1999 (a and b), "Modeling Mamala Bay Outfall Plumes. I. Near Field. II: Far Field, *J. Hydraulic Engineering*, Vol. 125, No.6.
- Roberts, P.J.W., 2003, "Dilution Modeling for the Cartagena Ocean Outfall", Report for the *World Bank*, 31 October 2003
- Roberts, P.J.W., 2004, "Additional Water Quality Modeling for the Cartagena Ocean Outfall", Report for the *World Bank*, 19 May 2004
- Roberts, P.J.W., 2005, "Modeling of Wind Effects on Bacterial Transport for the Cartagena Ocean Outfall", Report for the *World Bank*, 29 July 2005
- Roberts, P.J.W., 2006, "Modeling for the Cartagena Ocean Outfall", Report for the *World Bank*
- Roberts, P.J.W., and Snyder, W.H., 1993, "Hydraulic model study for the Boston outfall. I: Riser configuration. *J. Hydraulic Engineering*, 119(9), 970-987
- Roberts, P.J.W., and Snyder, W.H. & Baumgartner D.J., 1989c, "Ocean outfalls III, Effect of diffuser design on submerged wastefield", *J. Hydraulic Engineering*, 115, 49-70
- Roberts, P.J.W., and Snyder, W.H. and Baumgartner, D.J., 1989a, "Ocean outfalls I: Submerged waste field formation", *J. Hydr. Eng.*, 115, HY1, 1-25
- Roberts, P.J.W., and Snyder, W.H. and Baumgartner, D.J., 1989b, "Ocean outfalls II: Spatial evolution of submerged waste field", *J. Hydr. Eng.*, 115, HY1, 26-48
- Roberts, P.J.W., and Williams, N., 1992, "Modeling of ocean outfall discharges", *Water Science and Technology*, 9, 155-164
- Roberts, P.J.W., Hunt, C.D., and Mickelson, M.J., 2002, "Field and model studies of the Boston outfall", *Proc. Marine Waste Water Discharges, MWWD 2002*, Istanbul, 16-20 September
- Rodi, W., 1984. Turbulence models and their application in Hydraulics, State-of-the-art paper article sur l'etat de connaissance. *Paper presented by the IAHR-Section on Fundamentals of Division II: Experimental and Mathematical Fluid Dynamics*, The Netherlands.
- Rodi, W., 1993, "Turbulence Models and Their Application in Hydraulics, A State-of-the-Art Review", Third Edition, *IAHR Monograph Series*, A.A. Balkema / Rotterdam / Brookfield

- Rodi, W., 2004, "Numerische Berechnung turbulenter Strömungen in Forschung und Praxis", *Hochschulkurs vom Institut für Hydromechanik, Universität Karlsruhe*, 13-15.9.04
- Rodriguez, A., Sánchez-Arcilla, A., Redondo, J.M., Bahia, E., and Sierra, J.P., 1995, "Pollutant dispersion in the nearshore region: modelling and measurements", *Water Science and Technology*, Vol. 32, No. 9-10, 169-178
- Roldao, J., Carvalho, J.L.B., Roberts, P.J.W., 2001, "Field observations of dilution on the Ipanema Beach outfall", *Water Science and Technology*, Vol. 43, No. 11, 351-360
- Rosman, P. C. C., 1987, "Modeling Shallow Water Bodies via Filtering Techniques" *Ph.D. Thesis, Ralph M. Parsons Laboratory for Water Resources and Hydrodynamics, Civil Engineering Department, Massachusetts Institute of Technology*
- Rosman, P.C.C., 1989, "Modelos de Circulação em Corpos d'Agua Rasos", Capítulo 3 do livro Métodos Numéricos em Recursos Hídricos 1, *Associação Brasileira de Recursos Hídricos*
- Rosman, P.C.C., 1989, "Um system computacional de hidrodinamica ambiental", Capítulo 1 do livro Métodos Numéricos em Recursos Hídricos 5, *Associação Brasileira de Recursos Hídricos*
- Rosman, P.C.C., 1998, "Avaliação da Eficiência de Diluição do Emissário Submarino de Esgotos de Ipanema (ESEI), - Relatório Final sobre Modelagem Computacional", Relatório COPPETEC-ET-150663, 02/98, *COPPE / Universidade Federal de Rio de Janeiro, Brazil*
- Rouse, H., Yih, C.S., and Humphreys, H.W., 1952, "Gravitational convection from a boundary source", *Tellus*, 4
- Salas, H., 1994, "Emisarios submarinos; alternativa viable para la disposición de aguas negras de ciudades costeras en América Latina", CEPIS (*Centro Panamericano de Ingenieria Sanitaria, Lima, PE*)
- Salas, H., 2000, "Historia y aplicacion de normas microbiologicas de calidad de abua en el medio marino", CEPIS (*Centro Panamericano de Ingenieria Sanitaria, Lima, PE*), also published with older information in *Water Science Technology*, Vol. 18, No. 11, 1986
- SEPA, , 1998, "Initial dilution and mixing zones for discharges from coastal and estuarine outfalls", *Scottish environment protection agency (SEPA)*
- Sfeir, A.A., 1976, "The velocity and temperature fields of rectangular jets", *Int. J. Heat Transfer*, 19, 1289-1297.
- Shannon, N.R., Mackinnon, P.A., and Hamill, G.A., 2002, "Evaluation of a CFD model of saline intrusion in marine outfalls", *Proc. Int. Conf. Marine Waster Water Discharges 2002*, Istanbul, Turkey, 16.-20.Sep, 2002
- Shuval H, 2000, "A Preliminary Estimate of the Global Disease Burden Associated with Disease Caused by Wastewater Pollution of the Marine Environment". Unpublished report prepared for the Division on the Protection of Human Environment, *World Health Organization and GESAMP*, 10pp.
- Signell, R.P., Jenter, H.L., and Blumberg, A.F., 2000, "Predicting the Physical Effects of Relocating Boston's Sewage Outfall", *U.S. Geological Survey*, Woods Hole, MA, U.S.A.
- Silva, S., Ré, A., Pestana, P., Rodrigues, A., and Quintino, V., 2004, "Sediment disturbance off the Tagus Estuary, Western Portugal: chronic contamination, sewage outfall operation and runoff events", *Marine Pollution Bulletin*, 49, (2004), 154-162
- Simonin, O., R.E. Uittenbogaard, F. Baron and P.L. Viollet, 1989. Possibilities and limitations to simulate turbulence fluxes of mass and momentum, measured in a steady stratified mixing layer, In *Proc. XXIII IAHR Congress, Ottawa, August 21-25*, published by National Research Council Canada, A55-A62.
- Solic, M. and Krstulovic, N., 1992, "Separate and combined effects of solar radiation, temperature, salinity, and pH on the survival of faecal coliforms in seawater", *Marine Pollution Bulletin*, Vol. 24, No. 8, 411-416
- Stelling, G.S. and J.J. Lendertse, 1991. Approximation of Convective Processes by Cyclic ACI methods, *Proceeding 2nd ASCE Conference on Estuarine and Coastal Modelling, Tampa, 1991*.

- Stelling, G.S. and Van Kester, J.A.Th.M., 1994, "On the approximation of horizontal gradients in sigma co-ordinates for bathymetry with steep bottom slopes", *Int. J. Num. Meth. Fluids*, Vol. 18, 915-955
- Stelling, G.S., 1984. On the construction of computational methods for shallow water flow problems. Rijkswaterstaat communications, No. 35, The Hague, Rijkswaterstaat, 1984.
- Stelling, G.S., 2001, Modelling in 1,2, and 3 Dimensions, *The Croucher Foundation, University of Hong Kong*, February 5-12
- Stolzenbach, K.D., 2005, "Review of design approaches for the Cartagena submarine outfall", *Communication for the World Bank*, November 4
- Swamee, P.K., Jain, A.K., "Explicit Equations for Pipe-Flow Problems", *Journal of the Hydraulic Division of the ASCE*, 102, no HY5 (May 1976)
- Sweers, H.E., 1976, "A monogram to estimate the heat exchange coefficient at the air-water interface as a function of windspeed and temperature; a critical survey of some literature", *J. of Hydrology*, Vol. 30
- Telford, T., 1988, "Long sea outfalls", *Proceedings of the conference held in Glasgow 19-21 October 1988*, organized by the Institution of Civil Engineers, Co-sponsored by the Water Research Centre, ISBN 072771516 X, London, 1989
- Tetra Tech Inc, 2000, "Ocean Circulation and Plume Dispersion Modeling Review, with Emphasis on Orange County Sanitation District's Offshore Outfall and Wastewater Plume", Orange County Sanitation District, USA, (http://www.ocwatersheds.com/watersheds/pdfs/Ocean_Circulation_Plume_Dispersion_Modeling.pdf)
- Tian, X., Roberts, P.J.W. and Daviero, G.J., 2004a, "Marine wastewater discharges from multipoint diffusers. I: Unstratified stationary water", *J. Hydr. Eng.*, 130, 12, 1137-46
- Tian, X., Roberts, P.J.W. and Daviero, G.J., 2004b, "Marine wastewater discharges from multipoint diffusers. II: Unstratified flowing water", *J. Hydr. Eng.*, 130, 12, 1147-55
- Uittenbogaard, R.E. and Baron, F., 1989, "A proposal: extension of the k-e model for stably stratified flows with transport of Internal Wave Energy", In *7th Turbulent Shear Flows Symp.*, Stanford, August, paper 18.4, 21-23
- Uittenbogaard, R.E., J.A.Th.M. van Kester and G.S. Stelling, 1992. Implementation of three turbulence models in 3D-TRISULA for rectangular grids, report Z81, Delft Hydraulics.
- UNEP, 2002, "Water Supply & Sanitation Coverage in Regional Seas, Need for Regional Wastewater Emissions Targets?" <http://www.gpa.unep.org/documents/RS%20Sanitation%20&%20WET%20draft%20report>
- UNEP, 2004, "Guidelines on Municipal Wastewater Management", Version 3, http://www.gpa.unep.org/documents/wastewater/Guidelines_Municipal_Wastewater_Mgmt%20version3.pdf
- UNEP, *United Nations Environment Program*, 1996, "Guidelines for submarine outfall structures for Mediterranean small and medium-sized coastal communities", MAP Technical Reports Series No. 112, ISBN 92-807-1618-2 Athens
- USEPA (U.S. Environmental Protection Agency), 1994, "Water Quality Standards Handbook: Second Edition", EPA 823-B-94-005a, Washington, DC, USA
- USGS (United States Geological Survey), 2004, "Huntington Beach Shoreline Contamination Investigation Phase III, Coastal Circulation and Transport Patterns: The Likelihood of OCSA's Plume Impacting the Huntington Beach Shoreline", Final Report 04-1019 by Noble, M. and Xu J. (Ed's)
- Villegas, B., 2005, Personal communication, participant of project
- Wallis, I.G., 1977, "Initial dilution with deep water diffusers", *J. Water Pollution Control Federation*, 49(7), 1621-1626
- Weitbrecht V., Lehmann D. and Richter A., "Flow distribution in solar collectors with laminar flow conditions", *Solar Energy*, Vol. 73, No. 6, 2002

- WFD (*Water Framework Directive*), 2000, Official Publication of the European Community, L327, Brussels
- WHO, 1997, "Environmental matters, Strategy on sanitation for high-risk communities", Report by the Director-General. Executive Board, 101st Session, Provisional agenda item 12.3. Geneva, *World Health Organization*, (unpublished document EB101/19)
- WHO, 2000, "The world health report 2000 - Health systems: Improving performance", Geneva, *World Health Organization*
- Wilkinson, D. L., "Avoidance of seawater intrusion into ports of ocean outfalls", *Journal of Hydraulic Engineering*, Vol. 114, No. 2, February, 1988
- Wilkinson, D. L., "Purging of saline wedges from ocean outfalls", *Journal of Hydraulic Engineering*, Vol 110, No. 12, December, 1984
- Wilkinson, D. L., "Seawater circulation in sewage outfall tunnels", *Journal of Hydraulic Engineering*, Vol. 111, No. 5, May, 1985
- Wilkinson, D. L., and Wareham, David G., "Optimization Criteria for Design of Coastal City Wastewater Disposal Systems", *Proc. Clean Sea 96, Toyohashi*, 1996
- Wilkinson, D.L. and Wareham, D.G, 1998, "Optimization of Coastal City Wastewater Treatment and Disposal Systems to Achieve Sustainable Development", *Proc. of the 1998 IPENZ Conference*, 12-16, p. 6.3-6.7
- Wilkinson, D.L., and Nittim, R., "Model studies of outfall riser hydraulics", *Journal of Hydraulic Research*, Vol. 30, No. 5, 1992
- Williams, B.L., 1985 "Ocean Outfall Handbook", *National Water and Soil Conservation Authority*, Water&Soil Miscellaneous publication number 76, ISSN 0110-4705, Wellington
- Wood, I.R.; Bell R.G.; Wilkinson D.L., 1993, "Ocean Disposal of wastewater", World Scientific, Singapore
- World Bank, 1993, "World Development Report 1993: Investing in Health", New York, Oxford University Press
- World Bank, 1997, "Clear Water, Blue Skies: Chinas Environment in the New Century", Washington, DC, World Bank
- World Resources Institute, 1998, "A guide to the global environment: environmental change and human health", New York, Oxford University Press
- WRc, 1990, "Design Guide for Marine Treatment Schemes", Water Research Centre plc., Swindon
- Wright, S J., 1994, "The effect of ambient turbulence on jet mixing", in *Recent Research Advances in the Fluid Mechanics of Turbulent Jets and Plumes* (eds P A davies & M J Valente Neves), NATO ASI Series, Series E: Applied Sciences, Vol 255, Kluwer Academic Publishers, Dordrecht, NL
- Zhang, Xue-Yong and Adams, E.E., 1999, "Prediction of near field plume characteristics using far field circulation model, *Journal of Hydraulic Engineering*, Vol. 125, No.3
- Zhang, Xue-Yong, 1995, "Ocean Outfall Modeling - Interfacing Near and Far Field Models with Particle Tracking Method", Dissertation thesis, Massachusetts Institute of Technology, Boston, USA
- Zhu, J., And Shih, T.H., 1994, "Computation of confined coflow jets with three turbulence models", *J. for Numerical Methods in Fluids*, 19(10), 939-956
- Zielke W. & Mayerle R., 1999, "Küstengewässer" in: Zielke, W. [Hrsg.]: *Numerische Modelle von Flüssen, Seen und Küstengewässer*, DVWK Schriften 127, Bonn

A summary on outfalls references is also available at: <http://outfalls.ifh.uni-karlsruhe.de/>

Curriculum vitae

General Information

Birth data: 21st October 1972 • Marbach (Neckar) • Germany
Marital status: married, two children
Nationality: German
Private address: Douglasstr. 34 • 76133 Karlsruhe • www.bleninger.com
Office address: Institut für Hydromechanik • Universität Karlsruhe
Kaiserstr. 12 • 76131 Karlsruhe • Germany
bleninger@ifh.uka.de • www.ifh.uni-karlsruhe.de



Education

- Dipl.-Ing. • University Karlsruhe • March 2000 • Civil Engineering, subject Hydraulic & Environmental engineering
- Kepler - Gymnasium (high - school) of natural-sciences • 1983-1992 • Ulm, Germany

Professional experience

- Head of teaching department, research and teaching assistant • University Karlsruhe • Institute for Hydromechanics • April 2003 - present
- Research and teaching assistant • University Karlsruhe • Institute for Hydromechanics • July 2000 - March 2003

Lectureships

- Lecturer: „Environmental Fluid Mechanics“, Advanced School (one week) • University Karlsruhe • June 2006
- Lecturer: “Design of Ocean Outfalls for Heated Water and Wastewater Discharges”, short course • Seoul, South Korea • 9.9.-10.9.05
- Coordinator and lecturer: “Hydraulics of the waste water treatment plant – outfall systems”, short course • Catania, Italy • 24 - 25.09.04
- Lecturer: “Submarine Outfalls: Design Considerations and Environmental Performance Monitoring”, workshop • São Paulo, Brazil • 1-5.12.2003
- Coordinator and lecturer: “CORMIX course” • University Karlsruhe • 07-08.12.2000

Short term assignments

- Research stay • Georgia Institute of Technology, USA • December/January 2005/2006
- Research stay • Universidade de São Paulo, Brazil • Aug. 2002, Nov. - Dec. 2003 • “PROBRAL (DAAD project): “Reducing water pollution on the São Paulo Coast: Development of methodologies for planning and design of multiport diffusers for wastewater discharges”
- Research stay • Universidade Porto, Portugal • Sept. '98 • Experiments on particle laden jets

Professional Societies and memberships

- DWA (Deutsche Vereinigung für Wasserwirtschaft, Abwasser und Abfall, / German Association for Water resources, waste water and waste) • since 2001 • member of working group WW-3.4 "Mixing and Transport problems due to discharges"
- International Association for Hydraulic Engineering and Research (IAHR) • since 2003
- International Water Association (IWA) • since 2007 • member and secretary of specialist group “Wastewater treatment systems utilising submarine outfalls”
- American Geophysical Union • since 2007 • member
- EWB – Engineers without borders University Karlsruhe • since 2004 • founding member

Long submarine outfalls with a multiport diffuser are efficient discharge devices avoiding pollutant accumulation and collapse of ecosystems by dispersing the treated effluents. This thesis describes the hydraulic design and environmental impact prediction technologies for such installations. Focus are the hydrodynamics approached by computer models. First, a multiport diffuser design program was developed. Second, two model systems for discharge analysis, CORMIX for the near-field and intermediate-field and Delft3D for the far-field were coupled, and third a regulatory procedure is proposed to license and monitor outfall installations. The models have been applied for the planned outfall in Cartagena, Colombia, and successfully demonstrated the capabilities for outfall projects and the model improvements due to the implemented approach.